The hydrodynamics and heat transfer characteristics of liquid films on a rotating disc

by

C. BELL B.Sc. (Hons., Newcastle)

Thesis submitted for the degree of Doctor of Philosophy in the Faculty of Applied Science of the University of Newcastle upon Tyne.

Department of Chemical Engineering

University of Newcastle upon Tyne

June, 1975.

ACKNOWLEDGEMENTS

The author is aware of extensive indebtedness to many individuals and departments of the University too numerous to mention in full, but would like to extend particular thanks to the following:

Mr.J.E.Porter, Supervisor, whose creativity and zeal have been exemplary;
Professor J.D.Thornton, Head of Department, in whose laboratories this work was conducted;
Mr.A.K.Cole, Technician, for his fabricatory skill;
Mrs.L.Appiah and the Inter Library Loan staff for their determined pursuit of obscure references;
Mr.C.A.Currie and the workshop staff; Mr.D.Burman, Electrician, and Mr.R.Randles, Photographer, for their advice and assistance.

The author acknowledges the financial support of a Scientific Research Council award.

SYNOPSIS

This work is concerned with the hydrodynamics and heat transfer characteristics of the liquid film formed when a liquid flows across a rotating, heated disc.

Comprehensive reviews of both the hydrodynamic and heat transfer behaviour of planar gravitationally forced films, and rotating discs in homogeneous media of infinite extent, are presented in addition to the primary subject of this study.

For the liquid film on the rotating disc, various hydrodynamic models are studied and the controlling parameters identified. Results obtained with water films are in good agreement with the theoretical models.

A simple heat transfer model is developed as an extension to one of the hydrodynamic models. Experimental results for water films show fair agreement with the model and suggestions are made accounting for the discrepancies.

Suggestions for future work in both the hydrodynamic and heat transfer fields are made.

FOREWORD

The purpose of this foreword is to act as a guide to the reader of this work. Different people will read this work for different reasons and the hope is that this note used in conjunction with the index will enable the user to locate the desired information more quickly.

The work has been sectioned into two main parallel parts, 2: HYDRODYNAMICS and 3: HEAT TRANSFER. The first sub-section of each part (2.1 and 3.1) deals with previous work in the allied fields mentioned in the SYNOPSIS. For the hydrodynamic section only, a particular experimental technique review has been included (2.2). Next the literature survey proper for this work is conducted considering both previous theoretical and experimental results (2.3 and 3.2). This is followed by this work's contribution (2.4 and 3.3) a description of the equipment design (2.5 and 3.4), the experimental work (2.6 and 3.5) and the results and discussion (2.7 and 3.6). Conclusions and suggestions for future work end each main section.

Extensive use of non-dimensional groups has been made and the reader, if only intending to pursue the experimental results is advised to read the first few pages of the LITERATURE SURVEY (section 2.3), and note the groups used in the NOMENCLATURE.

NOMENCLATURE

in addition to the text definitions

ROMAN			DIMENSIONS
x, X	:	in flow direction	-
y, Y	:	normal to flow direction	-
r, R	:	in radial direction, also radius	-
t	:	time	T
t_R	:	residence time	T
T	:	temperature	Θ
T^*	=	$(T_o - T)/T_o - T_i)$	-
P	:	pressure	$ML^{-1} T^{-2}$
N	:	rotational speed	T^{-1}
R_o	:	body force in radial direction	$M L^{-2} T^{-2}$
Y_o	:	body force in vertical direction	$M L^{-2} T^{-2}$
a	:	wave amplitude	L
g_c	:	gravitational constant	$L T^{-2}$
Q	:	total volumetric flowrate	$L^3 T^{-1}$
Q'	:	volumetric flowrate per unit normal flow perimeter length	$L^2 T^{-1}$
U, V	:	velocity	$L^2 T^{-1}$
K	:	consistency index for power law non-Newtonian liquids	$MT^{n-2}L^{-1}$
n	:	index for power law non-Newtonian liquids	-
$\mathbb{A}$	:	Benjamin's amplification factor for waves (see page 12)	-
A	:	aspect ratio (= G/r_i)	
G	:	distributor/flow surface gap	L
H	:	disc edge/tank wall clearance	L
Z_o	:	disc/shroud clearance	L
Cv, Cp	:	specific heat	$H.M^{-1} \Theta^{-1}$
k	:	thermal conductivity	$H.\Theta^{-1} L^{-1} T^{-1}$
h	:	heat transfer coefficient	$H.\Theta^{-1} L^{-2} T^{-1}$
q	:	specific heat flux	$H.L^{-2} T^{-1}$
h_{fg}	:	specific latent heat	$H.M^{-1}$
M	:	Mach number of flow	-
k_m	:	mass transfer coefficient	$L.T^{-1}$
D_v	:	diffusivity	$L^2 T^{-1}$

GREEK		DIMENSIONS
θ	angle of plane inclination	deg
α	surface tension contact angle	deg
ϕ	wake angle	deg
σ	surface tension	MT^{-2}
ρ	density	ML^{-3}
μ	viscosity (1st coefficient)	$ML^{-1}T^{-1}$
λ	viscosity (2nd coefficient) } context will clarify	$ML^{-1}T^{-1}$
λ	wavelength	L
γ	$= C_p/C_v$	-
α_H	thermal diffusivity ($k/C_p\rho$)	L^2T^{-1}
ϵ	eddy viscosity	$M.L^{-1}T^{-1}$
ν	kinematic viscosity ($=\mu/\rho$)	L^2T^{-1}
τ	shear stress	$ML^{-1}T^{-2}$
η	$= y/\delta$ or see equation 152	-
ω	angular velocity	T^{-1}
K	Brauer group - equation 25	-
θ_o	body force in azimuthal direction	$M.L^{-2}T^{-2}$
Φ_v	viscous dissipation	$H.L^{-3}T^{-1}$
δ	film thickness	L

SUB-SCRIPTS

s	free surface
o	solid surface (except r_o - see below)
x, y, r, θ in	x, y, r, θ directions respectively
i	at inlet
e	at exit (except r_o)
a	air or average (text will signify)
L	liquid
v	vapour
N	Nusselt formulation (see equation 135.1)
c	condensation or critical
w	wavy
∞	in an infinite media
m	mean or mixed

SUPERSCRIPTS

—	averaged
+ , * , '	non-dimenionalised

DIMENSIONLESS GROUPS

Re	Reynolds	Qr/ν
Ta	Taylor	wr^2/ν
We	Weber	$\bar{U}_r/(\sigma/\rho\delta)^{\frac{1}{2}}$
Nu	Nusselt	$\frac{hL}{k}$ when L = r, x or $(\nu/\omega)^{\frac{1}{2}}$ text will clarify
Pr	Prandtl	$Cp\mu/k$
Sh	Sherwood	$k_m r/D_v$
Sc	Schmidt	$\mu/\rho D_v$
N_T	see equation 14	
β	see equations 13 and 94	
ϵ, ψ	see equation 77.1	

FIGURES

TABLES

PHOTOGRAPHS

INDEX

1. INTRODUCTION

The successful design of a heat exchanger requires the simultaneous satisfaction of often conflicting needs. FIGURE 1 details a typical design procedure for obtaining an exchanger design that should best suit the limitations of fluid nature, economics and existing (if any) plant locations. The essential requirements for the successful completion of the algorithm are essentially three fold. Firstly, the designer needs to have detailed and accurate data on the fluids involved. Such information is usually available fairly easily in the literature. The second requirement is knowledge of any special requirements that may single out a particular type of exchanger as the most sensible choice. Thus space limitations, corrosive fluids, high or low temperatures or pressures and so on could each determine the ideal type of exchanger over and above any economic considerations. Thirdly, the designer must have a detailed design technique available to actually design the required exchanger.

In most circumstances the above procedure is probably not knowingly followed by a designer. For most applications a conventional shell and tube heat exchanger will suffice and there are easily available inexpensive "off the shelf" exchangers and/or comprehensive design techniques. However, FIGURE 2 is an attempt to show those areas where the situation is not so well defined. FIGURE 2 is a chart showing, in columns, the various types of fluid that may have to be processed and, in rows, the various types of exchanger available. It can be seen from this figure that in general moving from left to right one progressively meets more difficult liquids and moving, down the figure, the exchangers available become more sophisticated and expensive. However, for the heat sensitive products the sophisticated exchangers are the most suitable. The reason for this advantage over, for example, the conventional shell and tube device, is the very low residence time of, for example, the rotating devices. The low residence time means that a higher processing temperature can be employed since the product of increasing decomposition rate (due to the higher temperature) and shorter time at the higher temperature will still be less overall than for conventional devices. A higher processing temperature has an additional advantage in that the ratio (death rate of thermophilic bacteria/decomposition rate of material) increases five fold for every 10°C rise in processing temperature (from figures in (1)). Thus VITER et al (2) in a pilot plant trial of a rotating conical heat exchanger used in concentrating an alcoholic extract of digitalis, found

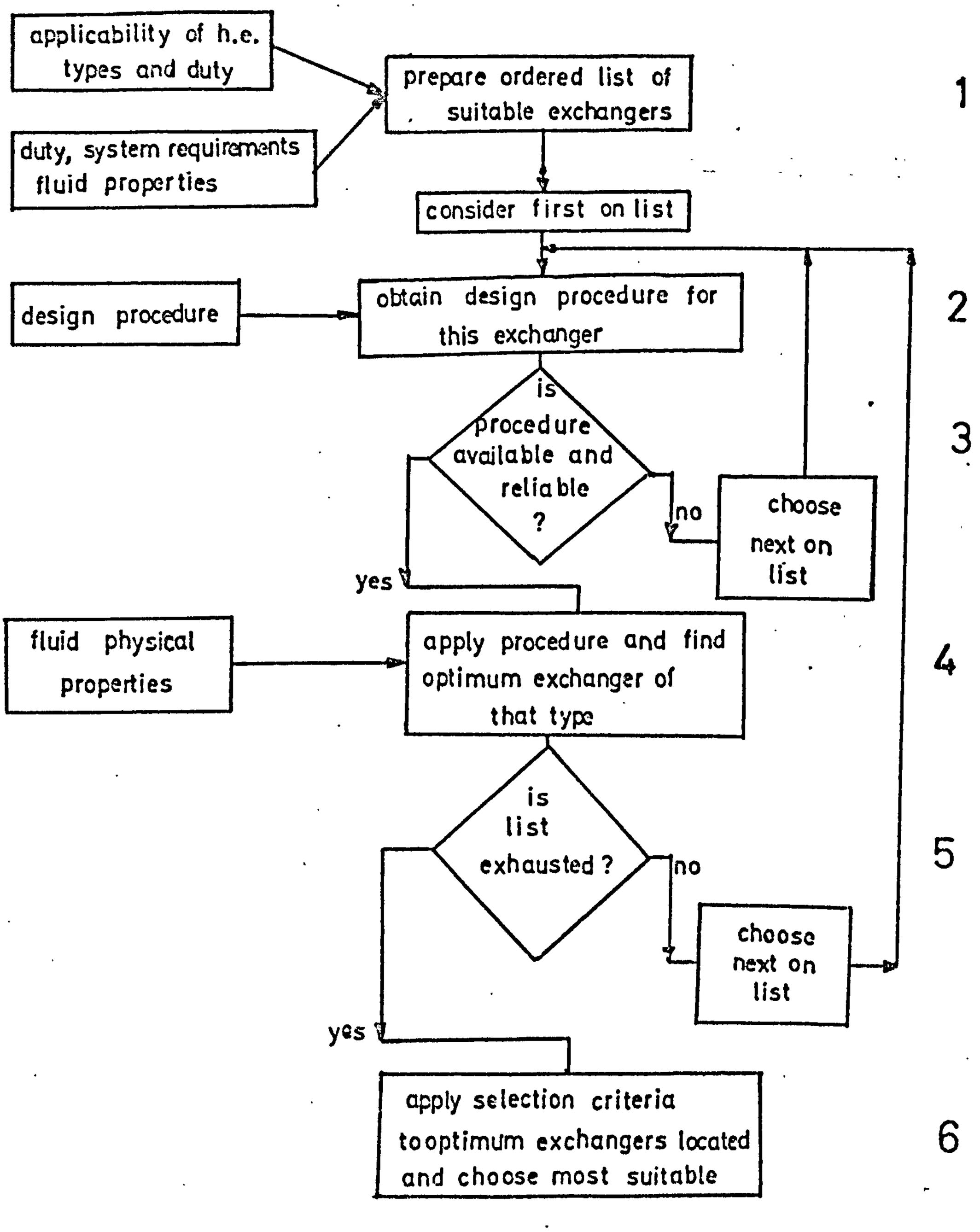

FIGURE 1 : A HEAT EXCHANGER DESIGN ALGORITHM

FIG 2 EXCHANGER CATEGORISATION

REGIME	EXCHANGER TYPE	MAX. VISC.(P)	SECONDS / PASS	SYSTEM PARAMS. FOAMING	SYSTEM PARAMS. SCALING	FLUID PROPERTIES GEN. NON H.S.	FLUID PROPERTIES GEN. MED H.S.	FLUID PROPERTIES GEN. VERY H.S.	FLUID PROPERTIES GEN. ULTRA H.S.	FLUID PROPERTIES LOW VISCOSITY NON H.S.	FLUID PROPERTIES LOW VISCOSITY MED H.S.	FLUID PROPERTIES LOW VISCOSITY VERY H.S.	FLUID PROPERTIES LOW VISCOSITY ULTRA H.S.	FLUID PROPERTIES HIGH VISCOSITY NON H.S.	FLUID PROPERTIES HIGH VISCOSITY MED H.S.	FLUID PROPERTIES HIGH VISCOSITY VERY H.S.	FLUID PROPERTIES HIGH VISCOSITY ULTRA H.S.
NATURAL CONV.	TANK/COILS	10	>10														
	SUBMERGED TUBES	10	>100														
FORCED CONV.	TANK/COILS + STIRRER	20	>1														
	SHELL TUBE	4	>10														
	EXTENDED SURFACE	4	>100														
	PLATE SPIRAL	4	>100														
FILM	CLIMBING-FALLING FILM	4	~1														
	SCRAPED SURFACE	200	<1														
	ROTATING DEVICES	100	≪1														
FLUID EXAMPLE NUMBER						1	2	3	4	5	6	7	8				

HEAT SENSITIVITY	MAX. TIME AT 373K
ULTRA	1s
VERY	10s
MEDIUM	500s

.1.
MOST INORGANIC CHEMICALS
SOME ORGANIC CHEMICALS

.2.
PINEAPPLE JUICE
TOMATO JUICE
BEER
MILK
EGG

.3.
TEA EXTRACT
APPLE JUICE
GRAPEFRUIT JUICE

.4.
COFFEE EXTRACT
PHARMACEUTICAL
PROTEIN EXTRACTS
CHERRY JUICE

.5.
AGAR-AGAR
CELLULOSE SOLNS.
GLUE
SOUPS

.6.
SUGAR SYRUP
FRUIT CONCENTRATES
GELATIN
MEAT STOCKS

.7.
YEAST EXTRACT
APRICOT CONC.
PEACH CONC.
PEAR CONC.

.8.
MALT EXTRACT
ENZYME EXTRACTS

VERY GOOD
GOOD
SATISFACTORY
USABLE, NOT SUITABLE
EXCESSIVE DEGREDATION

that degradation of the glucosides present fell by 25% over a conventional evaporator's product. In addition the evaporation rate was of the order of 800 kg/hr for a unit of 2.4 m^2 area.

Thin film and rotary equipment have been in use since about the beginning of the century. HICKMAN (3) was the first to successfully combine the advantages of the two fields into a rotary disc evaporator as early as 1944. Experimental investigation is still active and at least one commercial conical device (ALFA-LAVAL) is marketed. The incentive to do so is brought out by FIGURE 3 which shows the world growth of a certain small sector of the sort of heat sensitive products that rotary devices are best suited for. This figure shows that the world market up to 1970 has grown at about 4% per annum (about twice world population growth) and at an even faster rate more recently. Much practical research work has been carried on the more simply understood disc geometry (see 4, 5, 6, 7), but the field is yet understudied with much work remaining to be commenced and existing results to be confirmed. In particular the significant problems of variable physical properties and fluids of non-Newtonian rheology have yet to be studied. LEIDENFROST (8, 9) states that a rotating disc was considered as a heat exchanger for oils but the results of this work have not yet been published.

The rotating disc geometry has found many other uses apart from the field of evaporation and heat transfer. These include:

fluid atomisation (10, 11, 12, 13, 14, 15)
as a reactor surface (16, 17, 18, 19)
high speed pump (20, 21)
centrifugal extractor (22)
solid/liquid separator (23)

In all cases a full understanding of the hydrodynamics of the film on the disc surface is fundamental to the successful design of the unit for any of these purposes. The work described in this thesis is in two main parts. In the first the various analyses available for describing the hydrodynamics of the system are studied and compared to the available experimental data. In the second section, the process is repeated for the heat transfer problem. In each section studies in related areas of research, for example

1. film flow on plane walls under gravity
2. radially expanding film flow on a stationary disc

and 3. a rotating disc in a media of infinite extent are discussed.

FIG 3 WORLD GROWTH IN HEAT SENSITIVES

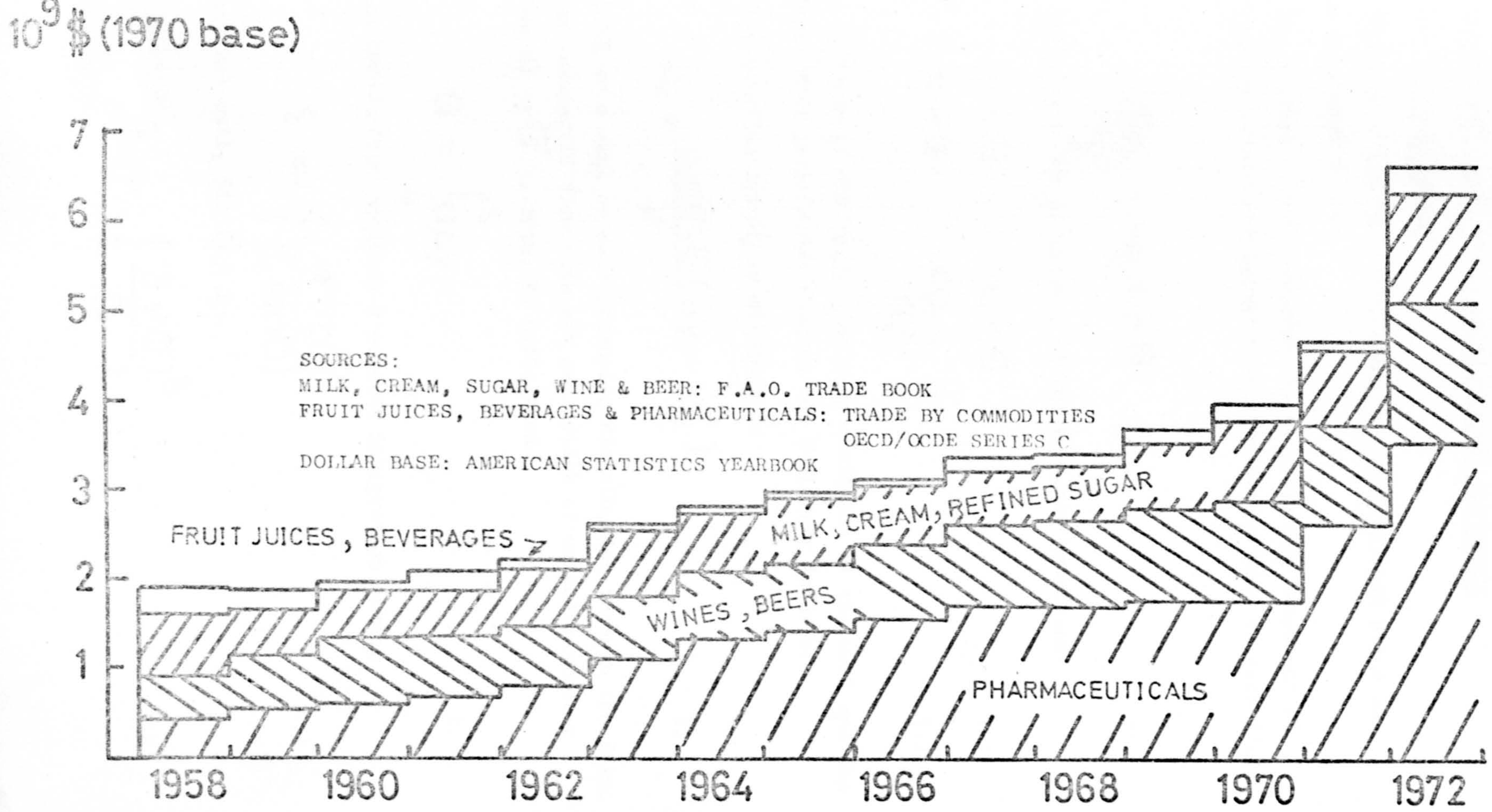

2. HYDRODYNAMICS

2.1. ASSOCIATED FIELDS

2.1.1. PLANAR FILMS UNDER GRAVITATIONAL INFLUENCE

A: FILM THICKNESS

Consider a liquid film flowing down an inclined plane as illustrated in FIGURE 4 over.

For a simple model consider the accelerating component of gravity along the film to be balanced by the viscous drag of each fluid layer,

Thus $$\nu \frac{d^2 u_x}{dy^2} = -g_c \sin\theta \qquad 1.$$

Integrate equation 1 twice, subject to the boundary conditions

$$y = 0 \qquad u_x = 0 \qquad 1.1$$

$$y = \delta \qquad \frac{du_x}{dy} = 0 \qquad 1.2$$

The first condition is the usual zero slip condition at the wall and the second implies zero interfacial drag at the fluid/air interface.

The solution for u_x so obtained is

$$u_x = \frac{g_c \sin\theta}{\nu}\left(\delta y - \frac{y^2}{2}\right) \qquad 2.$$

which gives u_x as a semi or half parabolic distribution through the film. Denoting the volumetric flow rate per unit width of wetted perimeter (units $m^3/sec\ m$) by Q' , then, by definition

$$Q' = \int_0^{\delta} u_x dy \qquad 3.$$

Substitution for u_x from equation 2 permits integration giving

$$\delta = \left(\frac{3\nu Q'}{g_c \sin\theta}\right)^{1/3} \qquad 4.1$$

or for a vertical wall, Sin $\theta = 1$

$$\delta = \left(\frac{3\nu Q}{g_c}\right)^{1/3} \qquad 4.2$$

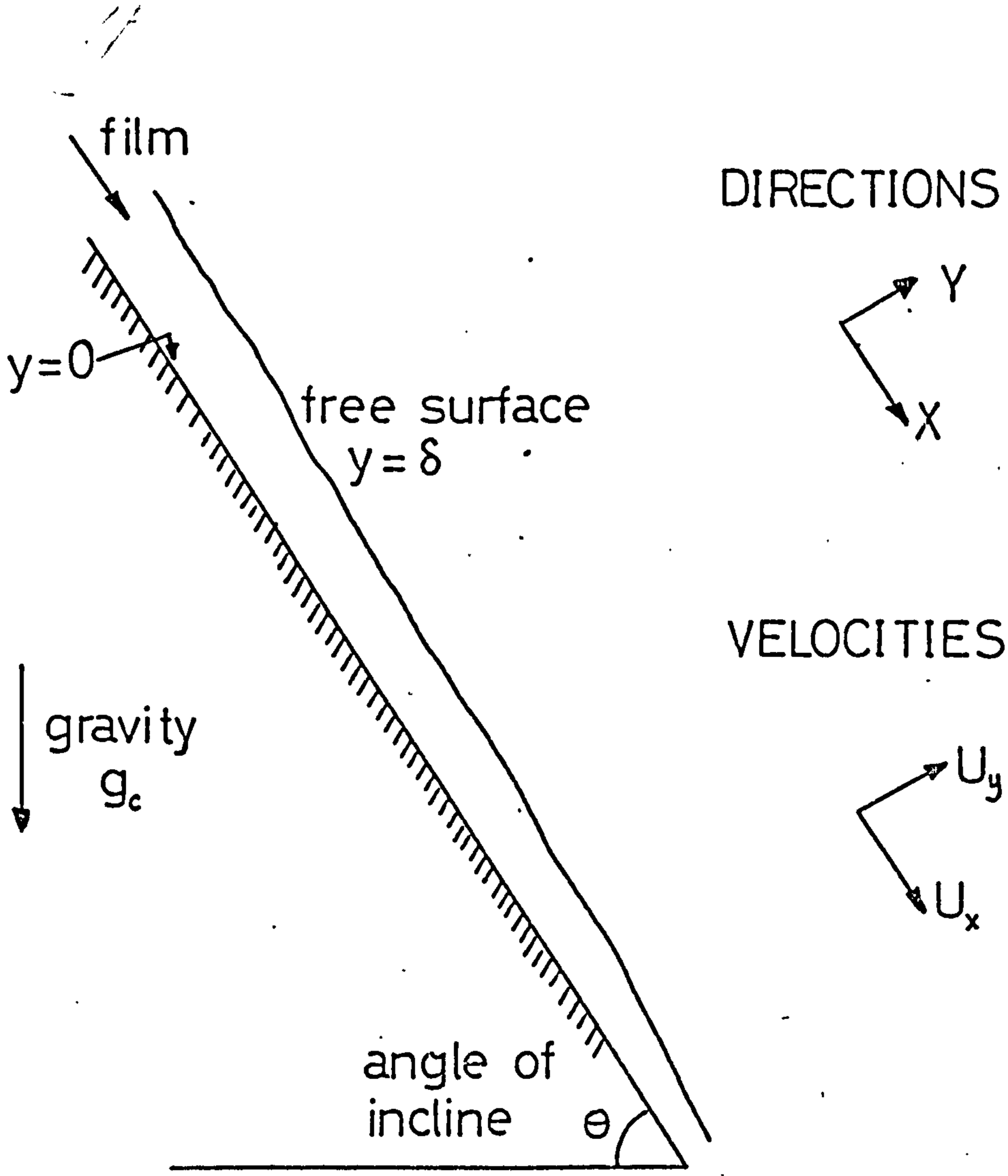

FIG 4 NOMENCLATURE FOR PLANE FILMS

This analysis was first performed by NUSSELT (24) for the case of steady, smooth film flow both without (as above) or with free surface interfacial shear. For interfacial shear equation 1.2 may be replaced by either

$$y = \delta \quad \tau = \tau_s \qquad \text{or} \qquad y = \delta \quad u_x = u_{sx} \qquad 5.1$$

when the subscript s refers to the free surface. The first boundary condition gives

$$u_x = -\left(\frac{\tau_s}{\rho} + g_c \delta\right)\frac{y}{\nu} + \frac{g_c}{2\nu} y^2 \qquad 5.2$$

and the second

$$u_x = \frac{g_c}{2\nu}\left(\delta y - \frac{y^2}{2}\right) + \frac{u_{xs}\, y}{\delta} \qquad 5.3$$

Returning to equation 4, the average velocity is given by

$$\overline{u_x} = \frac{Q'}{\delta} = \frac{g_c \delta^2}{3\nu} \qquad 6.$$

and so from equations 6 and 2 evaluated at $y = \delta$

$$\frac{u_{xs}}{\overline{u_x}} = \frac{3}{2} \qquad 7.$$

Equations 2, 4 and 7 provide a basis for experimental investigation of this simple model. However, before comparing the experimental information available to this theory, other models will be investigated.

DUCKLER and BERGELIN (25) proposed a theory which attempted to give an experimental basis to the analysis. If the Universal Velocity Profile (U.V.P.) concept developed by PRANDTL (26) and fitted to the data of NIKURADSE (27) for flow in tubes is assumed to be applicable to flow in thin films, then the velocity profile will be given as

for $0 < y^+ < 5 \qquad u^+ = y^+ \qquad 8.1$

$5 < y^+ < 30 \qquad u^+ = -3.05 + 5 \ln y^+ \qquad 8.2$

$y^+ > 30 \qquad u^+ = 5.5 + 2.5 \ln y^+ \qquad 8.3$

when $y^+ = \frac{u^* y}{\nu}$; $u^+ = \frac{u_x}{u^*}$; $u^* = \left(\frac{\tau_o}{\rho}\right)^{1/2} \qquad 8.4$

Each of expressions 8.1, 8.2 and 8.3 may be integrated in turn with respect to y^+ to give the specific flowrate thus:

$$Q' = \int_o^\delta U_x \, dy = \nu \int_o^{y^+} U^+ dy^+ \qquad 8.5$$

so that $0 < y^+ < 5$ $\qquad Q'/\nu = \delta^{+2}/2$ $\qquad 9.1$

$5 < y^+ < 30$ $\qquad Q'/\nu = 12{\cdot}5 - 8{\cdot}05\,\delta^+ + 5\delta^+ \ln \delta^+$ $\qquad 9.2$

$y^+ > 30$ $\qquad Q'/\nu = -63{\cdot}9 + 3\delta^+ + 2{\cdot}5\,\delta^+ \ln \delta^+$ $\qquad 9.3$

when δ^+ is the dimensionless free surface defined similar to y^+ in equation 8.4.

To a first approximation τ_o may be estimated from a simple force balance equating the wall shear stress to the fluid body force,

whence $$\tau_o = g_c (\sin\theta)\, \delta \rho \qquad 10$$

and so from equation 8.4 for a vertical film

$$\delta^+ = g_c^{1/2}\, \delta^{3/2}/\nu \qquad 11$$

Equations 9.1, 9.2 and 9.3 enable the film thickness to be found (implicitly) for a given flowrate and fluid viscosity.

The integration scheme outlined above may be applied to any given distribution of $U^+ = U^+(y^+)$. The distribution used above (U.V.P.) has two discontinuities within its operating range (both of value and derivative).

Various "smoothing" expressions have been proposed, for example, CHURCHILL and CHOI (28) recently proposed a continuous expression for $y^+ > 0.11$ (below which $U^+ = y^+$ may be used) as

$$U^+ = y^+ \left(1 + \left\{ y^+/A + B \ln y^+ \right\}^n \right)^{1/n} \qquad 12$$

The authors specify A = 5.5, B = 2.5 and n = 2 as correlating some experimental data on turbulent pipe flow. Analytic integration of equation 12 is, however, too involved and numerical integration indicates values not much different from the U.V.P. analysis.

The original paper by DUCKLER and BERGELIN contains an error, pointed out by PORTALSKI (29, 30) in that although the three expressions for U^+ must be integrated separately over their respective ranges, DUCKLER and BERGELIN claim that the final equation (equation 9.3)(valid only for turbulent flow, $y^+ > 30$) is valid for all $y^+ > 0$.

An estimation of turbulence onset may be obtained by setting $y^+ = 30$ into equations 9.2 and 9.3 resulting in (Q'/ν) values of 281.2 or 281.1 respectively.

DUCKLER (31) proposed a model in which the flow within the film is not stratified into distinct bands of laminar flow, transition flow and turbulent flow as in the U.V.P. model, but instead turbulence is allowed to exist at all values of y^+. DEISSLER'S (32) expression for eddy viscosity in tube flow was used for $y^+ \leq 20$ and von KARMAN'S expression for $y^+ > 20$. DEISSLER'S expression tends asymtotically to zero as $y^+ \rightarrow 0$ giving a perfectly laminar layer strictly speaking only at the wall. The numerical constants used in the eddy viscosity equations were those obtained from analysis of full tube flow data. The result of DUCKLER'S analysis was to obtain a numerical solution yielding δ as a function of (Q'/ν) with an additional parameter β.

β was defined as

$$\beta = \frac{1}{2}\left(\frac{\Delta\rho}{\rho}\right)\frac{\tau}{\rho}\left(\frac{g_c}{\nu^2}\right)^{1/3} \qquad 13$$

and DUCKLER concluded that the numerical value of β was an indication of the intensity of shear within the film. β ranged from 0 (laminar) to 4000 (turbulent). When $\beta = 0$, the results of the numerical study tended to agree to the simple model, equations 1 - 7.

FIGURE 5 shows a comparison of experimental data collected by FULFORD (33) from various sources published prior to 1962 with the analyses considered, viz. equations 4.2, 9.1, 9.2 and 9.3; and DUCKLER'S analysis. The figure uses the thickness parameter N_T employed by FULFORD. The experimental techniques employed in measuring the film thickness will be reviewed later. N_T may be viewed as a dimensionless film thickness and is defined as

$$N_T = \delta\left(\frac{g_c \sin\theta}{\nu^2}\right)^{1/3} \qquad 14$$

From equations 14 and 11 it can be seen that

FIG 5 GRAVITY INDUCED FLOW

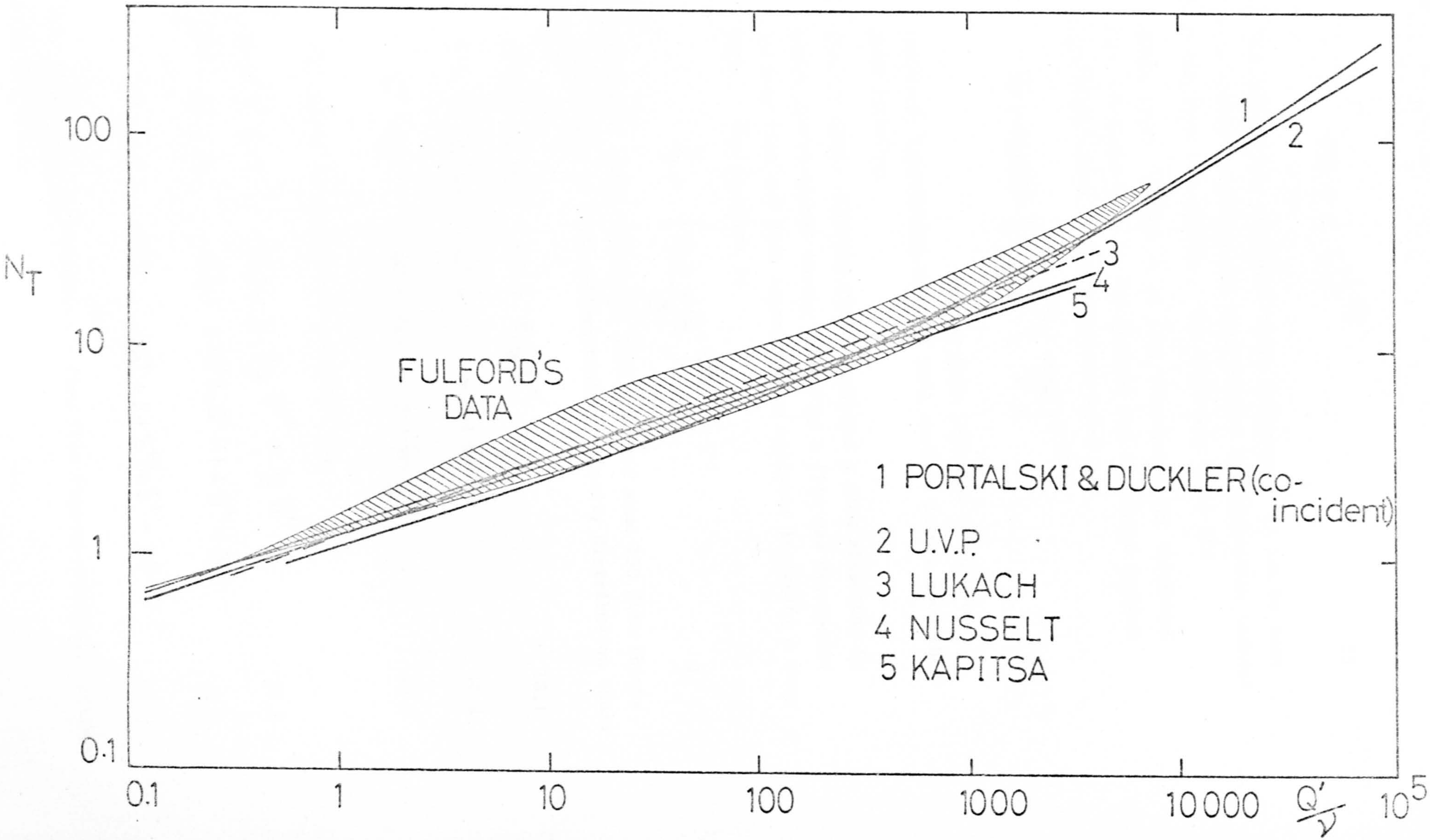

$$N_T = (\delta^+)^{2/3} \qquad 15$$

Also shown on this figure are three other analyses. It can be seen that the data scatter prevents any experimental discrimination between the various theories considered. The remaining lines are

1. LUKACH LINE: LUKACH et al (34) correlated the thickness data for water flow in the laminar and turbulent regimes (see later) over heated polythene tubes as

$$\delta = 0.805 \left(\frac{\nu^2}{g_c}\right)^{1/3} \left(\frac{4Q'}{\nu}\right)^{0.368} \qquad 16$$

and has been included to show the influence (apparently nil) of wall surface nature upon the hydrodynamics.

2. KAPITSA LINE: KAPITSA (35) considered a flow situation in which gravitational energy gained by a film was dissipated in wavy flow and thus represents an analysis including a wavy film. The equation is

$$\bar{\delta} = \left(\frac{2.4\,\nu Q'}{g_c}\right)^{1/3} \qquad 17$$

3. PORTALSKI LINE: PORTALSKI (36) analysed some 150 film thickness values to form a dimensionless velocity distribution thus:

$$0 < \delta^+ \leq 9 \qquad u^+ = 8/9\, y^+ + 1/2 \qquad 18.1$$

$$9 < \delta^+ \leq 30 \qquad u^+ = 1.7 + 3.1 \ln y^+ \qquad 18.2$$

$$\delta^+ > 30 \qquad u^+ = 5.1 + 2.1 \ln y^+ \qquad 18.3$$

for which the integrated equations are

$$0 < \delta^+ \leq 9 \qquad Q'/\nu = 4/9\, \delta^{+2} + 1/2\, \delta^+ \qquad 19.1$$

$$9 < \delta^+ \leq 30 \qquad Q'/\nu = 3.1\delta^+ \ln \delta^+ - 1.4\,\delta^+ - 8.2 \qquad 19.2$$

$$\delta^+ > 30 \qquad Q'/\nu = 3\delta^+ + 2.1\,\delta^+ \ln \delta^+ - 38.17 \qquad 19.3$$

The data shown contains measurements from film flow on vertical, inclined

plates and tube surfaces. FULFORD (37) has shown that applying a planar analysis to a curved surface of radius of curvature R leads to a correction term of the order of δ/R . Considering the normal film thicknesses and tube radii used in the experimental work ($\delta \simeq 20\mu m$, $R \simeq 2$ cm) it is obvious that little error is introduced by this procedure.

It appears that at low values of Q'/ν (of order 4) the simple analysis (equation 4.2) is followed. As Q'/ν is increased, some discrepancies appear. Observers of the film in this area report undulations commencing and the data tends to move towards the KAPITSA line. As Q'/ν is increased further, the average thickness data tends to return to the NUSSELT values, finally exceeding the simple models predictions at a Q'/ν of about 400.

KASIMOV and ZIGMUND (38) have treated the reduced two dimensional Navier-Stokes equations and the continuity equation and have obtained expressions for the film thickness as a function of the length of the flow path. They show that the NUSSELT model is strictly valid only over an infinitesimally small portion of the flow, after the flow has recovered from entry effects and prior to inertia forces taking effect.

B: SURFACE TO MEAN VELOCITY RATIO

Equation 7 indicates that

$$\frac{U_{xs}}{\overline{U}_x} = 1.5 \text{ for the NUSSELT analysis.}$$

If in a turbulent film PRANDTL'S power law for the velocity profile is assumed then

$$U_x = U_{xs} \left(y/\delta \right)^n \qquad 20$$

where n is a constant

thus
$$\overline{U}_x = \frac{1}{\delta}\int_0^{\delta} U_x \, dy = \frac{1}{n+1} U_{xs} \qquad 21$$

or
$$\frac{U_{xs}}{\overline{U}_x} = n+1 \qquad 22$$

For a $1/7^{th}$ power law distribution, the ratio is 1.143

The U.V.P. and PORTALSKI analyses may be used to give $U_{xs}/\overline{U}_x$ ratios as functions of Q'/ν as follows. Using the original expressions

for $U^+(y^+)$ and $\frac{Q'}{\nu}(\delta^+)$ and the definitions of equation 8.4,

then $$\bar{U}_x = \frac{Q'}{\delta} = \frac{Q'}{\nu}.\frac{\nu}{\delta} = \frac{U^+}{\delta^+}\left(\frac{Q'}{\nu}\right) = \frac{U_{xs}}{U_s^+}\delta^+\left(\frac{Q'}{\nu}\right) \quad 23$$

so $$\frac{U_{sx}}{\bar{U}_x} = \delta^+ U_s^+ / \left(\frac{Q'}{\nu}\right) \quad 24$$

when U_s^+ is the dimensionless surface velocity evaluated at δ^+. Thus for the U.V.P. model, for instance, at $\delta^+ = 4$

from equation 8.1 $U_s^+ = \delta^+ = 4$

from equation 9.1 $Q'/\nu = \frac{1}{2}\delta^{+2} = 8$

so from equation 24 $\frac{U_{sx}}{\bar{U}_x} = \frac{4.4}{8} = 2$ at $Q'/\nu = 8$

FIGURE 6 shows the analyses previously considered and the data of JACKSON et al (39), JACKSON (40) and FRIEDMAN and MILLER (41). The techniques used to obtain the values of U_{sx} will be considered in detail later. Also shown on FIGURE 6 are the experimental values of PORTALSKI (29) which were obtained using a novel technique. PORTALSKI argues that the rate of advance of a liquid front down a vertical, previously dry plate, is equal to the free surface velocity of the film. TINNEY and BASSET (42), however, note that a float placed behind the advancing front of a horizontal film itself advanced along the surface until it reached the front implying that the velocity of advance is less than the free surface velocity. Thus although PORTALSKI'S data fall to the expected turbulent value, they might be erroneously low. WEST and COLE (43) in a direct measurement of the surface velocity of a falling water film using surface drops of naphthalene reported velocity ratio figures in close agreement to those of PORTALSKI. It is apparent that PORTALSKI'S method requires further investigation.

FULFORD (33) made 226 determinations of $\frac{U_{sx}}{\bar{U}_x}$ by a surface pointer technique (see Section 2.2B) and found the average $U_{sx}/\bar{U}_x$ experimentally to be 1.543.

Possible explanations for the variation of the $U_{sx}/\bar{U}_x$ ratio with Q'/ν are suggested by FRIEDMAN and MILLER (41). They note that the film thickness data agrees to the simple NUSSELT model, implying that U_{sx} is behaving unexpectedly. The authors suggest that either

(a) the surface of the film is highly turbulent due to the free surface shear

FIG 6 VELOCITY RATIO FOR FALLING LIQUID FILMS

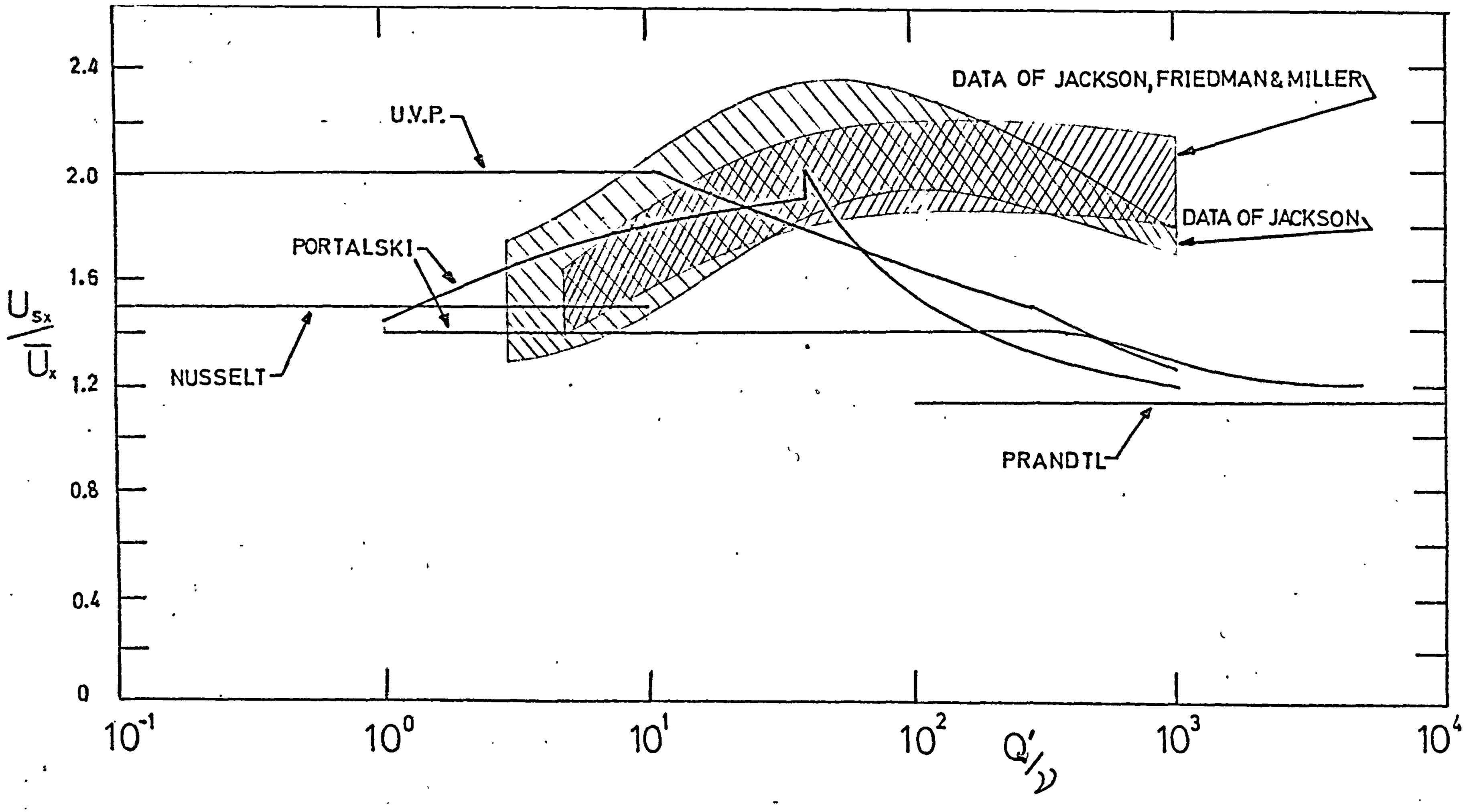

or (b) the presence of the free surface in some way invalidates the assumed differential equations as applied to the bulk of the film.

Since it would appear that the rise from the ratio of 1.5 first occurs in the flow area where waves first become apparent it could be that investigators have erroneously interpreted the wave celerity as the surface velocity. Thus FULFORD (37) notes that maximum values of $U_{sx}/\bar{U}_x$ have been reported in that region of flow where maximum wavelengths are observed,and tend to return to 1.5 again in that region where the wave velocity tends to equal the NUSSELT model value of U_{sx}.

C: VELOCITY PROFILES

Due to the extreme thinness of the flowing film measuring a velocity profile through it presents severe experimental difficulties and only limited information is available. In general the profile predicted by the NUSSELT model has been validated in the laminar and rippling laminar regimes. Thus GOODRIDGE and GARTSIDE (44), CLAYTON (45) and WILKES and NEDDERMAN (46) all report approximate semi-parabolic distributions. COOK and CLARK (47) report measurements of velocity to within 6 μm of the wall giving agreement to the NUSSELT model only in the smooth non-rippling zone. AGSJØRNSEN (48), using a residence time technique, reports agreement with the NUSSELT model up to a value of Q'/ν of 100, well into rippling film flow. GRIMLEY (49) reports a velocity profile which shows a maximum velocity some 25% below the free surface, with the velocity itself some 30% greater than the free surface. The experimental surface velocity was some 3 to 4 times the NUSSELT model value. It is possible that GRIMLEY'S experimental technique was at fault since he reports difficulty in maintaining neutrally charged particles in the film (the technique is discussed later in more detail), however, ATKINSON and CARUTHERS (50) provide general agreement to GRIMLEY'S finding that the maximum velocity occurred below the free surface rather than at the free surface as indicated by equation 2.

FIGURE 7 shows non dimensionally the typical profiles of the analyses considered compared to that of GRIMLEY.

D: REGIME TRANSITIONS

The simple NUSSELT model has implicit in its structure the assumption of the existence of a smooth laminar film. As has been

FIG 7 PLANE FILM VELOCITY PROFILES

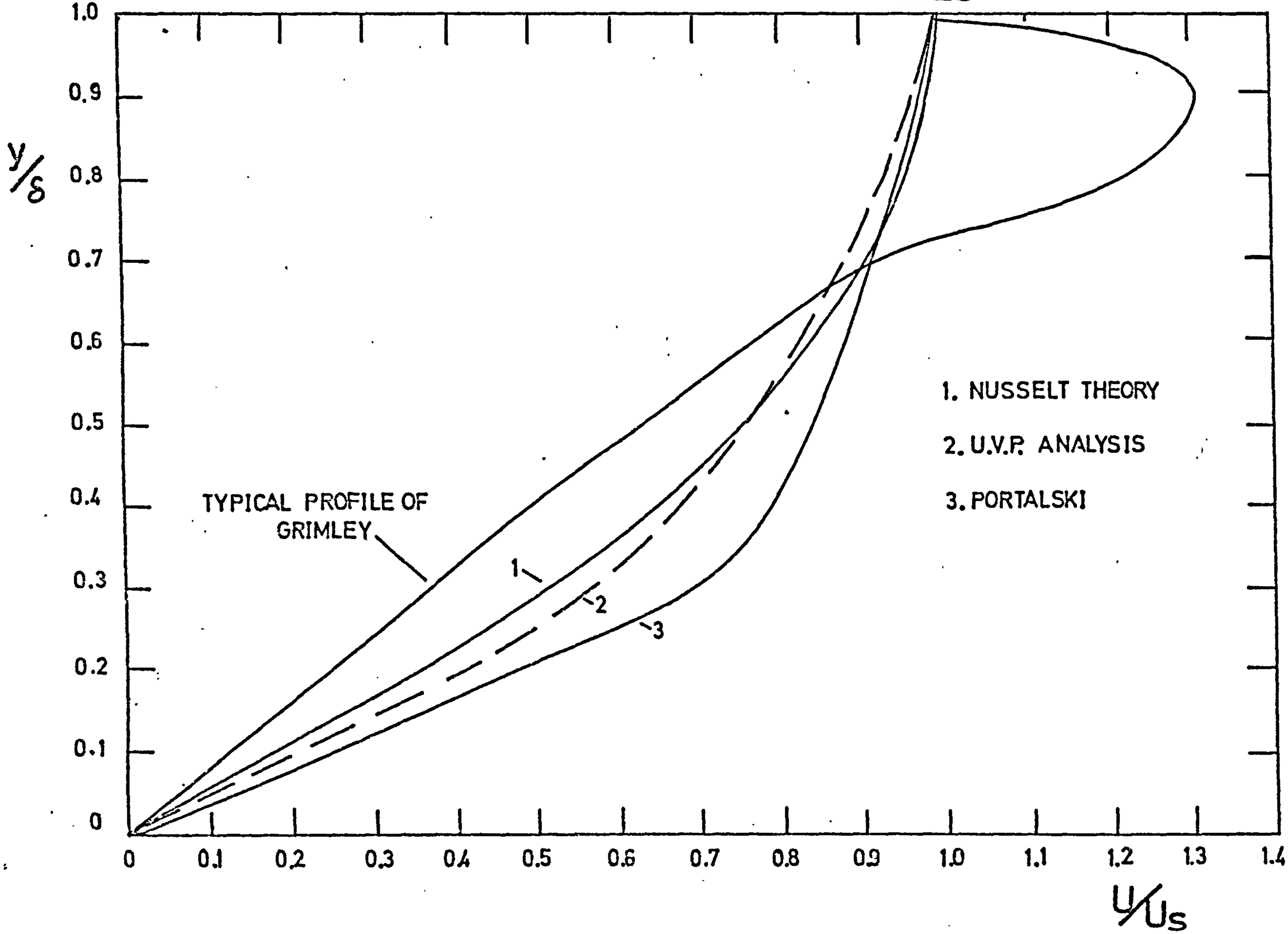

previously indicated, shortly after entry onto the plate the film begins to form ripples and as was seen in section A the mean thickness tends to that predicted by the KAPITSA model. It is possible to identify several regimes of film flow. Thus BRAUER (51) gives several inception flowrate values for water

$Q'/\nu < 4$: strictly laminar and smooth: NUSSELT theory

$4 < Q'/\nu < 10$: undulations across film: KAPITSA theory

$10 \leq Q'/\nu < 20$: sinusoidal waves gradually replaced by regular waves

$Q'/\nu > 20$: random waves

Up to a value of Q'/ν of 400 the fluid remains laminar in the bulk of the fluid. BRAUER states the transition boundaries for fluids other than water as functions of a parameter K, defined as

$$K = \frac{\rho \sigma^3}{g_c \mu^4} \qquad 25$$

and the first transition marking the end of the NUSSELT film flow

is $$Q'/\nu = 0.306\, K^{1/10} \qquad 26$$

The rippling transition is also agreed to by DAVIES (52), WILKES and NEDDERMAN (46) and KIRKBRIDE (53). The turbulence transition is a little less certain as it appears that turbulence is transmitted from the waves to a mainly laminar sub-layer (see for example STAINTHORP and WILD (54)), but depending upon the sensitivity of the detection device employed is visible at Q'/ν of order 250: KOSKY (55), DUCKLER and BERGELIN (25), PORTALSKI (36), WILKES and NEDDERMAN (46) and COOK and CLARK (47).

E: WAVES

When the film is introduced onto an inclined plate and the Q'/ν value is less than about 4 it flows indefinitely without rippling. If the plate is vertical or Q'/ν greater than 4 then at some point downstream from the entrance the smooth film surface begins to ripple. The smooth length increases with increasing flow rate, but not linearly as suggested by JACKSON (40), rather to a lower power (see FULFORD (37)). Work of BAUER (56) suggests that the smooth zone is an acceleration zone and ends

when the boundary layer (either laminar or turbulent) has reached the free surface.

In describing the mechanism of wave formation and effect there exists much theoretical and experimental work, not all complementary. A full review of the various theories is provided by FULFORD (37) and KRANTZ and GOREN (57). One interesting result is due to BENJAMIN (58). BENJAMIN took surface tension into account and was able to show that the results could be expressed in terms of an amplification rate, A , this being the amplification experienced by a wave of maximum instability in travelling 10 cm. The amplification rate is a function of the fluid physical properties and the group Q'/ν . Depending on A being < 1, 1 or > 1, then so the wave is damped, just propagated or amplified. For vertical surfaces, BENJAMIN shows A to be greater than unity for $Q'/\nu > 0$, i.e. all flows will be unstable. BENJAMIN explains the varying experimental critical Q'/ν values for wave onset as due to differences in the sensitivity of the detectors used by investigators. FULFORD suggests that more recent measurements have progressively given lower Q'/ν values for wave onset, due presumably to more sensitive detectors. PORTALSKI and CLEGG (59) noted that the amplification rate of waves on vertically falling glycerine/water films was in approximate agreement to BENJAMIN'S theory.

An indirect verification of BENJAMIN'S theory is reported by FULFORD (37) who states that BENJAMIN has shown analytically that for the onset of waves of a specified amplification rate on a smooth film

$$\frac{Q'}{\nu} \propto \left(\frac{\rho\sigma^3}{g_c\mu^4}\right)^{1/11}$$

The group and power index are in remarkable agreement to the experimental work of BAUER mentioned earlier.

In the study of waves the presence of surfactants has long been known to have a disproportionate effect upon the wave. Thus the Elder Plini (60) reports

"Omne oleo tranquillam ...."

KEULEGAN (61) obtained waves on clean water by a co-current air stream of velocity 3 - 4 m/s over the surface. On adding traces of soap to the water, no waves were formed at an air velocity of 12 m/s.

Surfactants are of basically two types, hydrophilic and hydrophobic (MOORE (62)) but in each case the stabilising power of the surfactant

seems to be in the effects upon surface viscosity and surface elasticity. In the surface viscosity effect the surface layers, in containing a disproportionate amount (compared to the bulk concentration) of the surfactant material, show an anomolous viscosity (usually greater than the bulk) effectively opposing any surface motion. Surface elasticity is a phenomenon exhibited to some extent by all surfactants in that strain is resisted by, effectively, a surface tension which varies with the rate of strain. Surface elasticity is the underlying phenomenon of the MARAGONI effect (see KITCHENER (63)).

Much experimental and theoretical work has been done on surfactants and their effects. One interesting point is noted from the work of LIN (64) where it is shown analytically that hydrophobic surfactants damp waves more effectively than hydrophilic surfactants. This is approximately as found experimentally by SMITH and CRAIK (65).

A difficulty of experimental wave investigations is that the film may be quite easily slightly contaminated. ANSHUS and ACRIVOS (66) explain an apparent 'critical' value of Q'/ν on wave inception as noted by TAILBY and PORTALSKI (67) (in that a flow of 82% glycerol in water on a vertical plate showed no waves for $Q'/\nu = 1.6$, but definite waves for $Q'/\nu = 1.75$) as due to an apparent increase in surface tension of only 9 dyne/cm over that of pure water. ANSHUS and ACRIVOS conclude that the effect of a surfactant will be to decrease the growth rate of the most unstable wave and increase the wavelength of the wave at inception. Both effects make the wave less easily detected.

F: ENTRANCE EFFECTS

In falling film literature experimenters often report great precautions taken to ensure that the film is evenly distributed over the flow surface entrance. The simple models considered so far take no account of the development of the velocity profile with flow distance. WHITAKER and CERRO (68) consider the development of a film in which the inlet velocity profile is taken as of plane Poiseuille type. WHITAKER and CERRO show that the analytic results of an earlier paper (CERRO and WHITAKER (69)) are applicable when the ratio of gravitational force shear to interfacial drag shear is very much less than unity. This ratio is shown to be approximately given by

$$\frac{\text{gravitational shear}}{\text{interfacial shear}} \propto \left(\frac{\rho_2 \mu_2}{\rho_1 \mu_1} \right)^{1/2} \qquad 27$$

when 1 refers to the upper fluid, 2 is the film fluid.
For water films with air as the interfacial fluid, this ratio is negligible. In the earlier paper the authors considered the numerical solution of the two dimensional boundary layer equations:

$$u_x \frac{\partial u_x}{\partial x} + u_y \frac{\partial u_x}{\partial y} = g_c \sin\theta + \nu \frac{\partial^2 u_x}{\partial y^2} \qquad 28.1$$

and

$$\frac{\partial u_x}{\partial x} + \frac{\partial u_y}{\partial y} = 0 \qquad 28.2$$

A further solution of the system equations 28 including fluid inertia showed that the boundary layer equations were applicable when

$$\frac{3}{2} \frac{Q'}{\nu} > 100 \qquad 29$$

The analytic results were shown (68) to be in close agreement to their own experimental results and those of LYNN (70). CERRO and WHITAKER (69) and LYNN (70) show that the velocity profile in developing from plane Poiseuille type to semi-parabolic type passes through a 'S' shaped profile in which the maximum velocity moves from half the film depth to some 75% of the film depth. This could provide an explanation for GRIMLEY'S experimental observations, which were discussed earlier (Section 2.1.1:C). LYNN showed that the development length was dependent upon the inlet conditions of flowrate and distributor gap, and varied from 6 to 13 times the eventual film thickness for Q'/ν values from 100 to 200 and inlet gaps of 50% and 110% of the eventual film thickness. AULT and ORVILLE (71) numerically investigated the effect of surface tension upon the development. They concluded the effect to be small, with typically a length of some 20 film depths required for 95% development of the surface velocity.

G: FILM BREAKDOWN

If the liquid feed rate to a vertically falling film is gradually reduced a repeatable sequence of events occurs. Initially the film is distributed evenly, but eventually begins to show signs of instability such as the formation of dry surface "pin holes" or "roping" of the flow (see NORMAN and McINTYRE (72)). If the film is brushed mechanically at this stage it will normally re-establish itself. If the liquid feed is reduced further, the area of dry patches increases until the liquid finally runs as rivulets. Hysteresis is considerable in that increasing the flowrate again may lead to a rivulet flow regime at a

flow rate that previously supported a film flow.

McPHERSON (73) studied the stability of a dry patch on the wall of an annular two phase flow. It was shown that the evaporation vapour thrust, the liquid film hydrostatic head and the vapour drag at the dry-out step were negligible compared to the surface tension, the liquid thrust at the stagnation point and the vapour/liquid shear force. McPHERSON combines these results into the form

$$F = F_e + F_\tau + F_\sigma \qquad 30$$

where F_e is the kinetic energy force of the decelerating liquid and vapour at the dry patch, F_τ is the shear force on the fluid and F_σ, the surface tension force. F is the total force on the dry patch and for stability F = 0. Should $F < 0$, then the patch advances upstream, $F > 0$ leads to re-wetting. McPHERSON'S paper contains details of expressions to calculate the values of the component forces.

HARTLEY and MURGATROYD (74) have considered two criteria for dry patch stability under both laminar flow and shear induced laminar/turbulent flow. The criteria considered were

1. equivalence of stagnation pressure of the fluid and surface tension at the most upstream point of the dry patch,

and 2. minimum total energy (kinetic and surface tension energy) contained in a flowing rivulet.

The first criteria studies conditions at the most upstream point of the dry patch, the second conditions in the rivulet flowing alongside the patch.

By employing the velocity profiles of the NUSSELT model, and the U.V.P. model, several analytic equations predicting the onset of film breakdown resulted. Only the NUSSELT model results agreed to a practical case, for which the results were

from criteria 1
$$\delta_c = 1{\cdot}72 \left(\frac{\sigma}{\rho}[1-\cos\alpha]\right)^{1/5} \left(\nu/g_c\right)^{2/5} \qquad 31.1$$

and
$$Q'_c = 1{\cdot}69 \left(\frac{\sigma}{\rho}[1-\cos\alpha]\right)^{3/5} \left(\nu/g_c\right)^{1/5} \qquad 31.2$$

from criteria 2
$$\delta_c = 1{\cdot}34 \left(\sigma/\rho\right)^{1/5} \left(\frac{\nu}{g_c}\right)^{2/5} \qquad 31.3$$

and
$$Q'_c = 0{\cdot}803 \left(\frac{\sigma}{\rho}\right)^{3/5} \left(\nu/g_c\right)^{1/5} \qquad 31.4$$

when δ_c is the film thickness at breakdown and Q'_c the minimum wetting rate.

PONTER et al (75) and RUCKENSTEIN (76) obtained results similar to equation 31.2. WILSON (77) has recently considered the modifications required to account for flow in the "collar" upstream of the dry patch.

The above analyses are performed for isothermal film breakdown. NORMAN (78) proposed that when the film was heated greater instability would exist in that the warmer troughs (which would generally have a lower surface tension σ) would thin as fluid was attracted to the cooler (and hence greater σ) crests of any waves present. PONTER and BOYES (79) observe that the analyses considered give repeatable results when heat transfer is occurring butmay be up to 1000% in error for isothermal flow. In view of NORMAN'S suggestion a possible explanation for the isothermal discrepancy could be as follows. In steady isothermal flow considerable hysteresis is noted in the film/rivulet transition, presumably due to low order "triggering" forces. When heat transfer is taking place, the additional instability due to the heated waves is sufficient to reduce the hysteresis and thus cause a more pronounced and repeatable transition to occur.

Although these analyses give the criteria for the existence of stability or otherwise of a film, they do not supply a mechanism of film breakdown. ROBERTS and TABOR (80) suggest that surface projections of the wall surface will be large in relation to the film dimensions. However, thicker films on smooth surfaces may rupture, apparently spontaneously. PADDY (81) shows that the nature of the solid surface, both chemical and topological, is important. PADDY showed by high speed photography of a thinning layer covering an upwards facing convex surface, that a dimple forms at the thinnest point of the film prior to rupture. FRENS (see 81) suggested that the dimple was caused by the presence of hydrophobic sols rising to the surface and causing the depression by virtue of their weight. DORMANT (see 81) suggested that free surface irregularities, such as capillary waves, might bring the liquid/air interface momentarily close to the solid/liquid interface when long range interaction continued to hold the liquid surface in the dimple shape. This interaction seems to be electrical in origin since experiments showed that rupture occurred more easily as the ionic concentration of ionic salt solutions was increased (see 82).

Whatever the main mechanism involved in the breakdown process

it seems certain that the physico-chemico properties of the thin fluid film must enter into any description of the actual rupture and reformation. In this respect, and with particular reference to system cleanliness, LUDVIKSSON and LIGHTFOOT (83) studied the climbing of squalene (a symmetrical triterpene) films on heated vertical metal plates. The authors noted that placing a non-spreading barrier (perfluoro-octylpoly methacrylate) in advance of the film caused an apparent slow down in film advance before reaching the barrier. This would imply the spread in front of the main film of a very thin film (possibly only adsorption layers), too thin to observe but with a disproportionate influence upon the main film advance.

H: NON-NEWTONIAN FLUIDS

The NUSSELT model derived earlier may be rederived for a non-Newtonian fluid described by a power law equation of the type

$$\tau = K\left(\frac{du_x}{dy}\right)^n \qquad 32$$

This results in an initial model of the form

$$\frac{d}{dy}\left(\frac{dv_x}{dy}\right)^n = -\left(\frac{\rho g \sin\Theta}{K}\right) \qquad 33$$

(cf. equation 1)

resulting in a velocity distribution of

$$v_x = \left(\frac{\rho g_c \sin\Theta}{K}\right)^{1/n}\left(\frac{n}{n+1}\right)\left(\delta^{\frac{n+1}{n}} - (\delta - y)^{\frac{n+1}{n}}\right) \qquad 34$$

(cf. equation 2)

Integrating for the flowrate

$$Q' = \int_0^{\delta} v_x dy = \left(\frac{\rho g_c \sin\Theta}{K}\right)^{1/n}\left(\frac{n}{2n+1}\right)\delta^{\frac{2n+1}{n}} \qquad 35$$

thus forming the ratio $v_{sx}/\bar{v}_x$ from equations 34 and 35

$$\frac{v_{sx}}{\bar{v}_x} = \frac{2n+1}{n+1} \qquad 36$$

(cf. equation 7)

ASTARITA et al (84) and CHENG (85) show how equations 34 to 36 may be used experimentally to obtain the consistency and power index for a non-Newtonian fluid under investigation. SYLVESTER et al (86 and 87) report investigation of the flow of glycerol/water mixtures and aqueous

carbopol solutions ($0.4 < n < 1$) and report good agreement for equation 36 using PORTALSKI'S technique for measuring U_{sx}. SYLVESTER et al repeat KAPITSA'S analysis for wavy flow for a power law fluid but obtained only approximate agreement between experimental wavelength for non-Newtonian fluids and the theoretical values. SYLVESTER et al noted that the non-Newtonian fluid showed significantly more stability to wave instabilities than did the Newtonian fluids. The authors advanced an explanation of this phenomenon based upon the surfactant effects of the large non-Newtonian polymer molecules.

2.1.2. RADIAL FLOW ON A STATIONARY DISC

WATSON (88) has studied the hydrodynamics of a radial outflow whose source is the centre of a stationary disc. FIGURE 8 shows the nomenclature used. WATSON studied the boundary layer equation

$$U_r \frac{\partial U_r}{\partial r} + U_y \frac{\partial U_r}{\partial y} = \nu \frac{\partial^2 U_r}{\partial y^2} \qquad 37.1$$

and

$$\frac{\partial}{\partial r}(rU_r) + \frac{\partial}{\partial y}(rU_y) = 0 \qquad 37.2$$

with the boundary conditions

at the wall $y = 0$ $U_r = 0$ 38.1

at the free surface $y = \delta$ $\frac{dU_r}{dy} = 0$ 38.2

WATSON was able to show that in that portion of the flow between the radius where the boundary layer has developed to include the free surface, and the radius where the hydrodynamic jump occurs, a similarity analysis is valid. The results of this analysis are

$$U_r = 0.0681 \left(Q^2 / \nu (r^3 + \ell^3) \right) z \qquad 39$$

$$\delta = 3.7988 \ \nu (r^3 + \ell^3)/Qr \qquad 40$$

when

$$\ell = 0.567 \ r_i \left(\frac{Q}{r_i \nu} \right)^{1/3} \qquad 41$$

z is a numerical value dependent upon η only ($\eta \equiv y/\delta$) and r_i is the radius of the inlet jet. The bounds for this solution are

1) the development of the boundary layer to the free surface depth

$$r_1 = 0.3155 \ r_i \left(\frac{Q}{r_i \nu} \right)^{1/3} \qquad 42.1$$

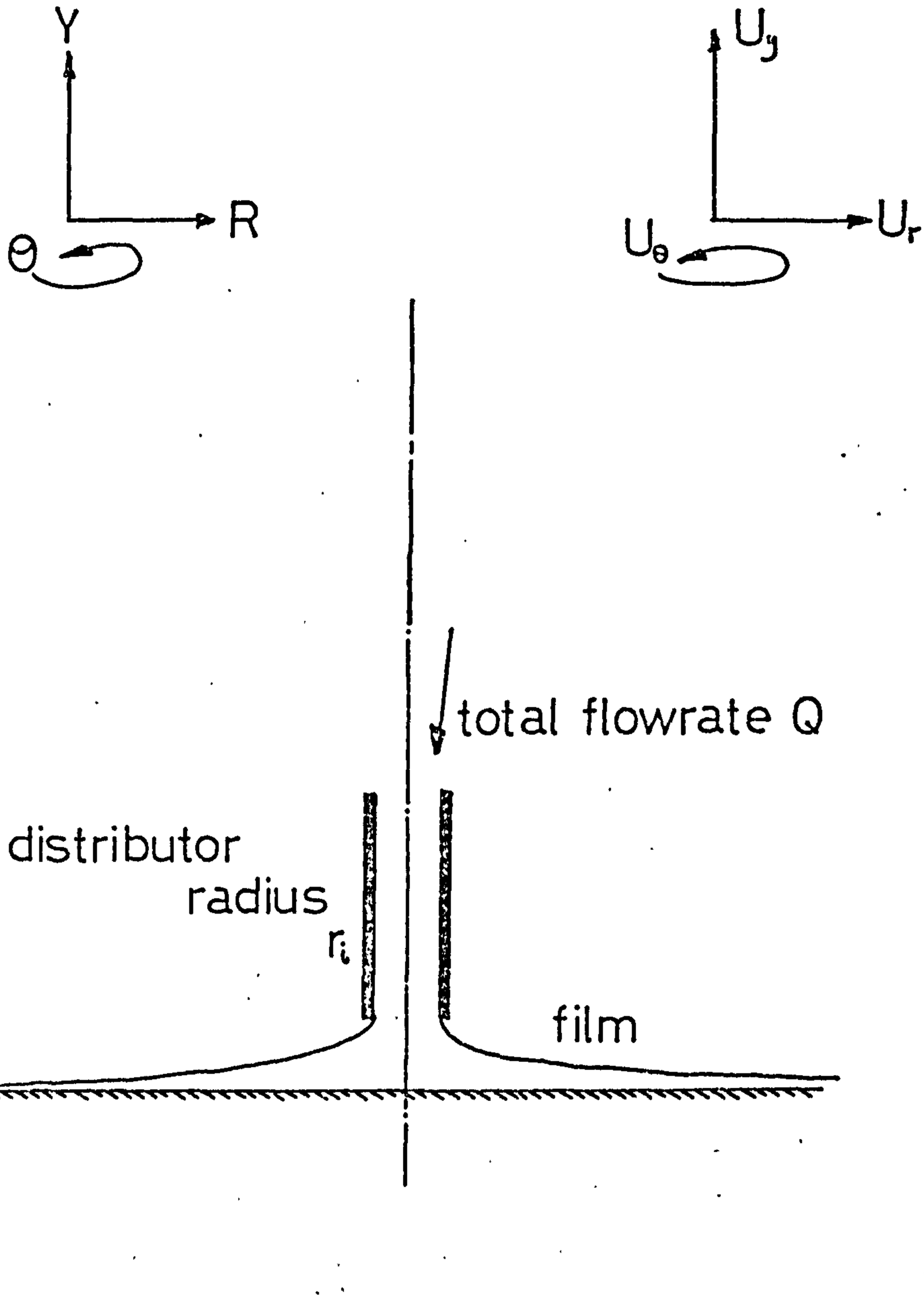

FIG 8 NOMENCLATURE FOR RADIAL FILMS

and 2) the jump radius r_2 given by

$$\frac{q_c d^2 r_i^2 r_2}{Q^2} + \frac{r_i^2}{2\pi r_2 d} = 0.10132 - 0.1297\left(\frac{r_2}{r_i}\right)^{3/2}\left(\frac{r_i \nu}{Q}\right)^{1/2} \qquad 42.2$$

when d is the film thickness subsequent to the jump.

WATSON reports experimental confirmation of equation 42.2 in that measured values of the jump radius and subsequent film depth are as predicted by equation 42.2.

GLINKIN and TYABIN (89) also considered the boundary layer equations 37.1 and 37.2. By assuming that the surface radial velocity was a function of r only, GLINKIN and TYABIN were able to show that the thickness at any radius was given by

$$\delta = \frac{\delta_i r_i}{r} + \frac{5\pi\nu}{3Q}\left(r^2 - \frac{r_i^3}{r}\right) \qquad 43$$

In equation 43, δ_i is the film thickness at the entry to the disc, r_i (the film is assumed to enter by means of a central vertical jet turning smoothly onto the disc). Examination of equation 43 shows that the film thickness initially falls with increasing radius until a certain critical radius is reached, after which the thickness increases with radius.

The radius at which the critical minimum thickness occurs is given as

$$r_c = \left(3Q\delta_i r_i / 10\pi\nu - r_i^3/2\right)^{1/3} \qquad 44.1$$

If r_i is small then equation 44.1 may be simplified to

$$r_c = 0.46\left(Q r_i \delta_i / \nu\right)^{1/3} \qquad 44.2$$

GLINKIN and TYABIN report experiments which confirm equations 43 and 44.2 for values of Q of 1590 and 70 cm^3/s, $r_i = 1.5$ cm and 0.5 cm. The liquid investigated was water. The experiments are reported to validate equations 43 and 44.2 when $r < r_c$, that is up to the minimum film thickness. After the minimum thickness, which must precede the hydraulic jump, the experimental/theoretical deviation was reported to increase considerably. Substituting for r_c from 44.2 into 43 gives the minimum thickness as

$$\delta_c = 3.28\left(\frac{\delta_i^2 r_i^2 \nu}{Q}\right)^{1/3} - 11.38\left(\frac{r_i^8 \nu^4}{Q^4 \delta_i}\right)^{1/3} \qquad 45$$

Locating the minimum thickness radius predicted from equation 40 (WATSON'S analysis) gives

$$r_c = 0.45 \left(Q r_i^2 / \nu \right)^{1/3} \qquad 46.1$$

(cf. equation 44.2)

with a minimum thickness of

$$\delta_c = 2.31 \left(r_i^4 \nu / Q \right)^{1/3} \qquad 46.2$$

(cf. equation 45)

Thus WATSON'S and GLINKIN and TYABIN'S analyses result in similar expressions (certainly on the controlling parameters) if

$$r_i = \delta_i \qquad 47$$

2.1.3. ROTATING DISC IN AN INFINITE MEDIA

The earliest study of the hydrodynamics of a disc rotating in a fluid of infinite extent was performed by von KARMAN (90). Von KARMAN considered the boundary layer equations (see Appendix F):

$$v_r \frac{\partial v_r}{\partial r} + v_y \frac{\partial v_r}{\partial y} - \frac{v_\theta^2}{r} = \nu \frac{\partial^2 v_r}{\partial y^2} \qquad 48.1$$

$$v_r \frac{\partial v_\theta}{\partial r} + \frac{v_\theta v_r}{r} + v_y \frac{\partial v_\theta}{\partial y} = \nu \frac{\partial^2 v_\theta}{\partial y^2} \qquad 48.2$$

$$v_r \frac{\partial v_y}{\partial r} = -\frac{1}{\rho} \frac{\partial p}{\partial y} + \nu \frac{\partial^2 v_y}{\partial y^2} \qquad 48.3$$

and the continuity equation

$$\frac{\partial v_r}{\partial r} + \frac{v_r}{r} + \frac{\partial v_y}{\partial y} = 0 \qquad 48.4$$

Von KARMAN assumed that a similarity solution existed (that is, the velocity profile magnitude depends linearly upon the radius and the shape of the profile is essentially constant at all radii).

Thus it was proposed

$$v_r = r f(y) \qquad 49.1$$

$$v_\theta = r \cdot g(y) \qquad 49.2$$

$$v_y = h(y) \qquad 49.3$$

$$\rho = \rho(y) \qquad 49.4$$

then equation set 48 reduces to

$$f^2 - g^2 + h\frac{df}{dy} = \nu\frac{d^2f}{dy^2} \qquad 50.1$$

$$2fg + h\frac{dg}{dy} = \nu\frac{d^2g}{dy^2} \qquad 50.2$$

$$h\frac{dh}{dy} = -\frac{1}{\rho}\frac{dp}{dy} + \nu\frac{d^2h}{dy^2} \qquad 50.3$$

and $$2f + \frac{dh}{dy} = 0 \qquad 50.4$$

Notice that the original partial differential equations have been reduced to an ordinary differential equation set.

Equation set 50 may be reduced to non-dimensional form using

$$F = f/\omega \qquad 51.1 \qquad\qquad P = p/\rho\nu\omega \qquad 51.4$$

$$G = g/\omega \qquad 51.2 \qquad\qquad \zeta = \left(\frac{\omega}{\nu}\right)^{1/2} y \qquad 51.5$$

$$H = (\omega\nu)^{-1/2} h \qquad 51.3$$

which after substitution gives the equation set

$$F^2 - G^2 + HF' = F'' \qquad 52.1$$

$$2FG + HG' = G'' \qquad 52.2$$

$$HH' = -P' + H'' \qquad 52.3$$

$$2F + H' = 0 \qquad 52.4$$

(' indicates differentiation with respect to ζ)

The appropriate boundary conditions for a disc in an infinite media are

$$y=0 \qquad v_r = v_y = 0 \qquad v_\theta = \omega r$$

or $\zeta = 0 \qquad F = H = 0 \qquad G = 1$ 53.1

$y = \infty \qquad U_r = U_\theta = 0 \qquad U_y = -C$

or $\zeta = \infty \qquad F = G = 0 \qquad H = -C$ 53.2

where C is a constant describing the far field approach to the disc.

An asymptotic solution for large ζ may be obtained using the boundary condition for $\zeta = \infty$ to reduce these equations to give

$$-CF' = F'' \qquad 54.1$$

$$-CG' = G'' \qquad 54.2$$

for which the solution is

$$F = A \exp(-C\zeta) \qquad 54.3$$

$$G = B \exp(-C\zeta) \qquad 54.4$$

leading to $$H = -C + \frac{2A}{C} \exp(-C\zeta) \qquad 54.5$$

Thus F and G tend to zero as ζ tends to infinity. In fact due to the exponential dependency of F and G on ζ, F and G are practically zero for some finite ζ. This provides the key to von KARMAN'S solution in that the upper boundary conditions are applied, not at infinity, but at some finite ζ.

However, COCHRAN (91) points out two errors in von KARMAN'S original paper, one in the algebraic expansion for G between 0 and ζ, and the second in the numerical evaluation of the boundary conditions of system 52. COCHRAN also notes that using other available boundary conditions with von KARMAN'S approximate method of solution, gives physically unreasonable results. COCHRAN obtained a numerical integration of equation set 52 using a matched expansion technique. By expanding according to a Taylor series about $\zeta = 0$ for F, G, H and P and using the basic equation set to provide equivalents, formal expansions are obtained in terms of $\exp(-C\zeta)$ involving two unknowns only, $A(\equiv F'(0))$ and $B(\equiv G'(0))$. As stated earlier, asymptotic values of F, G and H are known as ζ tends to infinity. COCHRAN'S technique was to search for values of A and B which would integrate up from $\zeta = 0$, satisfying the

lower boundary conditions ($\zeta = 0$) until at $\zeta = \zeta_o$ (ζ_o finite) a sufficiently close match appeared to the asymptotic expansions. Values of A = 0.51 and B = -0.616 give agreement between the two expansions to the third decimal place. The original paper by COCHRAN contains an error in the initial expansion for both F and H in the coefficient of ζ^6. Thus for F, COCHRAN'S value of $(\frac{1}{360} - \frac{AB}{90})$ should be $(\frac{1}{40} - \frac{AB}{90})$ and for H, COCHRAN'S value of $(-(1/80)A)$ should be $(-(1/180)A)$. These errors obviously lead to a discrepancy in the starting values of F and H, but to the fourth decimal place (the author's level of accuracy) there is no noticeable difference. However, since the solution is dependent upon the previous values obtained it may be that the error accumulates as the solution proceeds. Certainly OSTRACH and THORNTON (92) and SPARROW and GREGG (93) have noted differences from COCHRAN for $H(\infty)$. [(92) -0.8845; (93) - 0.88447; COCHRAN -0.8860].

Provided that the small influence of flow towards the plate can be ignored, the rotating disc in an infinite media exhibits an approximately constant thickness boundary layer, as shown by von KARMAN. In accounting for the small net inflow to the disc, MILLSAPS and POHLHAUSEN (94) showed that the boundary layer is a function of the radial distance along the plate, but for values of the parameter, R, where

$$R = \left(\omega/\nu\right)^{1/2} r \qquad 55$$

greater than about 15 the thickness increases only slowly with radius. For a disc in air at 100 r.p.m, $r > 2$ cm for a constant boundary layer. For water, the equivalent value is $r > 0.47$ cm. These figures show that for relatively small discs, say $r \approx 10$ cm, some 99% of the disc area has a constant boundary layer thickness in water. This has given rise to the term "uniformly accessible surface" (see LEVICH (95)) and the use of rotating discs as a reaction study tool for liquid phase reactions.

The physical interpretation of flow over a rotating disc in an infinite medium is that the disc entrains a layer of fluid on its surface which passes angular momentum to adjacent layers. Due to centrifugal action the rotating medium moves out along the disc and is twisted away from the direction of rotation due to the action of the Coriolis acceleration. New fluid is brought down onto the disc from all over the disc surface, the inflow being stronger at the centre line of the disc, but still present far above the disc at appreciable radii. The situation far from the disc centre line is shown diagramatically in FIGURE 9.

It will have been noted that in equation set 48 the pressure term was only included as a vertical distribution. The circumferential distribution of pressure is exactly zero due to the symmetrical nature of the system. The rejection of the radial distribution, $\partial p/\partial r$, is more suspect, and strictly speaking has been ignored only in comparison to the value of $\partial p/\partial y$. Since the fluid above the disc is stationary the primary pressure distribution far from the disc is a vertical one. The reverse situation of a rotating fluid over a stationary plate as studied by BODEWADT (96), includes the pressure distribution as a radial distribution. A solution involving pressure as both radial and circumferential distributions does not seem to have been obtained, although there will be regions where the two terms will be of comparable magnitude.

All the analytical work discussed in this section applies strictly to discs of infinite diameter. Since most of the fluid flow occurs as approximately boundary layer flow, the disc may be taken as being of infinite extent when the outer radius is much greater than the boundary layer thickness. POSTLETHWAITE et al (97) give the boundary layer thickness as

$$\delta_B = 2{\cdot}8 \left(\nu / 2\pi N \right)^{1/2} \qquad 56$$

when N is in (revolutions/sec)

For water at only 60 r.p.m. this implies a disc of diameter much greater that 0.2 cm may be regarded as infinite in extent. (Note however that equation 56 applies to a developed boundary layer).

GREGORY et al (98) investigated experimentally the velocity profiles existing over a disc rotating in air and found reasonable agreement under laminar flow conditions to the analysis of von KARMAN, thus validating the assumption of similar profiles over the range studied.

GREGORY et al also noted experimentally that toward the edge of the disc turbulence of the air flow was found. The onset of turbulence was correlated by the variable $\left[(\omega/\nu)^{1/2} r\right]^2$ and the upper limit of this value was found to be some 2×10^5. This observation has also been made by several investigators working on heat transfer from rotating discs (see Section 3.1.3:A later).

HANNAH (99) showed that von KARMAN'S and BODEWADT'S models are limiting situations of a more general situation in which suction or blowing from the disc surface is allowed. GREGORY and WALKER (100) were able to

FIG 9 VELOCITY PROFILE IN AN INFINITE MEDIUM

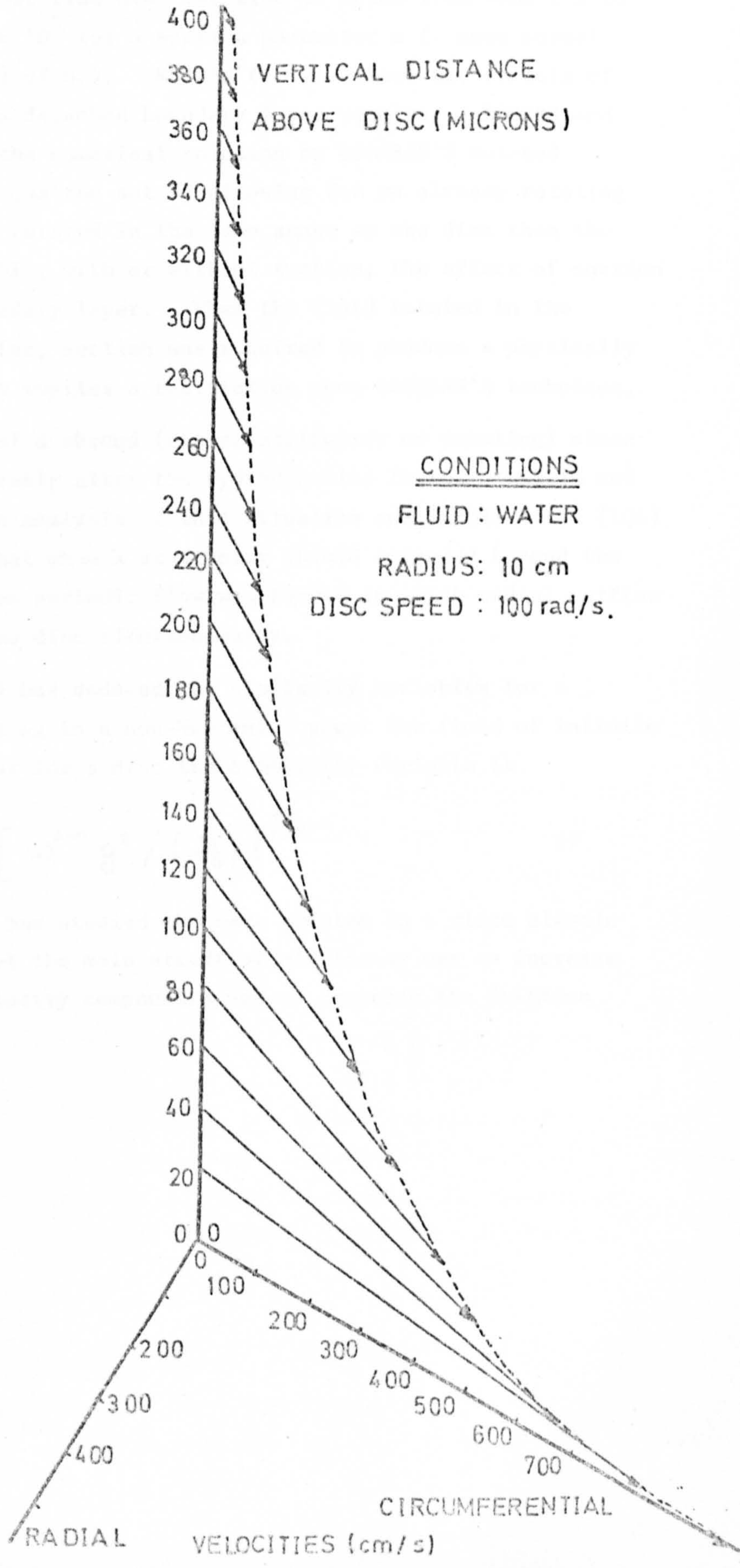

show experimentally that the effect of suction is to extend the value of $[(\omega/\nu)^{1/2} r]^2$ for which laminar flow over the disc is noted from some 2×10^5 (no suction) to some 4×10^5 for a suction parameter a (mean normal suction velocity/$\sqrt{\nu\omega}$) of 0.4. KUIKEN (101) reviews the effects of blowing and shows that a detached boundary layer results. ROGERS and LANCE (102) considered the numerical solution by COCHRAN'S matched expansion technique of equation set 52 allowing for an already rotating fluid. When the fluid rotated in the same sense as the disc then the solution method was stable, with or without suction, the effect of suction being to reduce the boundary layer. When the fluid rotated in the opposite sense to the disc, suction was required to produce a physically reasonable result, which implies a restriction upon COCHRAN'S technique.

The presence of a shroud (either stationary or rotating) close to the disc may considerably alter the hydrodynamics found. KREITH and VIVIAND (103) present an analysis of this situation and MAROTI et al (104) showed experimentally that when a stationary shroud extended beyond the edge of the rotating disc periodic flow was formed in which radial outflow and inflow existed on the disc simultaneously.

MITSCHKA (105) has deduced the similarity variables for a general body shape rotating in a non-Newtonian power law fluid of infinite extent and has shown that for a disc the similarity variable is

$$\zeta = \left[\omega^{2-n} y^2 / \left(\frac{k}{\rho}\right) \right]^{\frac{1}{n+1}} \qquad 57$$

ELLIOTT (106) has studied the same problem in a visco elastic medium and concluded that the main effect of elasticity was to increase the magnitude of the velocity components and to decrease the friction experienced by the disc.

2.2. EXPERIMENTAL TECHNIQUES

In validating any hydrodynamic model, measurements must be made upon the gross results of these phenomena, that is film thickness, surface velocity and velocity profile. In the following review of previously employed techniques one reference will be given for each technique. The reference will either be of important historical interest or a detailed explanation of the technique.

A: FILM THICKNESS MEASUREMENT

1. Micrometer Probe HOPF (107)

A needle is fixed to a micrometer held vertically over the flow surface. A zero reading of the flow surface is taken, the micrometer wound back and flow established. The micrometer is wound down to touch the film surface and the difference in the two readings gives the film thickness. A major advantage is simplicity and ease of operation, but with the disadvantages of limited accuracy and applicability to a rotating buckled surface.

2. Micrometer Probe with contact sensing HOYLE and ESPIG (108)

As for (1) above, but the visual observation of the needle touching the surface (both flow surface and film) is augmented by electrical contact. Disadvantages as for (1) and in addition, presence of spray or high voltages can give erroneous conduction whilst needle is still above film surface.

3. Shadowgraph of profile KAPITSA (109, 35)

A flow surface is placed sideways in between a light source, magnification lenses and a screen. The surface datum is noted on the screen. The flow is established and the new surface position noted. Calibration of the magnification system and measurement of the spacial difference between the two surfaces gives the film thickness. If the screen is replaced by a photographic plate, instantaneous profiles of the film surface may be obtained.

4. Weighing of Flow surface and film KAMEI and OISHI (110)

The flow surface forms one part of a balance and the weight of the flow surface with and without a fluid film is noted. By dividing the

difference by the flow area and the fluid density the film thickness is found. Cumbersome and only moderately accurate.

5. Drainage Techniques FULFORD (33)

A fluid film is established on a flow surface. The supply is diverted and simultaneously the surface is drained into a collector. The volume collected divided by the flow area gives the film thickness. Undrained droplets on the surface must be wiped off and weighed and, unless special precautions are taken over the distributor design, weir effects can give an erroneously high drainage quantity.

6. Electrical resistance HEWITT et al (111)

Electrodes are built in flush to the flow surface and the electrical conductivity of the flowing film once established noted. By calibrating with known depths of fluid and sizes and separations of electrodes, the flowing film thickness may be inferred. The fluid must be conductive and the flow surface of similar surface finish to the electrodes.

7. Capacitive methods BLACK (112)

A capacitive circuit is created between a small probe and a much larger parallel metal plate. A capitance reading is taken, film flow established and a second measurement made. Calibration of the probe and knowledge of the permittivity characteristics of the fluid material enable the film thickness to be inferred. Unless the probe has very small face dimensions, the film thickness sensed is the average over a considerable area. If the probe is of small area, then the separation between it and the metal plate must also be small for measurable capacitances to exist.

8. Light extinction of a dyed film CLEGG (113)

A light source is situated normal to a transparent flow surface and a light sensor placed in line on the far side of the surface. Flow of the film is established and the degree of extinction of the light caused by the film noted. Calibration of the source/sensor with known depths of fluid enables the film thickness to be inferred from the degree of extinction. Suitable absorbent dyes may have to be added to the film (possibly causing surfactant effects).

The sensor may be replaced by a standard photographic plate and photodensimetric measurements made subsequently.

9. Emission from a radioactive tracer JACKSON (40)

A radioactive emitter is added to the flowing film and a reading of the degree of emission taken. By calibrating the sensor against known quantitites of radioactivity, the amount of emitter in the film is found. If the inlet concentration of emitter is known, then the film depth is found by proportion.

10. Emission from an excited flourescer HEWITT (114)

A known quantity of light emitting material is added to the film and a small area subjected to excitation. The emission of the excited flourescer is noted. Calibration of the sensor against excited films of known depth enables the flowing film thickness to be found.

In addition to the above 10 methods should be added the method whereby an average velocity is obtained and δ then calculated from continuity considerations (see WATTS (115)).

The various merits and demerits of the 10 techniques have been collected in TABLE 1. Those techniques that have previously been used for films on rotating discs are listed in TABLE 1.

B: VELOCITY MEASUREMENT

1. Area method

Divide the flow rate supplied by the wetted perimeter and the film depth. Gives the mean velocity.

2. Progression of a marker FRIEDMAN and MILLER (41)

If a marker (dye drop or solid particle) is introduced into or onto the film it will tend to move with the film. Timing the time taken for the marker to cover a known distance gives the marker speed. It is assumed that the position (i.e. average depth or surface) of the marker is known and that the marker travels at the same speed as the film at that location.

3. Photographic Streak method GARTSIDE (116)

As for (2) above but the known distance per measured time concept is replaced by that of known time per measured distance. The marker is either illuminated continuously for a known period or else illuminated twice

TECHNIQUE	1	2	3	4	5	6	7	8	9	10
DESCRIPTION	POINTER	POINTER + ELEC.	SHADOW -GRAPH	WEIGHING	DRAINAGE	ELEC. RESIS.	CAPAC- ITANCE	LIGHT ABSORB.	RADIOACT. EMISSION	LIGHT EMISSION
COMPLEXITY 1 SIMPLE 2 AVERAGE 3 VERY COM	1	1	3	3	2	2	2	2	2	2
MOVABLE	Y	Y	Y	N	N	N	Y	Y	Y	Y
DIRECT	Y	Y	N	Y	Y	N	N	N	N	N
NO CALIBRATION	Y	Y	N	Y	Y	N	N	N	N	N
MAX. THICKNESS	Y	Y	Y	N	N	N	Y	Y	Y	Y
MEAN THICKNESS	N	N	Y	Y	Y	Y	Y	Y	Y	Y
INST. THICKNESS	N	N	Y	N	N	Y	Y	Y	Y	Y
ANY FLOW SURF.	Y	Y	Y	Y	Y	N	N	N	N	Y
ANY FLUID	Y	Y	Y	Y	Y	N	Y	N	Y	N
USED ON ROT. DISC	Y	Y	N	N	N	Y	Y	Y	N	N

Y=YES N=NO

TABLE 1 FILM THICKNESS MEASUREMENT COMPARISON

for very short periods with a known separation to the pulses. A photograph is taken (usually by the open shutter technique) and the subsequent photograph is analysed to give the distance covered by the particle (which appears as either a streak or a double dot depending on the technique) with respect to a known distance marked in the image field. Division of the distance by the known time of illumination/ pulse spacing gives the velocity. As for (2) above, assumptions about the depth location and particle slip are required.

4. Pressure drop of an adjacent gas stream JACKSON et al (39)

The pressure drop of an adjacent gas stream is measured with and without a film flow present. By calibration the difference in pressure drop over the length can be used to infer the surface velocity of the film flow.

5. Standing Wave Technique FULFORD (33)

If a pointer is touched to a moving film a set of stationary waves are set up upstream of the pointer. The existence of the waves has been examined by RAYLEIGH (see LAMB (117)) and if assumptions are made over the solution of the governing equations, the wave length can be related to the surface velocity of the film.

6. Ultramicroscope with Rotating Objective GRIMLEY (49)

An ultramicroscope is focussed to a pre-calibrated position and a liquid film carrying markers (in GRIMLEY'S work small lead iodide crystals) is established. The objective of the microscope is rotated at varying, but known, speeds until these markers in focus appear stationary. The tangential speed of the objective then equals the film speed of the marker.

7. Stereoscopic chronophotography WILKES and NEDDERMAN (46)

Stereoscopic photography is used to focus upon one pre-calibrated position in the film depth. Markers within the film are illuminated as under (3) above and velocities inferred as for method (3).

The relative advantages of these techniques are listed in TABLE 2, with those techniques previously employed for films on rotating discs noted.

TECHNIQUE	1	2	3	4	5	6	7
DESCRIPTION	FLOW AREA	DIST/TIME	TIME/DIST	PRESSURE DROP	STANDING WAVE	ULTRA MICROSCOPE	STEREO PHOTOGRAPHY
COMPLEXITY 1 SIMPLE 2 AVERAGE 3 VERY COM	1	2	2	2	1	3	3
SURFACE VEL	N	Y	Y	Y	Y	Y	Y
MEAN VELOCITY	Y	Y	Y	N	N	Y	Y
SLIP ASSUMPTION	N	Y	Y	N	N	Y	Y
NO CALIBRATION	Y	N	N	N	Y	Y	N
DIRECT	Y	N	N	N	Y	Y	N
MOVABLE	Y	Y	Y	N	Y	Y	Y
USED ON ROT DISC	Y	Y	N	N	N	N	N

Y=YES N=NO

TABLE 2 VELOCITY MEASUREMENT COMPARISON

2.3. LITERATURE SURVEY

2.3.1. THEORETICAL DEVELOPMENTS

A: CENTRIFUGAL MODEL

Taking equation F7.1 and simplifying the equation further by assuming

1) $R_o << \omega^2 r$ (viz. gravity forces are negligible compared to centrifugal forces)

2) $U_\theta = \omega r$

and 3) ignoring all other terms but the centrifugal force and viscous drag then

$$\nu \frac{d^2 U_r}{dy^2} = -\omega^2 r \qquad 58$$

when ω is the rotational speed of the disc. The physical interpretation of the model is that of the fluid rotating everywhere at the same rate as the disc, moving out over the disc purely radially with the driving centrifugal force balanced by the fluid's viscous drag.

Equation 58 may be integrated subject to the boundary conditions

at the disc surface $y = 0$ $U_r = 0$ 59.1

at the free surface $y = \delta$ $\frac{du_r}{dy} = 0$ 59.2

Condition 59.1 and 59.2 may be compared to conditions 1.1 and 1.2 used earlier. The solution to 58 is

$$U_r = \frac{\omega^2 r}{\nu}\left(\delta y - \frac{y^2}{2}\right) \qquad 60.1$$

The average velocity, $\overline{U}_r$, is given by

$$\overline{U}_r = \frac{1}{\delta}\int_0^\delta U_r dy = \frac{\omega^2 r \delta^2}{3\nu} \qquad 60.2$$

after substituting for U_r from equation 60.1

Equating $\overline{U}_r$ to the flow rate per unit area available for flow gives the film thickness in terms of the system parameters:

$$\overline{U}_r = \frac{Q}{2\pi r \delta} = \frac{\omega^2 r \delta^2}{3\nu} \qquad \text{(from equation 60.2)} \qquad 60.3$$

or $$\delta = \left(\frac{3}{2\pi}\ \frac{Q\nu}{\omega^2 r^2}\right)^{1/3} \qquad 61$$

Evaluating U_{rs}, the surface radial velocity from equation 60.1 at $y = \delta$ and comparing to equation 60.2 gives

$$\frac{U_{rs}}{\overline{U}_r} = 1.5 \qquad 62$$

This model is ascribed by ADLER and MARSHALL (118) to BAR (119) as its first proposer. The similarity to NUSSELT'S model for falling planar films (Equations 1.1 to 7) will be apparent.

The mean residence time of the film on the disc may be obtained as follows. Combining equations 60.2 and 61 to eliminate δ gives

$$\overline{U}_r = \left(\frac{\omega^2 Q^2}{12\pi^2\nu}\right)^{1/3} r^{-1/3} \qquad 63.1$$

noting that $\overline{U}_r = dr/dt$ over the depth at that radius

then integrating $$\frac{dr}{dt} = \left(\frac{Q^2\omega^2}{12\pi^2\nu}\right)^{1/3} r^{-1/3} \qquad 63.2$$

subject to $$t = 0 \quad r = r_i \qquad 63.3$$

$$t = t_R \quad r = r_e \qquad 63.4$$

gives $$t_R = \frac{3}{4}(12\pi^2)^{1/3}\left[\frac{\nu(r_e^4 - r_i^4)}{\omega^2 Q^2}\right]^{1/3} \qquad 65$$

when t_R is the residence time of the entire film in travelling between radii r_i to r_e.

Equation 61 may be written in non-dimensional form as

$$\frac{\delta}{r} = \left(\frac{3}{2\pi}\right)^{1/3}\left(\frac{Q\nu}{\omega^2 r^5}\right)^{1/3} \qquad 66$$

VENKATARAMAN (120) noticed that the group $\left(\frac{Q\nu}{\omega^2 r^6}\right)$ could be rewritten as Re/Ta^2 if the definitions

$$Re = \frac{Q}{r\nu} \qquad \text{and} \qquad Ta = \frac{\omega r^2}{\nu} \qquad 67$$

were employed.

The group Re, containing the flow rate, is a form of Reynolds number for the flow and the group Ta, containing the rotational speed, is the

Taylor number applicable to the flow. Notice that for a given flowrate and rotational speed, Re decreases and Ta increases with increasing radius. Thus equation 66 may be rewritten as

$$\frac{\delta}{r} = \left(\frac{3}{2\pi}\right)^{1/3} \left(\frac{Re}{Ta^2}\right)^{1/3} \qquad 68.1$$

or
$$\frac{\delta}{r}.Re = \left(\frac{3}{2\pi}\right)^{1/3} \left(Re^2/Ta\right)^{2/3} \qquad 68.2$$

or
$$\frac{\delta}{r}.Ta^{1/2} = \left(\frac{3}{2\pi}\right)^{1/3} \left(Re^2/Ta\right)^{1/6} \qquad 68.3$$

and equation 65 may be written as

$$\omega t_R = \frac{3}{4}(12\pi^2)^{1/3} \left(\frac{Ta}{Re^2}\right)_o^{1/3} \left(1-\left(\frac{r_i}{r_e}\right)^4\right)^{1/3} \qquad 69$$

when $\left(\frac{Ta}{Re^2}\right)_o$ signified a value of $\left(\frac{Ta}{Re^2}\right)$ computed at the outer radius.

Much use will be made of the groups Re and Ta in this work. The model outlined above has been derived for a non-Newtonian power law fluid by ZINNATULLIN (121).

Commencing with a shear stress equation of the type

$$\tau = K\left(\frac{dv_r}{dy}\right)^n \qquad 70.1$$

then equation 58 may be rewritten as

$$\frac{K}{\rho}\frac{d}{dy}\left(\frac{dv_r}{dy}\right)^n = -\omega^2 r \qquad 70.2$$

which after double integration subject to boundary conditions 59.1 and 59.2 gives

$$v_r = \frac{n}{n+1}\left(\frac{\rho}{K}\omega^2 r\right)^{1/n}\left[\delta^{\frac{1+n}{n}} - (\delta-y)^{\frac{1+n}{n}}\right] \qquad 71$$

Integrating again with respect to y and dividing by δ gives $\bar{v}_r$. Equating $\bar{v}_r$ to the flowrate divided by flow area gives an expression similar to equation 61,

$$\delta = \left(\frac{1+2n}{2\pi n}\right)^{\frac{n}{1+2n}} \left(\frac{Q}{r}\left(\frac{K}{\rho}\right)^{1/n}\left(\frac{1}{\omega^2 r}\right)^{\frac{1}{n}}\right)^{\frac{n}{1+2n}} \qquad 72.1$$

or
$$\frac{\delta}{r} = \left(\frac{1+2n}{2\pi n}\right)^{\frac{n}{1+2n}} \left(\frac{Q}{r^{\frac{1+3n}{n}}}\left(\frac{K}{\rho}\right)^{\frac{1}{n}}\left(\frac{1}{\omega^2 r}\right)^{\frac{1}{n}}\right)^{\frac{n}{1+2n}} \qquad 72.2$$

note that equations 72.2 and 66 are identical if $K = \mu$ and $n = 1$. TYABIN et al (122, 123) have derived similar equations for a visco-plastic medium which exhibits a critical yield stress. The equations for film thickness, once the material has yielded, are essentially unchanged.

YURCHENKO et al (124) have considered the centrifugal model in which two immiscible liquids are flowing out over the disc in two layers, one on the other. The results reduce to equations 60 to 62 for the limiting case as the upper layer tends to zero flowrate.

B: CORIOLIS MODEL

The model considered above was essentially formed by considering the primary force balance of the radial boundary layer equation. It is apparent that the physical interpretation of the model which results, viz. a fluid film which moves out over the disc under the action of centrifugal force, must give rise to a Coriolis force. This force will be circumferential in direction and will oppose the direction of rotation. The appropriate equations for solution (see Appendix F) are

$$\nu \frac{\partial^2 v_r}{\partial y^2} = - \frac{v_\theta^2}{r} \qquad 73.1$$

$$\nu \frac{\partial^2 v_\theta}{\partial y^2} = \frac{v_\theta v_r}{r} + v_r \frac{\partial v_\theta}{\partial r} \qquad 73.2$$

after neglecting lower order of magnitude terms.
Putting $v_\theta = \omega r$ into equations 73.1 and 73.2 gives

$$\nu \frac{\partial^2 v_r}{\partial y^2} = - \omega^2 r \qquad 74.1$$

$$\nu \frac{\partial^2 v_\theta}{\partial y^2} = 2 \omega v_r \qquad 74.2$$

Equation set 74 will tend to equal set 58 if

$$\omega^2 r \gg 2 \omega v_r \qquad 75.1$$

Using the results for v_r from the centrifugal model, then criteria 75.1 becomes $\omega \delta^2 / \nu \ll 1$, or further substituting for δ,

$$\frac{Q^2}{\omega \nu r^4} \ll 1 \qquad 75.2$$

Notice that the group in equation 75.2 may be written as (Re^2/Ta)

The limitations of the centrifugal model, then,are controlled by the magnitude of the group (Re^2/Ta). In the absence of experimental information of the deviation from the centrifugal model, theoretical estimates of the critical magnitude of Re^2/Ta must be made as indicated above. It is apparent that no matter how small the value of Re^2/Ta, any finite value whatsoever implies that equation 73.2 cannot be strictly taken as zero. However, for sufficiently small values of Re^2/Ta the solution of equation set 73 should closely approximate that of equation 58.

EMSLIE et al (125) wrote the Coriolis force using the free surface velocity which, if the various terms involved in the equations used are retained, results in the criteria

$$Re^2/Ta < \left(\frac{2\pi}{3}\right)^2 \qquad 75.3$$

VACHAGIN and NIKOLAEV (126) after obtaining a solution to equation set 74 (see later in this section) and comparing the results of this expansion with the centrifugal model, concluded that the models were nearly identical if

$$\frac{\delta}{r}.(Ta)^{1/2} \leq 0.5$$

or, equivalently,

$$Re^2/Ta \leq \frac{\pi^2}{144} \qquad 75.4$$

ZINNATULLIN et al (127) in their expansion of equation set 74 for non-Newtonian fluids (see later in this section) again compared the theoretical solution against that of the centrifugal model and concluded that they were nearly identical if

$$\frac{2}{\pi}\ \frac{Re}{Ta}\ \frac{r}{\delta} \leq 0.01$$

or equivalently $$Re^2/Ta \leq \frac{3}{16}\pi^2 \times 10^{-6} \qquad 75.5$$

The criteria of 0.01 is if anything over restrictive and notable deviations do not begin until a value of some 0.3 is exceeded, leading more reasonably to

$$Re^2/Ta \leq 0.05 \qquad 75.6$$

RAUSCHER et al (128) obtain two criteria from their expansion of the simplified three-dimensional Navier-Stokes equations (see later in this section).

Firstly, equating the magnitudes of centrifugal and Coriolis forces, equation 75.3 was deduced. Secondly, by considering the additional terms introduced into the expansion for δ, then for the centrifugal model to fit,

$$\delta/r \ll 1 \qquad 75.7$$

MATSUMOTO et al (129) considered the polynomial expansion of the equations equivalent to von KARMAN'S equations for a disc in an infinite media and concluded that the centrifugal model was found if

$$\frac{\delta}{r}(Ta)^{1/2} \leq 1$$

or, equivalently,

$$Re^2/Ta \leq \left(\frac{2\pi}{3}\right)^6 \qquad 75.8$$

An approximate solution to equation set 74 may be simply obtained. Differentiating equation 74.2 twice w.r.t. y, then substituting for from equation 74.1 gives

$$\frac{\partial^4 v_\theta}{\partial y^4} = -\frac{2\omega^2 r}{\nu^2} \qquad 76.1$$

Integrating four times one finds

$$v_\theta = -\frac{\omega^3 r y^4}{12\nu^2} + Ay^3 + By^2 + Cy + D \qquad 76.2$$

when A, B, C and D are functions of ω, ν and r only. Forming $\frac{\partial^2 v_\theta}{\partial y^2}$ and using equation 74.2 gives

$$v_r = -\frac{\omega^2 r y^2}{2\nu} + \frac{3Ay\nu}{\omega} + \frac{B\nu}{\omega} \qquad 76.3$$

using the boundary conditions

$$y=0 \qquad v_r = v_\theta = 0 \qquad 76.4$$

$$y=\delta \qquad \frac{dv_r}{dy} = \frac{dv_\theta}{dy} = 0 \qquad 76.5$$

gives for the constants

$$A = \frac{\omega^3 r}{3\nu^2} \qquad C = -\frac{2}{3}\frac{\omega^3 r \delta^3}{\nu^2} \qquad 76.6$$

$$B = 0 \qquad D = 0 \qquad 76.7$$

giving for the final distributions

$$v_r = \frac{\omega^2 r}{\nu}\left(\delta y - \frac{y^2}{2}\right) \qquad 76.8$$

and

$$v_\theta = \frac{\omega^3 r}{3\nu^2}\left(\delta y^3 - 2\delta^3 y - y^4/4\right) \qquad 76.9$$

VACHAGIN and NIKOLAEV (126) considered equation set 74 and assumed that v_θ and v_r were given by equations of the form $\omega r.f$ when f was a function of y alone. The end result of their analysis is

$$\frac{\sinh\left(2\frac{\delta}{r}.Ta^{1/2}\right) - \sin\left(2\frac{\delta}{r}.Ta^{1/2}\right)}{\cosh\left(2\frac{\delta}{r}.Ta^{1/2}\right) + \cos\left(2\frac{\delta}{r}.Ta^{1/2}\right)} = \frac{2}{\pi}\left(\frac{Re^2}{Ta}\right)^{1/2} \qquad 77$$

Equation 77 gives $\frac{\delta}{r}.Ta^{1/2}$ implicitly as a function of Re^2/Ta.
ZINNATULLIN et al (127) considered the equation set similar to 74 appropriate to non-Newtonian flow. A simplifying assumption used was that the velocity distributions in the radial and azimuthal directions were of semi-parabolic form as predicted by equation 71 for the centrifugal model. The resulting analysis gave the solution

$$\varepsilon^n\left(1-\sqrt{1-\varepsilon^2}\right)^{\frac{n+1}{2}} = \psi \qquad 77.1$$

when $\varepsilon = \frac{2}{\pi}\frac{Re}{Ta}\frac{r}{\delta}$

and $$\psi = 2^{\frac{5n+1}{2}}\left(\frac{n}{2n+1}\right)^n\left(\frac{Q}{\pi}\right)^{n+1}\left(\frac{\rho}{K}\right)\frac{1}{r^{3n+1}\omega^{2n-1}} \qquad 77.2$$

Equation 77.2 reduces to $\psi = \frac{8}{3\pi^2}\frac{Re^2}{Ta}$ for $n = 1$, $K \equiv \mu$

Equation 77.1 predicts that $\left(\frac{\delta}{r}.\frac{Ta}{Re}\right)$ will be a function of Re^2/Ta.
Equation 77.1 is valid only to a value of ε and ψ of unity although obviously from the definition of ψ the limitation is not explainable on physical grounds since Re^2/Ta may be increased to any value. Thus the limitation must arise from the assumption concerning the shape of the velocity profiles and equation 77.1 should be regarded as merely an indication of the effect of Coriolis force on the centrifugal model.

C: GENERAL MODEL

DORFMAN (130) considered the more comprehensive equation set derived in Appendix F. Taking equations F7.1 and F7.2, (neglecting the

pressure distributions) and the continuity equation F8, DORFMAN rewrote the system in non-dimensional form, obtaining a non-linear parabolic set. DORFMAN obtained a numerical solution of the resulting system after generalising the equations over a rectangular net. For solution the inlet radial velocity distribution was taken as the average fluid velocity leaving the distributor gap. DORFMAN expresses the results as functions of two groups $\emptyset$ and Re^* (the * is included to prevent confusion with the group Re used elsewhere in this thesis) defined as

$$\emptyset = \frac{\bar{U}_{ri}}{\omega r_i} = \frac{1}{2\pi}\left(\frac{Re}{Ta}\right)_i\left(\frac{r_i}{G}\right) \qquad 78.1$$

and $$Re^* = \frac{G^2\omega}{\nu} \equiv \left(\frac{G}{r_i}\right)^2 Ta_i \qquad 78.2$$

when G is the distributor/plate gap through which the fluid enters onto the disc surface. DORFMAN shows how as $\emptyset$ is decreased the fluid attains a fully developed profile in a shorter radius (for example at $\emptyset = 0.5$, developed flow is attained at about $r = 2r_i$).

RAUSCHER et al (128) considered equation set F5 neglecting the normal velocity and its derivatives. A polynomial expansion was undertaken, subject to the boundary conditions of no solid surface velocity and zero free surface interfacial drag. Surface curvature and tension were considered as boundary conditions. The resulting expansions are infinite, but the first significant terms of the expansion are (when expanded from the nomenclature employed in 128)

$$U_r = \frac{\omega^2 r}{\nu}\left(\delta y - y^2/2\right) \qquad 79.1$$

$$U_\theta = \frac{\omega^3 r}{\nu^2}\left(-\frac{2}{3}\delta^3 y + \frac{1}{3}\delta y^3 - \frac{y^4}{12}\right) \qquad 79.2$$

$$U_y = \frac{\omega^2}{\nu}\left(\frac{y^3}{3} - \frac{2}{3}\delta y^2\right) \qquad 79.3$$

Notice that equation 79.1 is identical to equations 76.8 and 60.1. Equation 79.2 is identical with equation 76.9. It is simple to show from the continuity equation that equation 79.3 follows from equation 79.1.e79.2 (Note that from equation 61, $\frac{\partial\delta}{\partial r} = -\frac{2}{3}\delta/r$).

REES (131) considered the simplified boundary layer equation set 48 and the corresponding non-dimensional equation set 52. REES was able to show that the free surface downward velocity at the film surface

was given by

$$-C = \frac{-Q}{\pi r^2 (\omega\nu)^{1/2}} \equiv -\frac{1}{\pi}\left(\frac{Re^2}{Ta}\right)^{1/2} \qquad 80$$

(see Section 2.4:B later)

In the equations considered there are five unknowns (H, F, G, F', G') and three explicit equations (equations 52.1, 52.2 and 52.4). In addition, definition equations link F to F' and G to G'. The boundary conditions are distributed such that H, F and G are known at the solid surface (F' and G' unknown) and at the free surface H, F' and G' are known (F and G unknown). The solution technique adopted by REES was to assume values for F' and G' at the solid surface and integrate (with respect to ζ) the appropriate equations until the known value of H at the free surface was found. The initial values of F' and G' were then modified according to the imbalance in the free surface values of F' and G' (which should be zero) and the procedure repeated until all known boundary conditions were satisfied. REES reported no difficulties with this procedure.

MATSUMOTO et al (132) followed essentially the same solution as REES but reported that the solution method was unstable in that small changes in the initial boundary conditions led to great changes in the free surface values of F' and G', and so a 'feed-back' method tended to oscillate about the true solution becoming more unstable with each iteration. MATSUMOTO et al outline a stable solution based upon the quasilinearisation technique. Solution was obtained to a value of ζ of unity, i.e.

$$\frac{\delta}{r}.(Ta)^{1/2} = 1 \qquad 81$$

MATSUMOTO et al (129, 132 and 133) also considered a polynomial expansion of the equation set 52. By assuming that F, G and H were representable as polynomial expansions in ζ, the derivative equations F' and G' are easily found. By limiting the expansion to a specified order of ζ, use of the relationships of equation set 52 and the boundary conditions give algebraic relationships between F, G, H, ζ and constants. MATSUMOTO et al considered expansions including terms up to ζ^5. For the second order expansion the results are

$$F = \zeta_0 \zeta - \tfrac{1}{2}\zeta^2 \qquad 82.1$$

$$G = 1 \qquad 82.2$$

$$H = -\zeta_0 \zeta^2 + \frac{1}{3}\zeta^3 \qquad 82.3$$

$$\zeta_0 = \delta\left(\frac{\omega}{\nu}\right)^{1/2} \qquad \zeta = y\left(\frac{\omega}{\nu}\right)^{1/2}$$

Note that equation 82.1 is equivalent to the centrifugal model, 60.1, and 82.2 gives $U_\theta = \omega r$. Equation 82.3 may be shown to be the matching normal velocity equation from continuity considerations. By comparing the polynomial expansions to the numerical solution MATSUMOTO showed that as ζ_0 increases, then so too does the mismatch between the expansions and the numerical solution. In each case the higher the degree of expansion the better the resulting match. It is possible to integrate the expansion for F to obtain the relationship

$$\frac{1}{2\pi}\left(\frac{Re^2}{Ta}\right)^{1/2} = \int_0^{\zeta_0} F\, d\zeta \qquad 83$$

when the 5th order polynomial for F results in

$$\frac{1}{2\pi}\left(\frac{Re^2}{Ta}\right)^{1/2} = \frac{1}{2}a_1\zeta_0^2 - \frac{1}{6}\zeta_0^3 - \frac{1}{12}b_1\zeta_0^4 - \frac{1}{60}b_1\zeta_0^6 - \frac{1}{360}a_1\zeta_0^6 \qquad 84.1$$

and a_1 and b_1 are obtained from the relationships

$$a_1 - \zeta_0 - b_1\zeta_0^2 - \frac{1}{3}b_1\zeta_0^3 - \frac{1}{12}a_1\zeta_0^4 = 0 \qquad 84.2$$

and

$$b_1 + a_1\zeta_0^2 + \frac{1}{3}(a_1b_1 - 1) - \frac{1}{3}b_1\zeta_0^4 = 0 \qquad 84.3$$

For any value of ζ_0, a_1 and b_1 may be found from equations 84.2 and 84.3 and then the resulting values used in equation 84.1 to obtain the respective flow parameter. MATSUMOTO et al (129) tabulate values of a_1 and b_1 for values of ζ_0 (0,.1, 1) and in comparison to the numerical results, deviation from the numerical expansion is of O (2%) for $\zeta_0 = 1$. Note that equation set 84 gives $\frac{S}{r}(Ta)^{\frac{1}{2}}$ implicitly as a function of (Re^2/Ta).

The only analyses so far examined which consider inertia forces within the fluid are those of DORFMAN and RAUSCHER. To the simplest order, inertia is involved in the radial flow equation thus

$$\frac{\partial u_r}{\partial t} - \frac{U_\theta^2}{r} = \nu\frac{\partial^2 U_r}{\partial y^2} \qquad 85$$

ADLER and MARSHALL (124) and WATTS (115) have performed a simple force balance on the film employing the centrifugal model's velocity profile results. Thus equating the forces involved in Newton's Law

$$\begin{matrix}\text{centrifugal}\\ \text{force}\end{matrix} - \begin{matrix}\text{viscous}\\ \text{drag}\end{matrix} = \text{mass x acceleration}$$

or
$$\delta\rho\omega^2 r - \mu\left(\frac{du_r}{dy}\right)_{y=0} = \delta\rho\frac{d\bar{u}_r}{dt} \qquad 86.1$$

In equation 86.1 the fluid is considered as a layer moving as a solid film over the disc.

Replacing $d\bar{u}/dt$ by $\bar{u}\,d\bar{u}/dr$ in 86.1 and using the centrifugal models results to form $(du_r/dy)_o$ in terms of $\bar{u}_r$ gives

$$\frac{d\bar{u}_r}{dr} = \frac{\omega^2 r}{\bar{u}_r} - \frac{12\pi^2\mu r^2\bar{u}_r^2}{\rho Q^2} \qquad 86.2$$

Notice that the force balance is written for a layer moving with a velocity $\bar{u}_r$ for all y, the results of the centrifugal model (from which u_r is a function of y) are employed to evaluate expressions for the viscous drag. VENKATARAMAN (120) derived an equation similar to 86.2. WATTS (115) derived an equation similar to 86.2 by considering the "momentum flow rate" at a given radius. By defining

$$M = \int_0^\delta \rho u_r^2\,dy \qquad 87.1$$

and equating the left hand side of equation 86.1 to the radial rate of change of momentum, dM/dr, then by using the centrifugal models velocity profile WATTS obtained the relationship

$$\frac{d\delta}{dr} = -\frac{\delta}{r} - \frac{10\pi^2 r^3\delta^3\omega^2}{3Q^2} + \frac{5\pi r\nu}{Q} \qquad 87.2$$

Insertion of 87.2 into the relationship

$$\frac{d\bar{u}_r}{dr} = \frac{d}{dr}\left(\frac{Q}{2\pi r\delta}\right) = \frac{Q}{2\pi}\left(-\frac{1}{\delta r^2} - \frac{1}{r\delta^2}\frac{d\delta}{dr}\right) \qquad 87.3$$

gives
$$\frac{d\bar{u}_r}{dr} = \frac{5}{6}\left(\frac{\omega^2 r}{\bar{u}_r} - \frac{12\pi^2\mu r^2\bar{u}_r^2}{\rho Q^2}\right) \qquad 87.4$$

Note that apart from the factor $5/6$, equations 87.4 and 86.2 are similar.

Equations 86.2 and 87.4 may be used to progress in radial steps from the distributor gap (where $\bar{U}_r$ is known by virtue of the flowrate and gap dimensions). The numerical solution of 86.2 and 87.4 has been performed and the results compared to the centrifugal model in FIGURES 10, 11 and 12. It will be observed that the effects of the entry gap rapidly die out and the solution approaches the centrifugal model value. Approach is most rapid for low flowrates and high rotational speeds. Solution was obtained using program SINT (Appendix B) with a radial step length of 0.001 cm. The various system parameters chosen (Q, r_i, ω, ν) were specified to enable a comparison to be made against some experimental data collected. This comparison is made later in Section 2.5.

VENKATARAMAN (120) considered equation set 74 written for the average velocities (the Coriolis force was written as $\bar{U}_r \bar{U}_\theta / r + U_r dU_\theta/dr$ its correct value). The azimuthal velocity was assumed to be represented by a quadratic chosen to satisfy the boundary conditions in the circumferential direction, viz.

$$y = 0 \;,\quad U_\theta = \omega r \qquad 88.1$$

$$y = \delta \;,\; U_\theta = U_{\theta s} \;,\quad \frac{\partial U_\theta}{\partial y} = 0 \qquad 88.2$$

VENKATARAMAN employed the resulting equation and the profiles of the centrifugal model to obtain

$$\bar{U}_r \frac{d\bar{U}_r}{dr} + \frac{12\pi^2 \nu r^2 \bar{U}_r^3}{Q^2} - \frac{\bar{U}_\theta^2}{r} = 0 \qquad 89.1$$

$$\bar{U}_r \frac{d\bar{U}_\theta}{dr}(1-\bar{U}_r) + 2U_\theta U_r - \frac{12\pi^2 \nu r^2 \bar{U}_r^2}{Q^2}(\omega r - \bar{U}_\theta) = 0 \qquad 89.2$$

Equation set 89 was solved numerically by VENKATARAMAN. Comparison to the other models is difficult owing to the limited range of the operating parameters studied.

D: TURBULENT FLOW

All the preceding models have implicitly assumed that the flow is laminar. Before considering the analytic solutions for turbulent flow several models which provide semi-empirical descriptions of turbulent flow will be examined.

ADLER and MARSHALL (118) and (134) assumed that a 'friction factor'

FIG10 INERTIA MODEL

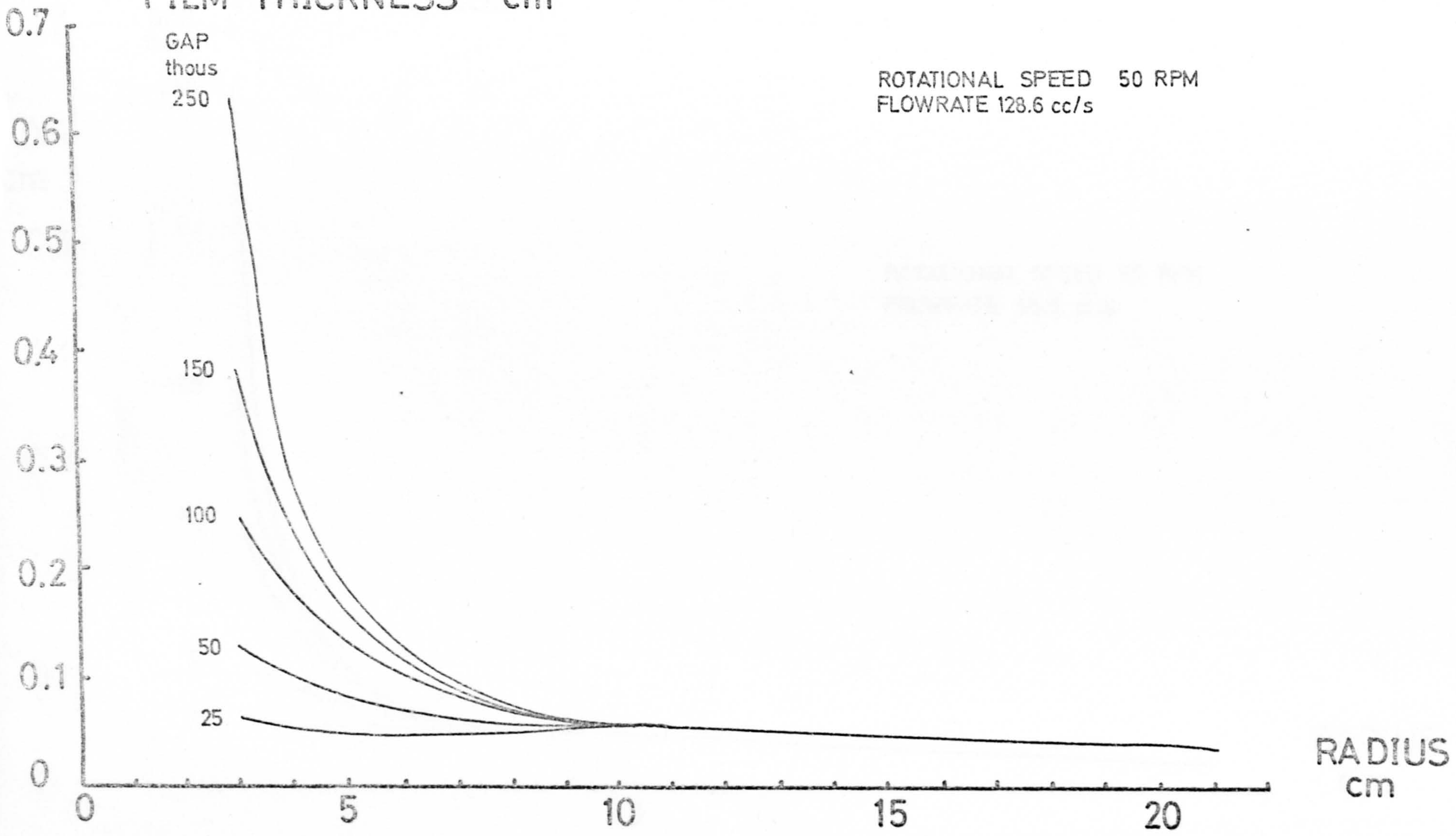

FIG11 INERTIA MODEL

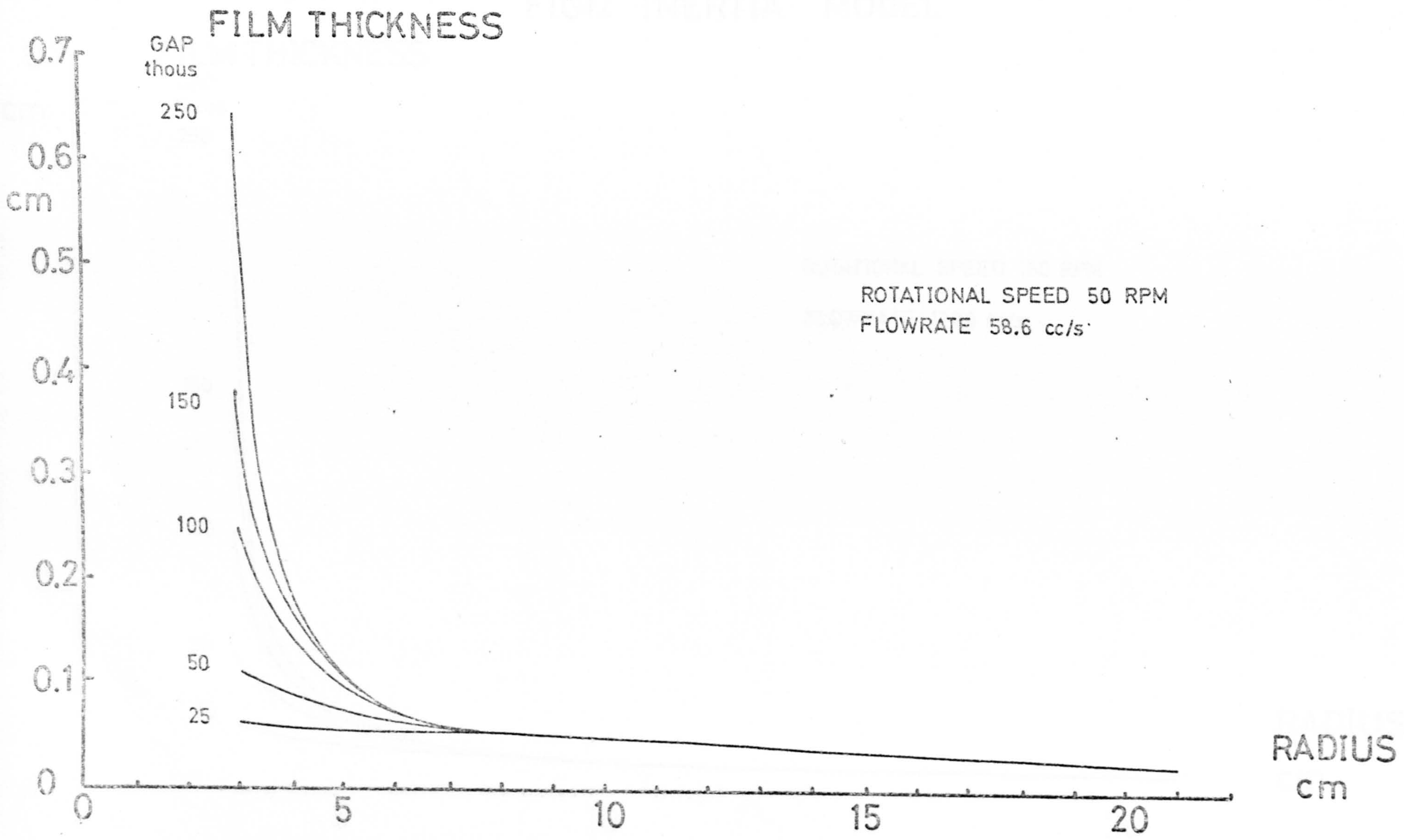

FIG12 INERTIA MODEL

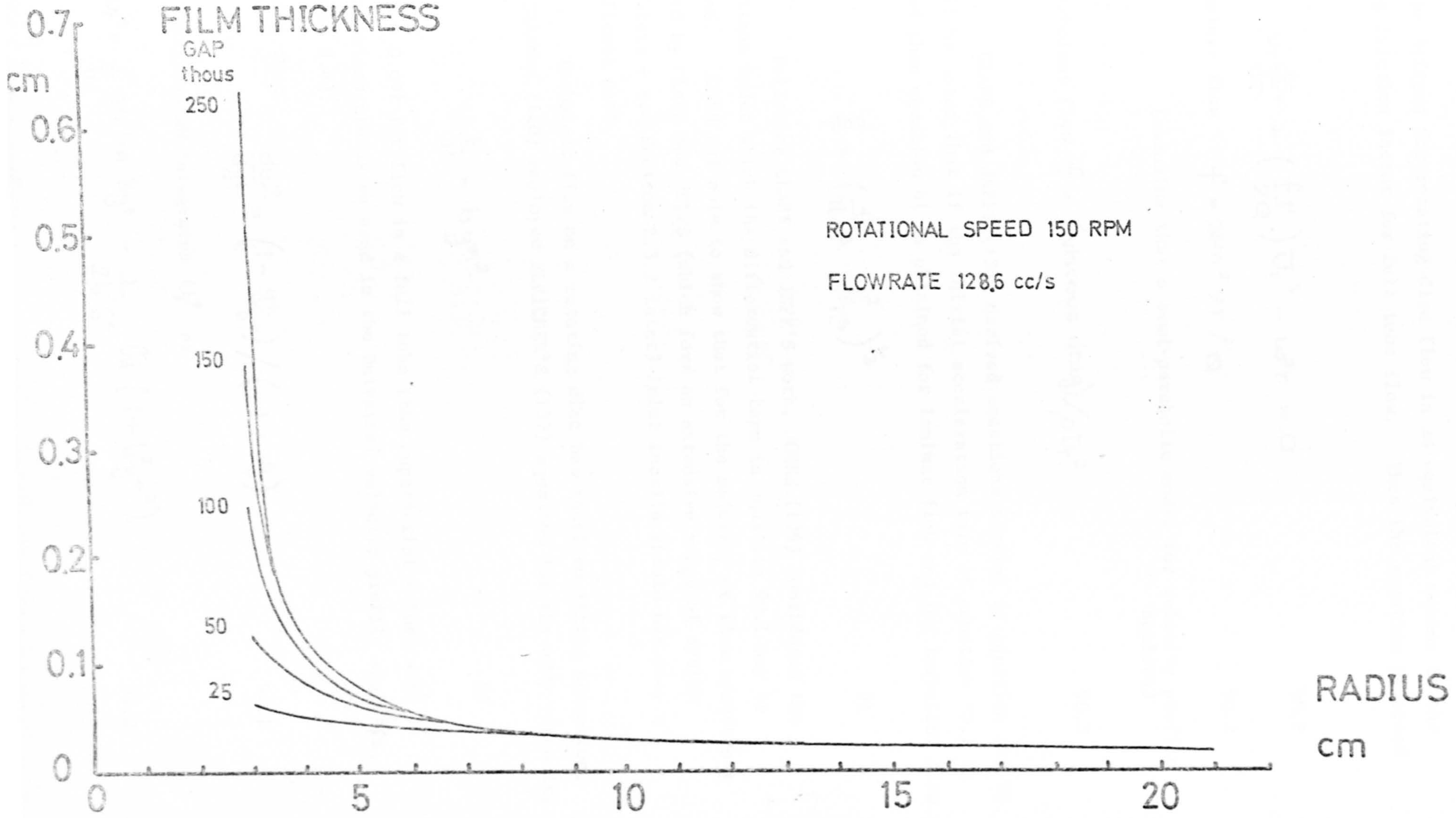

could be defined for rotating disc flow in an equivalent manner to the Fanning friction factor for full tube flow. Thus the equation proposed is

$$U_r \frac{d\bar{U}_r}{dr} + \left(\frac{f r}{2Q}\right)\bar{U}_r^3 - \omega^2 r = 0 \qquad 90.1$$

For laminar flow $$f = 24\pi^2 \nu r / Q \qquad 90.2$$

(assuming that a semi-parabolic model for velocity profile applies)

For turbulent flow $$f = (\text{viscous drag})/\rho \bar{U}_r^2 \qquad 90.3$$

CLARE and JEFFS (135) derived equations similar to equation set 90. It will be noted that if the initial acceleration term of equation 90.1 is ignored then equation 61 is obtained for laminar flow and for turbulent flow

$$\frac{\delta}{r} = \left(\frac{f}{16\pi^3}\ \frac{Q^2}{\omega^2 r^6}\right)^{1/3} \qquad 91$$

Following CLARE and JEFF'S work, JONES (136) considered the conditions under which the differential term in equation 90.1 may be ignored. JONES was able to show that for the majority of flow conditions studied by CLARE and JEFFS (which form an extensive range of system parameters - see Section 2.3.2 later) inlet inertia should not play a significant part.

Turbulent flow on a rotating disc has received little attention. VENKATARAMAN (120) employed SLEICHER'S (137) equation for the eddy viscosity

$$\frac{\varepsilon}{\nu} = b y^{+2} \qquad 92$$

when b = 0.091 for flow in a full tube (the superscript + indicates dimensionless groups as used in the Universal velocity profile analysis, equation 8.4).

Assuming that $$\frac{dU_r^+}{dy^+} = \left(1 - y^+/\delta^+\right) / \left(1 + \frac{\varepsilon}{\nu}\right) \qquad 93.1$$

then VENKATARAMAN integrates U_r^+ as

$$U_r^+ = \frac{1}{b}\arctan by^+ - \frac{1}{2b^2\delta^+}\ln\left(1 + b^2 y^{+2}\right) \qquad 93.2$$

which gives upon a second integration

$$\frac{1}{2\pi} Re = \frac{1}{b^2}\left[\left(X - \frac{1}{X}\right) \arctan X + 1 - \ln (1+X^2) \right] \qquad 93.3$$

when $$X = b\delta^+ \qquad 93.4$$

SLEICHER'S eddy viscosity is derived for single phase flow and three objections may be made against its use:

1. The presence of the free surface may be expected to dampen the turbulent intensity (see LEVICH (95)),

2. The coefficient b is derived from treatment of full tube flow data and may be different for film flow,

and 3. adjacent to the solid wall, ϵ varies as y^{+2}. ELROD (133) has shown theoretically that ϵ should vary as y^{+3} close to the wall. However, DAVIS (139) has used SLEICHER'S expression for plane film flow and obtained numerical results close to LILLELEHT'S data (see DAVIS (139)) for horizontal air/water film flow. The analytical expressions are strictly applicable for $\delta^+ \leq 30$.

WATTS (115) employed REICHARD'S (140) expression for eddy diffusivity:

$$\frac{\varepsilon}{\nu} = k\left(y^+ - \beta \tanh\left(\frac{y^+}{\beta}\right)\right) \qquad 94$$

when k and β are constants. The turbulent film thicknesses so obtained are greater than those obtained using DEISSLER'S expression and both are greater than those of the laminar model.

2.3.2. EXPERIMENTAL RESULTS

A: FILM THICKNESS

HICKMAN (3) reported qualitative measurements of the thickness of a flowing film on a rotating disc. HICKMAN concludes that 'for a wide range of flowrate'

$$\delta \propto \omega^n \qquad 95$$

The index, n, was not specified. HICKMAN shows photographs of a dyed

oil film flowing on the disc and the thinning of the film (inferred from the decreasing photographic image density) is obvious at increasing radii.

ESPIG (108, 141) studied water flow on a disc with a horizontal spindle. Thickness was indicated by a micrometer pointer with electrical surface contact indication. Fluid was introduced to the disc through a nozzle with a variable distributor/plate gap. No measurements other than film thickness are reported, and these showed considerable scatter about the correlation ($\delta/r\ (Ta)^{\frac{2}{3}}$) vs Re. This correlation scheme was obviously produced as an extension of film flow on a vertical plate (see equations 4.2 and 14) with the gravity term replaced by $\omega^2 r$. The correlation equation was deduced as

$$\frac{\delta}{r}^{max} = 1.12 \left(\frac{Re}{Ta^2}\right)^{\frac{1}{3}} \qquad 96.1$$

which compared to the equivalent KAPITSA correlation of

$$\frac{\delta}{r}^{max} = 1.06 \left(\frac{Re}{Ta^2}\right)^{\frac{1}{3}} \qquad 96.2$$

shows experimental thicknesses some 5% greater than theoretical. Note that equation 96.2 is based upon equation 17 deduced for sine waves on a falling plane film rewritten in terms of the rotating disc dimensionless groups. The equation has not been rederived to allow for the expanding nature of the flow with increasing radius and hence should not be expected to truly represent the nature of wavy flow on the disc.

GAZLEY and CHARWAT (142) and CHARWAT et al (143) studied the flow of water and water/surfactant mixtures on a rotating glass disc 38 cm in diameter. The diameter and rotating speed of the disc (1000 r.p.m.) mark an extension of earlier works system parameters towards more acceptable commercial values. Film thickness was inferred from the absorption of an infra-red light beam passed normal through the film and plate. GAZLEY and CHARWAT noted that the addition of surfactant considerably reduced the phenomena of surface disturbances, dry spots and waves observed in the pure water system. The scatter about the correlation groups (δ/r) and (Re/Ta^2) was less for the water/surfactant system compared to water, but the basic trends were indistinguishable between the two sets of results. This would seem to imply that the presence of waves did not significantly alter the film thickness observed. The data tended to fall below the centrifugal model for values of (Re/Ta^2) less than about 10^{-7} and then tended to rise over the model value. The correlating equation was

$$\frac{\delta}{r} = 1.6 \left(\frac{Re}{Ta^2}\right)^{0.4} \qquad 97$$

FIGURE 13 shows GAZLEY and CHARWAT'S data compared to the centrifugal model in dimensionless form. Also on FIGURE 13 are other experimental measurements referred to later. Due to the correlating groups chosen and the non-presentation of tabular data, ESPIG'S data has not been included on FIGURE 13. Owing to the difficulty of computation, the data shown graphically by GAZLEY and CHARWAT has not been reduced to independent values of δ/r, Re and Ta. Thus the alternative correlations (equation 68.2, 68.3) available cannot be compared to these experimental values.

VENKATARAMAN (120) employed a 5" diameter aluminium disc rotating at a maximum speed of 1500 rpm. VENKATARAMAN attempted to use a capacitive film thickness technique (technique 7 of Section 2.2), but was unable to obtain reproducible results. The technique finally employed was the micrometer probe method as used by ESPIG. The data collected, although of limited range showed very close agreement to the centrifugal model. The difficulty found by VENKATARAMAN in applying the capacitive technique was probably due to the fact that the probe head and the connections from the probe to the capacitometer were not shielded from stray fields and/or fringing effects.

VENKATARAMAN'S data is compared to the centrifugal model in FIGURES 13 and 14 and to the alternative correlations for this model in FIGURES 15 and 16.

CLARE and JEFFS (135) and CLARE and ASHWOOD (144) employed electrical measurement of the resistance of the flowing film (see technique 6, Section 2.2) to infer film thickness. Several experimental difficulties were experienced in creating the annular ring electrodes, maintaining electrical insulation between the rings and the remainder of the flow circuit and interpretation of the operative radii of the measurements taken. The ring electrodes were spaced some 1.9 cm apart and CLARE and JEFF S interpreted the measurement radii as the geometric mean of the inner and outer electrode rings. Comprehensive readings were taken for water dosed with calcium chloride to improve electrical conductivity ($CaCl_2$ concentration $\sim$ 1%). It was noticed that for any fixed radii and speed, increasing the flowrate from zero caused the measured film thickness to initially fall to a minimum then to increase. CLARE and JEFFS explain this minima as incomplete wetting of the disc surface and it is apparent that as the

FIG 13 GENERAL CORRELATION

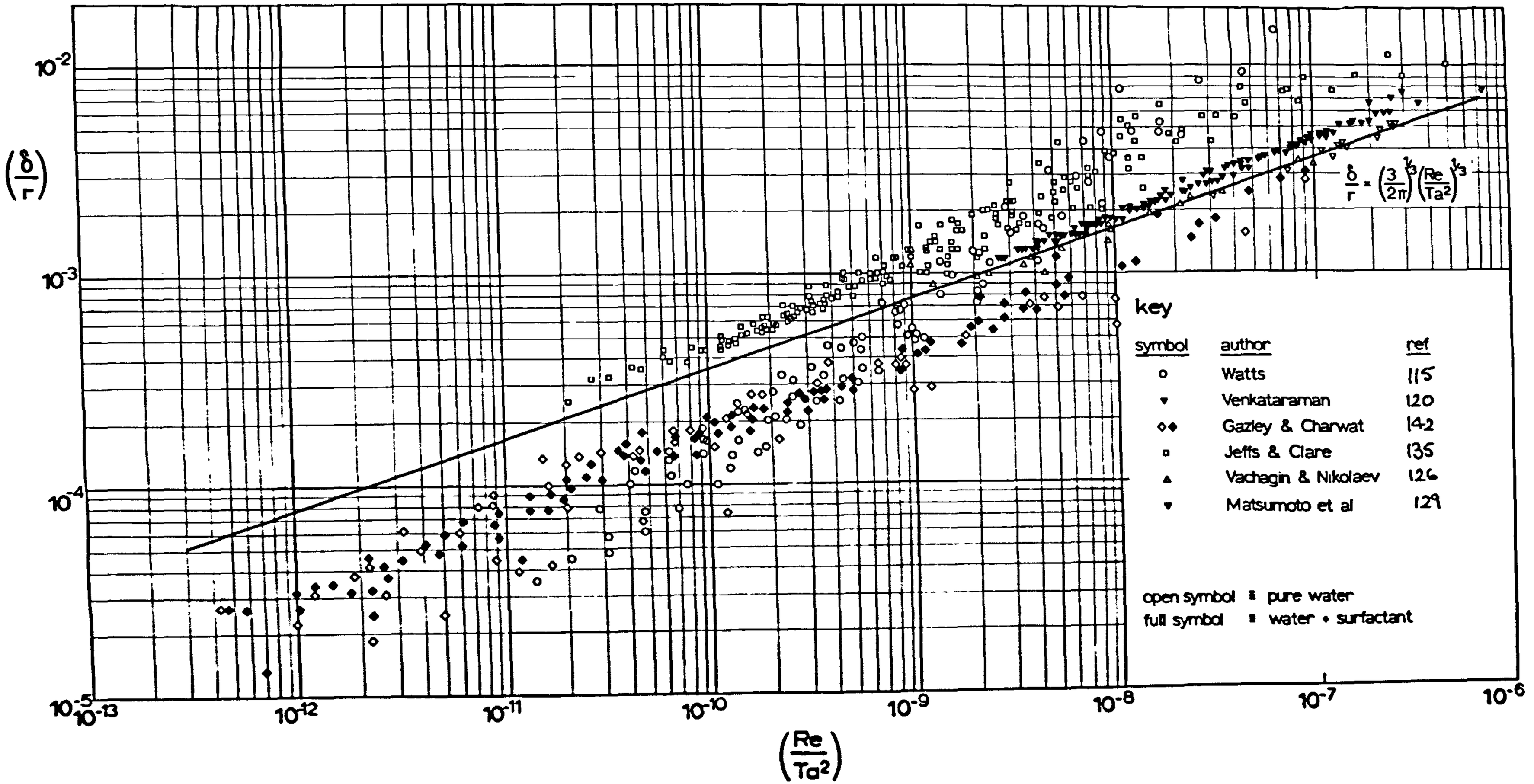

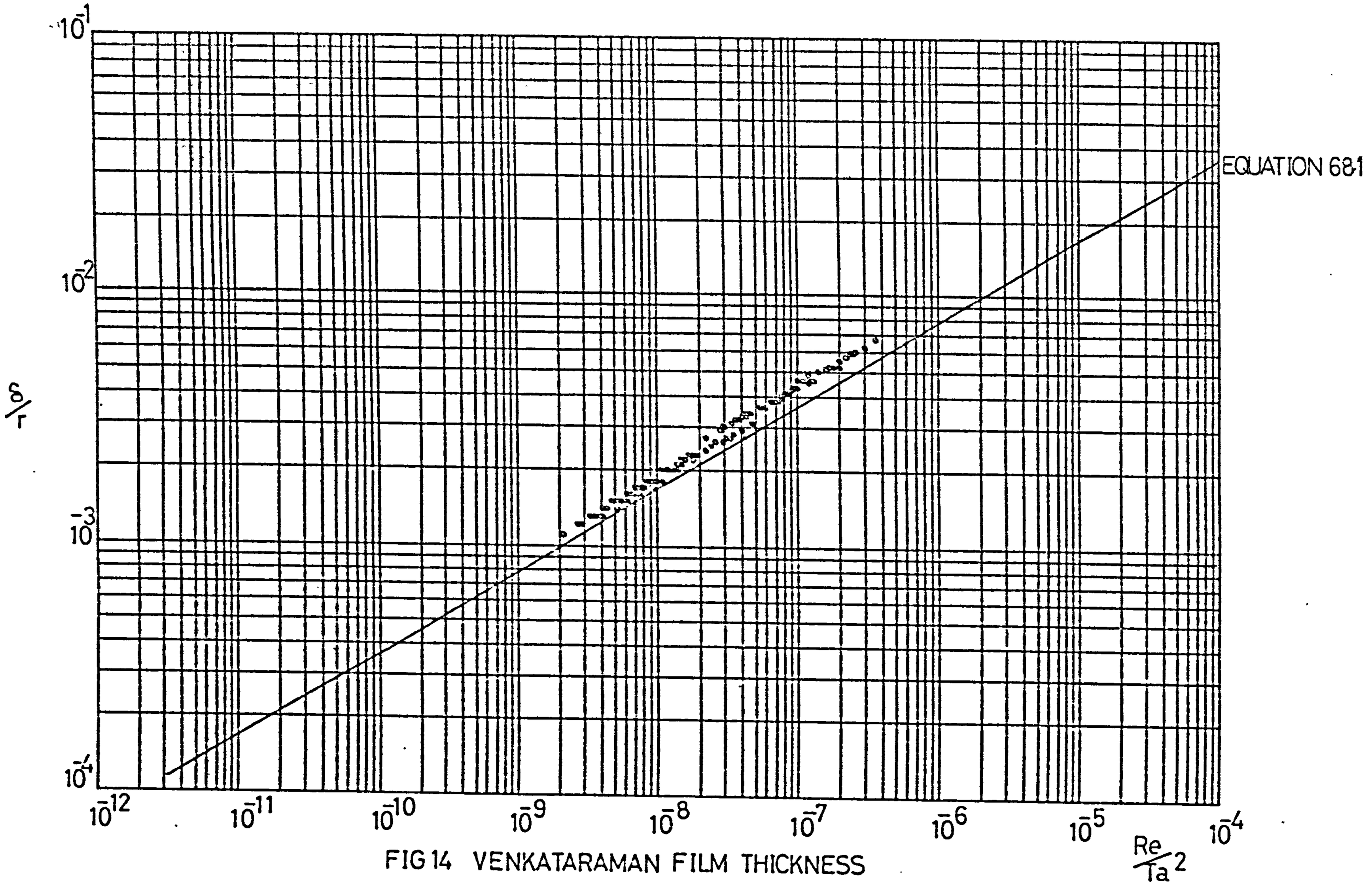

FIG 14 VENKATARAMAN FILM THICKNESS

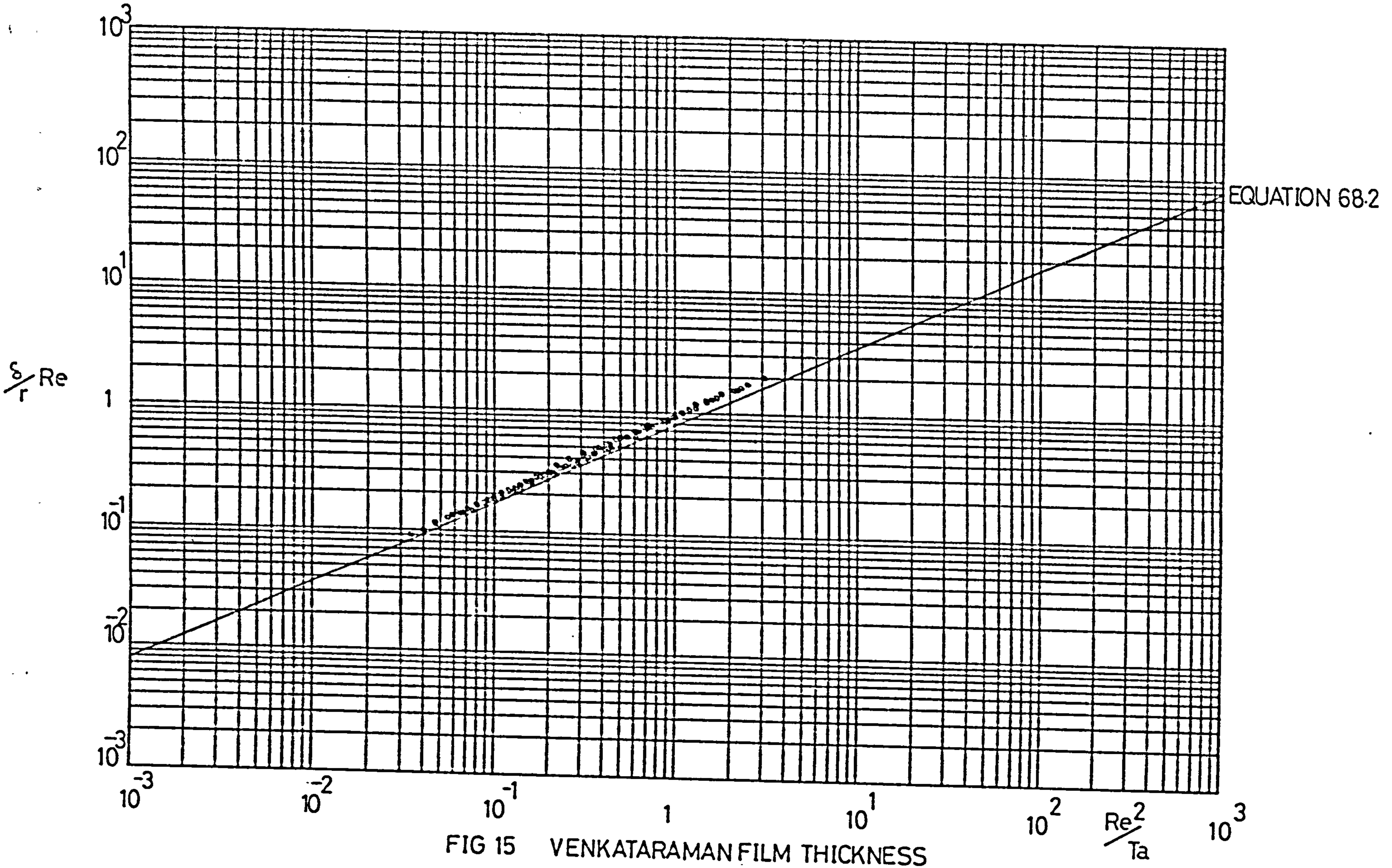

FIG 15 VENKATARAMAN FILM THICKNESS

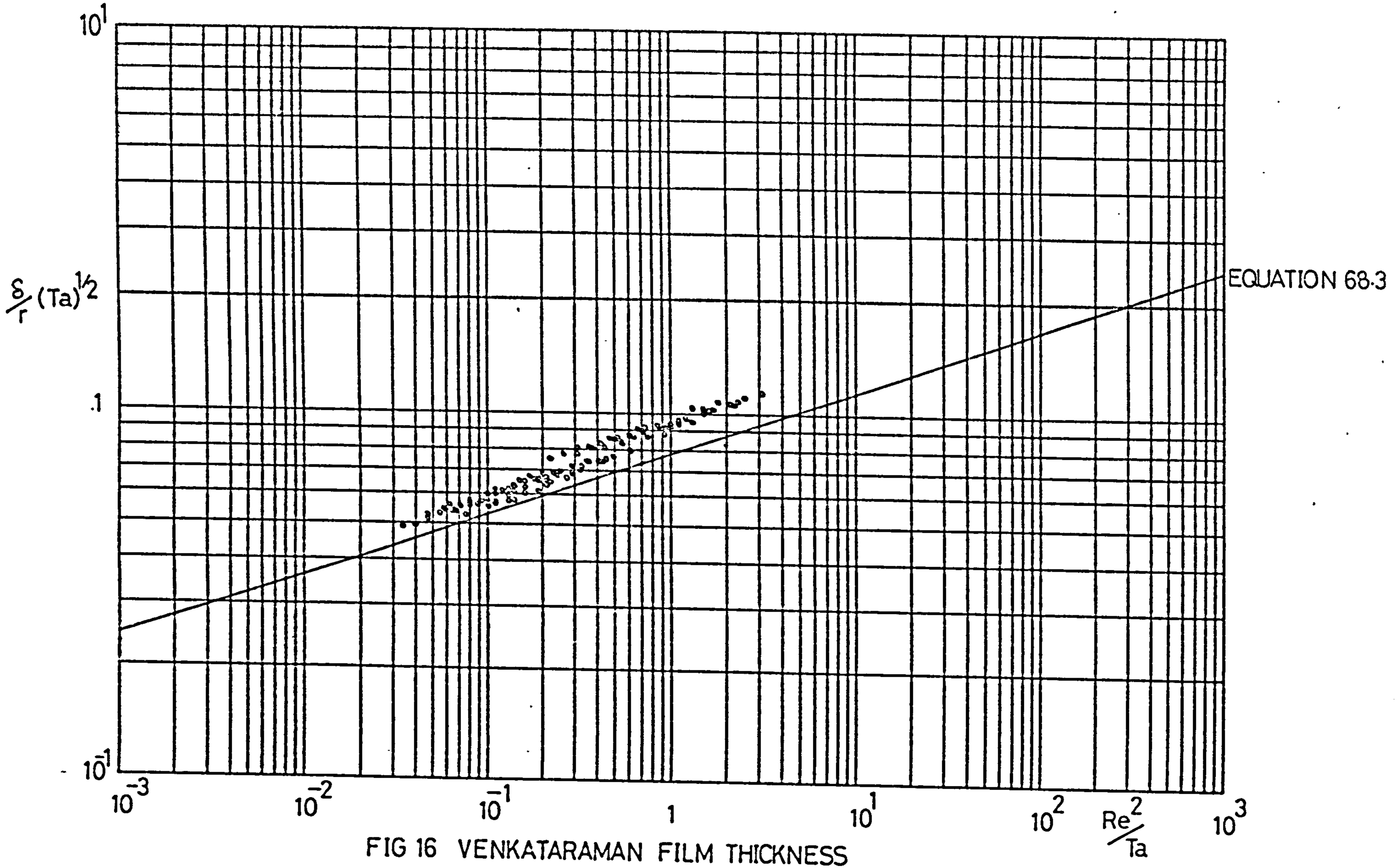

FIG 16 VENKATARAMAN FILM THICKNESS

flowrate increases (below the critical flowrate) the rivulets across the disc are broadening and thinning. Presumably at the critical flowrate the rivulets run together and form a smooth continuous film. It appears from the results given that the film becomes continuous rapidly over all radii with increasing flowrate, viz. at 3000 r.p.m. the film is continuous at the minimum radius (6.3 cm) at a flowrate of 9 cm^3/s and by a flowrate of 12.4 the film is continuous at the outer radius of 16.5 cm. CLARE and JEFFS compared the results to simple theories of laminar and turbulent flow (see Section 2.3.1,D) and concluded that if Re was less than a critical value, then the laminar flow model best fitted the data. The critical Re value was given as between 1600 and 5480. No reasonable explanation was offered for the variation found. In view of the work of YURCHENKO et al (see later) the variation could be explained as due to the neglect of the influence of the Taylor number. The experimental measurements of CLARE and JEFFS are shown on FIGURES 13 and 17, and compared to the alternate correlations for the centrifugal model in FIGURES 18 and 19.

WATTS (115) measured the mean velocity of carbon black particles in castor oil films and neutrally bouyant oil droplets in water and water/glycerol films. The path of the markers was recorded by high speed photography and from the average velocity recorded (since the depth of the particle could not be specified only an average value could be meaningfully recorded) the film thickness is computable. The results obtained for water are shown in FIGURES 13 and 20 against the centrifugal model, alternate correlations in FIGURES 21 and 22. For water/glycerol and castor oil the equivalent FIGURES are 23 and 24, 25 and 26 respectively. It will be noted that the pure water results are poorly correlated, the liquids of higher viscosity giving results of reasonable agreement to the centrifugal theory. In view of other workers results reported for water, the discrepancy between experimental and centrifugal model results seems to be more attributable to the technique used than to anomolous behaviour of the fluid as suggested by WATTS.

MATSUMOTO et al (129) considered fluid flow on a disc of diameter 12 cm rotating at speeds up to 9000 r.p.m. Film thickness was measured by micrometer probe with electrical contact sensing. The results obtained as seen from FIGURES 13, 27, 28 and 29 are in good agreement with the centrifugal model. The viscosity of the fluids investigated varied from 9.6 cS to 58.3 cS which implies fluids other than pure water. Presumably (although this is not stated) the fluids used showed Newtonian

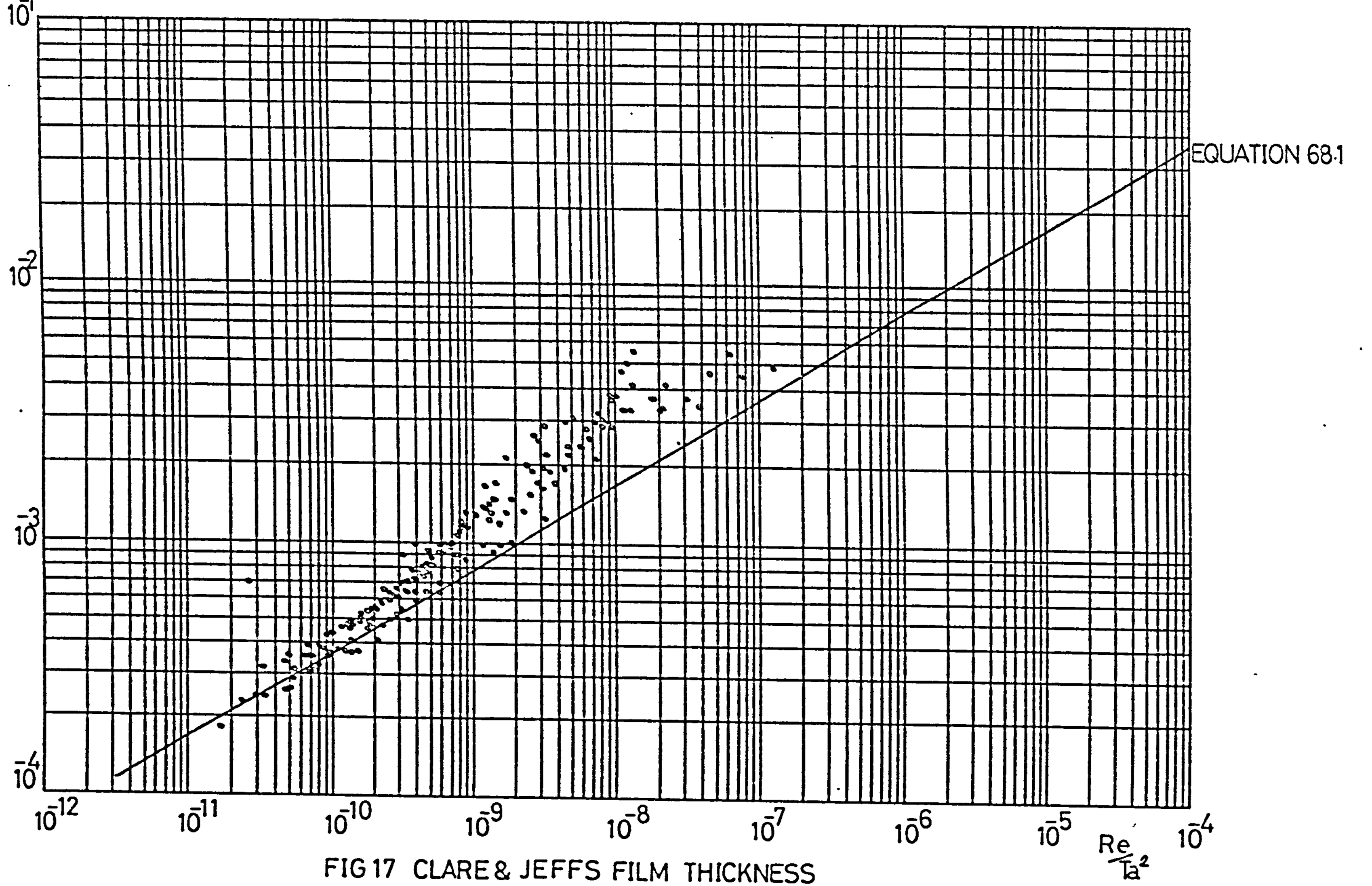

FIG 17 CLARE & JEFFS FILM THICKNESS

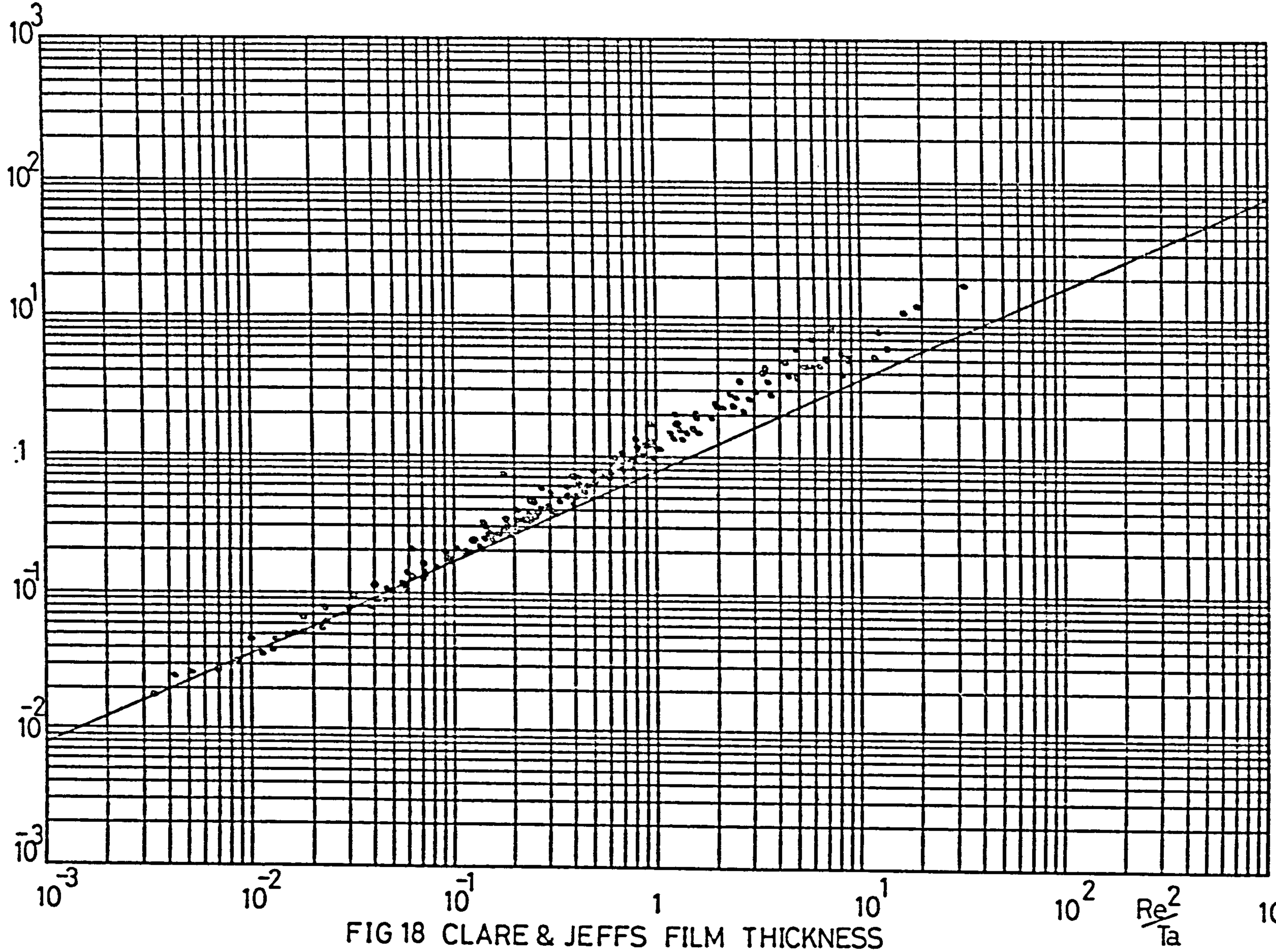

FIG 18 CLARE & JEFFS FILM THICKNESS

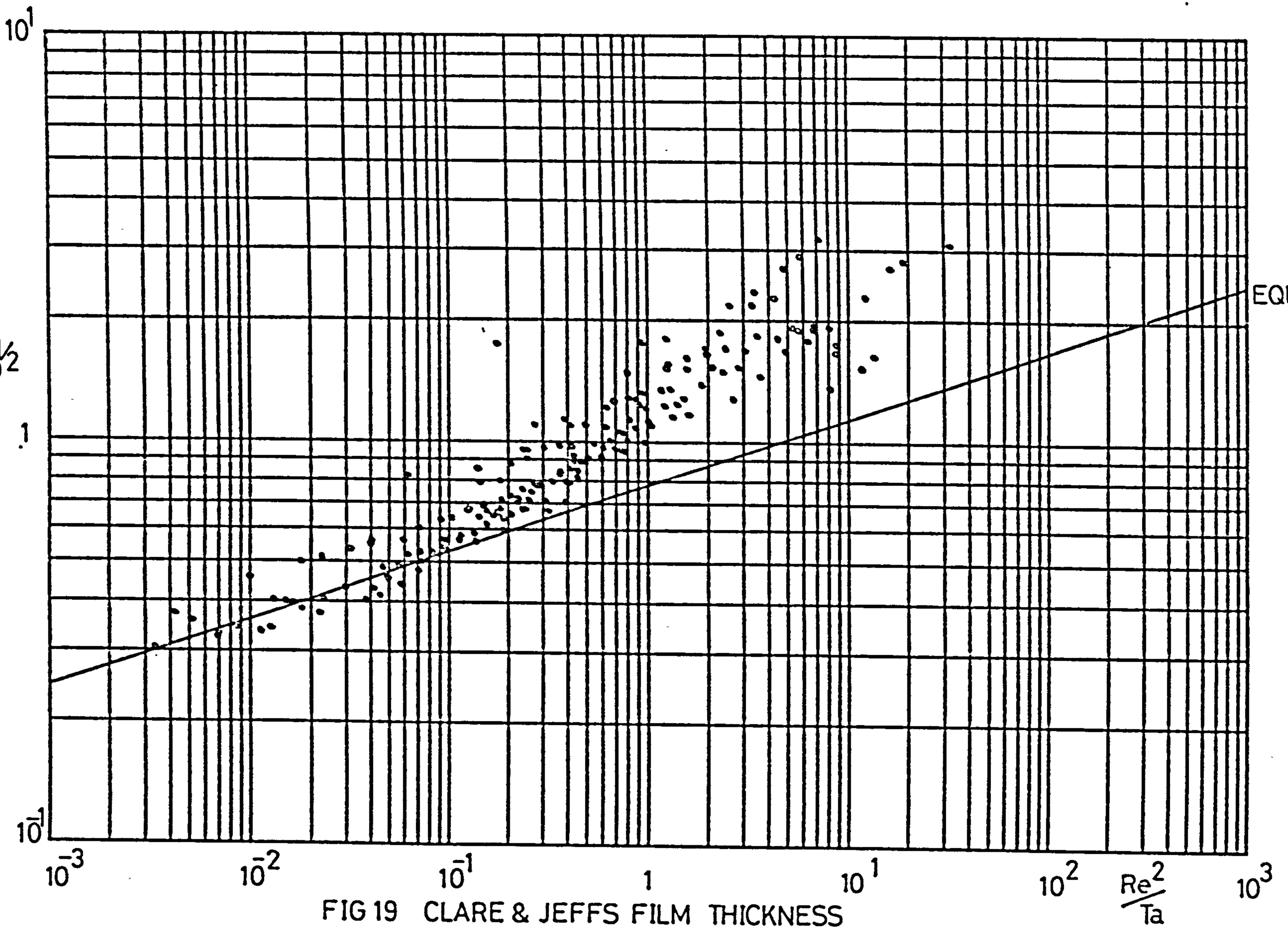

FIG 19 CLARE & JEFFS FILM THICKNESS

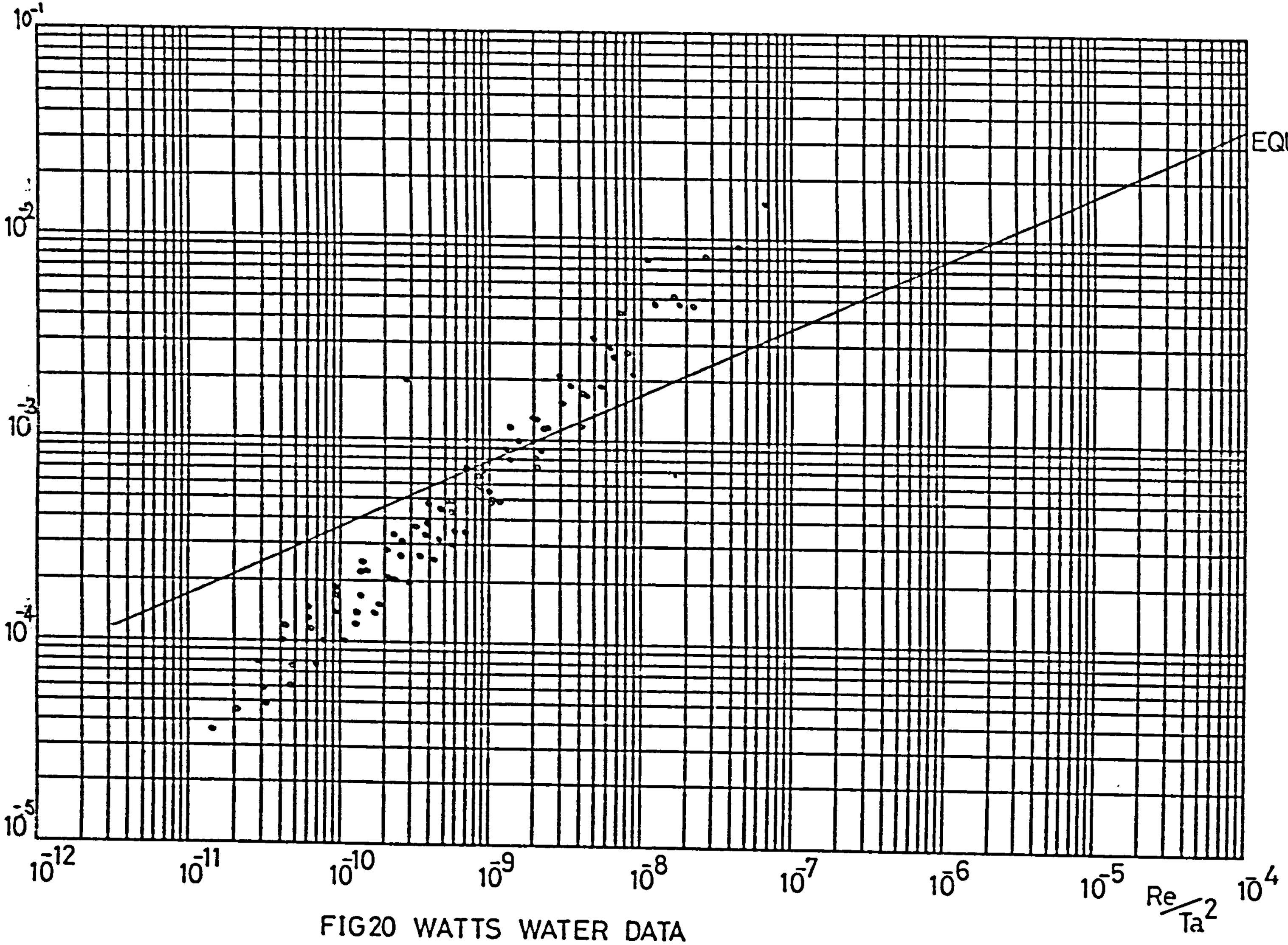

FIG20 WATTS WATER DATA

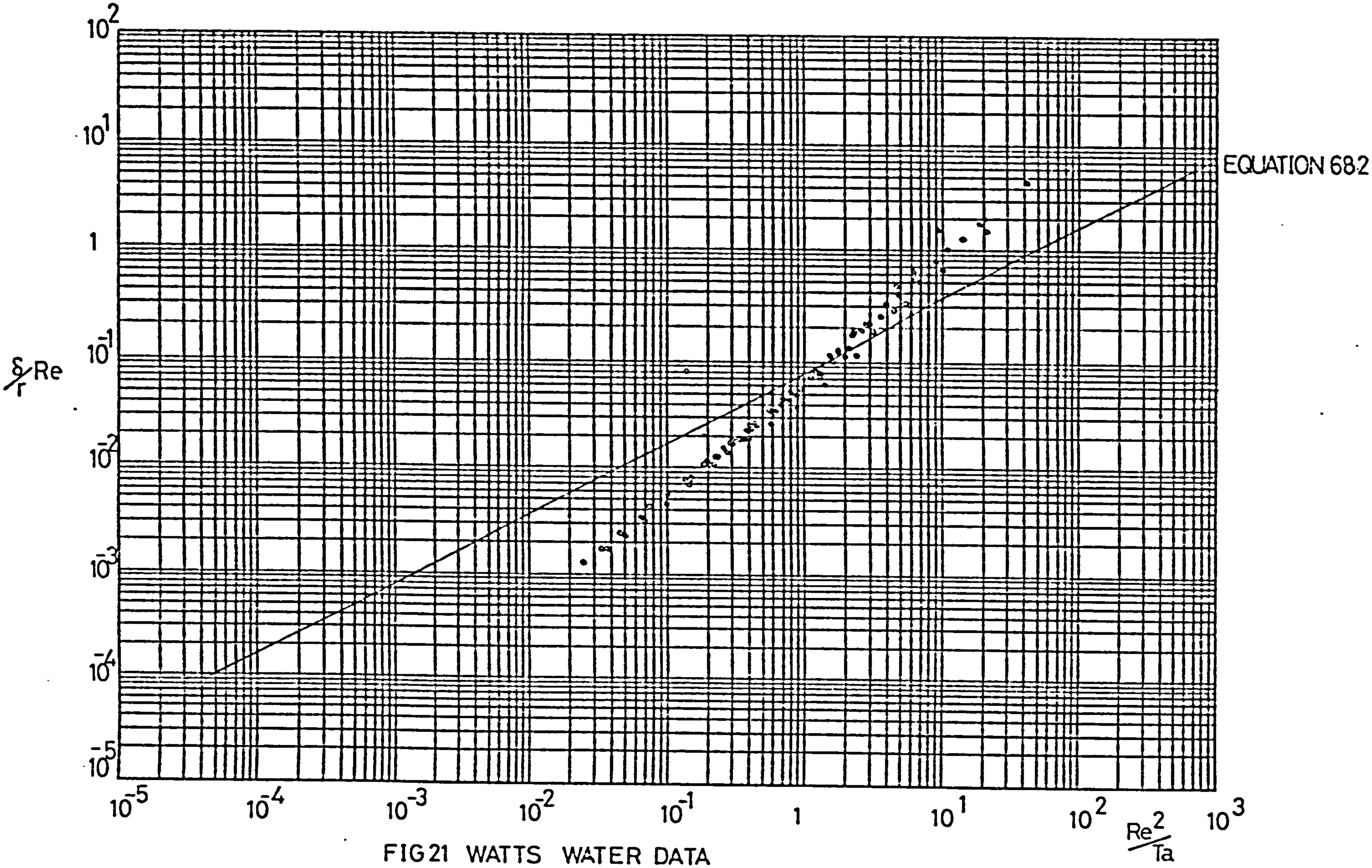

FIG 21 WATTS WATER DATA

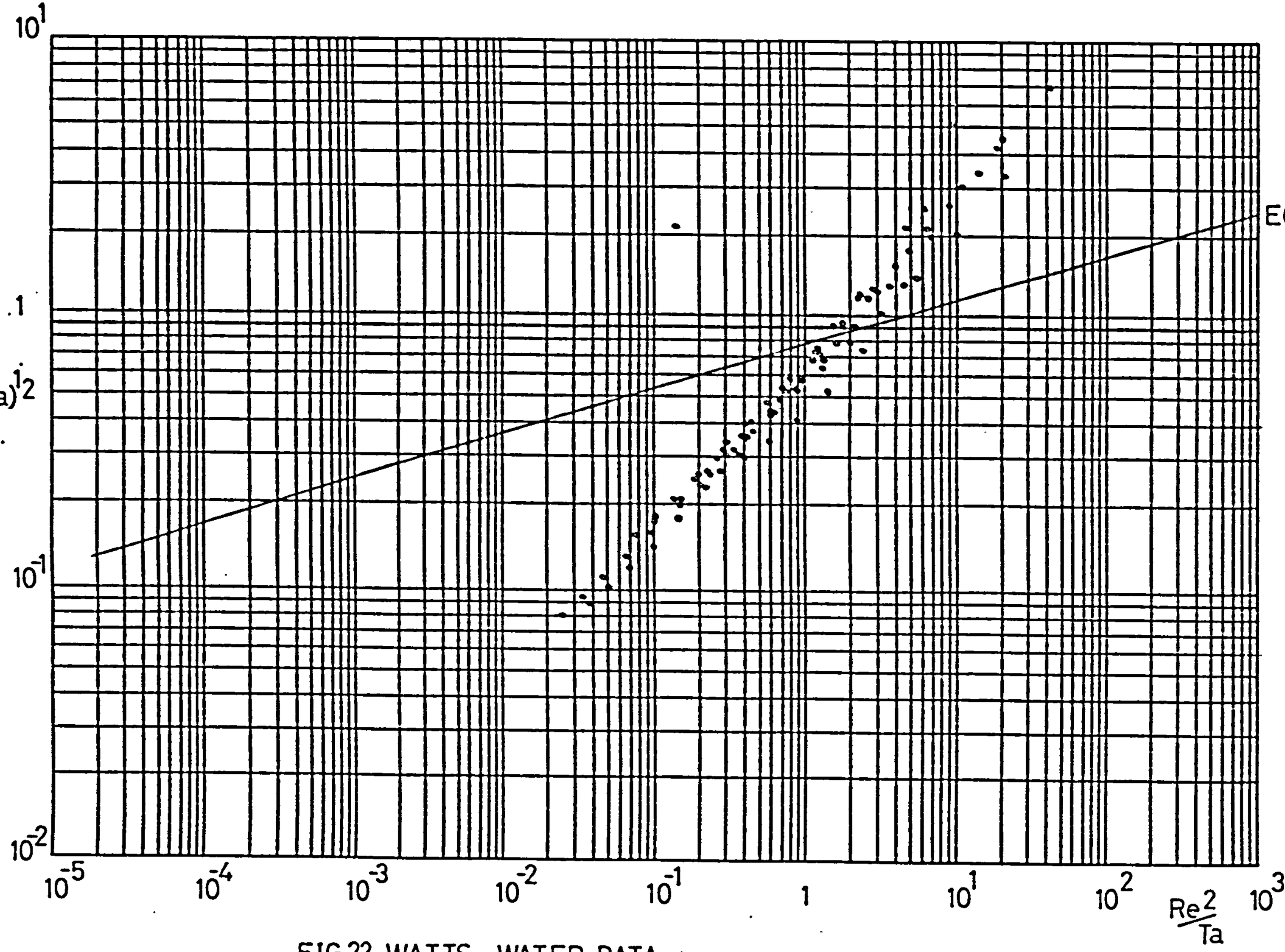

FIG 22 WATTS WATER DATA

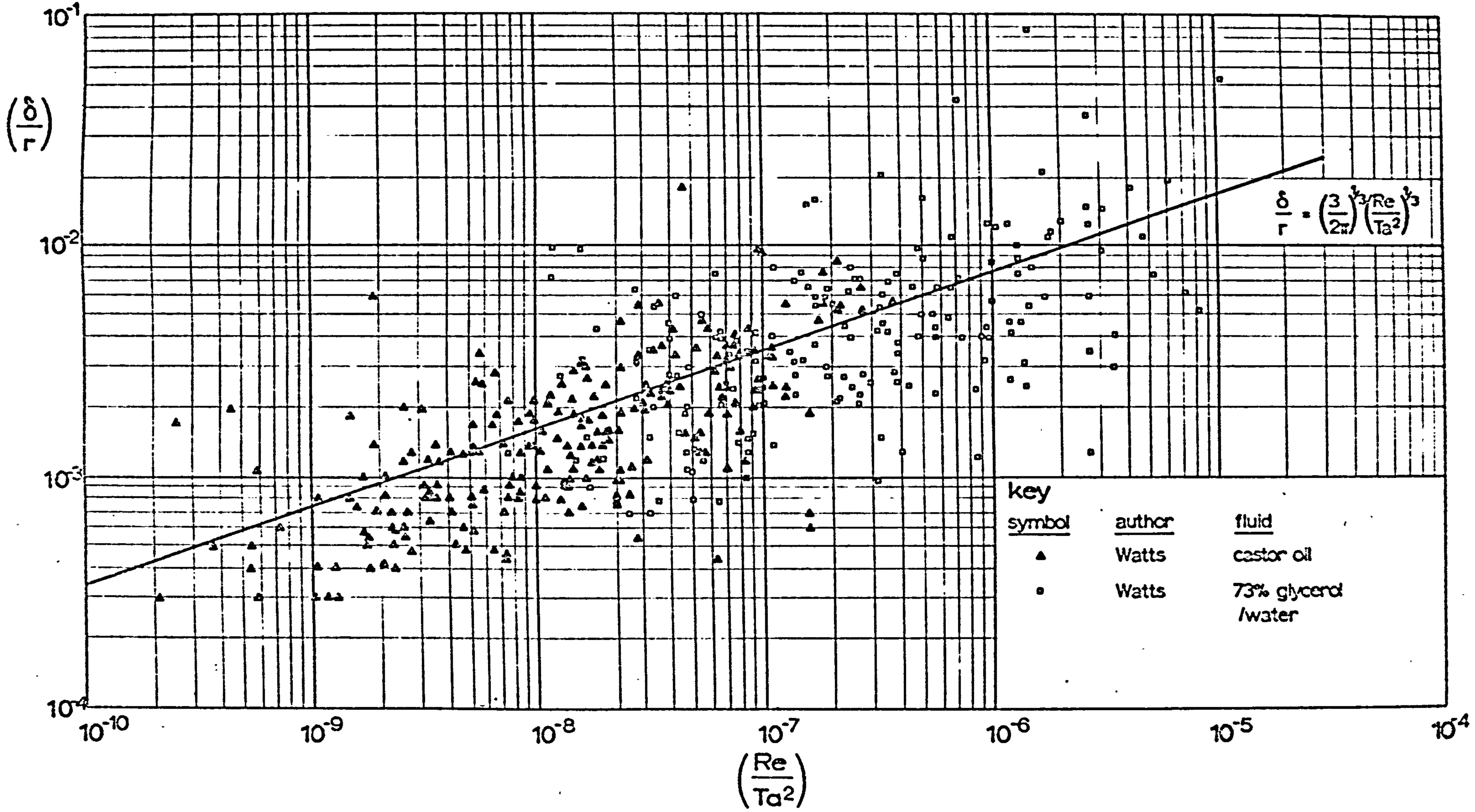

FIG 23 WATTS NON AQUEOUS & VISCOUS FLUIDS

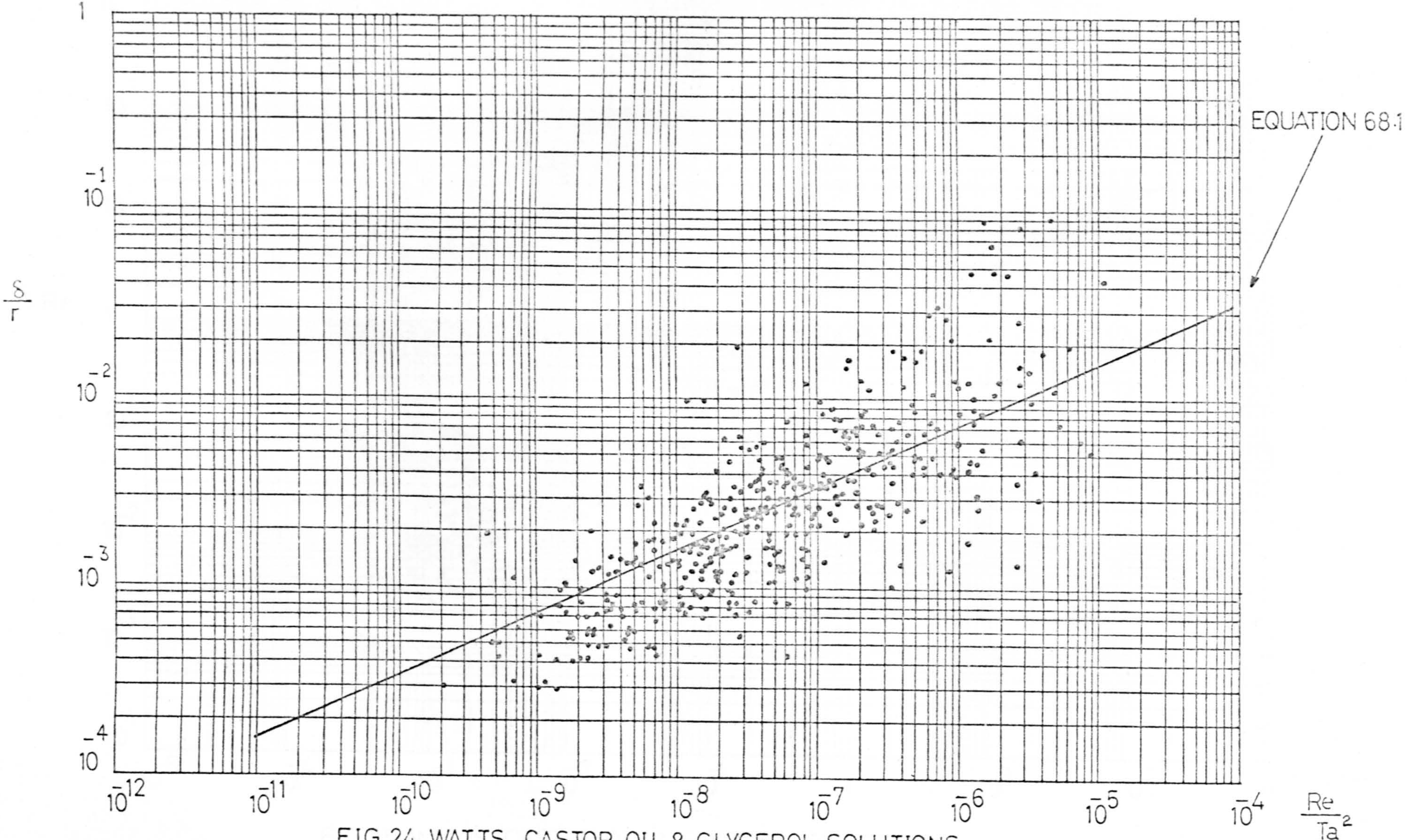

FIG 24 WATTS CASTOR OIL & GLYCEROL SOLUTIONS

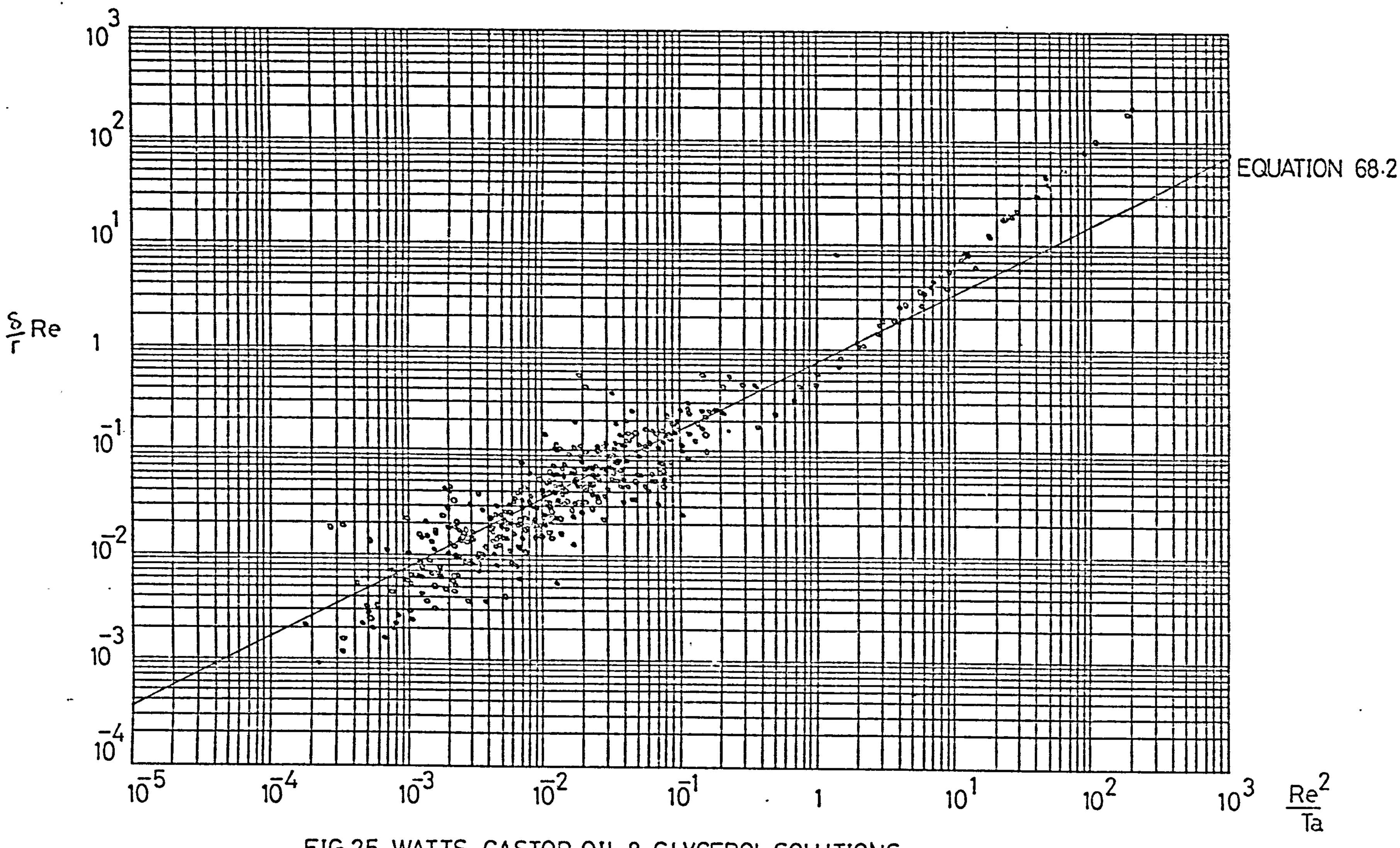

FIG 25 WATTS CASTOR OIL & GLYCEROL SOLUTIONS

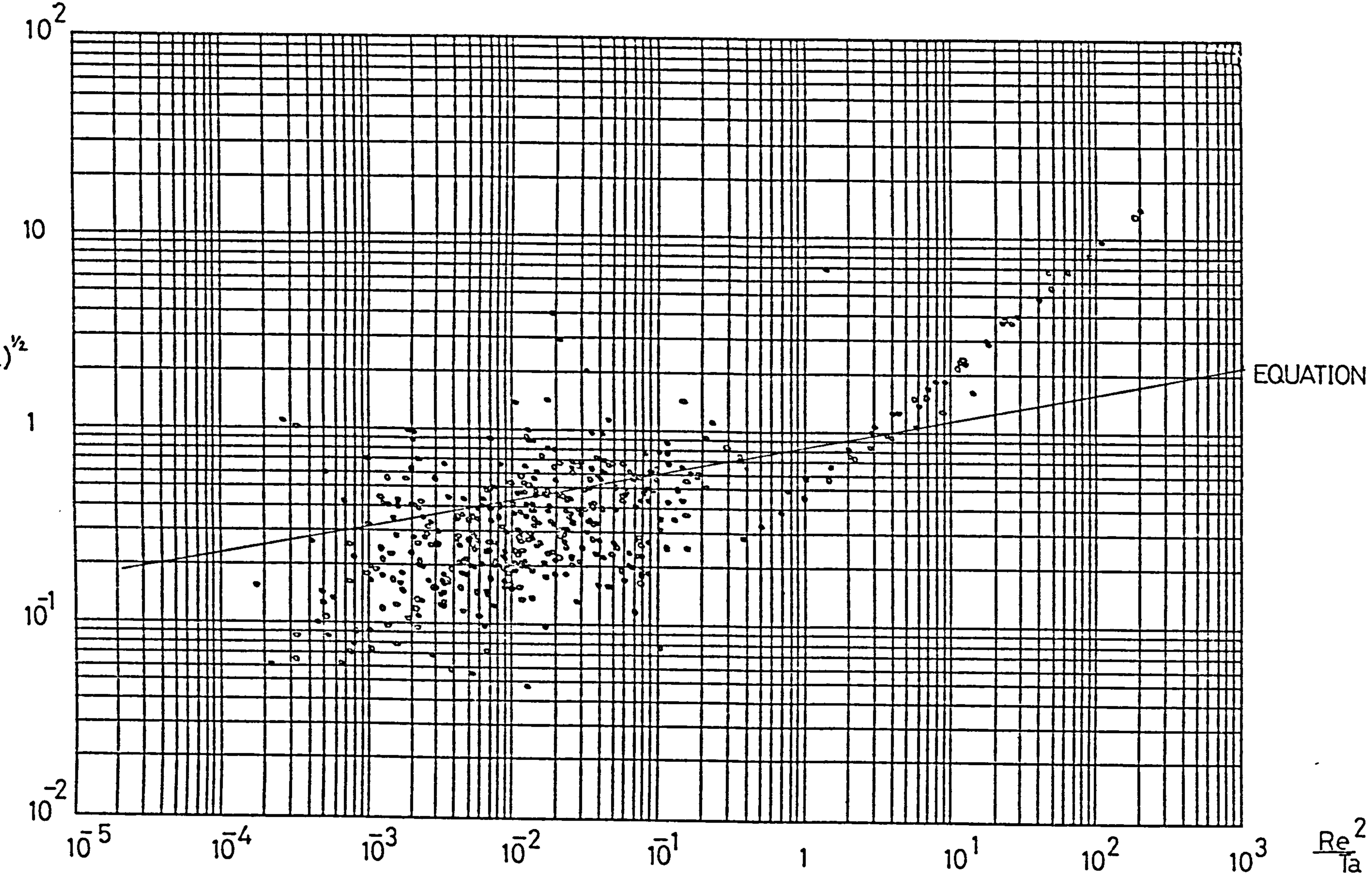

FIG 26 WATTS CASTOR OIL & GLYCEROL SOLUTIONS

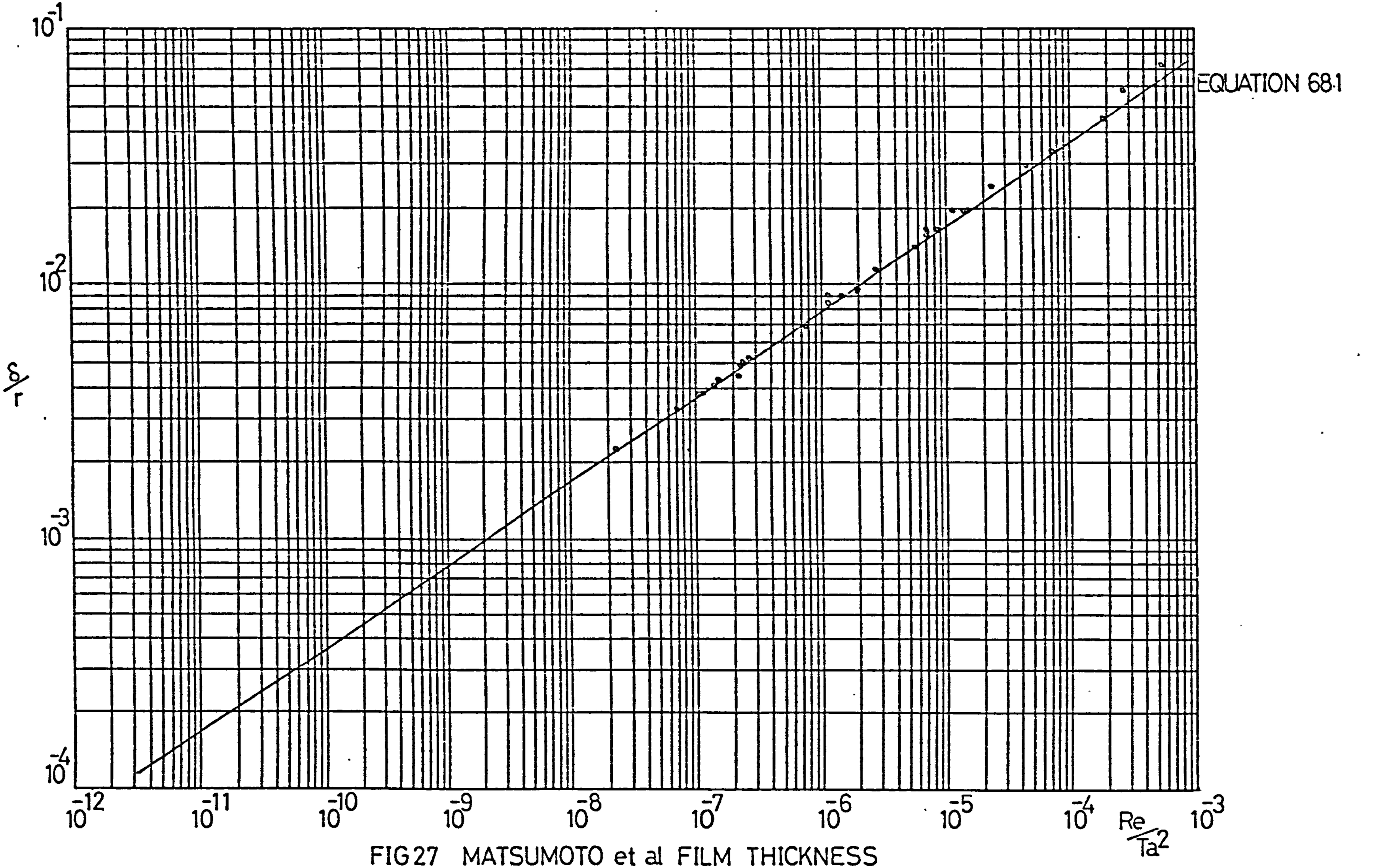

FIG 27 MATSUMOTO et al FILM THICKNESS

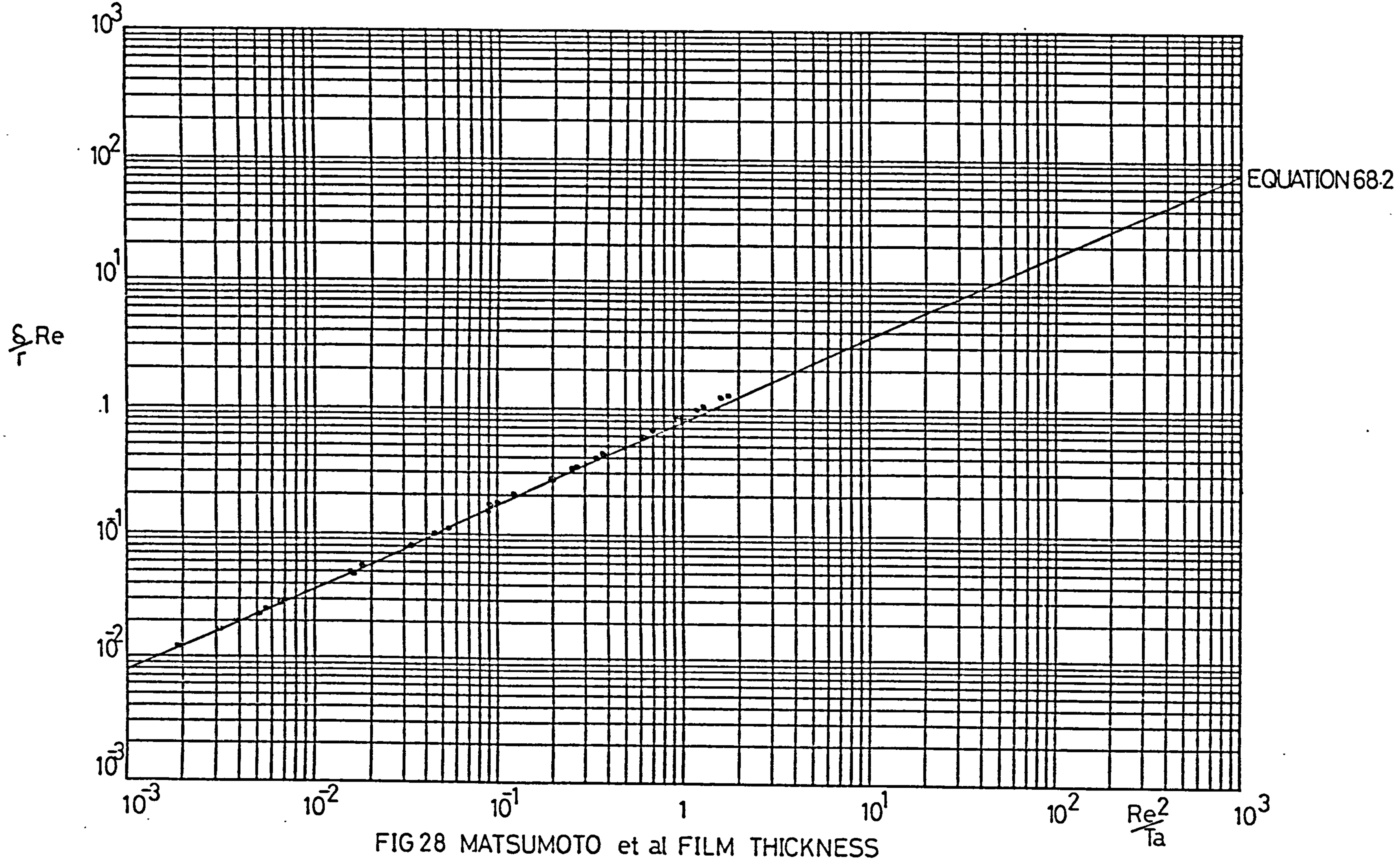

FIG 28 MATSUMOTO et al FILM THICKNESS

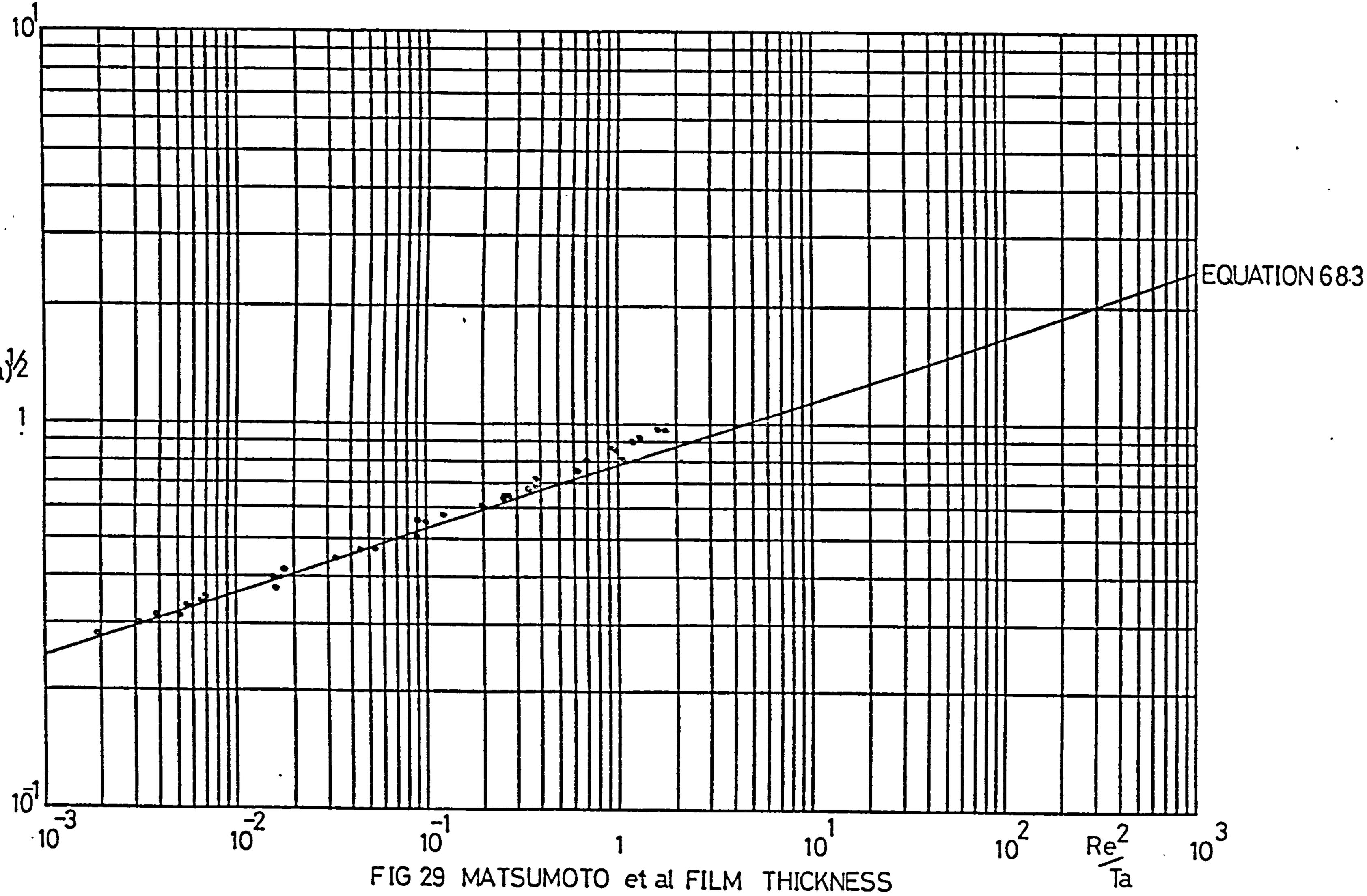

FIG 29 MATSUMOTO et al FILM THICKNESS

behaviour.

VACHAGIN and NIKOLAEV (126) studied the film flow of water over a disc of unstated diameter at a maximum speed of 2500 r.p.m. Poppy grains were mixed with the fluid and high speed photographs taken of the film. The average radial velocity at a given radius was thus found, from which the radial distribution of thickness may be calculated. The data is shown against the centrifugal model in FIGURES 13, 30, 31 and 32. Close agreement to the theoretical model can be seen.

Non-Newtonian flow on a rotating disc has been investigated experimentally by ZINNATULLIN et al (121, 126). In reference 121 thickness is measured by the micrometer probe/electrical contact method, in reference 126 by high speed filming of the average point value of the radial velocity (particles not stated). A 2% solution of polyacrylamide in water was investigated (K = 45.5 dyne sec^n/cm^2 and n = 0.535) in reference 121, and in reference 126 a 2.5% aqueous solution of carboxymethylcellulose for which K = 3.1 dyne sec^n/cm^2 and n = 0.67. The results are compared to the theoretical centrifugal model for a power law fluid (equation 72.2) in FIGURE 33. Also shown in FIGURE 33 is the previously considered data for water ($K \equiv \mu$, n = 1). It will be seen that the non-Newtonian data fits the model closer than the Newtonian water data. One possible explanation for this behaviour could be that the non-Newtonian fluid, consisting of long polymer molecules in water, exhibits strong surfactant like behaviour, and hence the flow is more stable to any disturbances present. VACHAGIN and NIKOLAEV (145) have, apparently, developed an analytical description of the flow on a cone of variable half angle with Coriolis force taken into account. Some data is reported for flow on discs (some 17 values) and comparison within the tabular entries indicates good agreement to the theoretical and experimental values. The results have not been considered further, however, since the fluid viscosity has not been stated and an English translation is not available at this time.

The various experimental system parameters considered by the investigators reported are summarised in TABLE 3.

B: VELOCITY MEASUREMENTS

On the rotating disc, two major directions for flow exist, radial and azimuthal. As reported in the previous section WATTS and VACHAGIN and NIKOLAEV have measured average radial velocities at a point on the disc.

TABLE 3 SUMMARY OF PREVIOUS WORK

INVESTIGATOR	REYNOLD	TAYLOR $\times 10^{-3}$	SPEED	FLOW	DISC RADIUS	FLUID	INLET TYPE	δ METHOD	POINTS	USED	REF.
			R.P.M	CM^3/S	CM						
HICKMAN	NS	NS	NS	NS	NS	WATER	NS	3	34	NONE	3
ESPIG ESPIG & HOYLE	10 – 1180	15 – 540	100 – 2000	0·6 – 24	19	WATER	1	2	39	39	141 108
GAZLEY & CHARWAT CHARWAT et al	6 – 1800	7 – 650	60 – 1080	0·3 – 13	14	WATER SURF.	1	3	162	162	142 143
VENKATARAMAN	0 – 300	30 – 190	300 – 1500	1·2 – 18	12.7	WATER	1	1	108	108	120
CLARE & JEFFS	150 – 4200	30 – 200	0 – 3000	12 – 163	10·1	WATER $CaCl_2$	2	4	182	182	135
MATSUMOTO et al	2 – 108	17 – 200	200 – 9000	5 – 30	12.7	WATER ? ?	2	2	35	35	129
VACHAGIN & NICHOLAEV	50 – 320	48 – 326	0 – 2500	2·4 – 24	7.2	WATER	1	5	17	17	126
ZINNATULLIN	3 – 2700	9 – 300	430 – 1150	0·2 – 40	6·5	WATER 2% PAC	1	2	34	34	121
ZINNATULLIN et al	2 – 3000	8·4 – 160	400 – 1200	0·2 – 40	6·5	WATER 2·5% CMC	1	5	27	27	127
WATTS	20 – 3000	1 – 5000	500 – 1500	60 – 180	30	VARI.	1	5	270	270	115

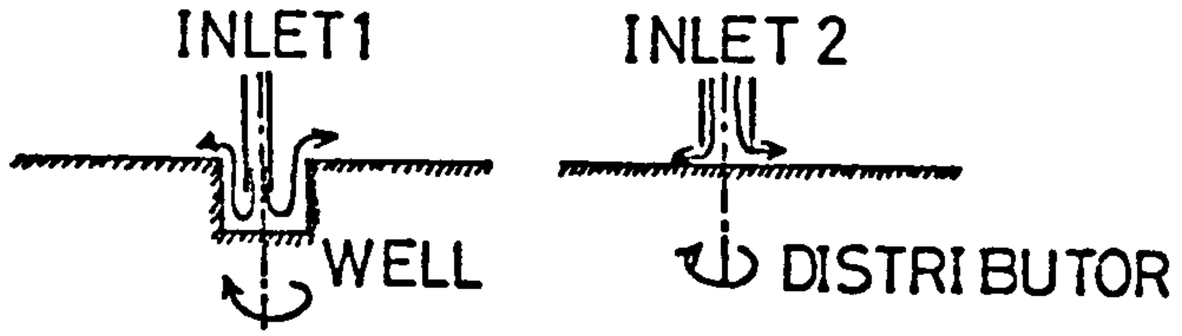

δ METHOD

1 MICROMETER
2 " " " " + ELECT. SENSING
3 PHOTODENSIMETRIC
4 ELECT RESISTANCE
5 AVERAGE VELOCITY

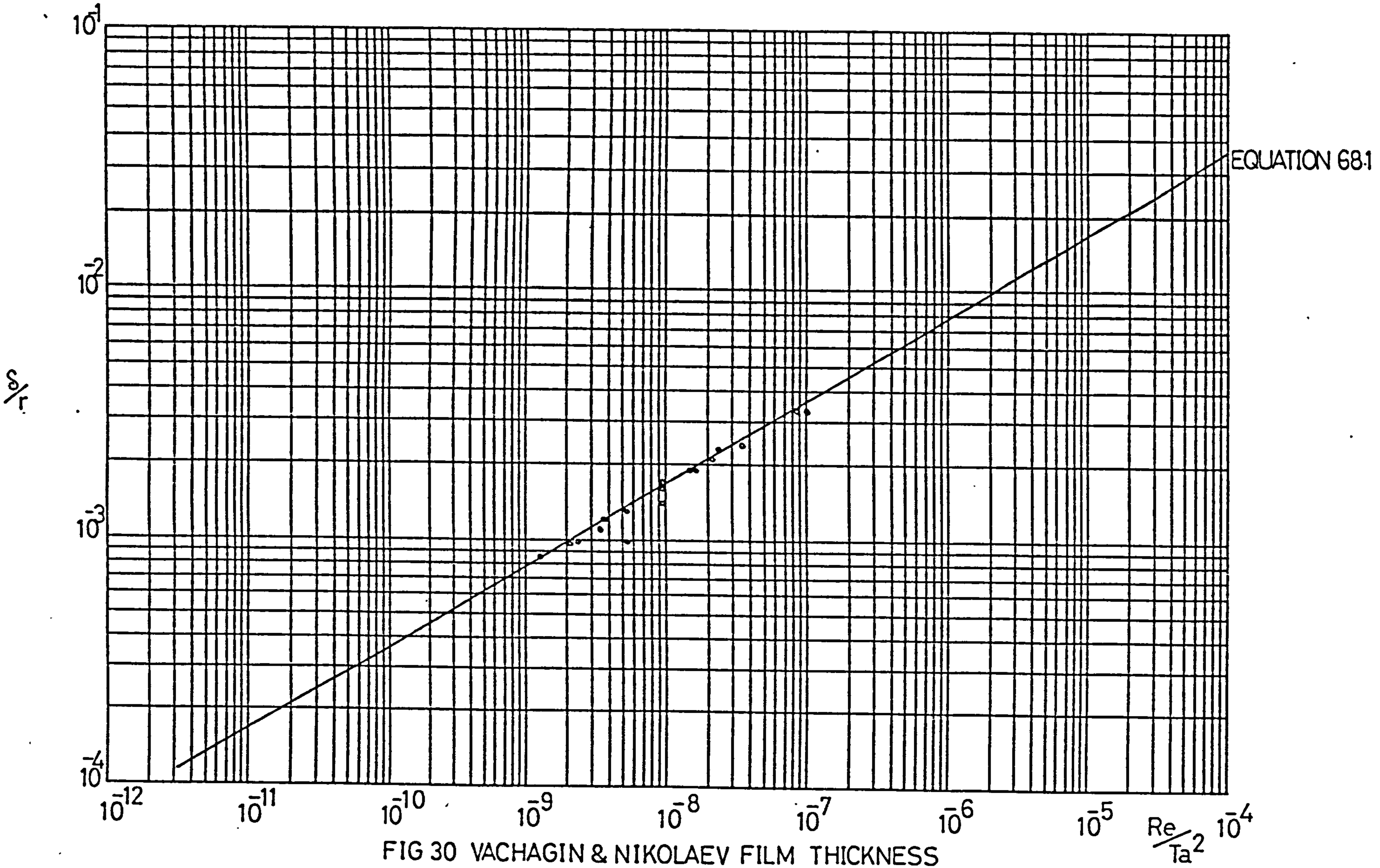

FIG 30 VACHAGIN & NIKOLAEV FILM THICKNESS

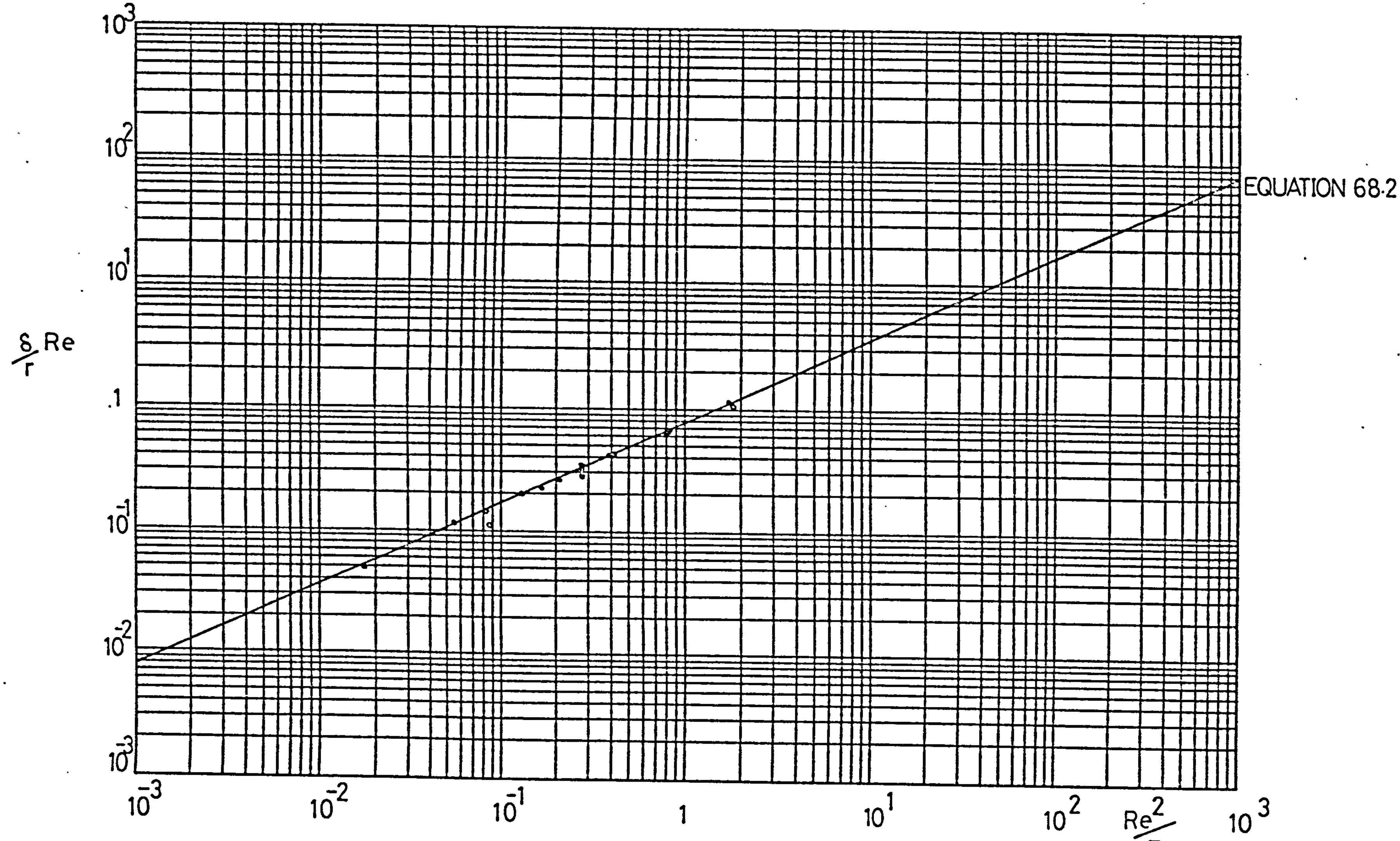

FIG 31 VACHAGIN & NIKOLAEV FILM THICKNESS

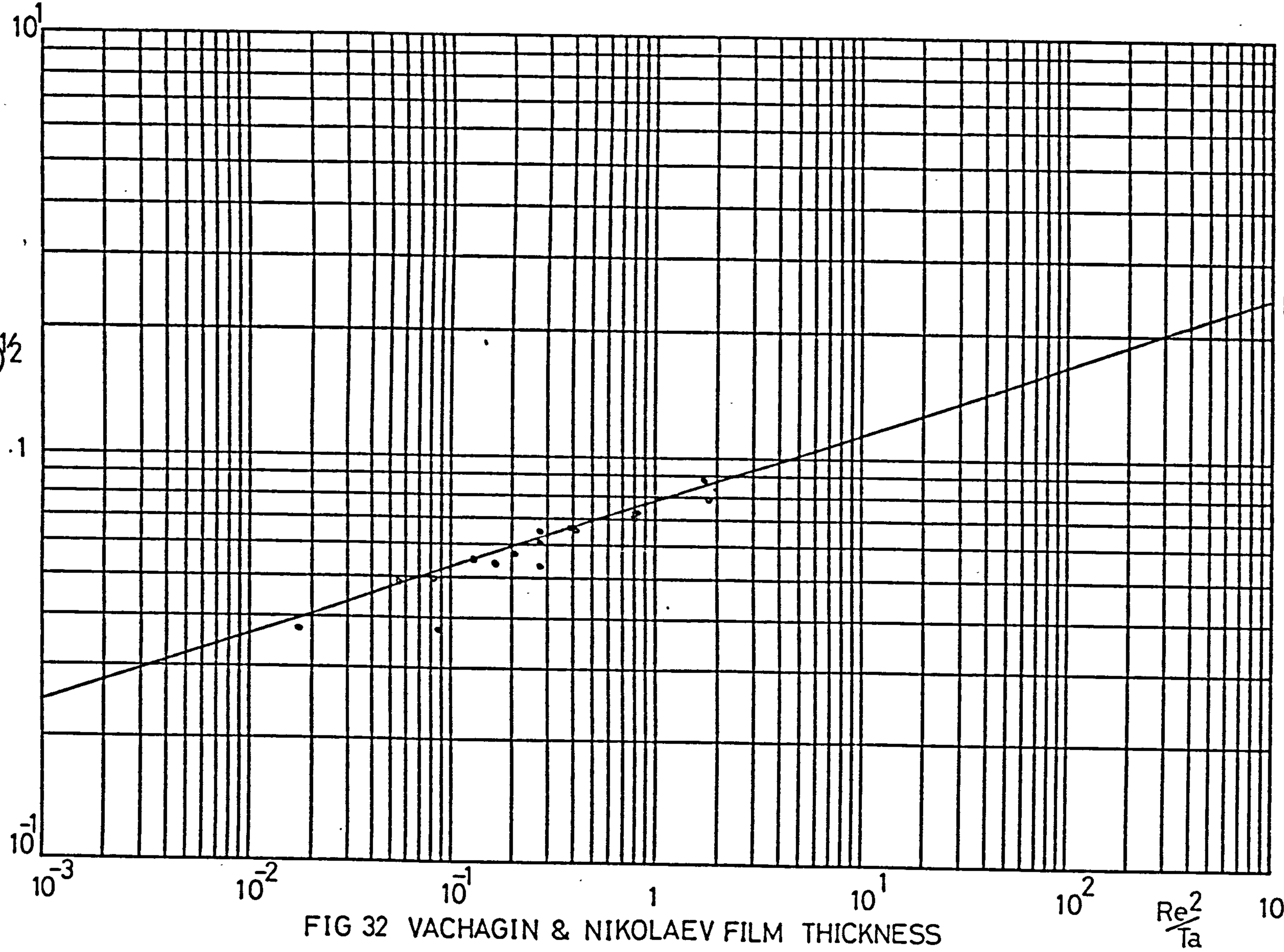

FIG 32 VACHAGIN & NIKOLAEV FILM THICKNESS

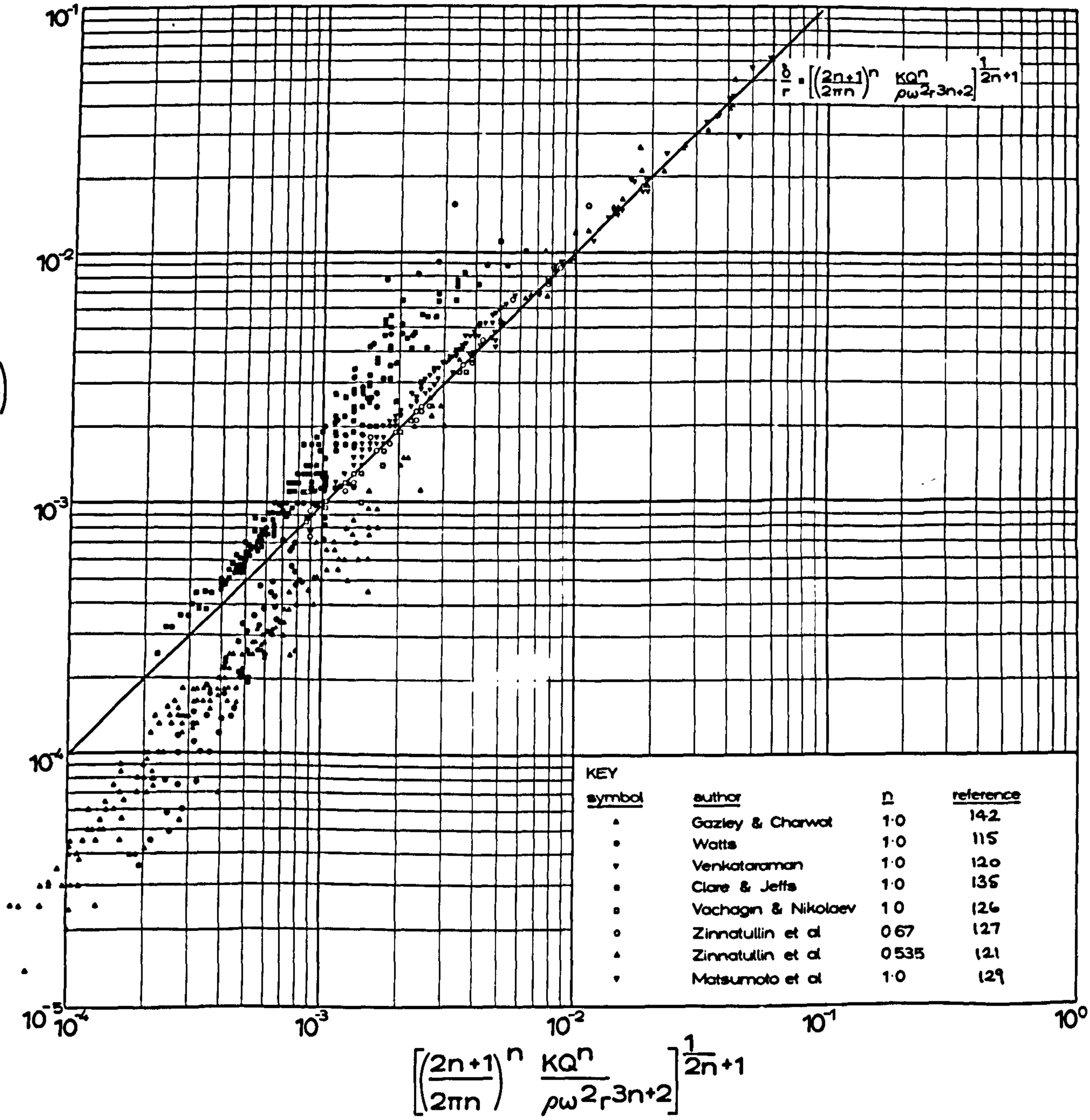

FIG 33 POWER LAW CORRELATION

VENKATARAMAN (120) measured the photographic displacement of fine aluminium particles introduced onto the film surface and obtained the dependency

$$U_{rs} \propto Q^{2/3} \omega^{2/3} \qquad 98$$

The dependency on Q and ω is as predicted by the centrifugal model, but the data was found to be independent of r. The centrifugal model predicts that U_{rs} varies as $r^{-\frac{1}{3}}$. For VENKATARAMAN the radius varied from 2.5 cm to 5.0 cm, which is a significantly smaller variation than that available in Q or ω. Thus the failure to find an experimental dependency upon r could be explained as being due to an insufficient experimental variation of radius.

CHARWAT et al (142) used an elegantly simple technique to check the relative ratio of U_{rs} to $U_{\theta s}$. By touching a pointer to the free surface a wake is developed. The angle of this wake to the radial direction at that point will be given by a simple force consideration as

$$\tan \alpha = \left. \frac{U_\theta}{U_r} \right|_s \qquad 99.1$$

Using the numerical expressions for the first order solutions of U_θ and U_r given by RAUSCHER (equation set 79), then

$$\frac{U_\theta}{U_r} = \left(\frac{1}{3}\right)^{1/3} \left(\frac{Re^2}{Ta}\right)^{1/3} \left[\frac{\eta_b^2 - 2 - 1/4\, \eta_b^3}{1 - \frac{1}{2}\eta_b} \right] \qquad 99.2$$

which gives for the angle of the flow path to the radial

$$\phi = \tan^{-1} \left(C \cdot \left(\frac{Re^2}{Ta}\right)^{1/3} \right) \qquad 99.3$$

when the constant C varies as η ($\equiv y/\delta$) giving C = 1.7334 for $\eta = 1$ (free surface), C = 1.647 ($\eta = 0.5$) and C = 1.337 ($\eta = 0$). Thus although the angle of the wake will depend upon the depth to which the pointer penetrates the film, the variation is not major.

CHARWAT et al found reasonable agreement between equation 99.3 and experimental values measured.

No measurement of velocity profiles in the rotating film has been attempted to date.

C: WAVES

CHARWAT et al (142) have investigated the wave patterns found upon the rotating film. Their qualitative observations are in agreement to ESPIG and HOYLE'S observations. CHARWAT et al note three distinct flow regimes in the 'laminar' flow region,

1) a smooth undisturbed flow

2) concentric ring waves: ring waves which move outward and decay at large radii with the remaining outer portion of flow smooth

3) spiral waves: stationary with respect to disc, opening in a spiral in the direction of rotation. Tend to decay at large radii, but usually break up into a very rough and random pattern of disconnected wedge-like wavelets.

CHARWAT et al found that for water at a fixed speed, increasing flowrate gradually caused the smooth film to form concentric waves and, at higher flowrates, spiral waves formed at greater radii. At a fixed flowrate increasing the rotational speed gradually damped any concentric waves present, formed a smooth film and finally caused spiral waves to form. Results for isopropyl and methyl alcohols showed similar behaviour. It is worth emphasising that the flow/speed parameters considered were small ($0 < Q <$ 8 cc/s, $0 < \omega < 12$ rps). GAZLEY and CHARWAT concluded that the concentric waves were formed by the entry effects of the impinging fluid jet. The authors developed a model for the existence of the spiral waves by considering the boundary layer equation set 74 written with $U_\theta = \omega r$, employing a perturbation expansion and searching for a periodic solution existing as a spiral. Adequate agreement was reported between experimental and model values for the spiral opening angle, that acute angle formed by the radius and crest direction. Further, the model predicted that the radius at which spiral waves would commence to be visible would be primarily correlatable by the group $(Q\omega)$, which was found to be agreed experimentally. The authors were able to measure the amplitude of the spiral waves which was found to increase to a maximum with increasing radius before decaying. The maximum amplitude was some 30 - 50% of the local film thickness and occurred close to the beginning of the wavy flow. The maximum amplitude was correlated against the mean film thickness (as proposed by LILLEHAT and HANRATTY (146) for planar films). A linear correlation was obtained.

It is worth noting that DE GRAAF (147) was unable to form a

completely smooth film for water on a rotating disc, finding instead that the film at the low speeds and flowrates tended to break down into rivulets.

D: FILM BREAKDOWN

The rotating disc exhibits easily observed dry patches at low speeds and flowrates, but with increasing speeds the changes in flow regimes are difficult to observe with any real precision. As already mentioned, CLARE and JEFFS (136) observed an incomplete film at a flowrate of less than some 10 cm^3/s at a speed of 3000 r.p.m., and also noted that little variation in flowrate (order 3 cc/s) was required to cause the film to completely reform over all the disc from a film previously breaking down at low radii. BUTUZOV and RIFERT (148) noted a broken film for $Q < 4$ cc/s in the speed range $95 < \omega < 290$ r.p.m. CHARWAT et al (142) noticed that a very thin film was ruptured apparently by air-borne dust particles settling on the film. For thicker films (say $\delta > 20\mu m$), breakdown could occur spontaneously and was correlatable to the Weber group

$$We = \bar{U}_r \Big/ \left(\frac{\sigma}{\rho\delta}\right)^{1/2} \qquad 100$$

The Weber group was also useful in correlating wave activity and the breakdown mechanism could be similar to that shown by PADDY (see Section 2.1.1:G) in which surface waves on the film cause such local thinning that spontaneous rupture occurs in the wave troughs. It appears from CHARWAT et al's work that the minimum film thickness supportable by a clean disc is of order 10 - $15\mu m$.

E: TURBULENCE

Due to the extreme thinness of the film and the difficulty of observing motion relative to the disc on a rapidly rotating disc, the transition from laminar to turbulent film flow is very imprecise. Doubtlessly, DUCKLER'S (31) view, that turbulence will build smoothly at some mid-portion of the film until at a higher value of the turbulence forcing group (i.e. increasing Re say) turbulence will be spread throughout the film, is correct. With this view there will be no sharply defined transition from laminar to turbulent flow as shown by full tube flow, for instance.

As already reported, CLARE and JEFFS (135) concluded that the controlling parameter for turbulent flow is the group Re, laminar flow exhibited for Re < 2000 - 6000. YURCHENKO et al however (124) showed that the group (Re Ta) controlled the onset of interfacial mixing of a two layer film. YURCHENKO et al concluded that this mixing marked the onset of turbulence. The critical value found was

$$(Re\ Ta) = 3 \times 10^{8} \qquad 101.1$$

RIFERT (149) concluded that deviations in heat transfer measurements to a rotating evaporating film was explainable in terms of film interfacial turbulence and that the turbulent criteria was

$$(Re\ Ta) = 5.1 \times 10^{8} \qquad 101.2$$

The evidence for turbulent flow or otherwise requires greater investigation.

F: INTERFACIAL DRAG

The various models considered have neglected certain phenomena, such as interfacial shear, surface tension etc, which are strictly bound to effect the models' formulation.

The addition of interfacial shear to the centrifugal model was shown by CHARWAT et al to be negligible if the air/water interface drag could be represented by the classical drag of an air flow induced by a rotating disc. From SCHLICTING (150), the air/solid surface drag is given by

$$\tau_o = \mu_a (0.510\ \omega r)\left(\frac{\omega}{\nu_a}\right)^{1/2} \qquad 102.1$$

(all physical properties of air)

CHARWAT et al deduced the expressions

$$U_{rs} = \frac{\omega^2 r \delta^2}{2\nu} + \delta\left(\frac{\mu_a}{\mu_L}\right)(0.510\ \omega r)\left(\frac{\omega}{\nu_a}\right)^{1/2} \qquad 102.2$$

and

$$\frac{\delta}{r} = \left(\frac{3}{2\pi}\right)^{1/3}\left(\frac{Re}{Ta^2}\right)^{1/3} - 0.255\left(\frac{\rho_a}{\rho_L}\right)\left(\frac{1}{Ta}\right)^{1/2}_{air} + O\left(\frac{\mu_a}{\mu_L}\right)^2 \qquad 102.3$$

From equation 102.3 it can be seen that the effect of induced air flow is to create a thinner film. Typical corrections are small, of

the order of 1 - 2% for most practical purposes. Equations 102.2 and 102.3 are derived assuming that the liquid/air interface is stationary. In fact the liquid is moving and so the film correction should probably be greater, that is the film is thinner still. No work has been performed allowing for interfacial drag on a rotating film with a moving interface. GAY (151) has studied drag on planar water films and concluded that up to a water velocity of 1 cm/s no alteration of the drag occurred compared to that experienced by a solid interface. Thus the additional corrections are likely to be very small.

2.4. THEORETICAL

A: CORIOLIS MODEL

The partial differential equations taken as representative of the Coriolis model will be

$$\nu \frac{\partial^2 U_r}{\partial y^2} = - \frac{U_\theta^2}{r} \qquad 103.1$$

$$\nu \frac{\partial^2 U_\theta}{\partial y^2} = 2 \frac{U_\theta U_r}{r} \qquad 103.2$$

Note that the second equation is strictly only equal to the true boundary layer azimuthal equation (equation 73.2) if $U_\theta = ar$ when a is some constant. This approximation was made, however, to reduce the non-linearity of equation 73.2.

Non-dimensional equation set 103 using the following substitutions

$$U = \frac{U_r \delta^2}{\nu r} \qquad Y = \frac{y}{\delta} \qquad V = \frac{U_\theta}{\omega r}$$

Then the equations become

$$\frac{\partial^2 U}{\partial Y^2} = - \left(\frac{\delta}{r} (Ta)^{1/2} \right)^4 V^2 \qquad 104.1$$

$$\frac{\partial^2 V}{\partial Y^2} = 2UV \qquad 104.2$$

The appropriate boundary conditions are

at the disc surface

$$y = 0 \quad U_\theta = \omega r \quad U_r = 0$$

$$Y = 0 \quad V = 1 \quad U = 0 \qquad 105.1$$

and at the free surface

$$y = \delta \quad \frac{dU_\theta}{dy} = \frac{dU_r}{dy} = 0$$

$$Y = 1 \quad \frac{dU}{dY} = \frac{dV}{dY} = 0 \qquad 105.2$$

The continuity equation is

$$Q = \int_o^{\delta} 2\pi r\, v_r dy = \int_o^{1} 2\pi r \left(\frac{\nu r U}{\delta^2}\right)(\delta dY) = \frac{2\pi r^2 \nu}{\delta^2}\int_o^{1} U dY$$

$$\text{or} \qquad \frac{1}{2\pi}\left(Re\,\frac{\delta}{r}\right) = \int_o^{1} U dY \qquad 106$$

Notice that the two groups uniquely defined by the model are $\frac{\delta}{r}(Ta)^{\frac{1}{2}}$ and $\frac{\delta}{r}Re$. Rearrangement of these groups gives the equivalent groups $\frac{\delta}{r}.(Ta)^{\frac{1}{2}}$ and $\frac{Re^2}{Ta}$.

Solution of equation set 104 subject to the boundary conditions 105 was obtained using two techniques. It will be seen that equations 104 need to be solved simultaneously and the most convenient method of performing the iterations required is by an analogue method. The analogue solution was performed on the Department's EAL HYBRID 48 analogue computer and the circuit diagram is given in FIGURE 34. Multipliers 1 and 2 prepare the right hand side of equation 104.1 for integration by integrator 3. The initial condition on dU/dY required in integrator 3 is set at 0. Integrator 8 integrates the output of 3 with the initial U condition U(0) = 0 (or ground). The right hand side of equation 104.2 is prepared by multiplier 12 from integrator 8's output and the current value of V. Integrator 13 produces dV/dY with dV/dY(0) = 0 for the initial guess and integrator 18 produces V with the initial condition V(0) = 1 (set as -1 V). At the end of the first COMPUTE period track stores 7 and 17 switch from TRACK to HOLD and the difference between the values U'(1) and V'(1) (when ' ≡ d/dY) and the desired boundary condition (zero) is followed by track stores 6 and 16 respectively. During the next COMPUTE period integrators 4 and 14 pass a proportion (depending upon the setting of potentiometers 5 and 15) of the previous COMPUTE periods error in U' and V' at Y = 1 to the initial condition for integrators 3 and 13 respectively.

The system continues to pass through COMPUTE/RESET cycles until the error in the value (U'(1) - 0) and (V'(1) - 0) as indicated by the track store memory pairs 6/7 and 16/17 becomes zero. When this occurs each integration cycle produces the same distributions for U and V and the solution has converged. The rate of this convergence is governed by the values of potentiometers 5 and 15. The profile of U is integrated by integrator 9 with two track stores 10 and 11 providing a steady display of the previous COMPUTE integration during each current COMPUTE cycle.

The flexibility of the analogue solution method is obvious from

FIG 34 ANALOG CIRCUIT

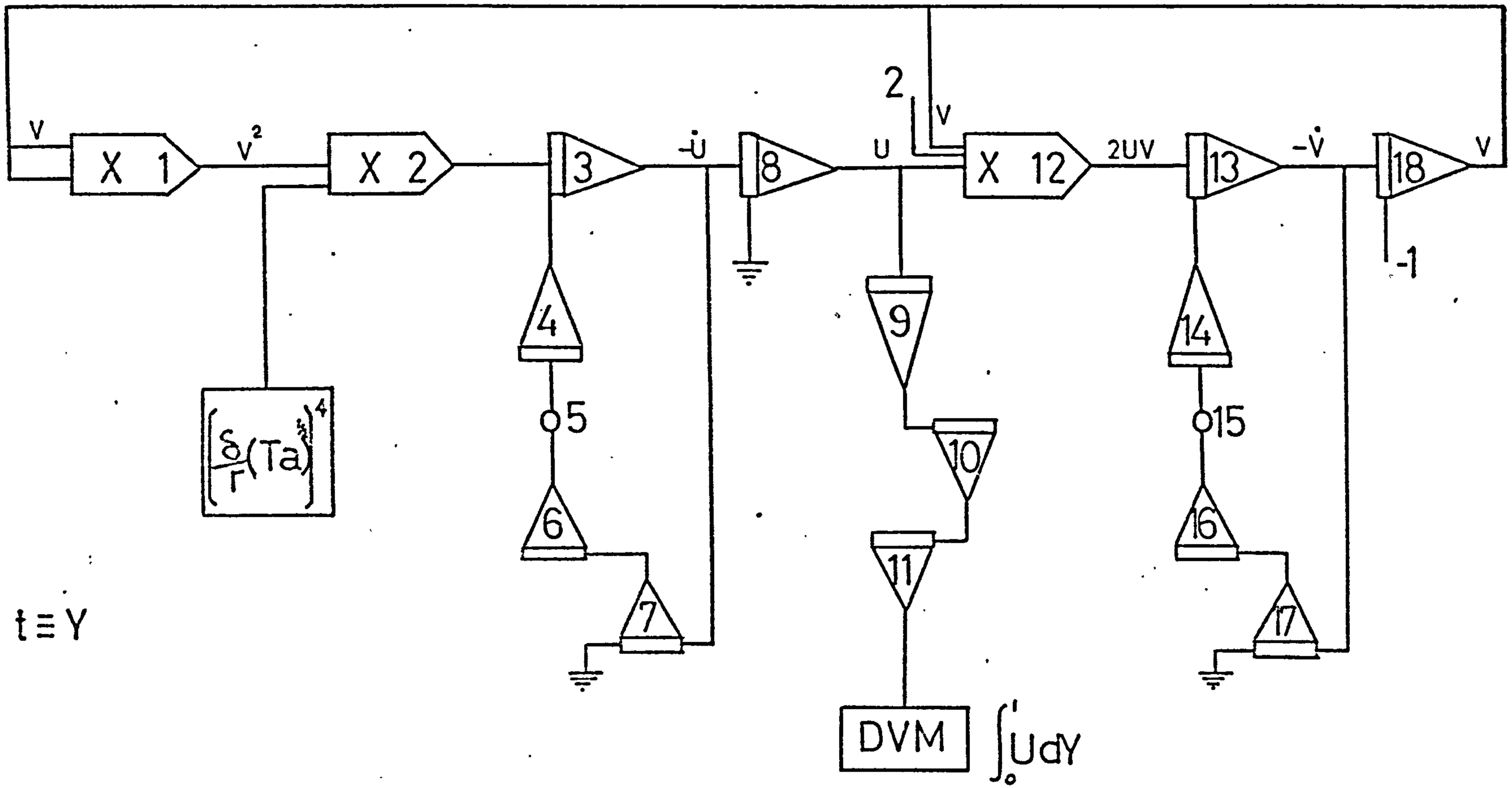

FIGURE 34. By adjusting the 2 input to multiplier 12 other values of the Coriolis influence may be investigated. By reducing the multiplier of multiplier 12 from two to zero the feed back value of V to the start of the computing chain is always -1 (V = 1 or $U_o = \omega r$) which corresponds to the boundary conditions of the centrifugal model considered earlier. Thus several differing analytical models may be studied with only slight modification to the basic circuitry shown. When the multiplier was set to zero as indicated above agreement within 1% to the analytical solution of the centrifugal model was obtained. Note the calculations of potentiometer and time constant settings have not been shown.

The circuit input consists of setting a value of $(\frac{S}{r} Ta)^{\frac{1}{2}})^4$ on one potentiometer and the resulting output voltage displayed on the voltmeter represents $\int_o^1 UdY$ or $\frac{1}{2\pi} \frac{S}{r}$ Re. From these measurements conjugate values of Re^2/Ta, $\frac{S}{r} (Ta)^{\frac{1}{2}}$ and $\frac{S}{r}$ Re may be calculated. Velocity profiles were also produced on a graph plotter linked to the velocity integrators directly.

In order to check the accuracy of the analogue solution, a digital solution was performed on the IBM 360 computer. The program used is listed in APPENDIX G: PROGRAM CORIOL. The program was found to be stable only to a value of Re^2/Ta of about 10. Extension of this limit would have required considerable reprogramming which in view of the match with the analogue solution where contiguous (error of 5% at worst) seemed unwarrented.

Typical velocity profiles are shown in FIGURE 35 and values of (Re^2/Ta) and $(\frac{S}{r} Re)$ are tabulated in TABLE 4. FIGURE 37 (later) shows a comparison of the analogue solution to the centrifugal model.

B: GENERAL MODEL

By use of non-dimensional groupings and similarity transformations the partial differential equation set 48 considered earlier may be reduced to the ordinary differential equation set 52, viz.

$$F'' = F^2 - G^2 + HF' \qquad 52.1$$

$$G'' = 2FG + HG' \qquad 52.2$$

$$H' = -2F \qquad 52.3$$

when $F = \frac{U_r}{\omega r}$, $G = \frac{U_\theta}{\omega r}$ and $H = \frac{U_y}{(\omega \nu)^{\frac{1}{2}}}$

TABLE4 THEORETICAL MODELS FILM THICKNESS COMPARISON

$\frac{Re^2}{Ta}$	$\frac{\delta}{r}Re$			
	centrifugal model eqn 60.2	CORIOLIS MODEL		GENERAL SOLUTION**
		analogue*	digital	
0.001	0.007819	0.0079	0.00786	0.0078
0.01	0.03628	0.036	0.0366	0.0364
0.06	0.1198	0.126	0.122	0.132
0.1	0.1684	0.17	0.1721	0.172
0.6	0.556	0.56	0.591	0.596
1.0	0.7816	0.78	0.851	0.862
6.0	2.581	3.5	–	3.72
10.0	3.628	5.33	–	6.69
60.0	11.98	28.2	–	–
100.0	16.84	45.97	–	–

* interpolated

** formed from program SIM output

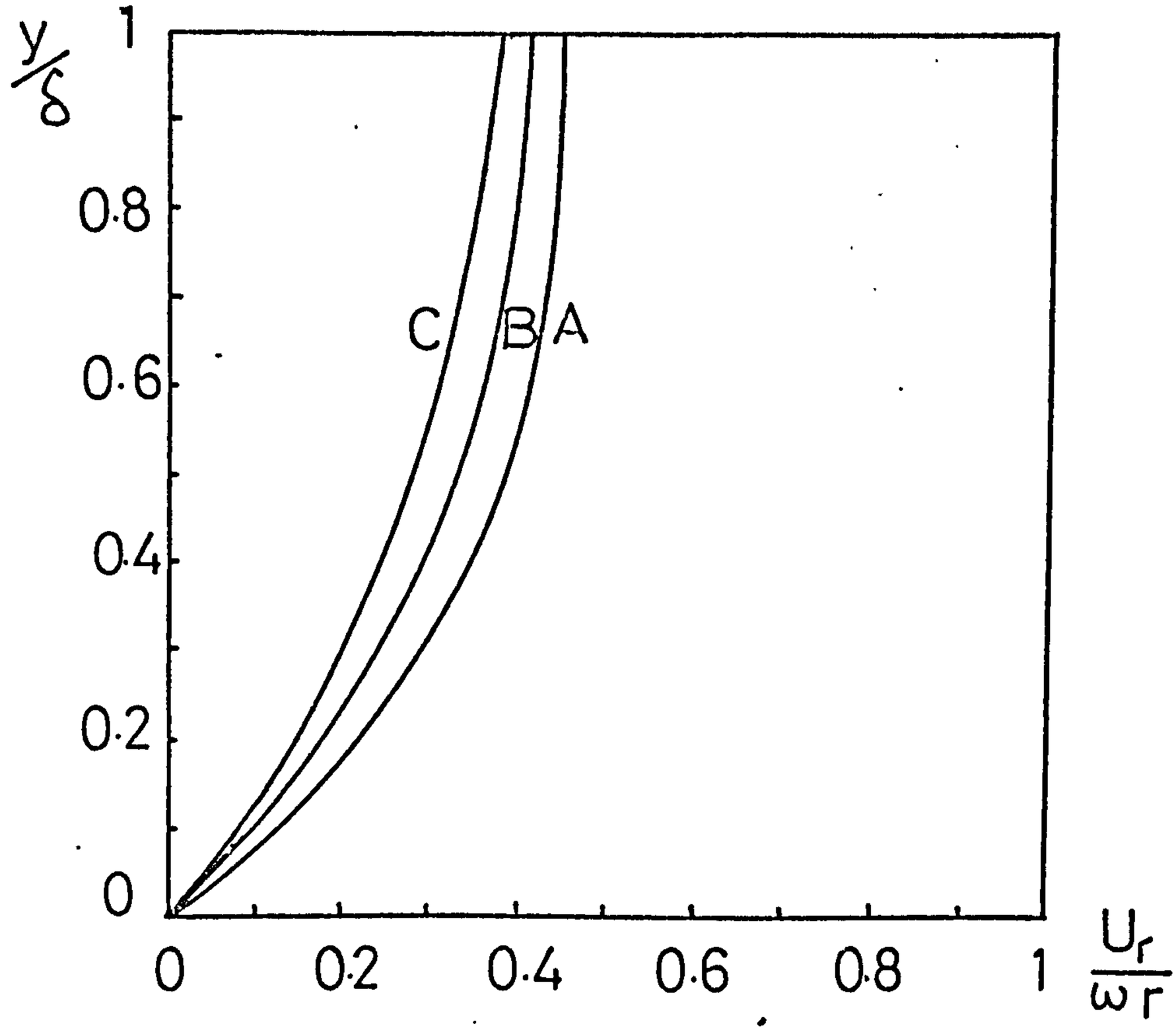

FIG 35 ANALOGUE SOLUTION

VELOCITY PROFILES

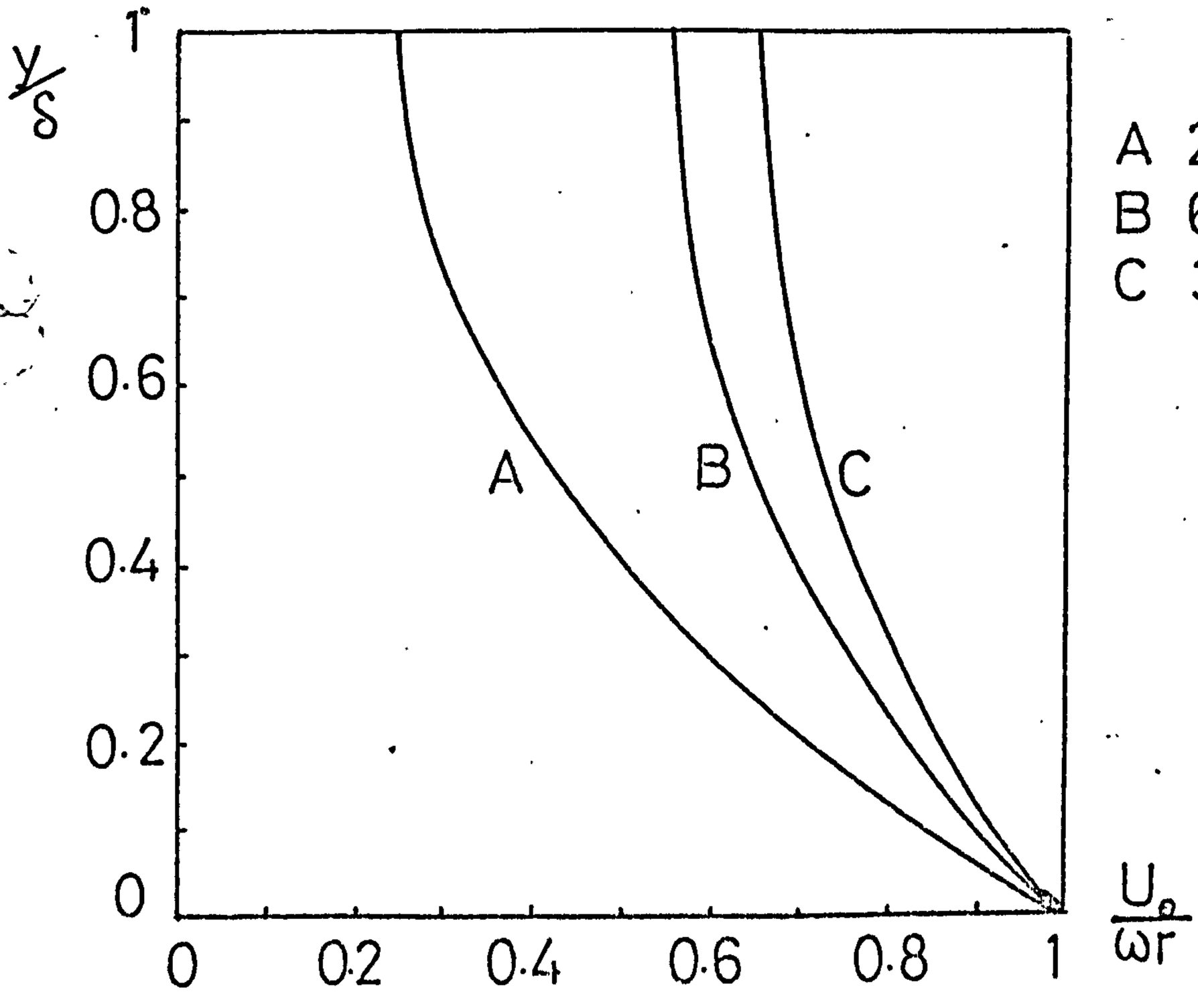

and the prime (') denotes differentiation with respect to ζ , when $\zeta = \left(\frac{\omega}{\nu}\right)^{1/2} y$.

The appropriate boundary conditions to equation set 52 are

at the disc $y = 0$ $\quad U_r = U_y = 0, \quad U_\theta = \omega r$

$\zeta = 0$ $\quad F = H = 0 \quad G = 1$

and at the free surface $y = \delta, \ \frac{du_r}{dy} = \frac{du_\theta}{dy} = 0, \quad Uy = -C$

$\zeta = \frac{\delta}{r} (Ta)^{1/2} \quad F' = G' = 0 \quad H = -D$

REES (131) obtains a value for D, the downward velocity at the free surface, as follows:

from the definition of F and ζ ,

$$\int_0^{\delta(\frac{\omega}{\nu})^{1/2}} F d\zeta \equiv \int_0^{\delta} \frac{u_r}{\omega r} \left(\frac{\omega}{\nu}\right)^{1/2} dy = \frac{1}{(\omega\nu)^{1/2} r} \int_0^{\delta} u_r \, dy \qquad 107.1$$

but from the continuity considerations

$$\int_0^{\delta} u_r dy = \frac{Q}{2\pi r} \qquad 107.2$$

hence, from equation 107.1

$$\int_0^{\delta(\frac{\omega}{\nu})^{1/2}} F d\zeta \equiv \frac{Q}{2\pi (\omega\nu)^{1/2} r^2} \qquad 107.3$$

Integrating equation 52.3 between $\zeta = 0$ and $\zeta = \delta \left(\frac{\omega}{\nu}\right)^{1/2}$

$$H\left(\delta\left(\frac{\omega}{\nu}\right)^{1/2}\right) - H(0) = -2\int_0^{\delta(\frac{\omega}{\nu})^{1/2}} F d\zeta = -\frac{1}{\pi}\left(\frac{Re^2}{Ta}\right)^{1/2} \qquad 107.4$$

Since H(0) is zero (from the boundary conditions), then the boundary condition D, the downward velocity at the free surface is

$$H(\text{free surface}) = -\frac{1}{\pi}\left(\frac{Re^2}{Ta}\right)^{\frac{1}{2}} \qquad 107.5$$

In this work the numerical solution method of REES was repeated. Equation set 52 is rewritten with the variables y_i, i = 1, 5, thus

$$y_1 = H \qquad 108.1$$

$$y_2 = F \qquad 108.2$$

$$y_3 = G \qquad 108.3$$

$$y_4 = F' \qquad 108.4$$

$$y_5 = G' \qquad 108.5$$

and equation set 52 becomes

$$y_4' = y_2^2 - y_3^2 + y_1 y_4 \qquad 109.1$$

$$y_5' = 2y_2 y_3 + y_1 y_5 \qquad 109.2$$

$$y_1' = -2y_2 \qquad 109.3$$

and by definition $y_2' = y_4$ 109.4

$$y_3' = y_5 \qquad 109.4$$

The boundary conditions for equation set 109 are

$$\zeta = 0 \quad y_1 = y_2 = 0 \quad y_3 = 1 \qquad 110.1$$

$$\zeta = \delta\left(\frac{\omega}{\nu}\right)^{1/2} \quad y_4 = y_5 = 0 \quad y_3 = -\frac{1}{\pi}\left(\frac{Re}{Ta}^2\right)^{\frac{1}{2}} \qquad 110.2$$

Notice that equation set 109 provides a complete differential scheme of 5 unknown and 5 equations. Solution of the system is complicated by the fact that at the solid surface only three boundary conditions are known out of the five required. The system is unique, however, since two other boundary conditions (y_4, y_5) are available, albeit at the free surface.

The solution method employed by REES was repeated for this work. Initial values for all five variables at the solid surface were assigned, y_1, y_2 and y_3 being correct values, y_4 and y_5 guesses (actually set to zero). Integration of the five differential equations was performed from $\zeta = 0$ until the value of y_3 in the integration just exceeded the specified boundary value calculated from the input of Re^2/Ta for this run. Interpolation was used to give the free surface values of y_4 and y_5 (F' and G'). Had the correct values of y_4 and y_5 been specified at the solid surface, then the free surface values would be zero or nearly so. The displacement from zero was used to provide a better estimate for y_4 and y_5 at the solid surface as follows

$$y_4^*(0) = y_4(0) - 0.5\, y_4 \left(\delta\left(\frac{\omega}{\nu}\right)^{\frac{1}{2}}\right) \qquad 111.1$$

$$y_5^*(0) = y_5(0) - y_5\left(\delta\left(\frac{\omega}{\nu}\right)^{\frac{1}{2}}\right) \qquad 111.2$$

The * in equation set 111 represents the new estimate. Equations 111 are those employed by REES and differing values of the feedback ratios (0.5 and 1 in equations 111) were used to attempt to reduce the iterations required. However, no distinct advantage was noticed for any other values.

The procedure was then repeated with the new (and hopefully more accurate) values for $y_4(0)$ and $y_5(0)$, until such time as the free surface boundary conditions ($y_3 = \frac{1}{\pi}(Re^2/Ta)^{\frac{1}{2}}$, $y_4 = y_5 < E$) were satisfied. E represents the acceptable error of the solution and was set to 0.0001 for most runs.

Initial computations on an IBM 360 computer showed the above technique very wasteful of C.P.U. (central processing unit) time and an attempt was made to reduce this wastage by use of a 'double error' loop. Full details are given in APPENDIX G: PROGRAM SIM, but briefly, the technique was adjusted to perform iterations for y_4 and y_5 to a gradually improving degree of accuracy in the computations for each step. This modification greatly improved the compution time, by a factor of up to 20. Typical results are tabulated earlier in TABLE 4. FIGURE 36 shows the velocity profiles resulting from the solution. FIGURE 37 is a comparison of the results of the centrifugal model, the Coriolis analogue solution and the similarity solution. It will be seen that divergence from the centrifugal model begins at values of (Re^2/Ta) order 1. The general model tends to be slightly higher than the Coriolis model. However, note that each model makes very major assumptions (the general that a similarity solution exists, and the Coriolis model that the azimuthal velocity may be taken as a linear distribution to a first approximation) and so the obvious conclusion that inclusion of more terms in the general model leads to a more thicker film still may be in error.

The numerical results of PROGRAM SIM were obtained only for values of (Re^2/Ta) less than 10. At higher values the instabilities in the variation of $y_4(0)$ and $y_5(0)$ as noted by MATSUMOTO et al (but not REES) were found and the solution method becomes unstable. In this respect it is worth noting that the technique used by MATSUMOTO et al to overcome this instability was reported to have been applied only to a value of Re^2/Ta of order (2) within the range for which the conventional technique is still stable. A fuller investigation of the technique is therefore warranted.

FIG36 SIMILARITY MODEL VELOCITY PROFILES

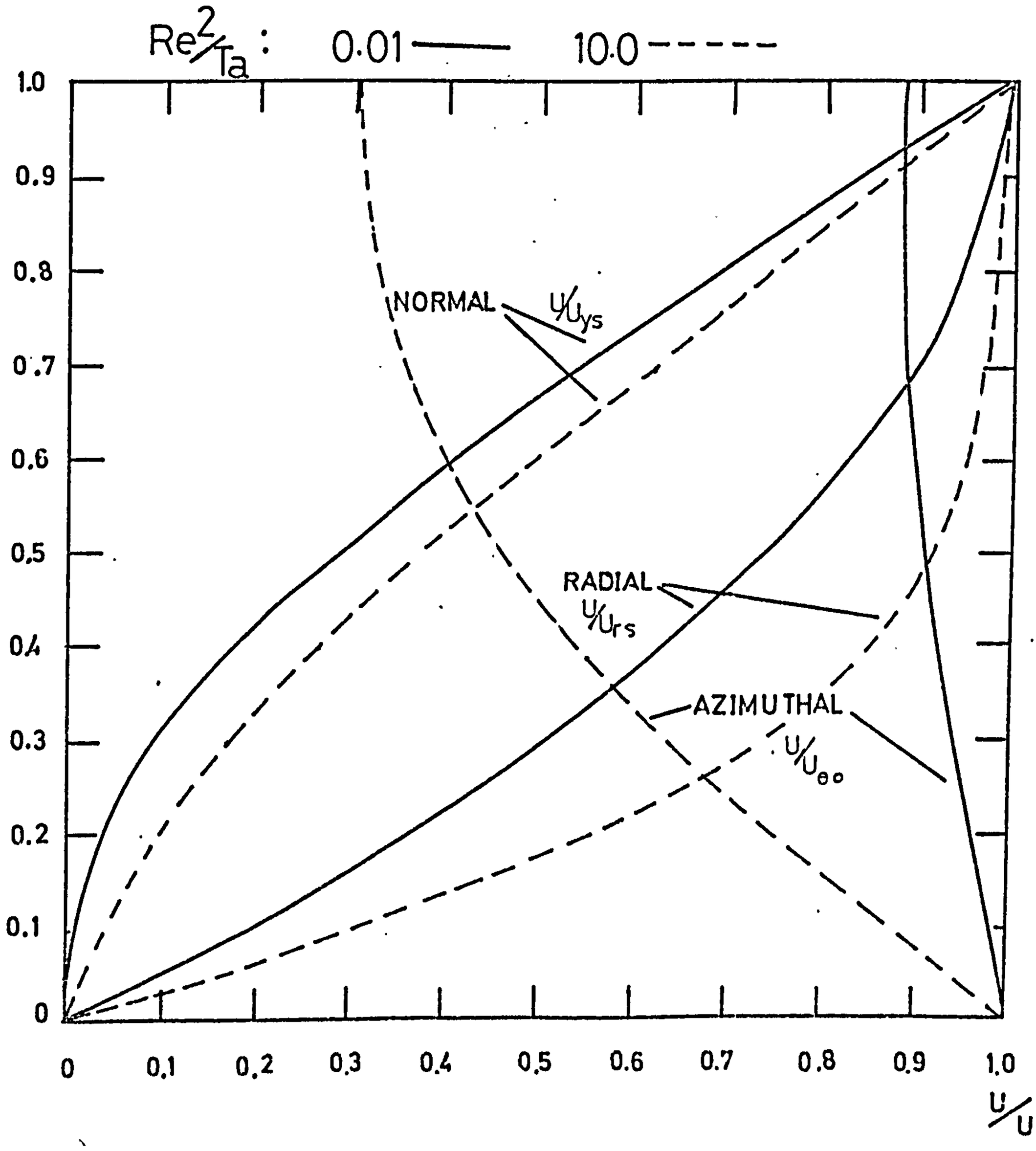

FIG37 THEORETICAL HYDRODYNAMIC MODELS

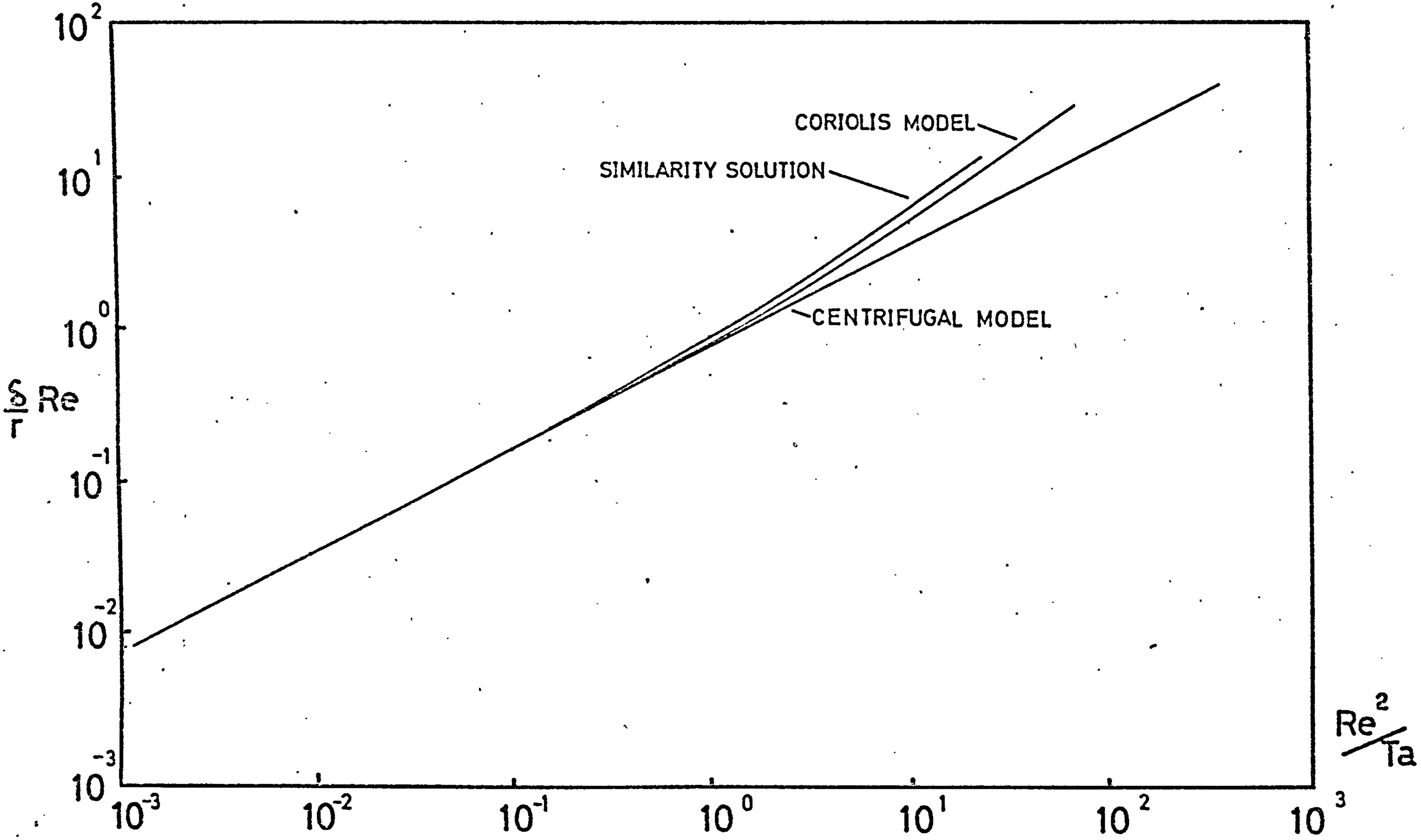

C: INERTIA MODEL

The following is presented as a summary of the theoretical work performed for the inertial model. Solution was not found possible due to the non-linearity of the final equation, but the work does indicate the important groups likely to govern any further study of inertia.

The general equation assumed is

$$\nu \frac{\partial^2 v_r}{\partial y^2} + v_r \frac{\partial v_r}{\partial r} = -\omega^2 r \qquad 112$$

with the boundary conditions

$$y = 0 \qquad v_r = 0 \qquad 113.1$$

$$y = \delta \qquad \frac{dv_r}{dy} = 0 \qquad 113.2$$

$$r = r_i \qquad v_r = \frac{Q}{2\pi r_i G} \qquad 113.3$$

when G is the distributor gap.

Non-dimensionalising may be performed using

$$r^* = \frac{r}{r_i} \quad , \quad y^* = \frac{y}{\delta} \quad , \quad U_r^* = \frac{U_r G r}{Q} \qquad 114$$

when equation 112 becomes

$$\left(\frac{Re'}{Ta^2}\left(\frac{r}{\delta}\right)^2 \frac{r^*}{A}\right) \frac{\partial^2 v_r^*}{\partial y^{*2}} + \left(\frac{Re}{Ta}\frac{r^*}{A}\right) r^* v_r^* \frac{\partial v_r^*}{\partial r^*} = -1 \qquad 115$$

when A is the aspect ratio ($\equiv G/r_i$)

Due to the non-linearity of the second group this equation is difficult to solve.

Notice that if the second group is ignored, then from the bracketted terms of the first group the controlling parameters are seen to be Re/Ta^2 and $(\frac{r}{\delta})^3$ since r^*/A becomes equivalent to r/δ for the far field solution so implied. These groups are in accordance with the centrifugal model considered previously.

This work, then, indicates that the additional groups defining the action of inertia upon the fluid are Re/Ta and r^*/A. Any experimental data collected should be studied in terms of such groups.

D: FILM BREAKDOWN

The model of HARTLEY and MURGATROYD (74) for planar film flow will be re-derived for the case of rotating film breakdown. Consider a dry patch on a rotating disc. The fluid runs radially up against the leading 'nose' of the patch and flows in rivulets alongside each edge of the patch. As with HARTLEY and MURGATROYD'S original paper criteria for the existence of the dry patch will be derived from consideration of flow both at the dry patch leading edge and in the rivulet alongside the edge of the patch.

1. AT THE STAGNATION POINT

The flow is brought to a halt at the upstream edge of the patch and thus the kinetic flow energy must be converted to a stagnation pressure. This will be balanced by the surface tension force resolved into a plane parallel to the solid surface. The contact angle, α, of the fluid is considered known, although practical tests show that measurement of α may be extremely difficult. Equating the two forces gives

$$\sigma(1-\cos\alpha) = \int_0^{\delta} \frac{\rho}{2} v_r^2 \, dy \qquad 116$$

Using the centrifugal model velocity profile (equation 60.1) and performing the integration gives

$$\sigma(1-\cos\alpha) = \frac{1}{15} \frac{\omega^4 r^2 \rho}{\nu^2} \delta^5 \qquad 117$$

or rearranging for δ as the critical film thickness (greater values of δ will give a stagnation pressure greater than the surface tension force, hence rewetting should occur)

$$\delta_c = (15)^{1/5} \left(\frac{\nu^2}{\omega^4 r^2}\right)^{1/5} \left(\frac{\sigma(1-\cos\alpha)}{\rho}\right)^{1/5} \qquad 118.1$$

Substituting for δ_c (from the centrifugal model equation 61) gives

$$Q_c = 10.63 \left(\frac{\nu r^4}{\omega^2}\right)^{1/5} \left(\frac{\sigma(1-\cos\alpha)}{\rho}\right)^{1/5} \qquad 118.2$$

2. IN THE RIVULET

The model proposes that the rivulet is stable when the sum of

the kinetic flow energy and the surface flow energy is minimum. The two energies are given by

$$\int_0^{\delta} \frac{\rho}{2} v_r . v_r^2 dy + \sigma v_{sr} \qquad 119$$

Using the centrifugal model velocity profiles equation 119 becomes

$$\frac{1}{35} \frac{\rho \omega^6 r^3 \delta^7}{\nu^3} + \frac{1}{2} \frac{\sigma \omega^2 r \delta^2}{\nu} \qquad 120$$

Differentiating equation 120 with respect to δ and equating to zero (for the minimum condition) gives

$$\frac{7}{35} \frac{\rho \omega^4 r^2 \delta^5}{\nu^2} = -\sigma \qquad 121$$

rearranging and taking the positive fifth root of δ gives

$$\delta_c = \left(\frac{35}{7}\right)^{1/5} \left(\frac{\nu^2}{\omega^4 r^2}\right)^{1/5} \left(\frac{\sigma}{\rho}\right)^{1/5} \qquad 122$$

Using equation 122 to obtain the critical flowrate gives

$$Q_c = 5.5 \left(\frac{\nu r^4}{\omega^2}\right)^{1/5} \left(\frac{\sigma}{\rho}\right)^{2/5} \qquad 123$$

Notice that apart from the inclusion of the contact angle α, the two criteria are of the same form. In equations 118 and 123 the suffix c represents the critical flowrate. For flows less than Q_c the film is unstable and, from the model's predictions, will flow in rivulet form.

2.5. EQUIPMENT

2.5.1. GENERAL

The work described in this thesis consists primarily of two parts, hydrodynamic studies and heat transfer studies. Similarly the equipment may be viewed as serving either of these two investigations. At the design stage, hydrodynamic equipment had to be sized and chosen with reference to the ultimate heat transfer investigation. However, to assist in maintaining division of the two studies in this work, only that design directly applicable to the hydrodynamic study has been considered here, the heat transfer design being considered later. It should be borne in mind though that the two designs were, in fact, conducted simultaneously.

2.5.2. HYDRODYNAMIC EQUIPMENT DESIGN

A: GENERAL CONSIDERATIONS

The purpose of the experimental investigation is to collect experimental information to enable a comparison to be made between the various hydrodynamic models developed and the experimental data. Thus measurements are required of the film thickness, velocity profile and surface velocity with varying radius, rotational speed, flowrate and fluid physical properties. In addition, the inertial models indicate that the entrance method of the fluid onto the disc will also be an independent parameter.

At the outset it was decided that direct measurement of a velocity profile within the film was beyond present experimental capabilities, and an indirect method (based, for example, upon residence time techniques) would require considerable development. It was decided, therefore, to conduct a thorough investigation of film thickness variation, and to collect some indicative data of other phenomena.

The film thickness measurement technique selected was the capacitometer method outlined in Section 2.2:A. This method is capable of giving instantaneous or time averaged, local or area averaged measurements of film thickness depending upon the mode of operation. The principle of operation is described more fully in APPENDIX H and the probe design in Section 2.5.2:E later. The measurement equipment chosen was a WAYNE-KERR type TC 100 meter commercially available. The equipment operates on a

comparison principle between the unknown sensed capacitance and a known calibrated capacitance within the circuitry. Sensitivity is good, of the order of 0.2 pF with a linear range 0.2 to 20 pF and stability is excellent. The meter takes a triaxial cable for input, the centre core carrying the sensed capacitance to be measured, the next core a capacitance measurement of the area around the sensor to prevent fringing of the sensor field and the third core provides a conventional screen around the two inner cores. The meter provides an analogue signal both visually and electronically.

The selection of this capacitance film thickness technique demanded that the rotating plate be metal and that all the flow circuit and metal work of the rig be earthed. In addition the fluid chosen for the experimental runs would have to have a known permittivity requiring either a well documented fluid or a calibration procedure. The liquid chosen for the tests was distilled water owing to the ease of supply and commercial importance of aqueous based fluids. It is recommended that additional work such as reported here is repeated for other liquids.

The major parts of the equipment design are concerned with the rotating disc (and immediate equipment) and the flow circuit. These will be considered in greater detail below.

B: MECHANICAL DESIGN

The rotating disc employed in this work is shown in section in FIGURE 38. It is 48 cm in diameter with an intended flow area of from 6 cm to 44 cm diameter.

The material for the disc manufacture was supplied by VICKERS LTD. and is a standard brass, 60% copper, 0.5% lead, remainder zinc. The raw weight was 50 kg and the machined weight some 12 kg. All design stresses were calculated for a speed of 2000 r.p.m. As can be seen from FIGURE 38 the disc is machined on both upper and lower surfaces. Almost all this machining is required for the heat transfer work described later. The upper surface of the disc was finished with chromium plating prior to the start of the experimental program.

The disc forms part of the rotating equipment as shown in FIGURE 39. FIGURE 39 is to scale and shows in addition the equipment used in the ultimate heat transfer runs. That area blacked out in the tracing cover may be ignored in the following description. The disc is held by sixteen ½" B.S.F. cap screws to the rim of a rolled brass chamber of

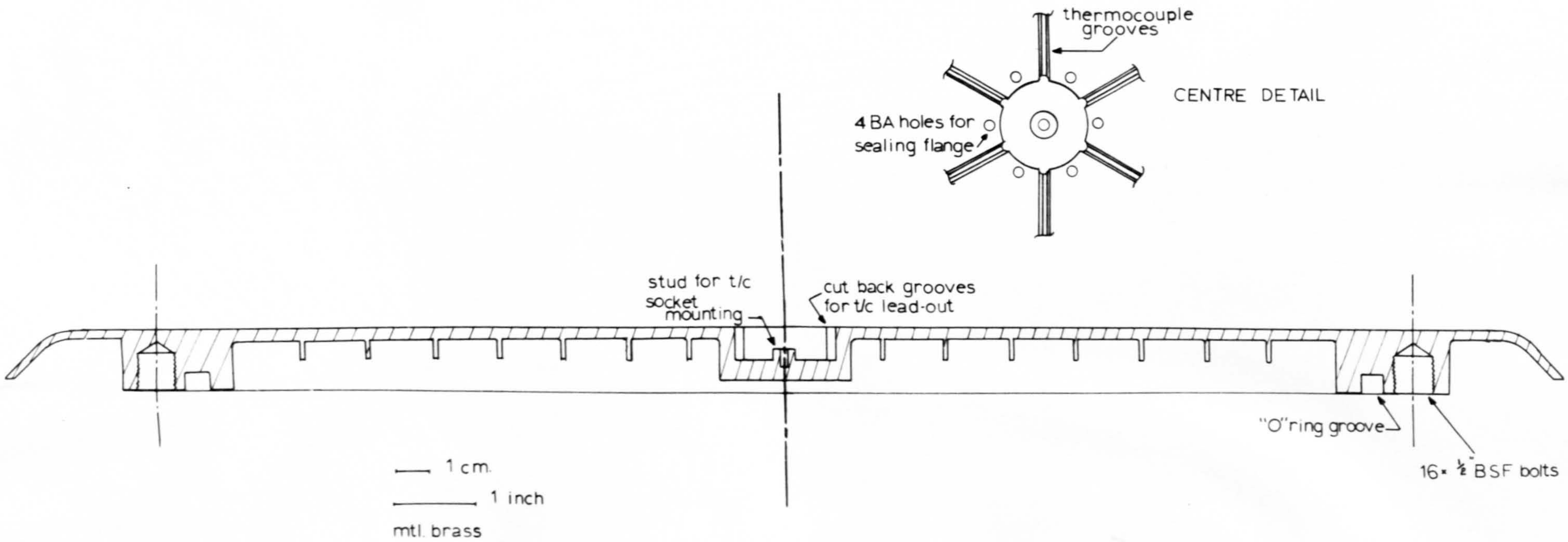

FIG 38 DISC CROSS-SECTION

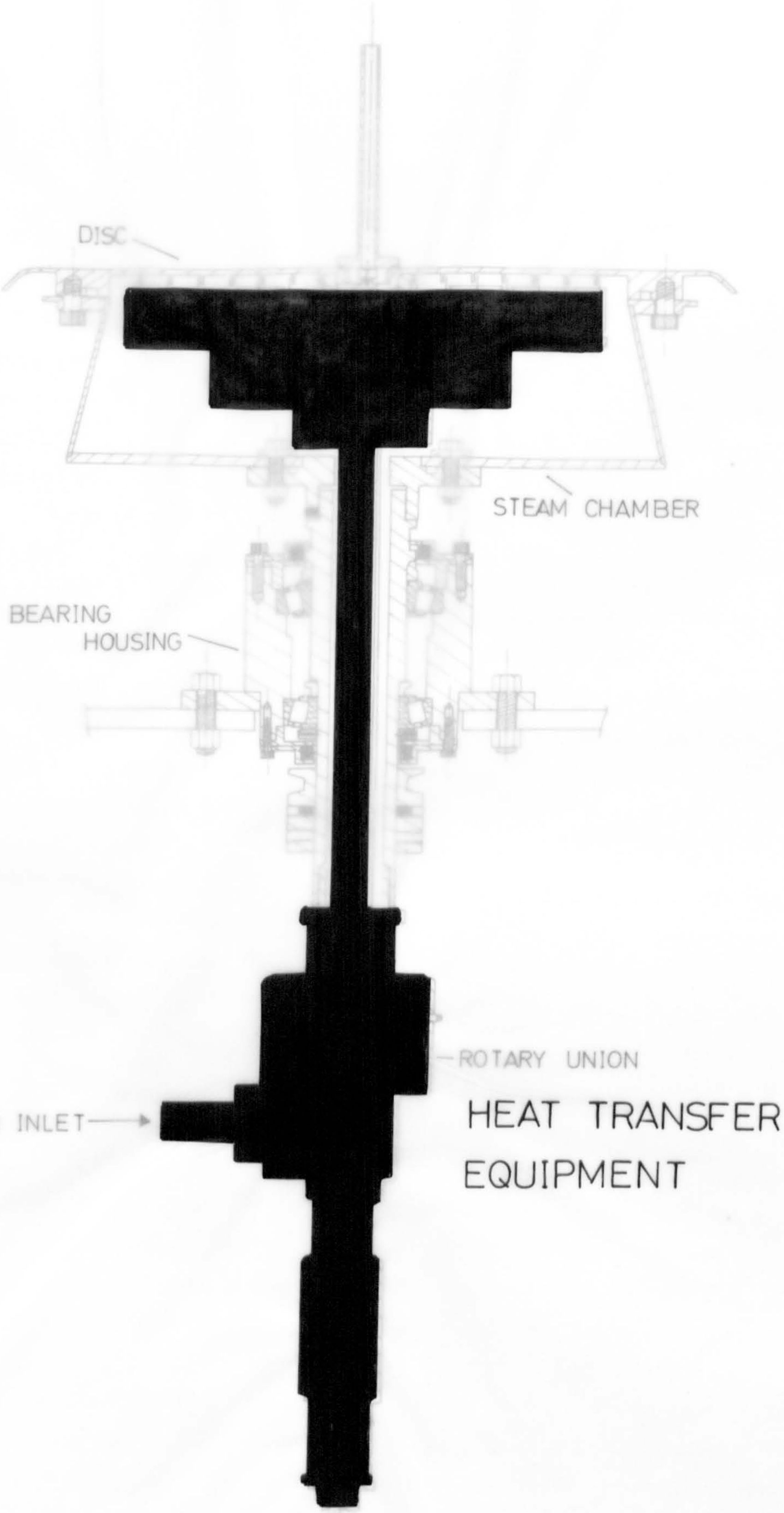

FIG 39 EQUIPMENT CROSS SECTION

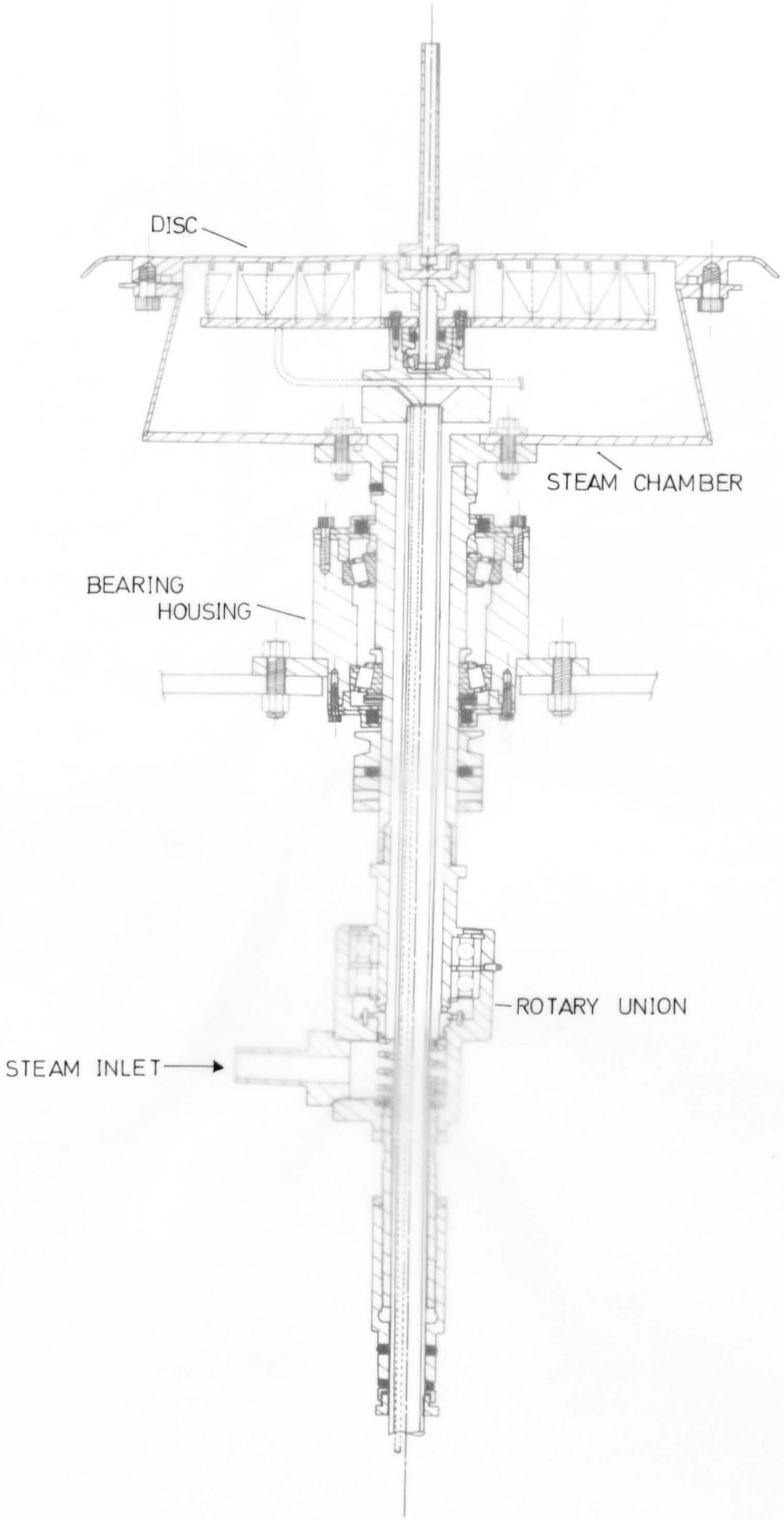
DISC
STEAM CHAMBER
BEARING
HOUSING
ROTARY UNION
STEAM INLET

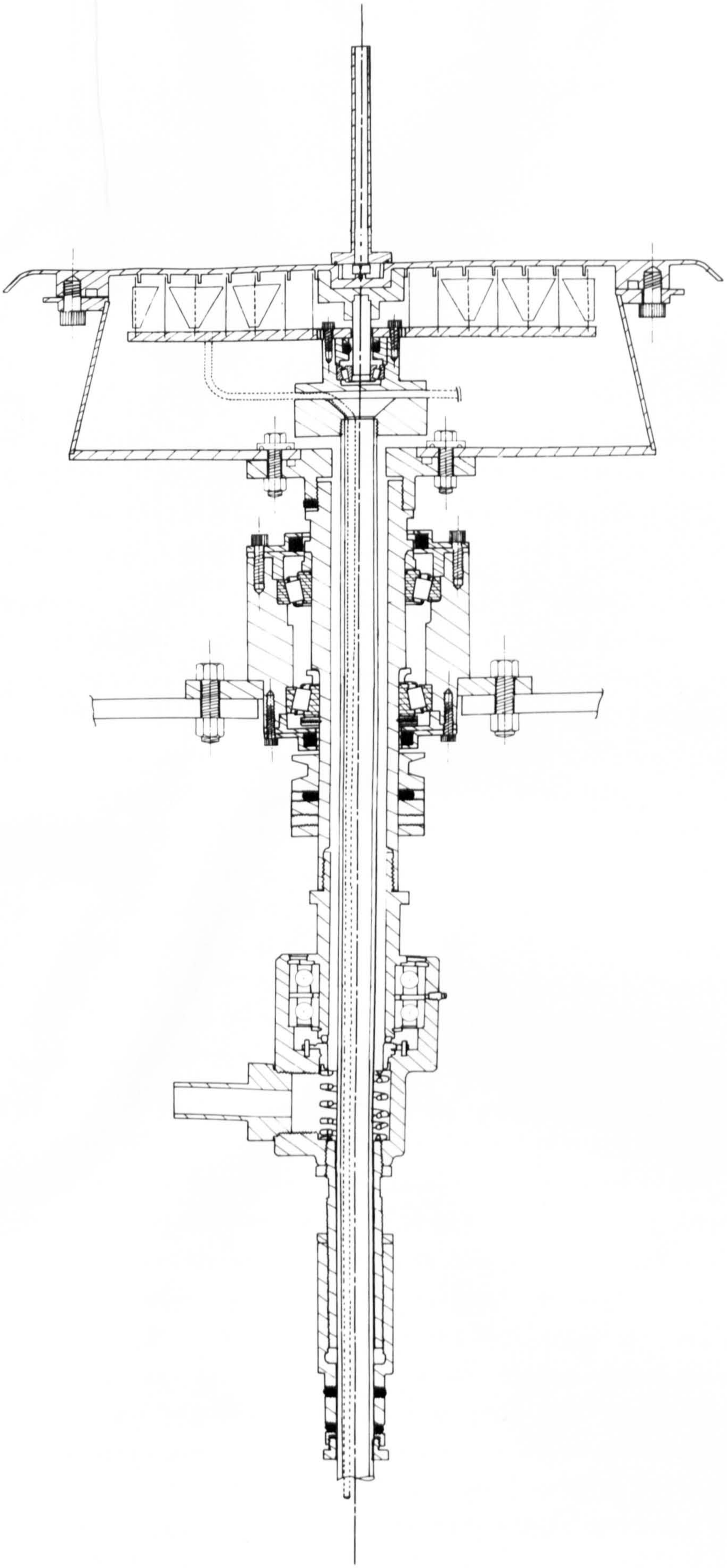

truncated cone like shape. This chamber is intum bolted to a mild steel flange by eight ¼" bolts. The flange screws onto a shaft mounted in a bearing housing. This shaft extends through the housing and ends in a screwed bore. The shaft is bored out to 3.7 cm diameter (1½"). The bearing housing contains two tapered bearings (mounted back to back) manufactured by TIMKEN (upper bearing: cup 39412, cone 39250; lower bearing: cup 382, cone 389A). The bearings were selected on size considerations and are amply suited to the mechanical load. The housing, a strong 15 cm diameter mild steel body is bolted to the main framework by eight ⅜" bolts via a ½" (1.75 cm) thick sheet of mild steel plate. The beginnings of the plate are visible on FIGURE 39. Lubrication of the bearings is by packed CASTROL LM grease, leakage along the shaft prevented by ANGUS GACO oil seals.

Beneath the support plate the extended shaft carries a 'V' belt block. The block consists of a 'V' belt groove (designed according to B.S. 1440) for an 'A' section belt, six grub screws (for retaining purposes) and six tapped holes. These latter holes were intended to be used for rotating balancing arms, however subsequent dynamic balancing obviated the necessity for this technique. The shaft and flange were tested on an AVERY balancing machine (type 7206 capacity 9 kg) and were found to be balanced within the machine limits (some 0.51 g cm). Since the majority of the out of balance forces would derive from the fabricated chamber beneath the disc it was decided to dynamically balance this chamber alone. Balancing was undertaking by PARSONS on an AVERY 7207 balancer (capacity 90 kg). A flange of spare material was left on the chamber and by removing certain portions of this, balance was achieved.

The mild steel plate that the rotating equipment is bolted to is supported in turn within a framework some 1.5 m x 1 m x 1 m formed of 5 x 5 cm mild steel square tube. A cross platform some 80 cm high supports the plate for the bearing housing and positions the disc face some 110 cm high. The entire box framework is mounted on a second ½" mild steel plate and is made more rigid by 4 diagonal 1½" angle-iron braces bolted into position. The front face of the box is drilled and tapped to take a safety screen of expanded mesh. The box framework and associated structure can be seen in PHOTOGRAPH 1. The base plate of the framework carries, at some distance behind the disc assembly, a short vertical plate. To this plate is bolted a ¾ HP NECO motor (D.C. power) with an 8.9 cm V pulley. This pulley is connected by the A section V belt mentioned earlier

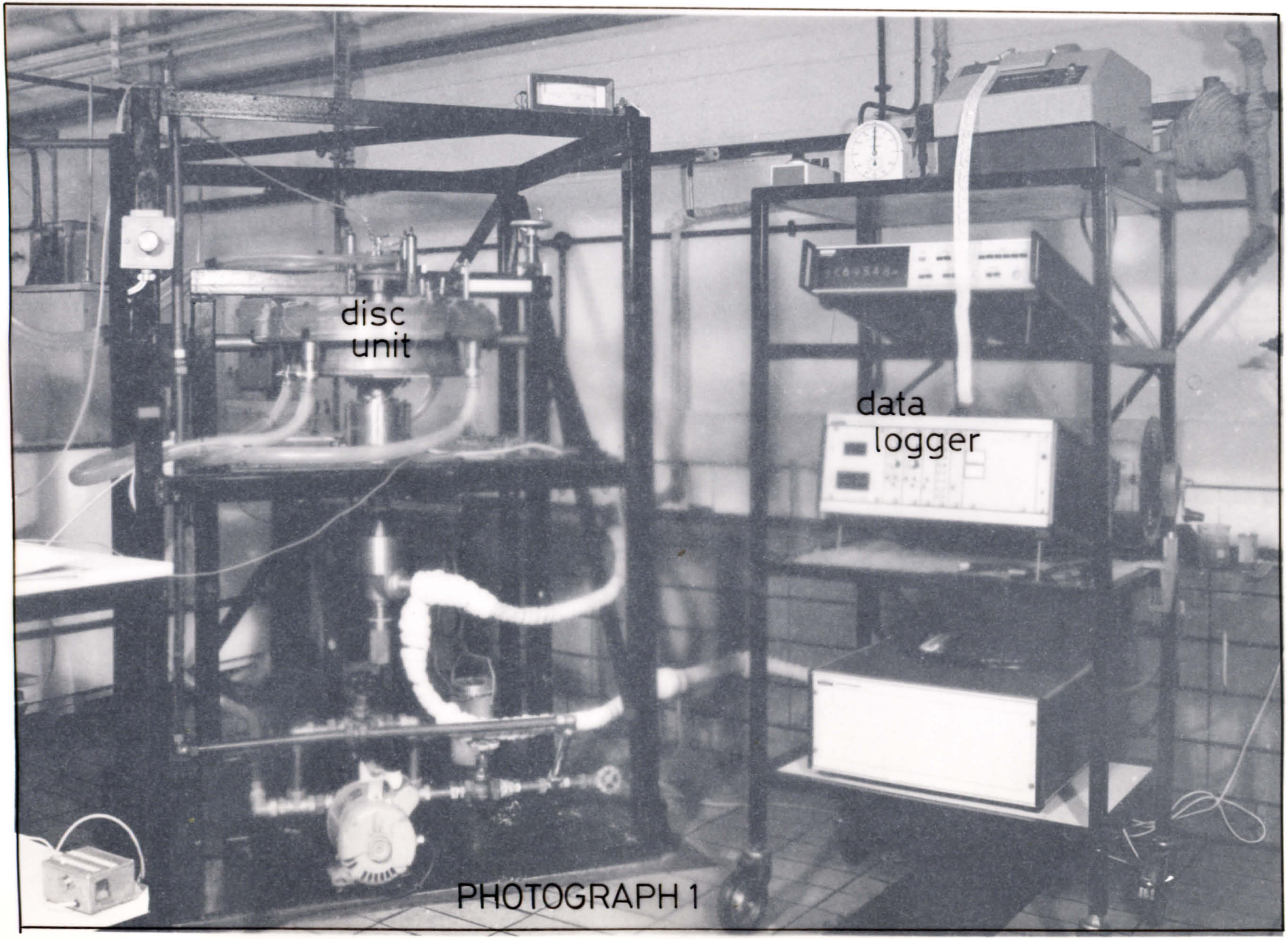

PHOTOGRAPH 1

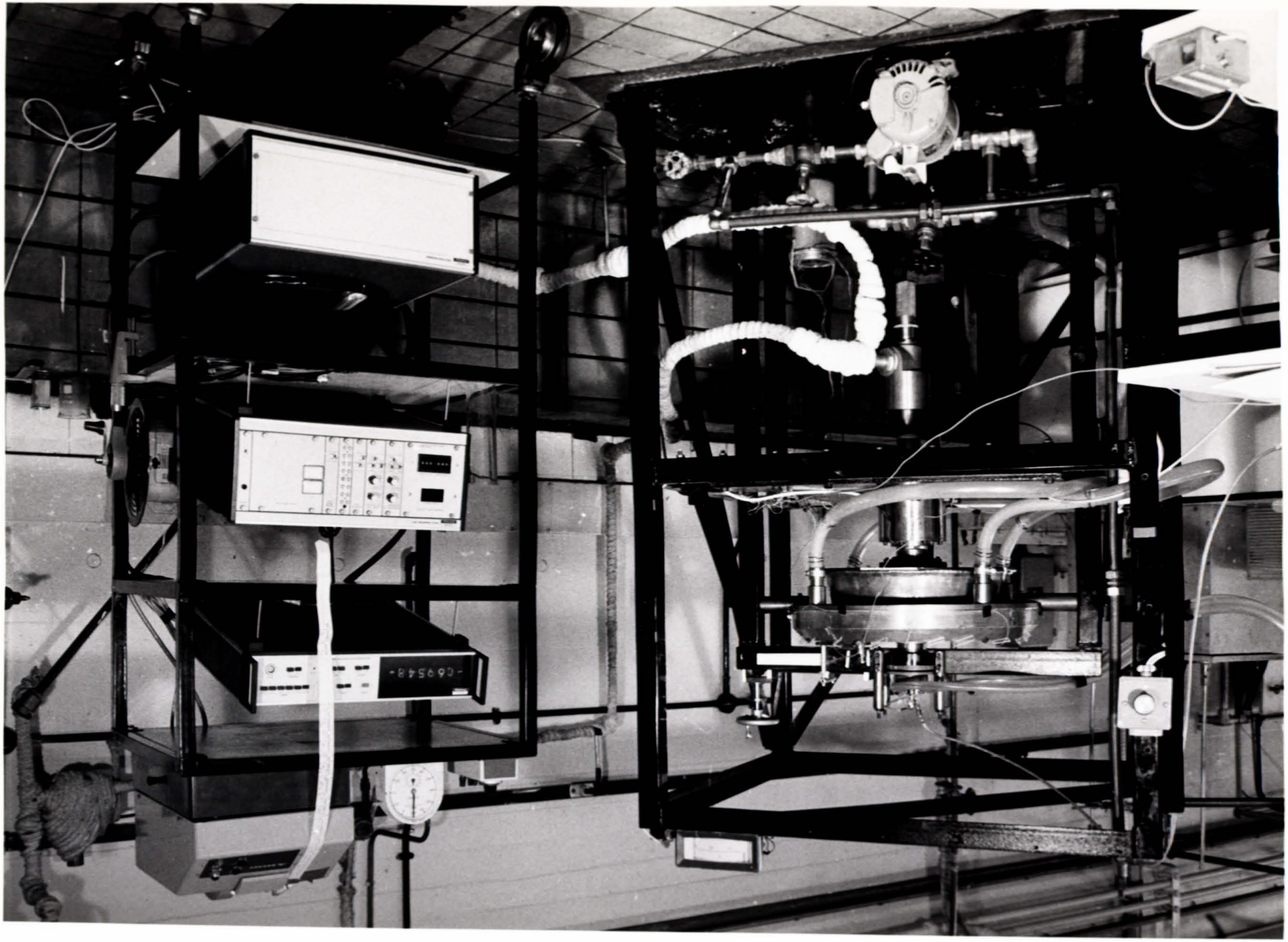

to the rotating disc pulley. The size of this pulley (7.5 cm) enables the maximum motor speed of 890 r.p.m. to drive the disc assembly at speeds up to 1050 r.p.m. The screw threads on the rotating assembly are all locked by set screws and are all designed so that with the designed sense of rotation (clockwise looking vertically downward) all screws are tightened by inertia loads in deceleration. The control circuit for the motor is described later.

The framework base carries two vertical posts of 5 x 5 cm tubing bolted to the bearing plate and base plate in such a way that the inclination of the posts may be adjusted. The upper ends of the tubes are blanked by ½" plates, centrally drilled and tapped to ½" B.S.F. Across these two posts is located a section of heavy U channel (7.5 cm x 5 cm x 0.5 cm) which carries a central circular bush. The purpose of the bush will be outlined in the next section. The channel is bolted through over-sized holes to the ends of the upright posts. In this manner the location and pitch of the central bush can be varied considerably. The base of the right hand trough (facing the equipment) of this cross channel is machined smooth and level ready to receive the film thickness probe carrier described later.

It will be noticed from FIGURE 39 that the centre of the disc is surmounted by a short spindle. This is, in fact, a vertical tube through which the surface thermocouple leads for the heat transfer tests were led. The tube was held to the disc by six 4 BA cap screws. Sealing was achieved by 'O' rings around the outer portion of the flange and around each cap screw. Corrosion of the mild steel heads of the cap screws was delayed by coating exposed surfaces with silicon rubber solution. The entire framework was supported on a ½" thick rubber mat to evenly distribute the load over the laboratory floor and give some insulation from environmental vibration.

C: FLUID CIRCUIT

The liquid circuit is shown diagrammatically in FIGURE 40. Liquid under test is held in a 0.06 m^3 tank (15 gallon) and flows through isolating gate valve V1 into the pump P1. Valve V1 enables the tank to be isolated for maintenance on the remaining circuit to be performed without system drainage. Pump P1 is a JABSCO type pump driven by a 1.5 HP three phase electric motor. This pump was chosen due to its ability to pump highly viscous materials almost as easily as low viscosity liquids.

FIG40 FLUID CIRCUIT

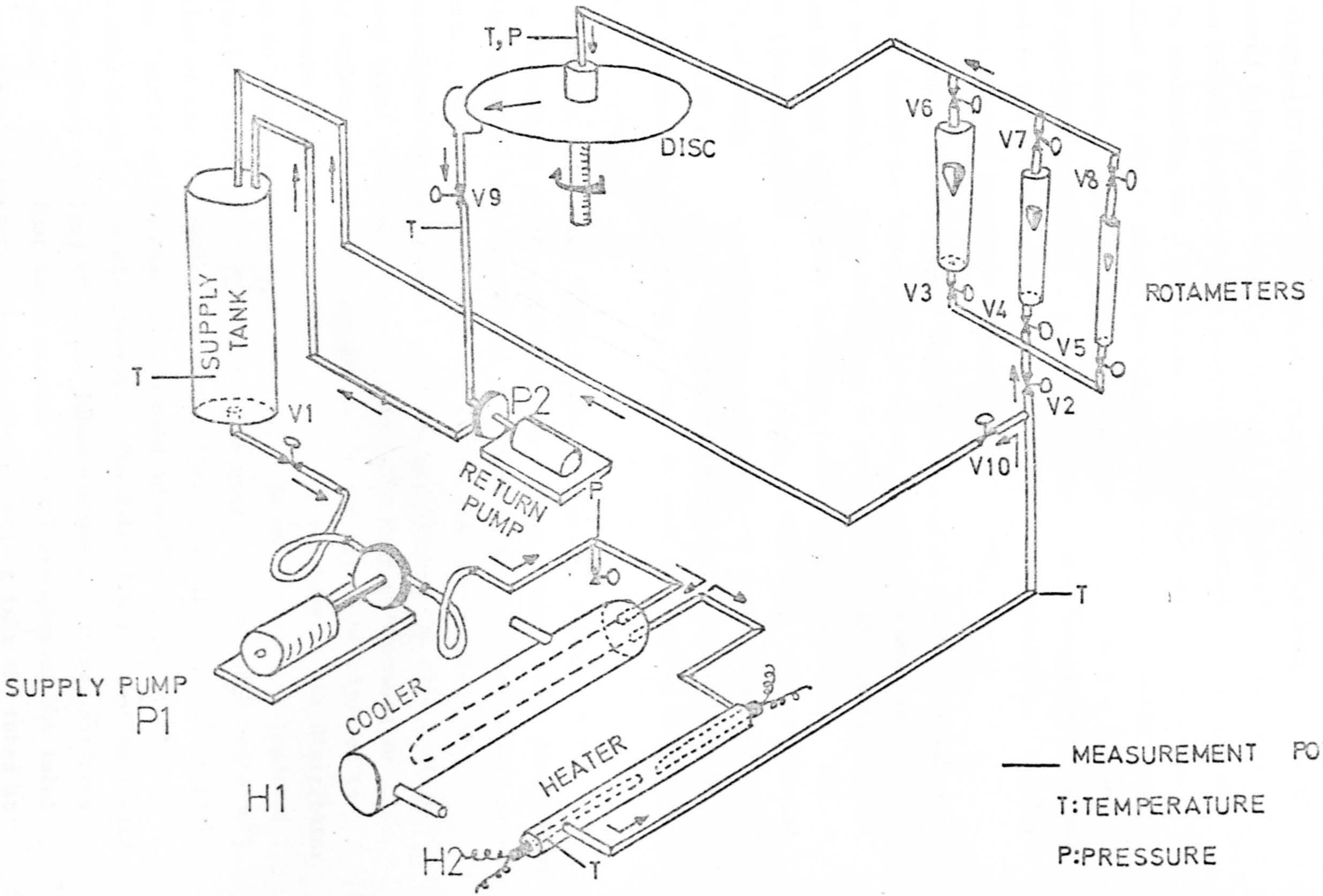

Pump P1 passes liquid through a heat exchanger H1 constructed in the department's workshop. The exchanger is a conventional small (1 m) multitube (33 tubes) double-pass shell and tube exchanger. Test fluid is passed through the tubes, mains water is applied to the shell. Liquid then passes through a trim heater (H2) consisting of a length of copper tube containing two 3 kW heaters, one at each end. One heater is controlled by a simple on-off switch, the other by a 10 A solid state voltage controller. Continuously variable heating rates of 0 - 2.5 and 3 - 5.5 kW are thus available. A surface thermocouple (copper-constantan) is attached to one of the heaters to monitor heater temperature. Display is on a panel mounted CAMBRIDGE temperature indicator.

Cooled or heated liquid from the exchangers travels through a trim valve V2 before passing to any of a bank of three rotameters connected in parallel. Each rotameter is preceded by fine control valves (V3, V4 and V5) and followed by isolation valves (V6, V7 and V8). The rotameters (from ROTAMETER Co.Ltd.) are types METRIC 14XP, METRIC 35XP and METRIC 47P, allowing smooth and overlapping delivery rates from 1.67 x 10^{-5} m^3/s to 1.25 x 10^{-3} m^3/s. To prevent excess pressure at valve V2 during low flowrate runs valve V10 allows a by-pass of fluid to return to the tank.

From the rotameters fluid is fed via four ½" diameter P.V.C. tubes to a distributor at the centre of the rotating disc. This distributor is shown in FIGURE 41 and consists of a screwed brass body with a mild steel jacking nut. When positioned over the centre line of the disc, the jacking nut allows the distributor gap (the gap between the disc surface and the body edge) to be adjusted and set. The body is threaded to 20 TPI and markings on the jacking nut enable the gap to be adjusted in values accurate to 25μm. The lower portion of the body of the distributor is screwed to accept various types of ends. In the experiments reported in this thesis a sharp edged distributor was used (included edge angle 30°). The interior of the distributor was smooth finished. Liquid leakage past the central 'stalk' of the disc is prevented by a ½" oil seal mounted in the inlet tube block of the distributor. The inlet tubes accepting liquid from the rotameters are four ½" copper tubes pressed and silver soldered into the block. These four tubes provide spacial symmetry of the inlet fluid around the distributor. To prevent any jetting from the tubes at the higher test flowrates a set of three baffles are hung from small tubes which pass coaxially down from the inlet tubes. The baffles are off-set

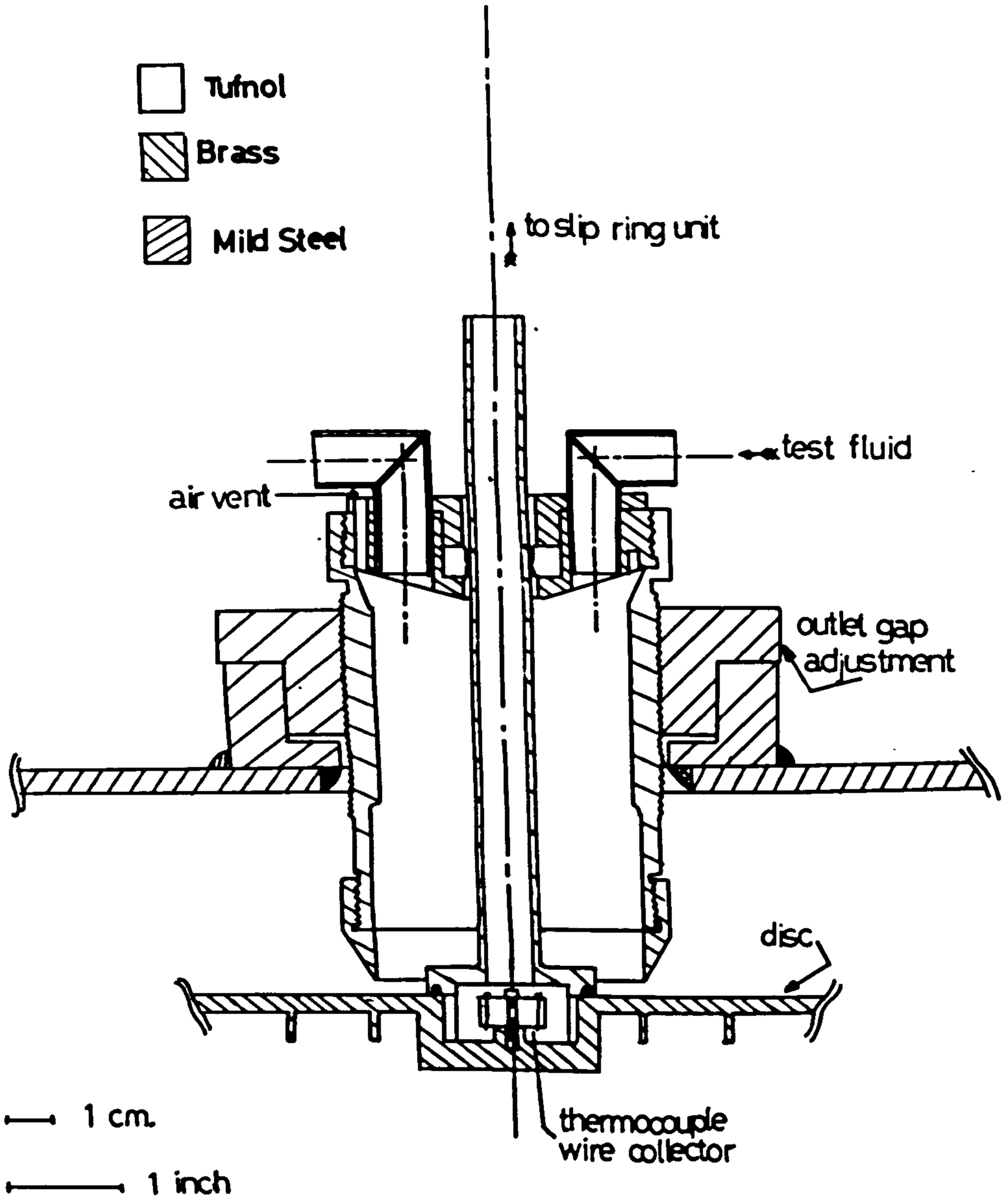

FIG 41a DISTRIBUTOR

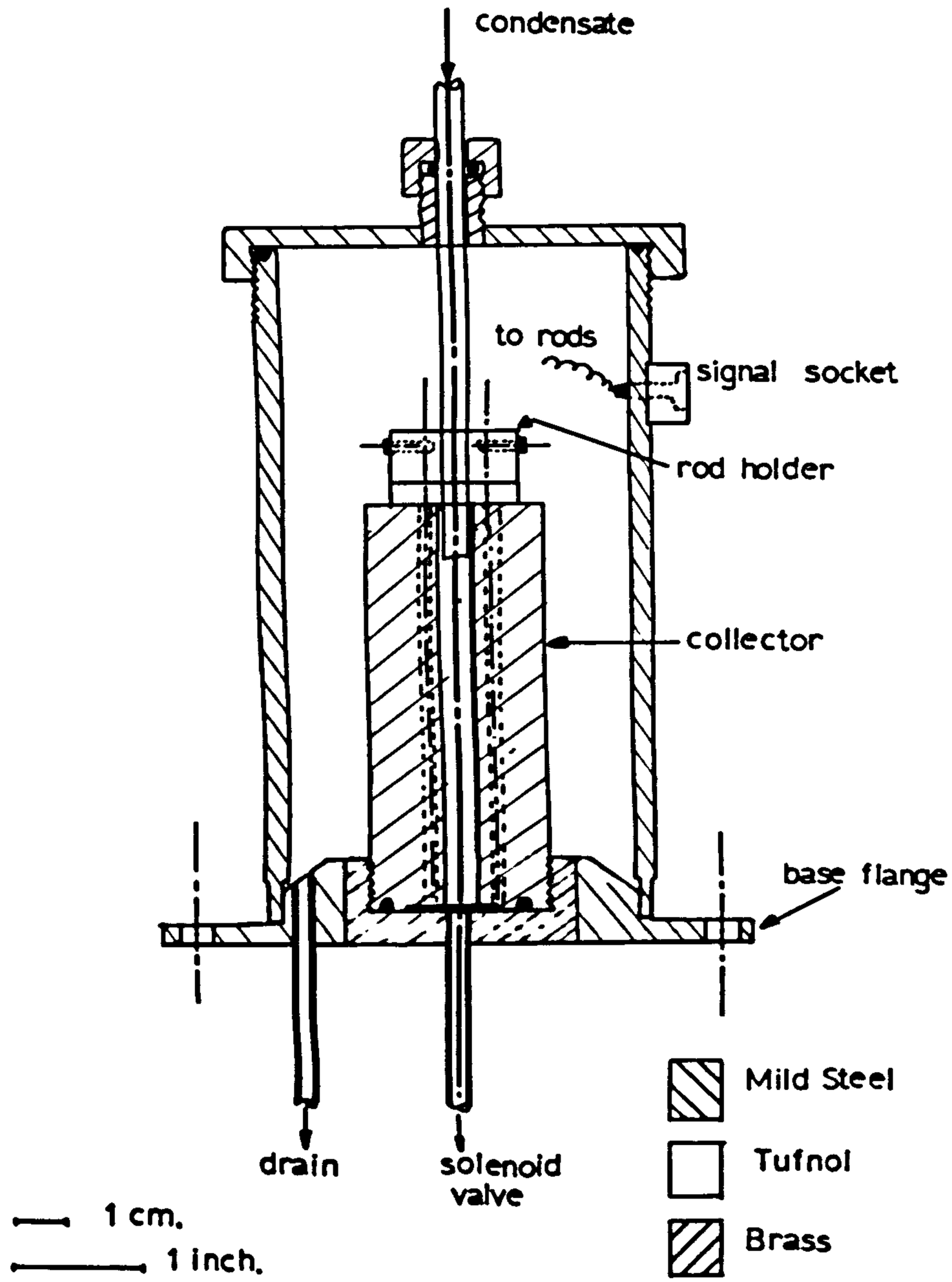

FIG 41b CONDENSATE TANK

and thoroughly distribute the inlet fluid. The small tubes also carry thin thermocouple leads inside and enable a measurement of fluid temperature to be made at entry to the disc surface. Distributor pressure is monitored by a water manometer from a pressure tapping on the distributor. The manometer is situated on the control panel.

After crossing the disc, the fluid is collected in an annular ring collector. The device is shown in PHOTOGRAPH 2. and consists of a heavy brass ring (44 cm i.d. x 54 cm o.d. x 1 cm thick) supporting two brass rings (1½ mm thick) some 4 cm apart. The inner ring is a plane cylinder some 3 cm high, the outer a cylinder of equivalent height surmounted by approximately a further 3 cm of cone of some 60° half angle. In operation the disc edge rests between the two rings, the outer collecting liquid thrown off by the disc, the inner forming a sufficiently deep trough to allow the liquid to drain away.

The design of the fluid collector represents a compromise. The rotating disc acts as an air pump and forces air out along its radius. A very high (much exceeding the top surface level of the disc) outer collector wall would interact with this air flow and possibly give rise to an unexpected "end-effect". On the other hand, too low a wall risks allowing splashes of the spun-off fluid to escape. In compromise the outer collecting wall protrudes some 1 cm above the level of the plate. In practice this performed adequately at low speeds and by placing a few downward facing vanes about the edge of this collector, tendencies to spray at high speeds was overcome.

Three thermocouples were held in the hold-up liquid of the collector to enable outlet temperature of the fluid spun off the disc to be measured. The collector is supported on two mild steel pegs which bolt into the framwork uprights mentioned in Section 2.5.2:B earlier. Tendency to pivot about these pegs is prevented by a rear bracing strut.

Liquid from the collector leaves by four 2.5 cm bore brass tubes pressed and sealed into the collector base plate. The four separate streams are brought together by a simple adaptor before passing to a small pump P2, (initially a mains centrifugal pump, later a JABSCO mains pump) mounted on the rigs base plate. Output from the pump is returned overhead to the supply tank.

All metal in the flow circuit is brass or copper. All metal tube junctions are of INSTANTOR type and tubing bore is 2.5 cm (1"). To

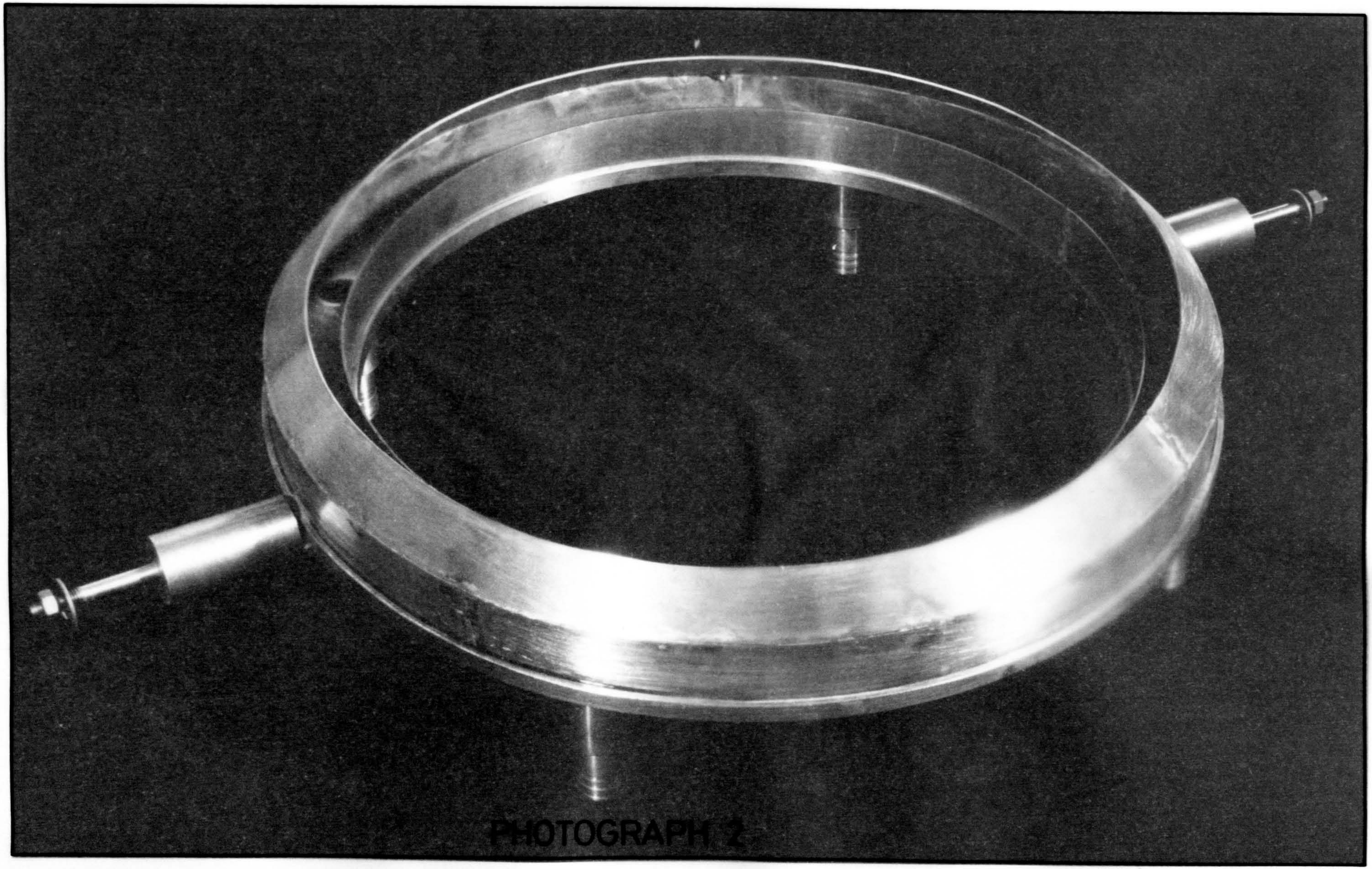

PHOTOGRAPH 2

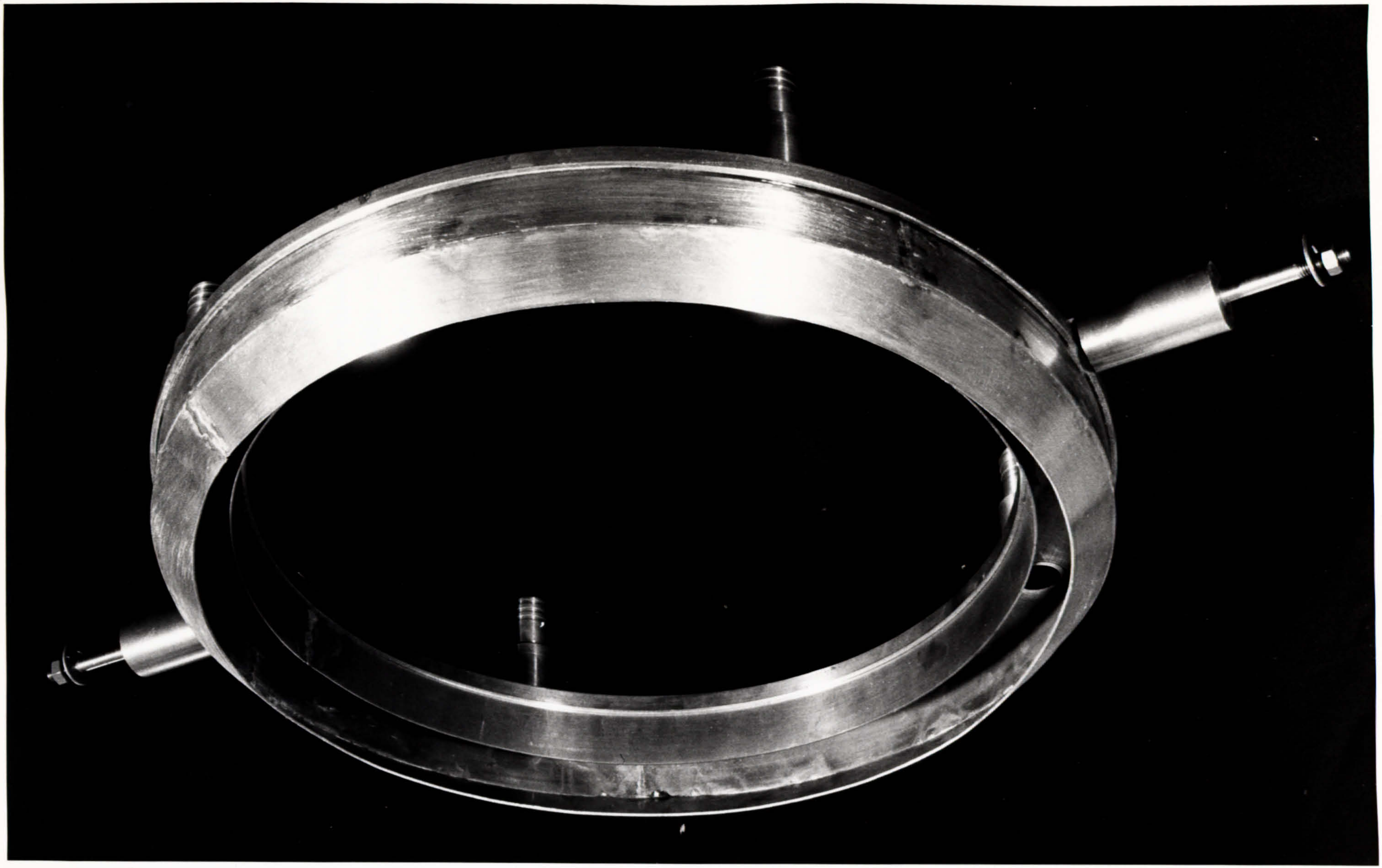

minimise unnecessary vibration transmission to the disc, connections to and from pump P1, to pump P2 and to the distributor were made in 2.5 cm bore flexible P.V.C. tubing. Operating the equipment for limited times without drainage pump P2 showed no change in the surface patterns of the disc film compared to those present when pump P2 was used. Hence vibration from pump P2, mounted on the disc framework, had negligible effect.

PHOTOGRAPH 3 shows the control panel servicing the rotating disc. Visible on the back panel are the three rotameters (on the right) with the heater switches and distributor manometer to their right. In the centre of the panel is the motor control and emergency stop button. On the table is the capacitometer and smoothing circuit (see later). Visible behind the panel are the heater/cooler (floor lower left), main pump (floor, centre) and supply tank (rear, right). The flexible supply pipes can be seen crossing to the rotating disc equipment.

In addition to the locations already mentioned temperature was also monitored at the exit from the heater/coolers and within the supply tank. Pressure was also monitored at the outlet of pump P1.

D: MOTOR CONTROL CIRCUITRY

The driving motor for the disc is controlled by a variable D.C. supply from a mains rectifier (NECO Ltd.). This supplies a constant field voltage and a variable armature current. The armature voltage and current are monitored by two moving coil meters mounted on the control panel. The supply from the rectifier to the motor is interrupted by the circuitry shown in FIGURE 42. Depressing the left most ON button causes the first relay to energise and pass the rectifier output to the next relay. Depressing the right most ON button energises the second relay and passes the rectifier supply direct to the motor. There are four possible OFF buttons, three emergency, one normal. Depressing any of the emergency stops (which are situated: one at the disc equipment front (left corner), one at disc equipment rear, one centre of control panel) de-energises relay 2 causing the supply to the motor and main pump P1 to cease (pump P2 continues to drain the collector) and further, shorts the motor armature across the emergency load resistor. Depressing the normal stop leaves the pump P1 functioning, disconnects the motor supply (by de-energising relay 1) and shorts the motor armature across the normal load resistors. When the armature is shorted in this manner across a resistor the motor

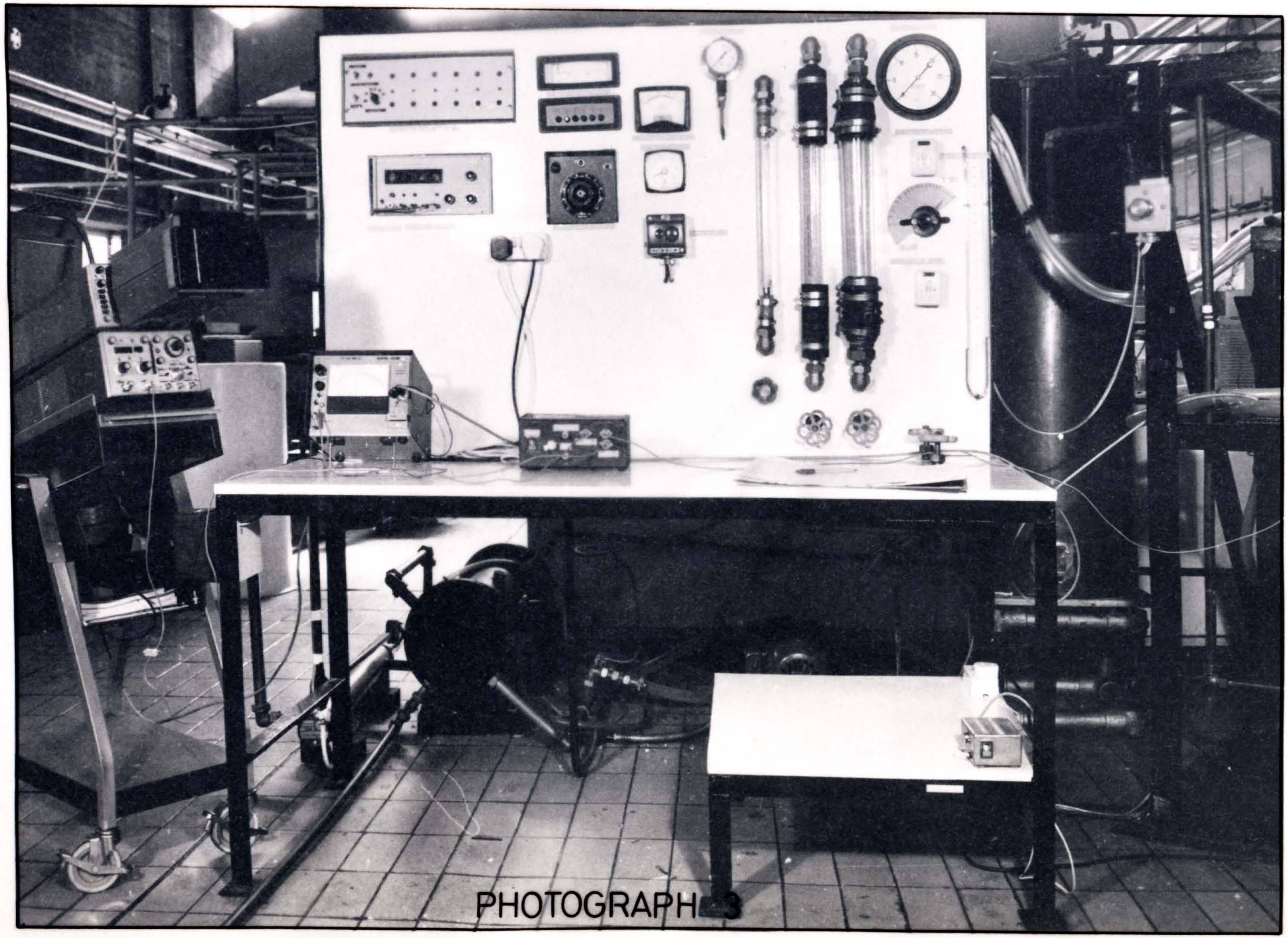

PHOTOGRAPH 3

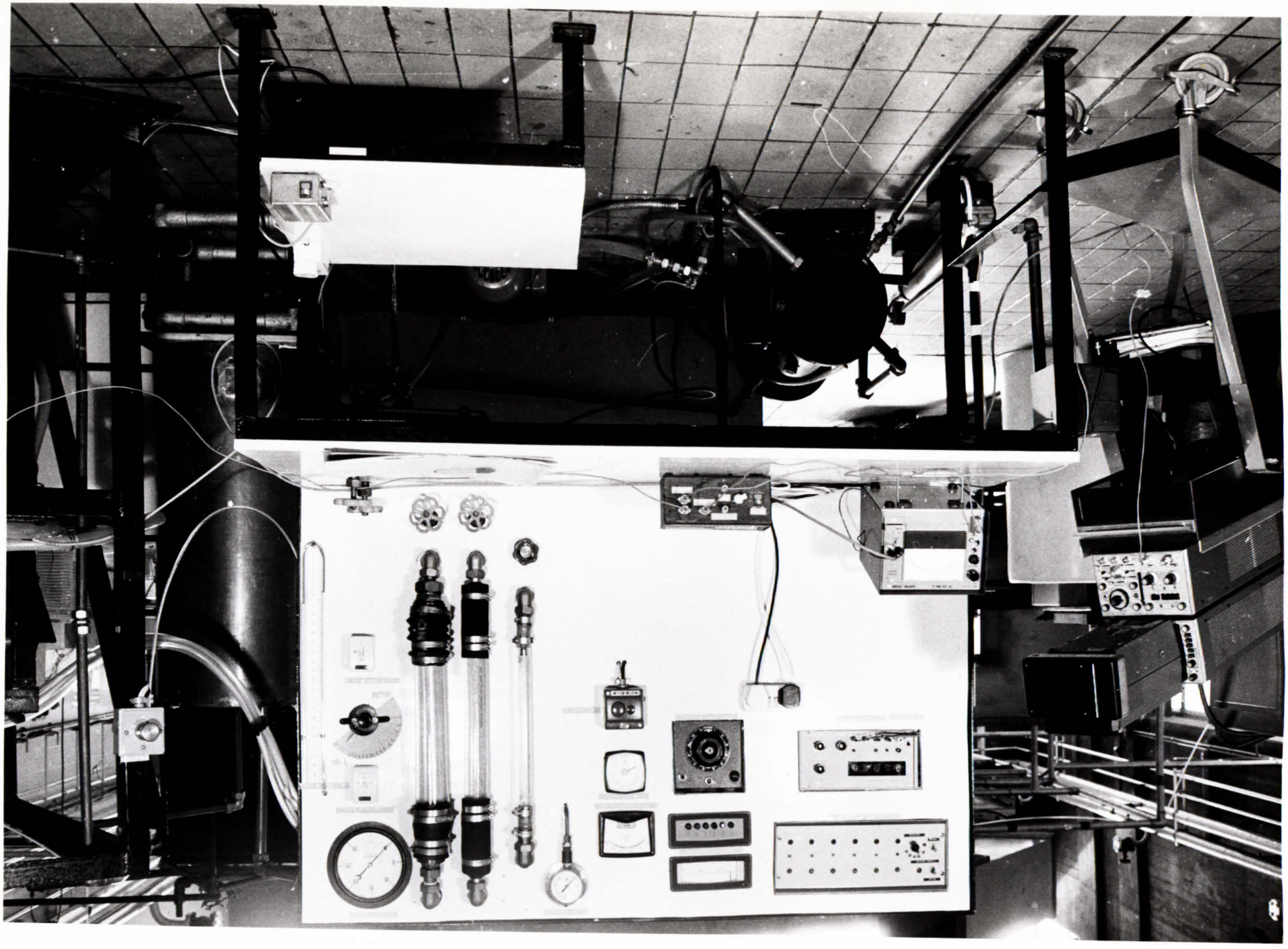

FIGURE42 POWER CONTROL

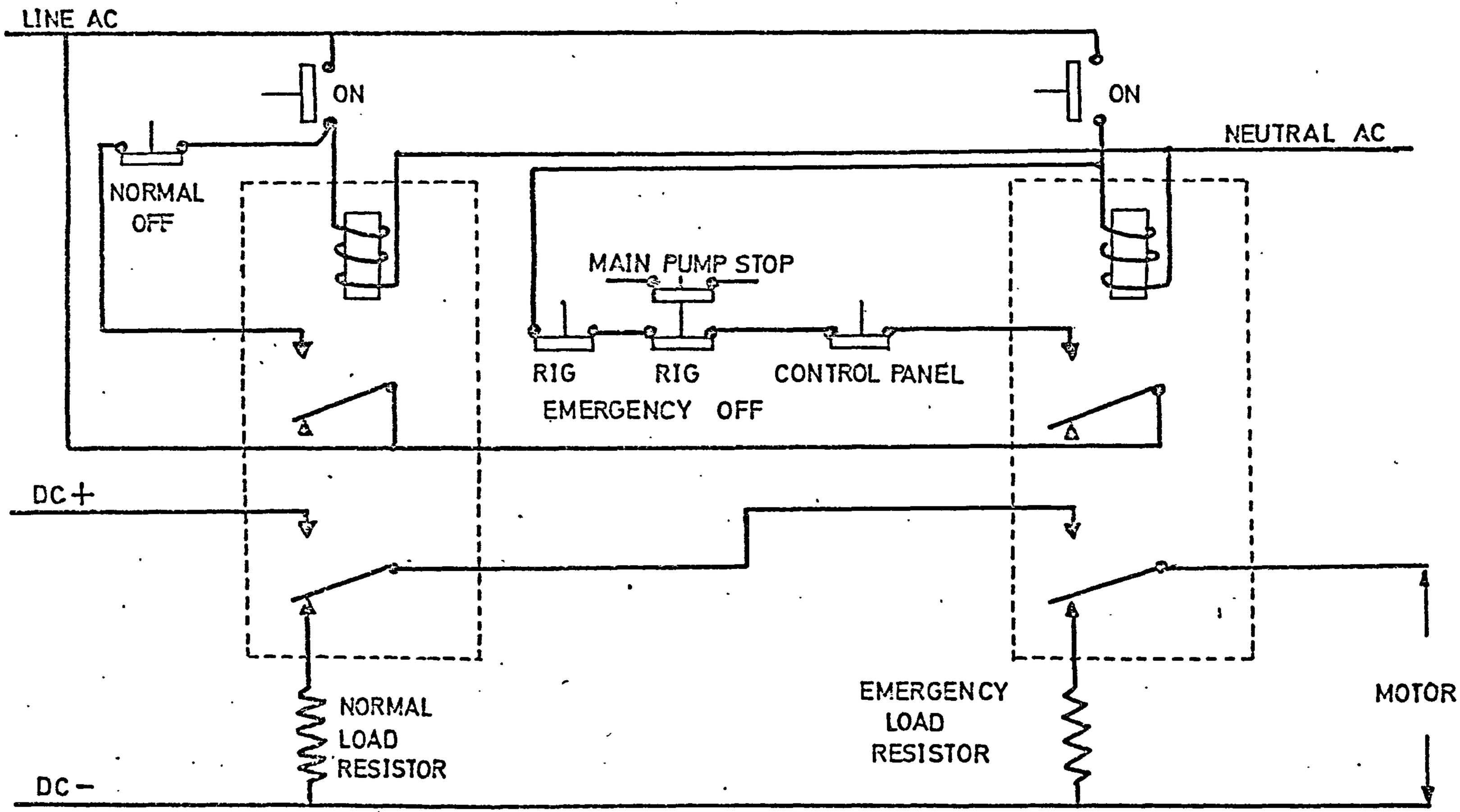

becomes, in effect, a generator absorbing power from the angular momentum of the rotating disc and degrading the electrical energy produced into heat in the load resistors. The smaller the resistance of the load resistors, the more rapidly will this degradation occur and the disc stopped.

In practice no load resistors were used in this circuit owing to the considerable friction of the oil seals, greased bearings, etc., which quite quickly stopped the disc once the motor supply was removed at all but very high speeds. The circuit is supplied, however, for future use on this equipment.

E: CAPACITANCE PROBE TRACKING DEVICE

The capacitance probe is required to move radially to any location desired. Positions should be repeatable and accurate, and the device self-contained. The device finally constructed is shown in PHOTOGRAPH 4. It consists of a 20 T.P.I. heavy mild steel screwed shaft supported by two end plates on a base plate. The shaft carries a mild steel plate with a cross piece along the upper edge. Two silver steel rods parallel with the shaft reduce backlash in the plates movement. The shaft ends with a 24 tooth bevel gear by OSBORNE Ltd. The matching 12 tooth gear is mounted vertically and is driven by a hand wheel. The hand wheel stock carries a pointer and dial. The dial is graduated in 25 μm parts and placement accuracy of the device is of the order of 10 μm. The number of total rotations of the shaft is counted by a small mechanical counter (VEEDER-ROOT Ltd.) fitted to the shaft.

The tracking cross piece carries two aluminium uprights which end in a T shaped tufnol block beneath the framework (in the photograph these are shown removed and to one side). The T block piece contains a 12 mm hole accurately aligned during manufacture to be within 12 μm of the overhead shaft centre line. In use the unit is aligned by dowel pins (in the cross piece U channel of the disc framework) to lie along a radius of the disc. The underslung T piece carriage is then free to move along a radius. The probe is pressed firmly into the T piece locating hole and enables film thickness measurements to be made from radii from 5 cm to 21 cm approximately.

F: CAPACITANCE PROBES

A cross-section and table of dimensions for the probes and holder used in the thickness measurements are given in FIGURE 43. The

PHOTOGRAPH 4

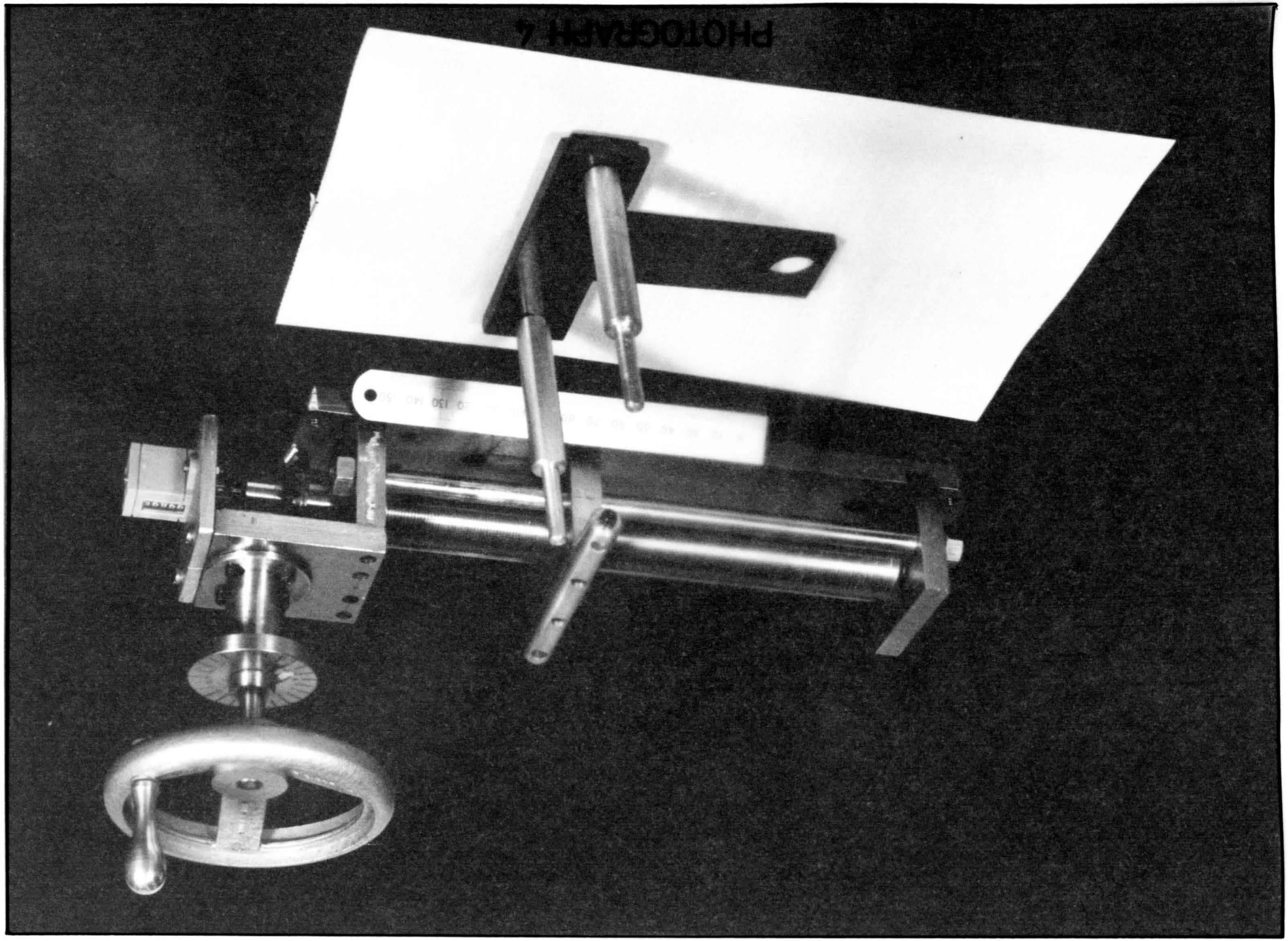

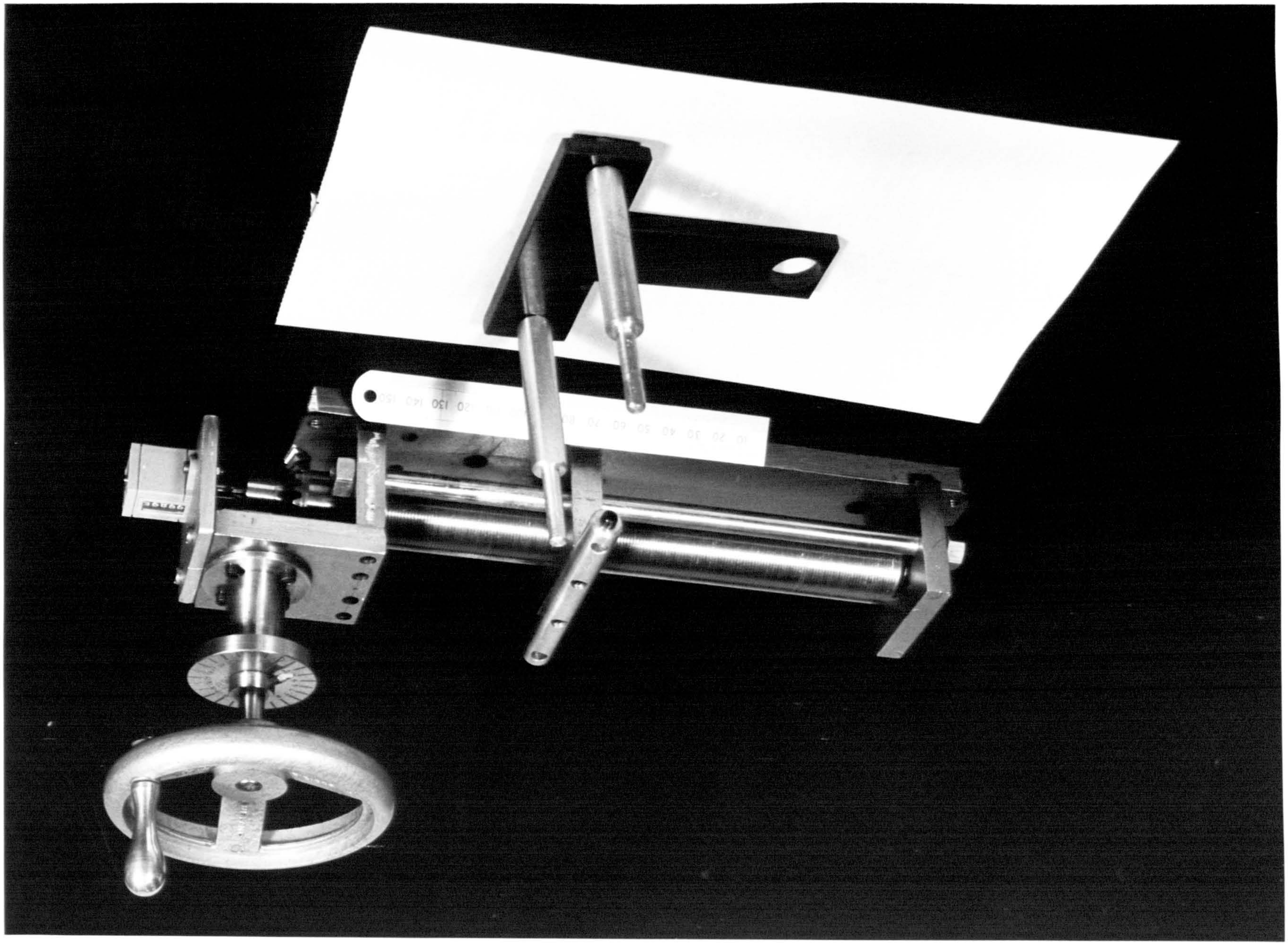

FIG 43 CAPACITANCE PROBES

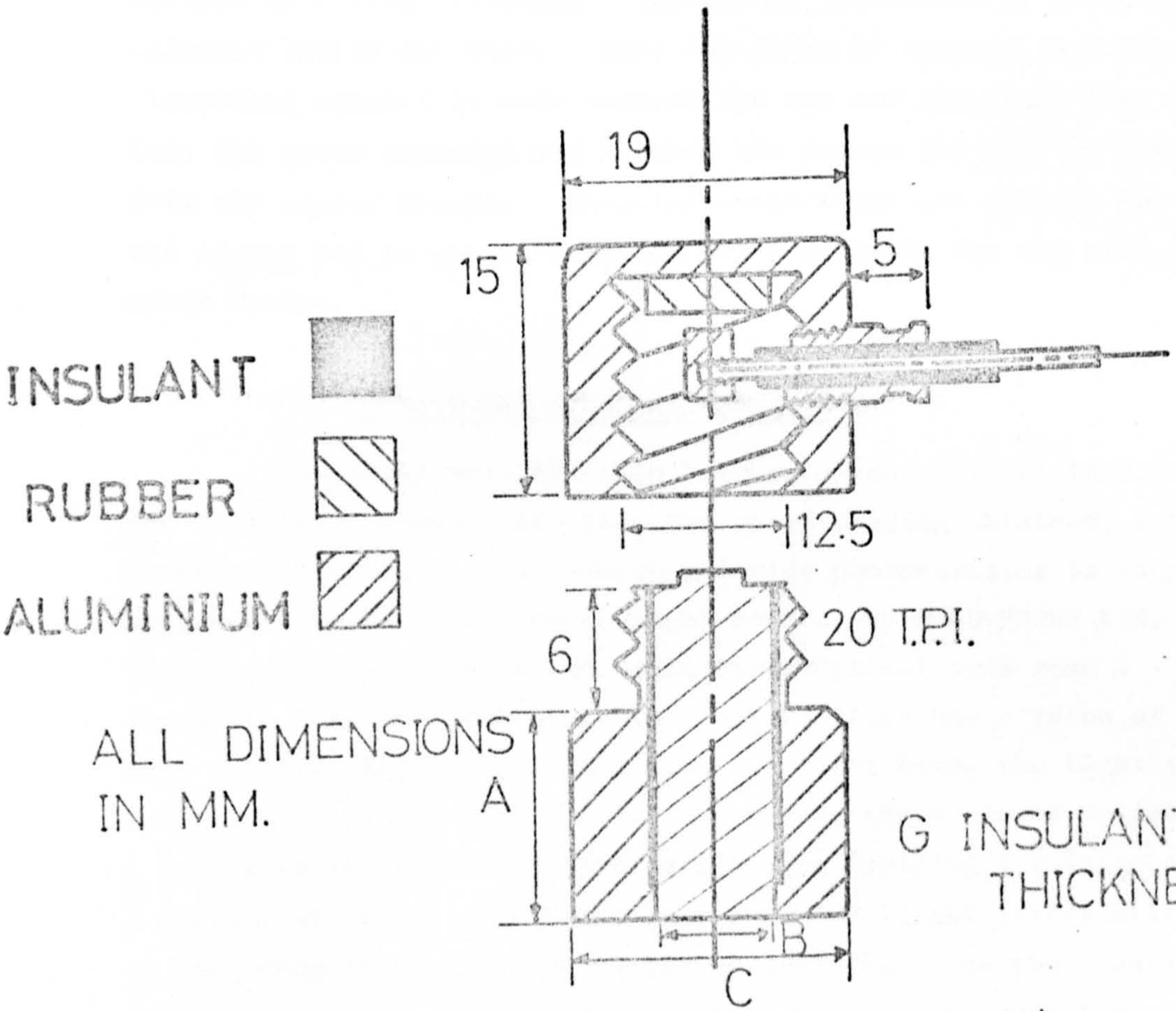

	LONG				SHORT			
G	.15	.25	.15	.15	.15	.25	.15	.15
A	13	13	13	13	4	4	4	4
B	4	6	7.5	8.5	4	6	7.5	8.5
C	18	18	18	18	18	18	18	18

probes themselves consist of a central aluminium stud insulated from an outer aluminium tube by tufnol and ISOPON resin. The centre aluminium piece was machined and a tufnol bar drilled and secured over the spindle of the aluminium by resin. When set the tufnol was machined to size to form a neat collar over most of the aluminium shanks length. The outer aluminium shape was machined (leaving a very precise clearance at the outer face) to suit the prepared tufnol/aluminium composite. After assembly and applying further resin to completely fill any air holes the probe was finished by carefully machining the face to a high finish and preparing the central stud/rear screw.

The cap was bored from one piece of aluminium and threaded to suit the probes. A rubber gasket insulates a side entrant copper rod covered in P.V.C. sleeving. The rod is terminated by a small copper cylinder inside the unit. When the probe is screwed into the cap electrical contact is made between the cap and the outer edge of the probe (via the screw threads) and between the copper rod and the inner probe rod (via the copper block). Co-axial connections are made to the cap and the copper rod to give a screened probe suitable for use with the capacitometer device.

G: ROTATIONAL SPEED MEASUREMENT

To avoid possible slip between a conventional tachometer and the rotating assembly affecting the speed reading obtained, a photo-electronic method was employed. A cadmium selenide photoresistor is supplied in a proprietry unit, with a small light source, by HIRD-BROWN Ltd. The light beam is arranged to cross the resistor's optical axis some 1 - 2 cm from the unit. In the dark state the photoresistor has a value of some 200 kΩ. When a reflecting object intersects the light beam, the light state resistance falls to some 1 kΩ. By connecting a second resistor of value 1 kΩ in series with the photoresistor and applying a voltage of some 6 V a voltage of nearly zero (dark state) or 3 V (light state) will be found at the connection. In the equipment described, the photo unit was housed in a black perspex housing fixed to the bearing support plate of the rig beneath the rotating chamber. The disc undersurface was painted matt black (JOY camera black paint) and a white sector (30^{o} included angle) added. The voltage dividing was performed in a shielded aluminium box fitted to the rig and power to the lamp and resistors was supplied from a solid state rectifier (visible on the lower shelf of the control panel -

PHOTOGRAPH 3). The chopped signal formed when the disc rotated was taken to an ADVANCE timer/counter unit (type TC 12A) and analysed to give the time per rotation.

Natural light was prevented from entering the photoresistor (and hence reducing the discrimination of the on/off state) by forming a viewing aperture for the resistor through a 1 cm hole in a black plastic plate 10 cm square. This plate was interposed between the unit and the chamber undersurface. The clearance along which natural light must pass between the undersurface and the plate is of the order of 3 mm. Viewing the voltage output with the disc rotating showed a saw-tooth signal characteristic of the slow rise time/fast decay for cadmium selenide resistors. At high rotational speeds (ω>600 r.p.m.) the signals tended to 'merge', however, by adjusting the variable triggering level of the timer, repeatable and steady speeds were indicated.

2.5.3. DISC AND ASSOCIATED EQUIPMENT ASSEMBLY

The procedure described below was followed several times during the experimental program.

Firstly the framework was checked with a T spirit level and any gross alterations in level adjusted with packing. With the disc and U channel cross piece removed the flange of the rotating steam chamber was checked using a COOKE engineers spirit level (accurate to 1 in 10,000) and by adjusting the chamber/flange and bearing housing/plate bolts the surface made level. The collector ring was lowered over the chamber and rested on the bearing plate. The disc was placed in position and the holding cap screws located to finger tightness. Using the engineers spirit level the cap screws were tightened to give as level an average disc surface as possible (better than $^{1}/_{5}{}^{o}$). The collector ring was then lifted into position and bolted into place on the uprights. The disc was then fitted with a special mild steel former shaped to give a vertical cylinder at the disc centre line when firmly bolted to the disc. With this in place the U channel was loosely bolted into position and the distributor body and jacking nut located in the centre boss. Using a clearance tool (fabricated from a portion of tube of internal diameter equal to the former diameter, external equal to the distributor body internal diameter) the channel was adjusted until the distributor body was positioned about the former with equal clearance at all radial and vertical locations. The channel retaining bolts were then tightened, a final check made and the distributor

body lifted clear. The former was then unbolted from the disc and the normal protective tube bolted into position. The upper block of the distributor (containing the inlet tubes) was then screwed into the distributor body and the unit again located in the channel centre boss. Care was taken to ensure that the distributor oil seal was not scratched on the disc's central tube at this time. Connection of the flexible flow tubes to the distributor and from the collector completed the disc setting up.

The probe carrier was assembled as follows. The carrier without the under hanging T piece was located in the U channel base by the dowel pins and the fastening bolts tightened. The probe to be used was selected and screwed into the cap. The cap was then pressed home into the tufnol T piece and one of the vertical arms of the T piece removed. The T piece was then slid under the U channel and the removed arm replaced on the protruding edge of the T. The two uprights were then pushed home into the carrier cross piece, the clearance between the T piece and the U channel undersurface adjusted and the locking screws on the carriage cross piece set.

Prior to any tests being conducted the trueness of the disc was checked using the capacitance probes. A test in which the probe faced a grounded water surface (hence level) showed that over the length of the probe carriage (some 16 cm) the probe lifted some 30 μm. Allowing for this slight variation, the true profile of the disc surface was evaluated and is shown in FIGURE 44. It will be seen that the disc shows (with respect to the 20 cm radius) a trough of some 1000 μm depth at about 17 cm radius tapering to 100 μm by 5 cm radius. Superimposed upon this radial variation is a circumferential variation consisting of a ripple of some $\pm$ 250 μm at the outer radii, $\pm$ 100 μm at inner radii. This buckling of the plate is undoubtedly due to the unrelieved machining stresses and the heat treatment necessary for the production of the surface thermocouples (see later).

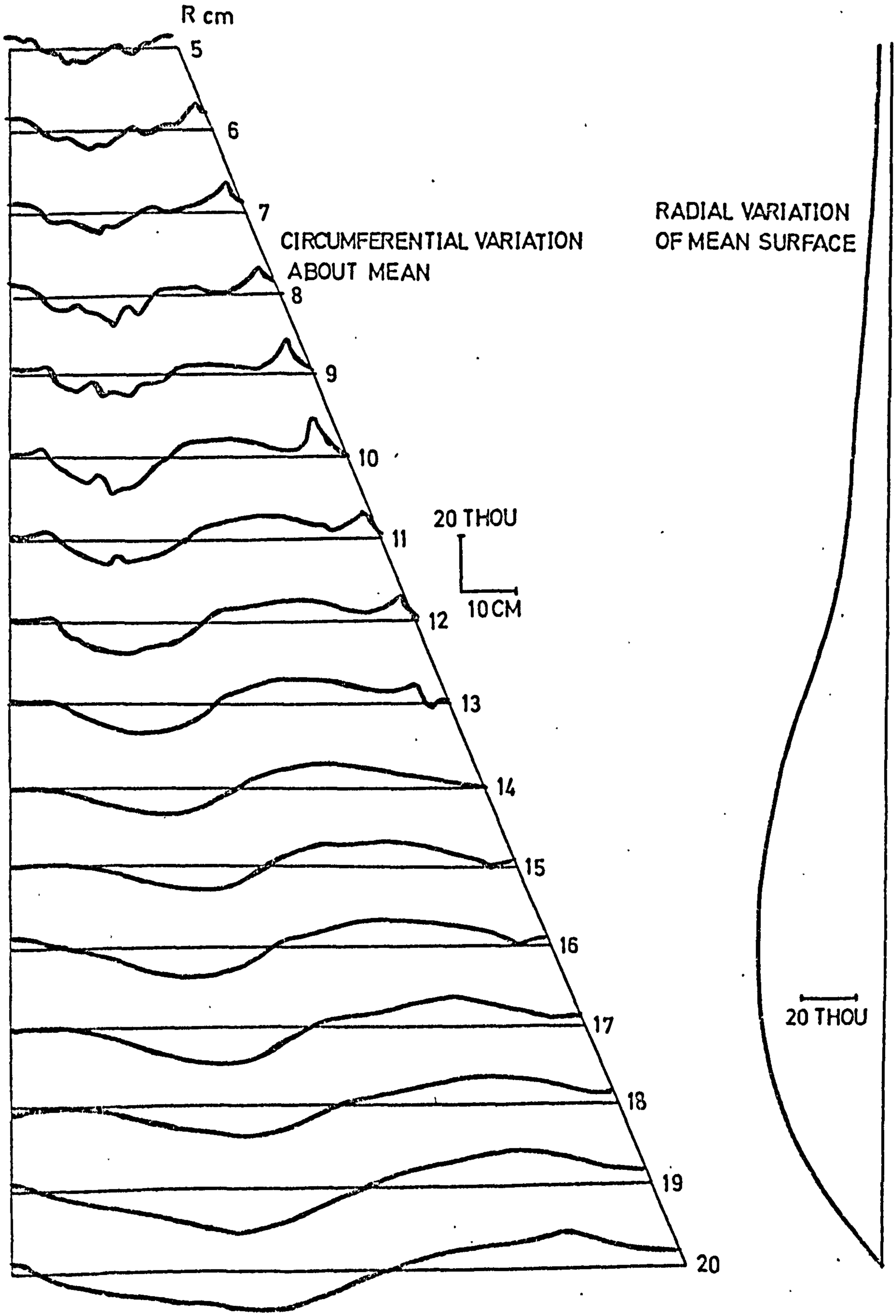

FIG44 DISC SURACE PROFILE

2.6. EXPERIMENTAL

2.6.1. CALIBRATION

A: TRACKING DEVICE

To enable a probe position to be inferred from the reading of the handle and counter, the probe carriage had to be standardised as follows. The T shaped undercarriage was set up with the capacitance probe replaced by a small brass bush 12 mm in diameter at one end, tapering to a point over a length of some 3 cm. The mechanical counter was disconnected and the carriage aligned at a known marker on the disc. This marker consisted of a thin brass plate some 10 cm long, tapering to a point at one end and dished to an arc of radius 1½ cm at the other. By placing the marker on the disc and firmly setting the edges of the dished end against the screwed down distributor body, the point end of the marker was automatically positioned on a radius of 12.17 cm, $\pm$ 50μm. The mechanical counter was then hand wound to read 0113 units and carefully fitted to the tracking unit drive shaft. Moving the hand wheel to increase the counter reading causes the radius of the tracker to decrease. Thus the radius of the tracker can be inferred from the following equation:

$$r = 12.17 + 0.127 \times \left[113 - (C + \frac{R}{50})\right] \qquad 124$$

when C is the mechanical count reading, R the hand wheel pointer value (0 - 25 x 2) and r the radius in cm.

B: ROTAMETERS

In order to calibrate the rotameters used, a special calibration rig was constructed. In essence this consisted of a glass tube some 15 cm i.d. and 120 cm long, mounted vertically. The lower end of the tube was connected to a system of slide valves, and the upper end was left free. The slide valves could divert a supply to the unit between a return from the unit and the base of the glass cylinder. A pump and drain system enabled the filled cylinder to either be left filled or drained. From the free end of the cylinder two 1 cm diameter copper tubes, each carrying a float switch, were inserted. The float switches were designed and manufactured in the Department to give an extremely rapid and positive on/off contact when immersed in a liquid. The switches were designed

such that immersion in a liquid caused the lower switch to make contact and the upper to break contact. The switches were connected in series across a 9 V D.C. supply and a solenoid operated timer.

Water from the rotameters was fed to the inlet of the rig and the slide valves arranged to return the flow immediately to the supply tank. The differential height of the two float switches was checked (having first been calibrated by filling the differential volume with a graduated cylinder) and the volume (from 1 to 16 ℓ) indicated noted. The rotameter reading was noted and the temperature of the supply water adjusted until steady. The slide valve was rapidly moved causing the flow to divert to the cylinder. As the liquid level rose first the lower float switch was operated (causing the timer to commence), then the upper switch was operated (stopping the timer). The slide valves were returned to their initial positions and the time indicated for the filling noted. Whilst the filling operation was being performed visual checks confirmed that the rotameter reading remained steady. The rotameters were thus checked over all their operating range for water at both 20°C and 50°C. Within the accuracy of the equipment (50 cc in 16 ℓ volume, ½s in time) no discrepancy to the manufacturers calibration curves was found. These calibration curves are shown in FIGURES 45, 46 and 47 for the 14X, 35X and 47 rotameters respectively.

C: TEMPERATURE MEASUREMENT

The equipment contains indicative and recording temperature sensing probes. The recording probes were manufactured from copper-constantan thermocouple wire (36 S.W.G. by SAXONIA Co. Ltd.) threaded into small bore (1 mm o.d.) modellers brass tubing. The junction was made with soft solder and was soldered into place at one end of the tube. Each thermocouple was constructed with its own ice point junction. These junctions were shielded by glass envelopes, 10 cm long by 3 mm diameter. The completed tubes were mounted in a large oil bath (3 ℓ) with a thermostatic heater. Temperatures were varied from 40°C to 110°C and were checked against a mercury and glass (0.5°C) thermometer. The output of the thermocouples was logged on paper tape by the Department's data logging system, SOLARTRON-SCHLUMBERGER analogue scanner, data transfer unit and digital volt meter A211. This equipment is visible on the right of PHOTOGRAPH 1. The calibration was repeated over the range 5 - 50° with the oil replaced by water. At any given temperature the discrepancy

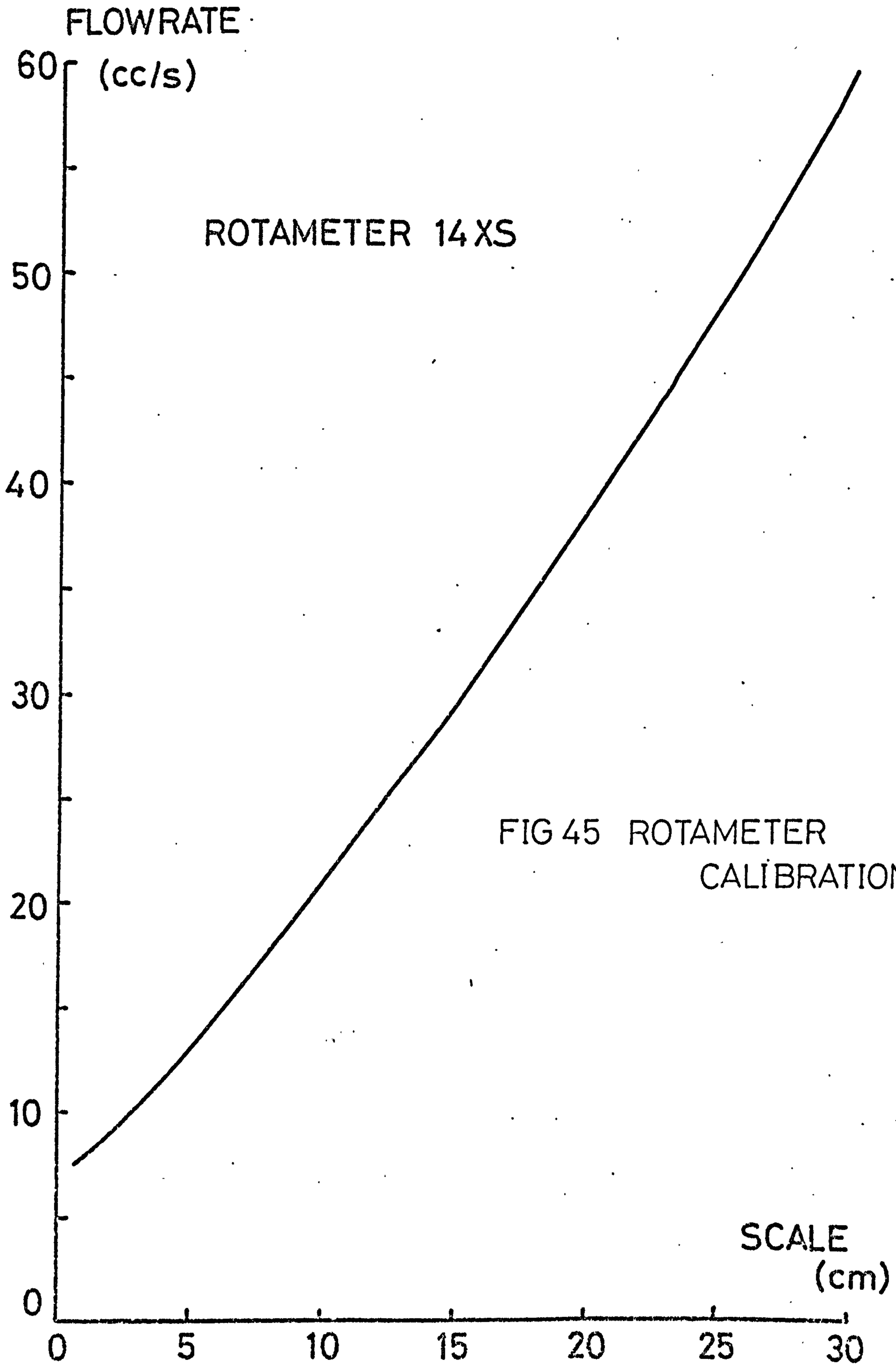

FIG 45 ROTAMETER CALIBRATION

FIG 46 ROTAMETER CALIBRATION

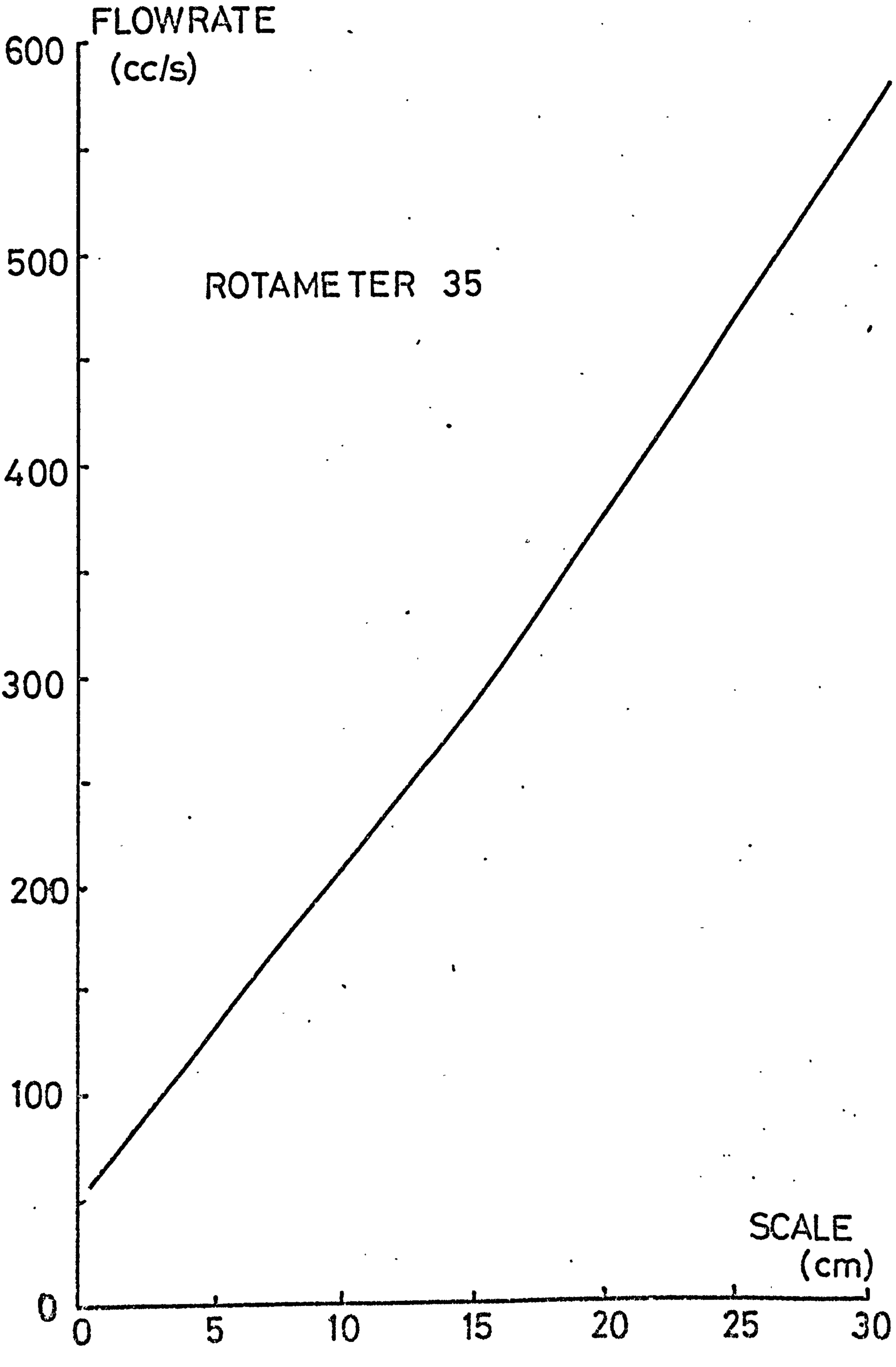

FIG 47 ROTAMETER CALIBRATION

between thermocouples was small, of the order of 0.005 mV. The final voltage/temperature characteristic was correlated by a semi-linear fit thus

$$T = 27.1\,E - E^{1.75} \qquad 125$$

when E is the e.m.f. (in mV) of the thermocouple and T is the temperature in degrees Centigrade. Accuracy of equation 125 is $\pm$ 1% over the range 0 - 110°C. Seven of the ten thermocouples manufactured were chosen for use in the work reported.

D: CAPACITANCE PROBES

It is shown in APPENDIX H that the liquid film thickness is given by

$$\delta = \frac{\Delta V}{M\left(1 - \frac{\mu_a}{\mu_L}\right)} \qquad 126$$

when ΔV is the dry plate sensor output less the plate and film output, M is the gradient of a gap/voltage plot for an air gap with the probe used (units Volts/length) and the third term represents the influence of the nature of the liquid used compared to air.

Calibration experiments were conducted with each probe to determine the value of M. A 2 - 3" micrometer was checked against slip gauges for accuracy. A special brass collar was made for the spindle of the micrometer which when fastened to the spindle formed a disc normal to the micrometer anvil. A tufnol holder was made to grip the anvil and take the probe holder. A probe was selected, screwed into the holder and the unit connected to the measuring instrument. The return earth was connected to the micrometer framework and the whole device gripped by a pair of laboratory stands. The micrometer was advanced until the disc on the spindle touched the probe face. Taking care not to disturb the disc/probe contact, the micrometer backlash was taken up and the micrometer reading noted. The analogue output from the measuring instrument was connected to the data logger and the output voltage adjusted to give -1.0 volts. The micrometer was now wound back a known amount (usually 250μm) and the new output voltage noted. This was repeated until the analogue output had reached +1.0 V. The whole procedure was then followed with the remaining probes.

The variation of the voltage output with air gap may be seen in FIGURE 48. It will be seen that each probe exhibits a linear range bounded by a non-linear range at very small and very large gaps. Accuracy of the gap was better than 2.5μm. The lower non-linearity is probably due to non-parallel effects in the disc/probe orientation and the upper deviation is most likely caused by fringing effects. Within the linear range least squares curve fitting was employed to evaluate M. The results are

Probe diameter	range	M (Volts/cm)
8.5 mm	25 - 2000μm	6.64
7.5 mm	25 - 1600μm	8.47
6.0 mm	25 - 1100μm	13.0
4.0 mm	25 - 350μm	33.5

The regression coefficients for the correlations was better than 0.9999.

2.6.2. PROCEDURE

A: FILM THICKNESS EXPERIMENTS

Prior to all experiments the tank liquid was checked to ensure that the surface showed no signs of dust or debris. If necessary the water was changed or replenished. Every two weeks the entire system was drained, flushed and recharged with distilled water. The disc surface was dusted, cleaned with a damp tissue and then polished dry. The correct probe was fitted to the probe cap and the assembly fitted into place beneath the U channel over the disc. The disc was then brought up to the speed at which the run was to be conducted and the bearings allowed to reach a steady working temperature. This required some 40 minutes at the higher speeds. All electronic equipment was switched on and the ice point thermocouples recharged with distilled water ice-cubes.

The offset voltage of the capacitance measuring instrument was adjusted to give a suitable reading on the digital voltmeter. The disc was stopped and the clearance between the probe and the disc checked to ensure that the probe would operate within its linear range. The disc was brought up to speed again, the radius count of the tracking device noted and the data logger started. A data tape of some 100 readings of the output voltage of the capacitometer was obtained and labelled.

The disc was stopped again and the distributor body screwed down

FIG48 CAPACITANCE PROBE CALIBRATION

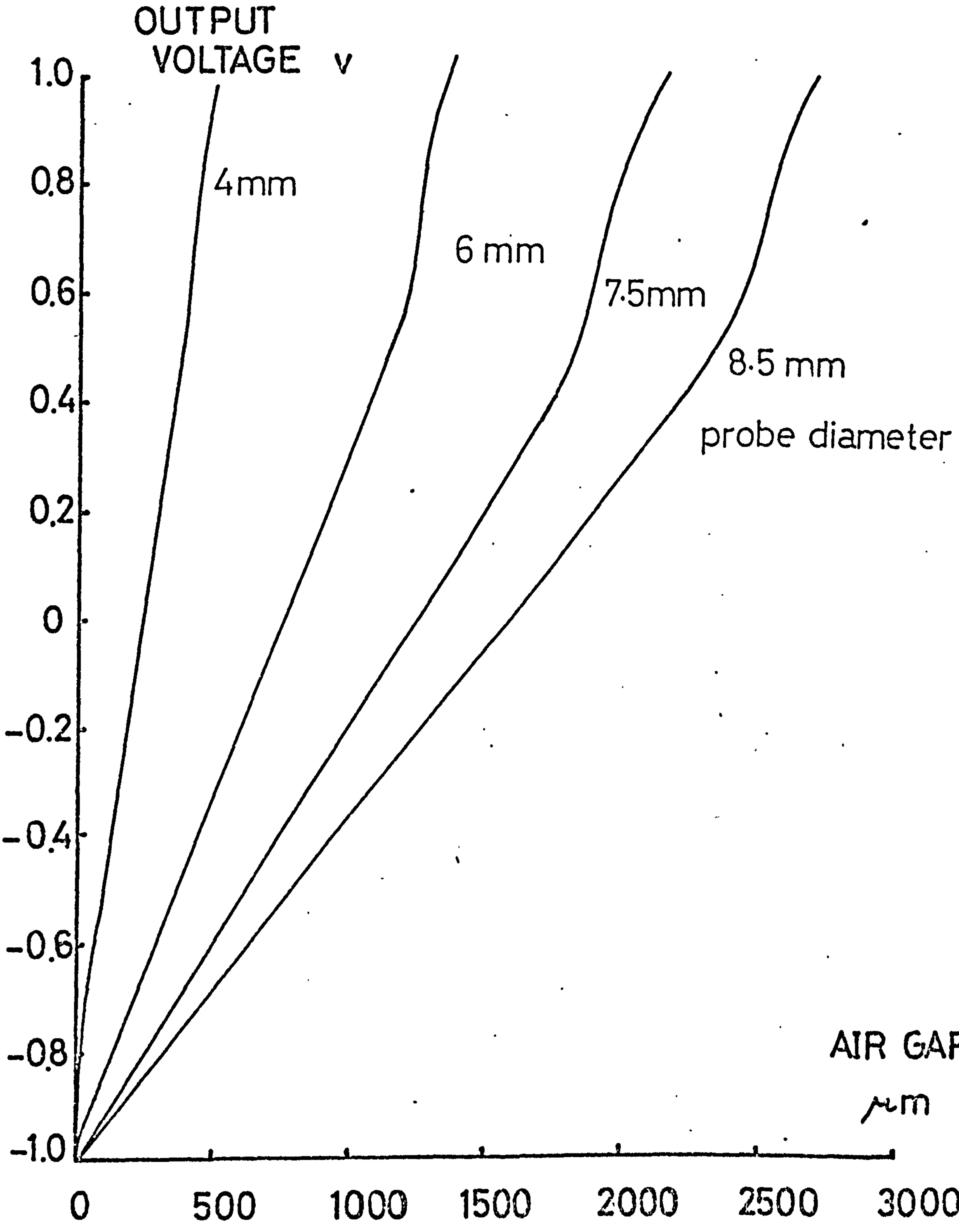

until the gap almost closed. The drainage and main pump was started with the rotameter inlet valves closed. Cooling water or heating was applied to the experimental liquid as necessary. The inlet of the rotameter selected for the flowrate required in the run was opened slightly and water allowed to fill the intervening system up to the distributor gap. Opening a drainage tap taken off the pressure tapping cleared the distributor of any entrained air. The disc was brought to speed once more and the distributor gap opened either to the value required for the run or sufficiently to ensure that the liquid entered the disc smoothly. The rotameter setting was adjusted and the equipment allowed to come to an equilibrium.

The data logger was again started and a second data tape of some 300 points taken of the instrument output with a film present and conjugate readings of the inlet and outlet thermocouple outputs. The two tapes collected were then processed by a PDP 8e computer to give the film thickness.

The data tapes were used to provide the "official" results of the experiments. However, whilst conducting the runs note was taken of the approximate average voltages visible on the voltmeter. These, and approximate system parameters, were used to calculate rough film thicknesses. These results were plotted immediately on a large scale graph to check the regions in which results had been or still had to be collected. This technique ensured an even distribution of the parameters studied.

Early experiments revealed that the length of the sampling period used to establish the average capacitometer outlet voltage was critical to the average so obtained. With long samples (say 1000 - 2000 samples), the average output at a given rotational speed was fairly well defined. With smaller samples, the mean showed considerable variation. The reason for this lies in the fact that the logger system, when driving a paper tape punch, samples at a rate of about 1 per second. At disc speeds of 60 r.p.m. or multiples the sampling "sees" a stationary disc and hence the "average" for the datum voltage is steady. At any other speed, the disc is precessing with respect to the sample point and hence, since there is a radial variation in the disc profile, sufficient samples must be taken to ensure a sufficiently widespread non-biased distribution. To sample 2000 values requires a long time and is wasteful of paper tape. The solution to the problem of achieving a representative mean consisted of smoothing the instantaneous output of the capacitometer.

FIGURE 49 shows the circuit employed. In essence the circuit consists of an operational amplifier used with unity gain and with a selectable capacitance in the feed-back loop. The calibration procedure employed is as follows. A millivolt calibrator (MANARP ELECTRONIC INSTRUMENTS Ltd.) was used to supply a constant reference voltage from 0.1 mV to 1 V to the input socket. The variable 50 KΩ resistor was adjusted to give an identical voltage at the output. The 500 KΩ resistor was adjusted with the input switched to the non-inverting input of the op. amp (after circuit modification) to give unity gain once more. With the input grounded the 10 KΩ resistor was adjusted to give an output of 0 V with respect to earth. When the amplifier had been so calibrated connections were made to the capacitometer output and the logger input. The capacitance values employed in the unit gives fixed circuit time constants of 0.1, 1.0 and 10.0 seconds. To ensure that the filter circuit worked satisfactorily the following experiment was conducted. The signal from the capacitometer was simultaneously fed to an oscilloscope and the filter circuit. The output from the circuit was logged for 1000 s with each of the three feed back capacitors in turn, and for the filter circuit removed (capacitometer direct to logger). Analysis of the oscilloscope trace by planimetry and digital analysis of the direct and filtered tapes gave an average agreed to within 1%. The operational amplifier was found in the calibration procedure to have gain slightly greater than unity, 1.0018. This was not corrected and was allowed for in the analysis programs (see APPENDIX G).

The filter circuit (the unit is visible to the left of the capacitometer in PHOTOGRAPH 3) was employed in all the experiments reported herein.

At the close of an experimental session, the main pump was stopped and the water in the distributor and feed tubes allowed to drain onto the disc. The rotameter valves were closed and the disc speed gradually reduced. The disc surface was dried using tissues, covered with clean tissues and all electrical equipment made safe.

B: ENTRANCE GAP EXPERIMENTS

In order to collect some information on the entry inertia effect, film thicknesses were measured with specific entry gaps. The disc was cleaned and a datum calibration tape taken as in (A) above. The distributor gap was closed and water from the rotameter selected allowed

FIG 49 FILTER CIRCUIT

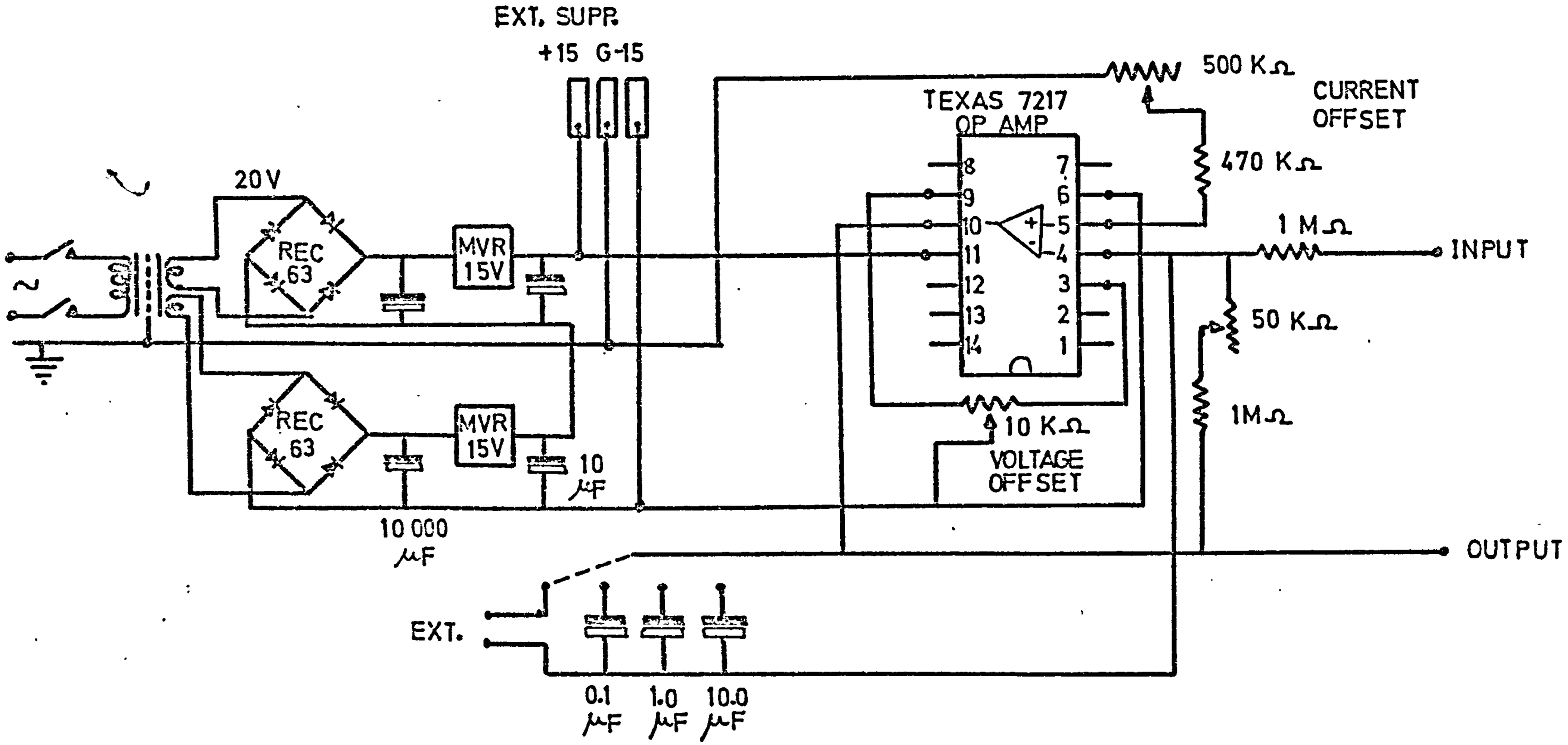

to fill the distributor. The distributor jacking nut was now wound back a specific amount (usually $\frac{5}{8}$ of a full turn, corresponding to a 625μm gap increment) and after allowing the film to stabilise the 'wet' output voltage of the capacitometer recorded as usual. The distributor gap was then opened a further increment and another 'wet' reading made. This process was repeated until the maximum gap studied (250 thous, 0.635 cm) was reached. The disc was then dried, the probe moved to a new radius and the process, including the datum reading, repeated. In this way, profiles of the change of film depth with radius were built up. To check that the stopping and starting of the disc and flow had no effect on the film thickness, the probe was occasionally left in one place whilst the disc and flow were stopped. Upon restarting the new film thickness never varied from the old by more than 5% if at all.

Usually as the gap opened so the film thickness at any radius tended to increase. Occasionally, and especially at short radii, this could lead to flooding of the probe. If this occurred the disc and flow were stopped and the probe surface redried. The probe carrier was then raised and a slip gauge of known thickness placed on the disc beneath the probe. Providing that the air gap between the probe and the gauge was within the linear range of the probe, the datum 'dry' plate zero was now taken with respect to the slip gauge surface. In this way a false zero was established for the air gap. When the water film was re-established, after removal of the gauge, then to the indicated film depth (with respect to the slip gauge surface) was added the gauge thickness. This thickness should be corrected for the relative permittivity of water compared to the metal. Since for water $\mu_L \approx 80$ and for metal $\mu_M \approx 1000$ then the correction is about $1/80$ or some 1.25%, and the correction was ignored. The maximum film thickness measured in this way was some 0.25 cm thick.

C: SURFACE VELOCITY EXPERIMENTS

Surface velocity was measured using the surface wave technique outlined earlier (Section 2.2:B). The pointer consisted of a length of the thin brass tubing (as used to strengthen the thermocouples) with a fine needle inserted at one end. Just prior to the needle the tubing was bent into a right angle. The tube was gripped by a clamp which tightened onto the surrounding collector ring. This clamp enabled the inclination of the tube to be adjusted and ensured that the needle just touched the film surface. With the disc stationary the tube length was

aligned along an axis and the needle positioned at the desired radius.

A Polaroid camera was held rigidly in a framework clamped on the top of the box framework of the rig. The camera was held in such a way that it viewed the needle and the tube from vertically above. With the disc illuminated from the side by a 1 kW quartz iodine lamp, a ruler was placed on the disc surface adjacent to the needle and a photograph taken. This photograph enabled the reduction of the lens and the focus of the camera to be checked. At the same radius, but at another point on the circumference, the capacitance probe was set up as indicated earlier to measure by inference the experimental film thickness at the point under the needle.

The film flow was established on the rotating disc as outlined earlier. The needle was gently lowered until it could be seen to touch the film surface and ripples seen upstream of the pointer. Viewing through the camera viewfinder the side illumination was adjusted to show the ripples in the best relief and a photograph taken. Typical photographs are shown in PHOTOGRAPH 5. Details of the system parameters (flowrate, speed etc.) were noted on the rear of the photograph. The procedure was then repeated for various other parameters.

The technique was found to be practical only within a fairly narrow band of flowrates and speeds etc., owing to the clarity with which the ripples can be photographed and hence the wavelength subsequently evaluated. However, the technique had the distinct advantage of experimental simplicity.

D: FILM BREAKDOWN

In order to test the theory for film breakdown developed earlier the following procedure was employed. Flow was established on the disc as previously noted with the capacitance probe positioned at the outmost radius (21.2 cm). A speed was selected and a high flowrate established. The flowrate was gradually reduced until visual and indications from the capacitometer (which suddenly showed marked variations as alternately wet and dry portions of the disc were presented) showed a breakdown of the film at the edge. This was repeated with a very low flowrate which was gradually increased, this time until the film was just reformed.

At very high speeds visual identification became difficult and a stroboscope was employed to help freeze the movement.

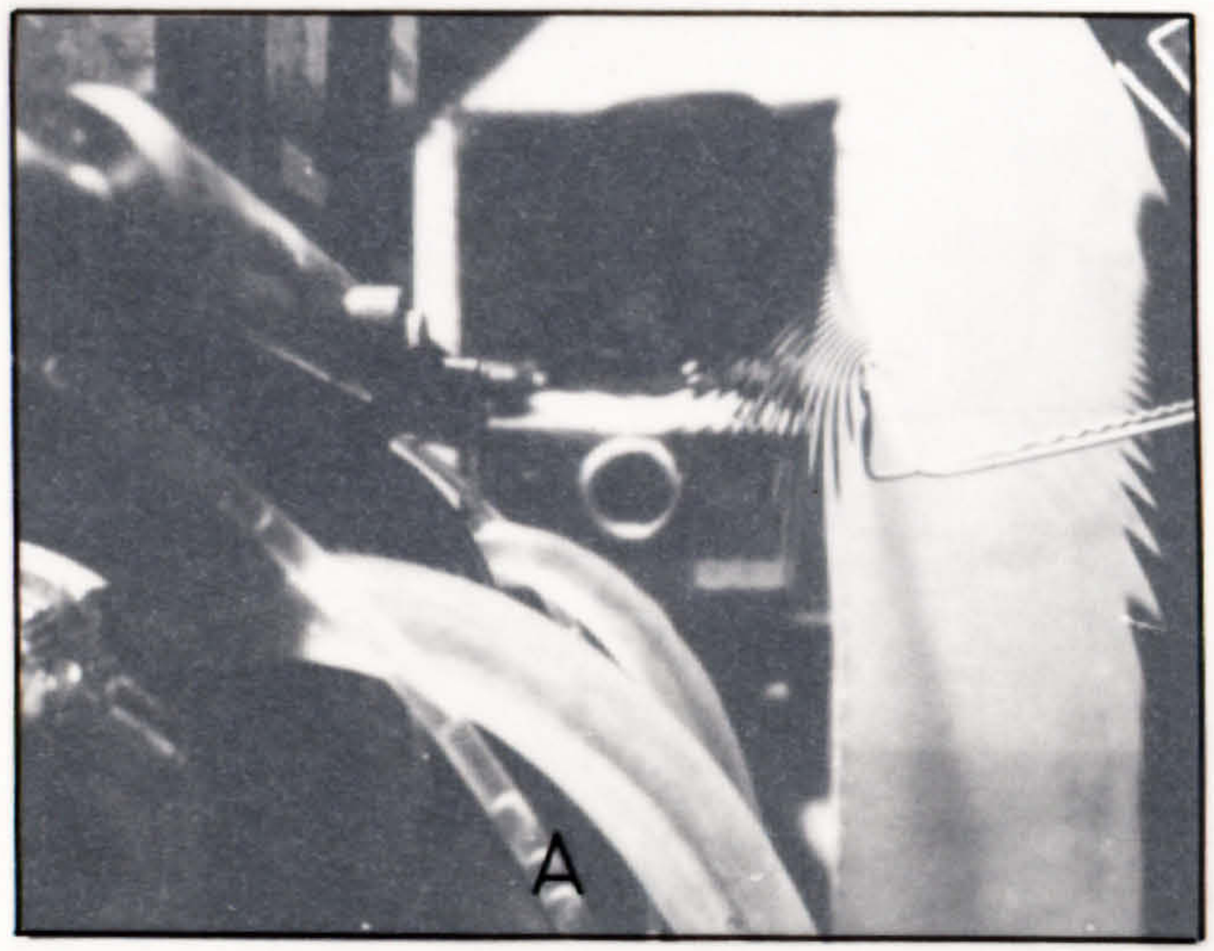

Q = 80 cc/s δ = 400 μm

ω = 50 rpm

R = 16 cm

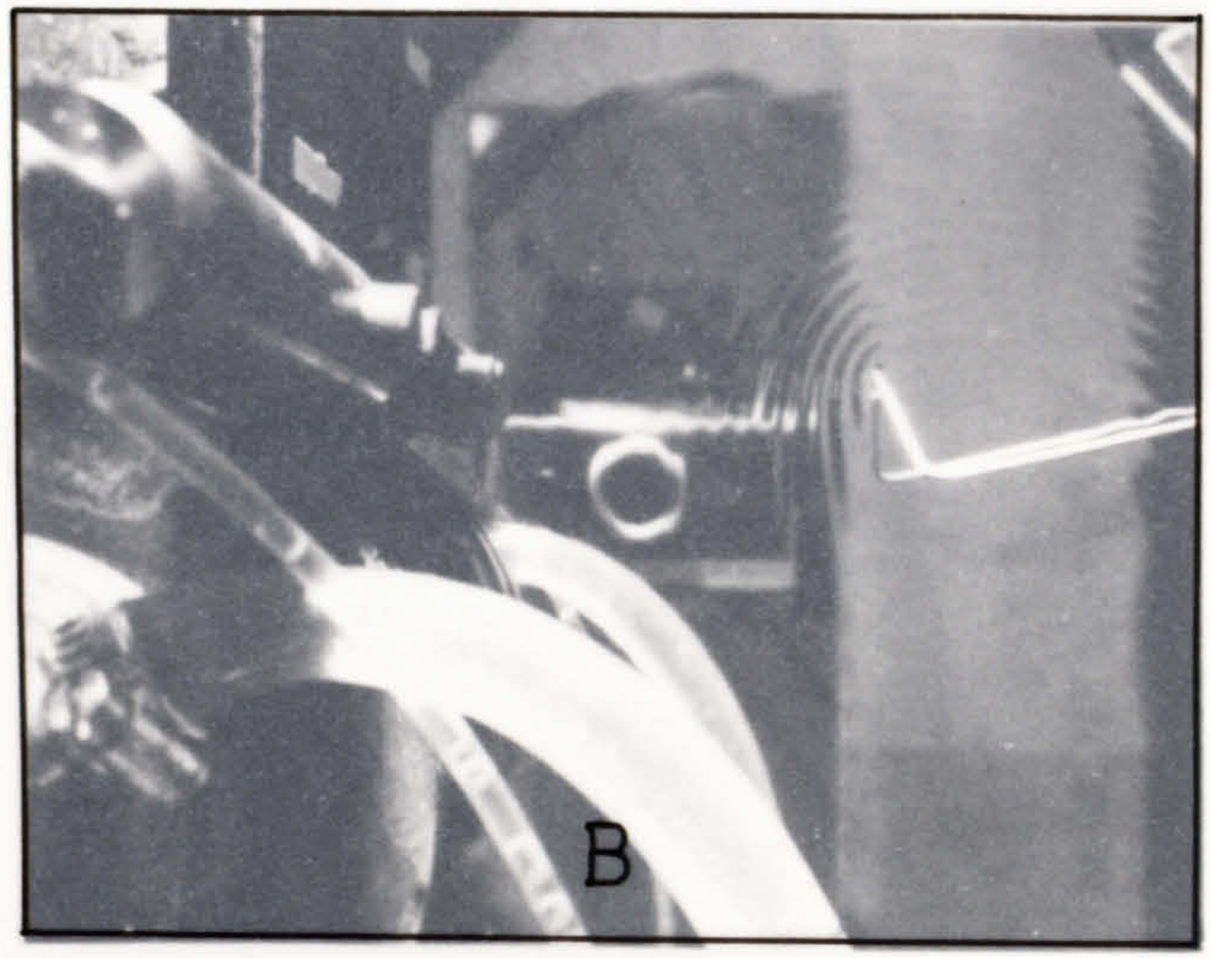

Q = 150 cc/s δ = 776 μm

PHOTOGRAPH 5

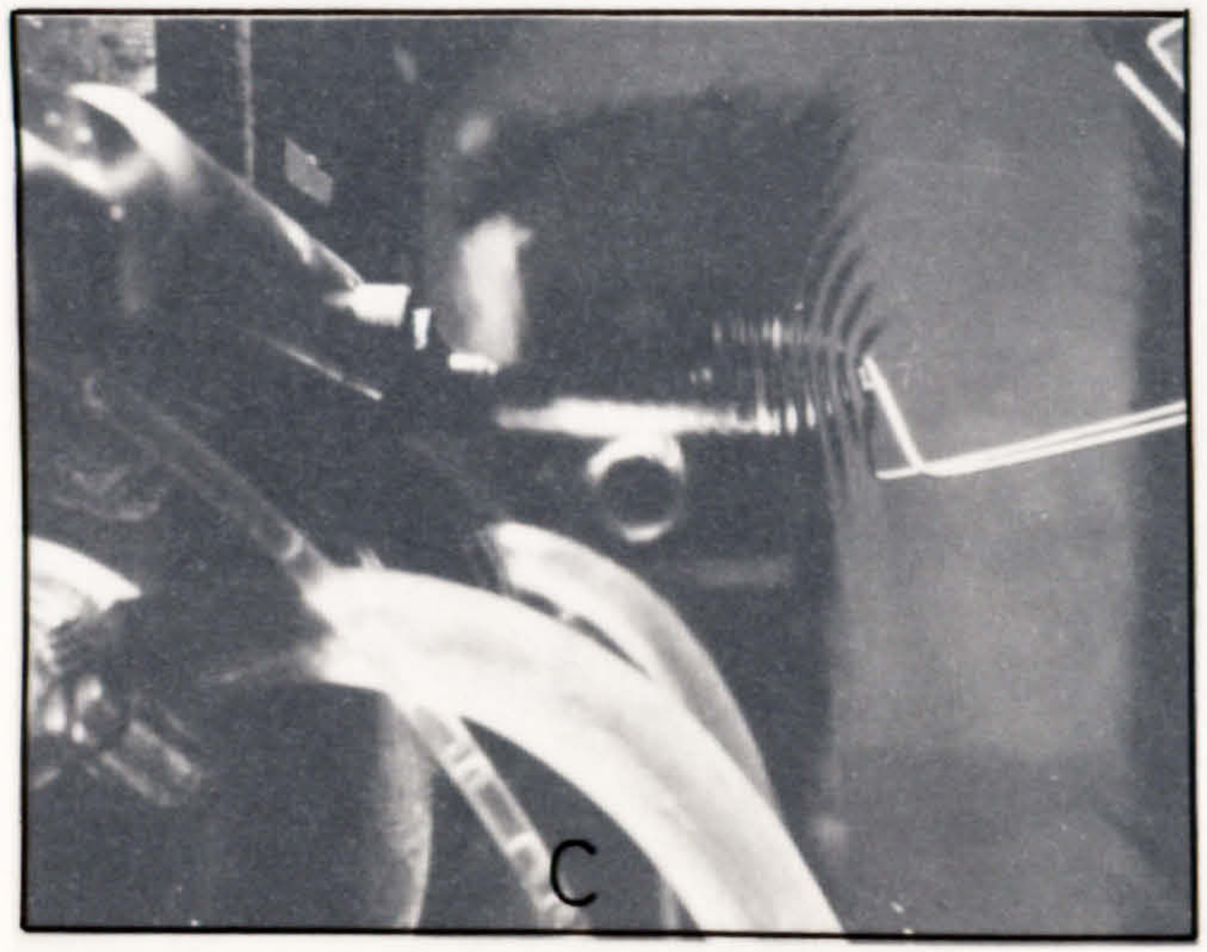

Q = 225 cc/s δ = 920 μm

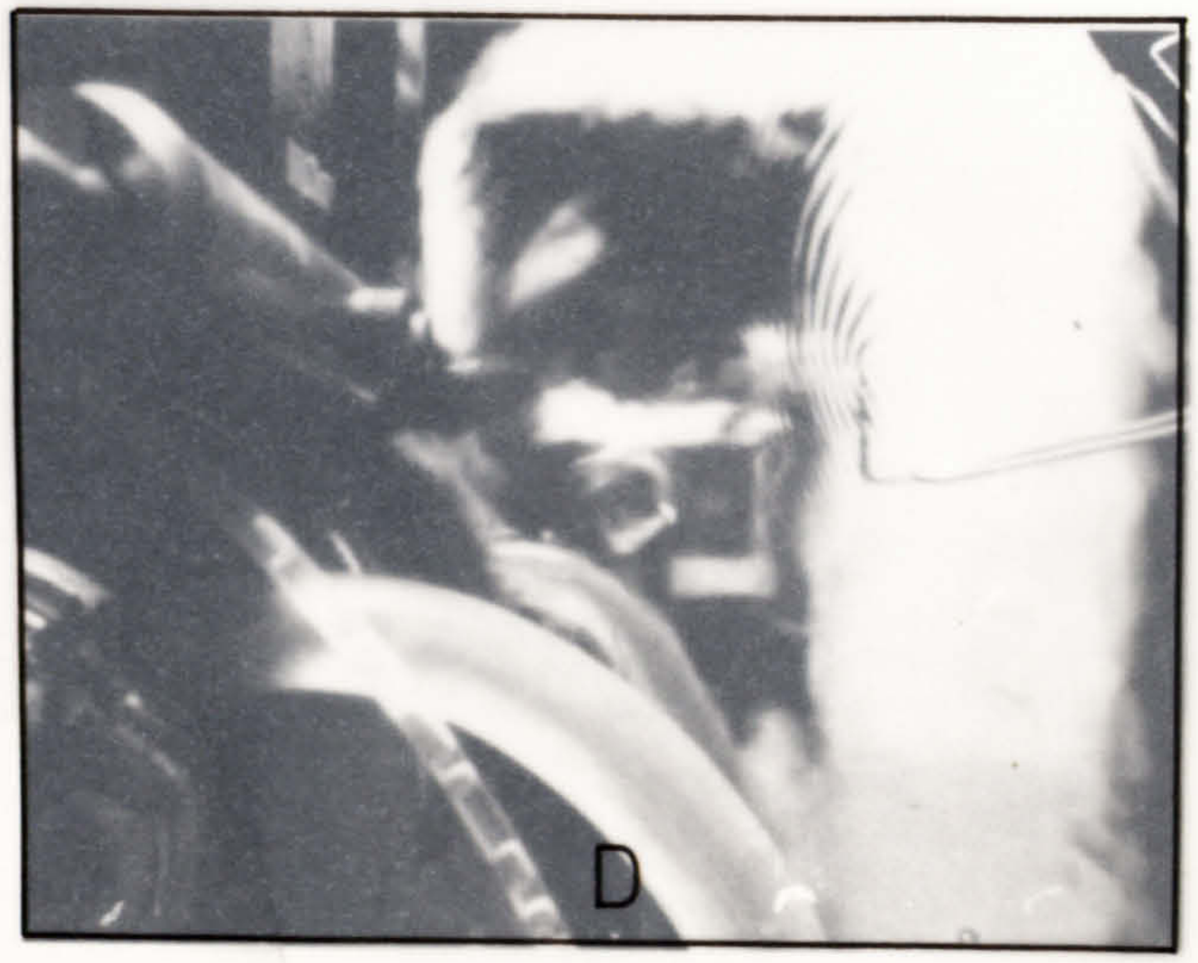

Q = 340 cc/s δ = 976 μm

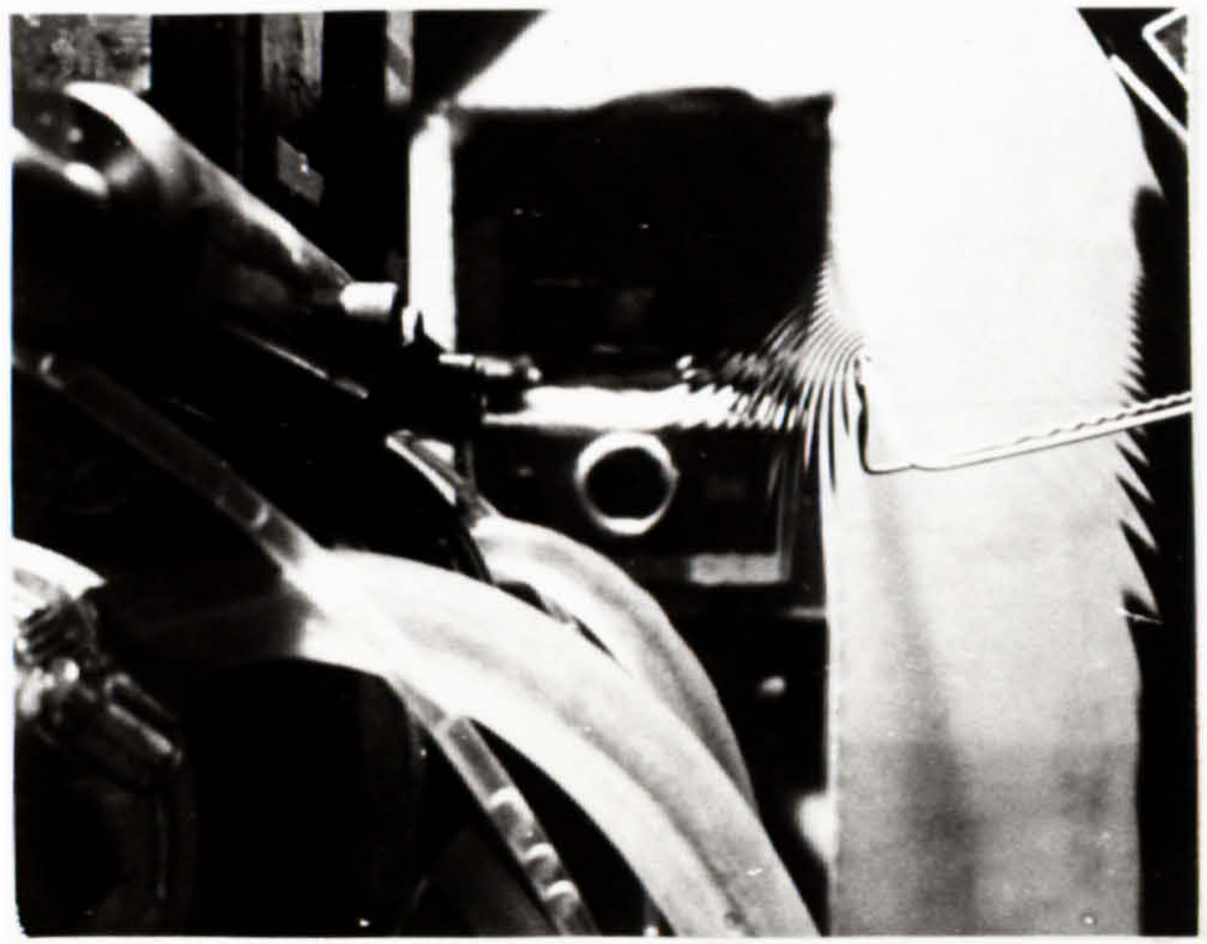

Q = 80 cc/s δ = 400 μm

Q = 225 cc/s δ = 920 μm

ω = 50 rpm

R = 16 cm

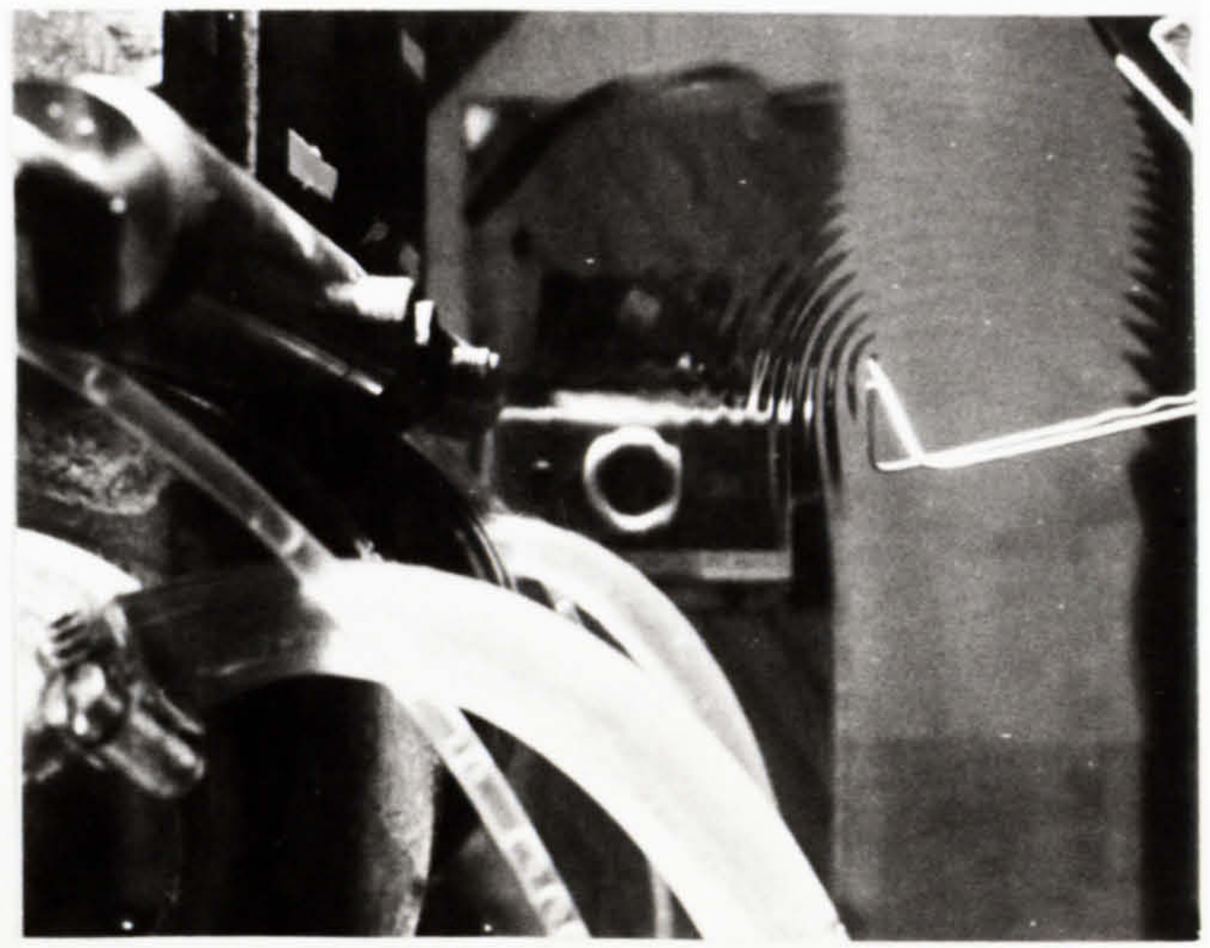

Q = 150 cc/s δ = 776 μm

Q = 340 cc/s δ = 976 μm

It was found impossible to consider breakdown at radii other than the edge of the disc. This was due to the fact that the broken film presented a 'jagged' radial distribution and the only way a mean breakdown radius could be obtained would have been through planimetric studies of a normal photograph of the entire disc. This was impossible on the present disc owing to the masking of the disc by the distributor and associated holder.

E: WAVES

Apart from the qualitative work indicated later, quantitative measurements of wave amplitude were performed as follows. The filter between the capacitometer and the voltmeter was removed and a connection made to an oscilloscope (HEWLETT-PACKARD 189A). The oscilloscope beam was reduced to the lowest intensity in 'conventional' mode and a Polaroid camera fitted to the screen. The disc was set up as before and a dry calibration tape made (with a filter switched in) with the disc rotating at a specific speed. The oscilloscope was triggered by a parallel timing pulse taken from the speed measuring equipment and a trace of the dry surface radial profile taken (with the electronic filter switched out) with the camera in open shutter mode. Triggering of the oscilloscope was stopped and film flow established on the disc. When conditions had equilibrated, the oscilloscope was again allowed to trigger from the timing pulse (thus ensuring that the disc surface was always in phase in each photograph) for a period of some 10 minutes, the camera again open shuttered. A 'wet' data tape was taken then, with the filter switched in.

At the end of the second sampling, the photograph was removed and the voltage and time settings of the oscilloscope noted. Typical results can be seen in PHOTOGRAPH 6. It will be seen that the basic disc radial profile (the single intense sine-wave like trace) is duplicated by a thicker offset band. This band represents the multiple tracing of the instantaneous film thickness on the disc. The thickness of the band is indicative of the amplitude of the waves. To obtain quantitative values for this amplitude, the mean film thickness obtained from the data tapes is related to the photographic distance A + $\frac{1}{2}$B when A is the length of the dark band between the intense sine wave and the lower portion of the wave band (corresponding to minimum film thickness) and B is the width of the wave band (or wave amplitude).

The analysis of the above results is outlined in APPENDIX J.

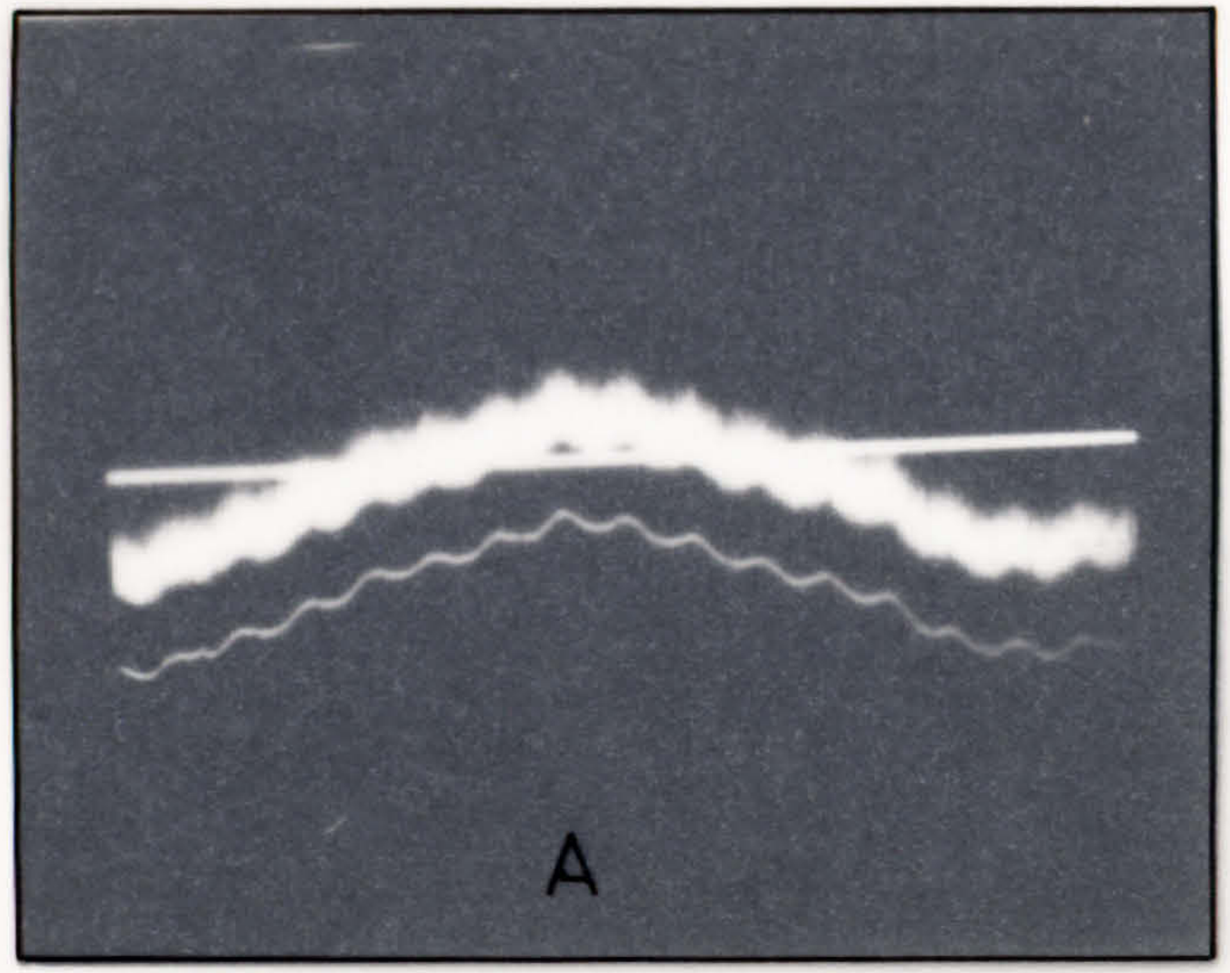

ω = 300 rpm

R = 15 cm

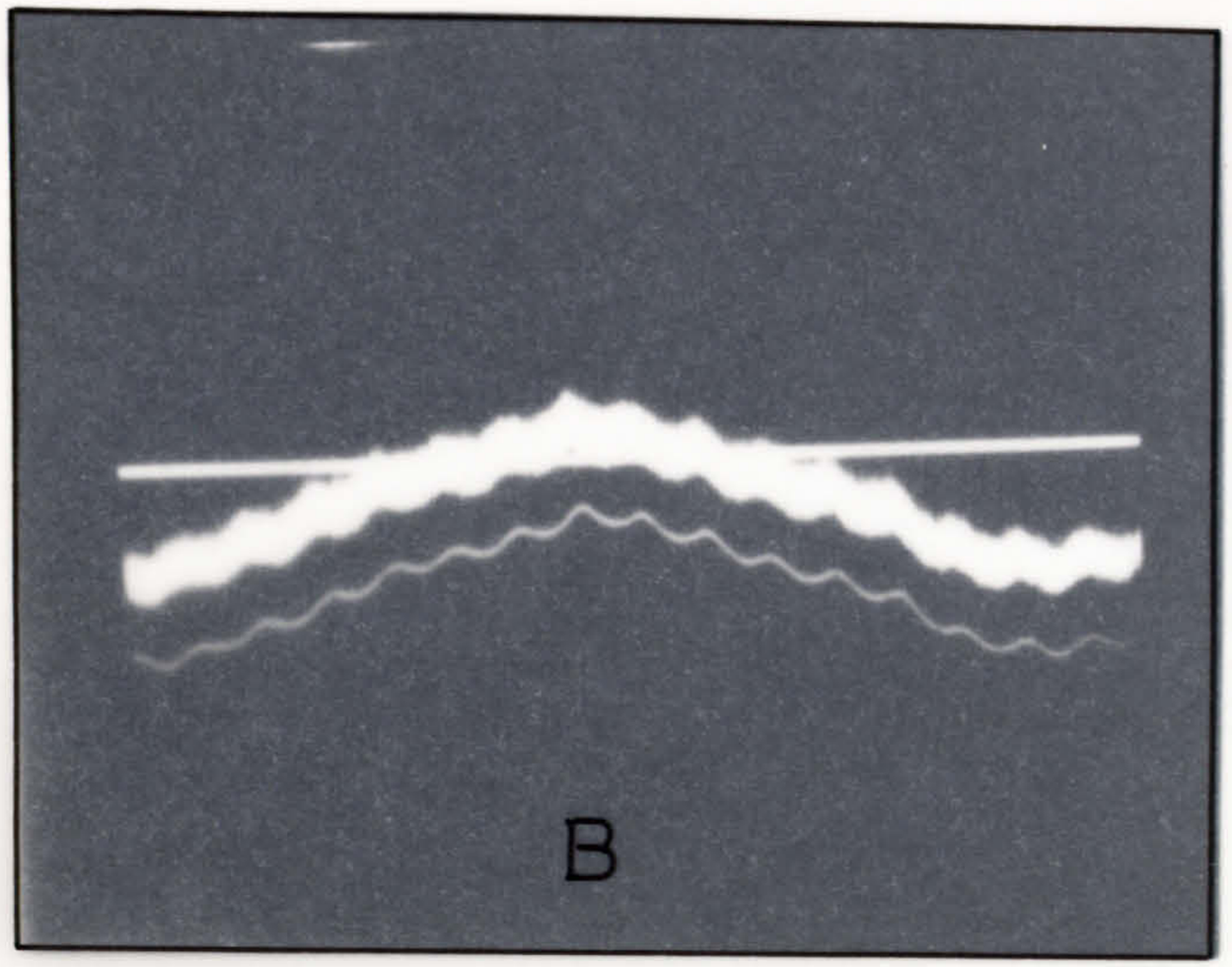

Q = 50 cc/s δ_m = 124 μm

Q = 100 cc/s δ_m = 154 μm

PHOTOGRAPH 6

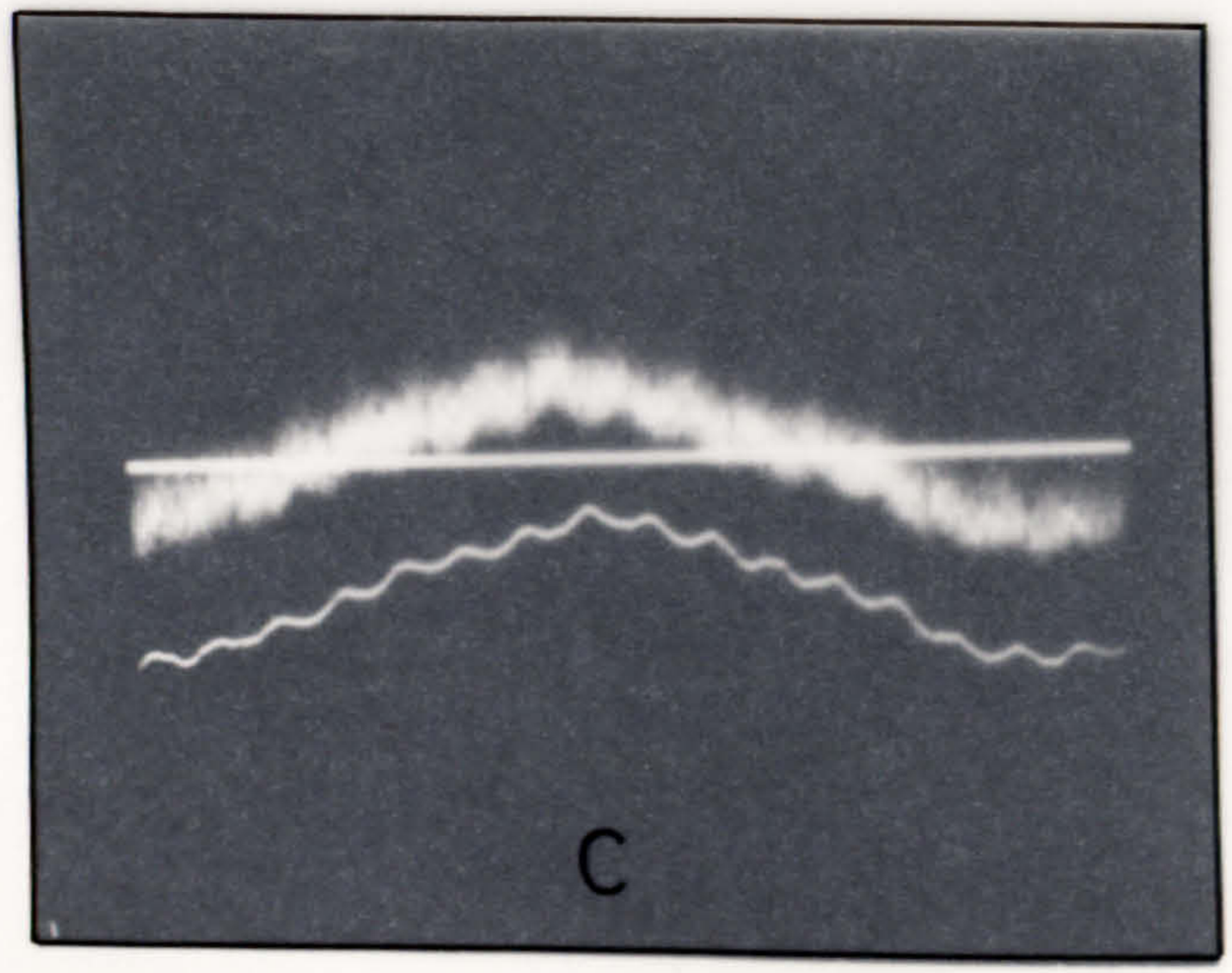

Q = 200 cc/s δ_m = 195 μm

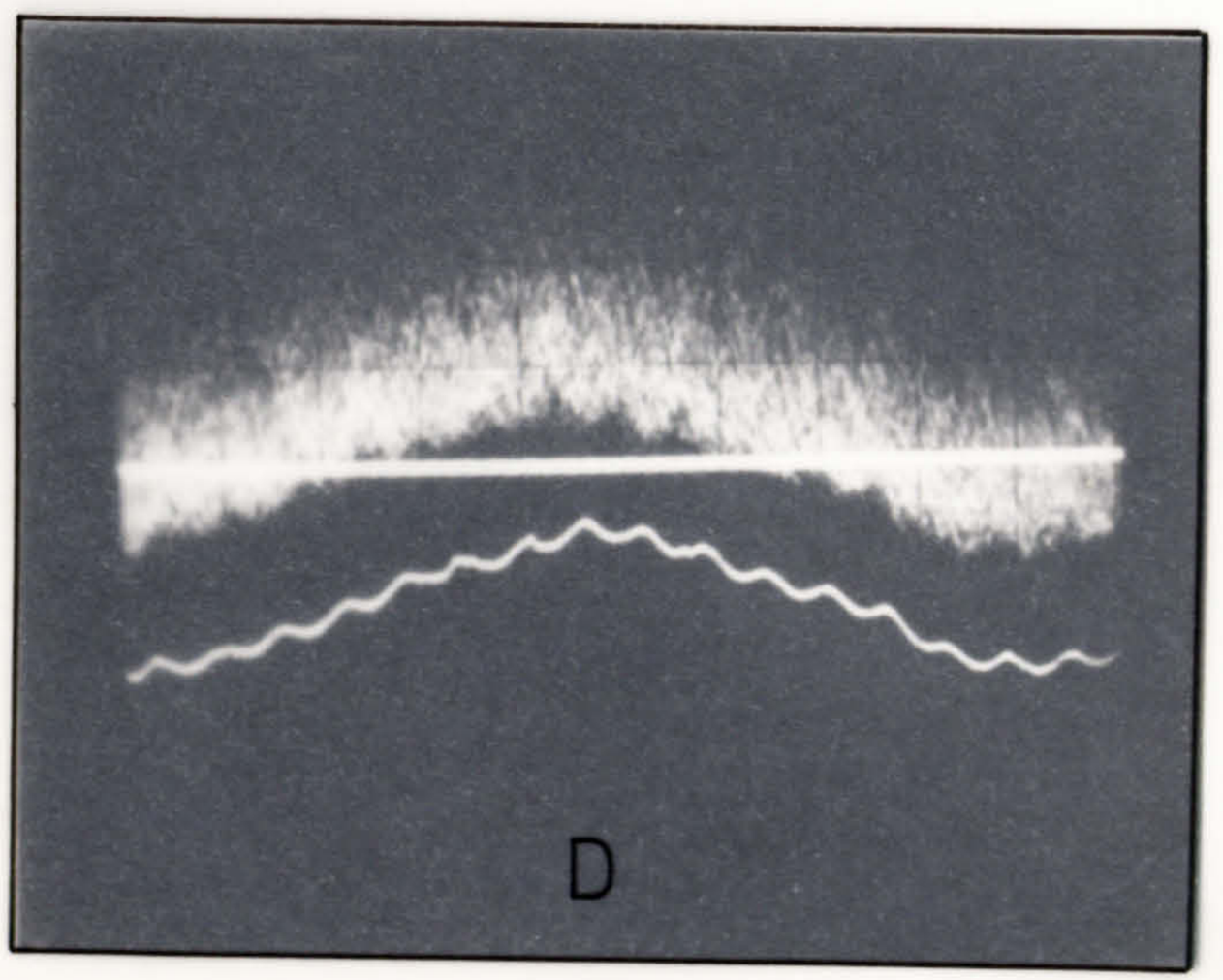

Q = 300 cc/s δ_m = 225 μm

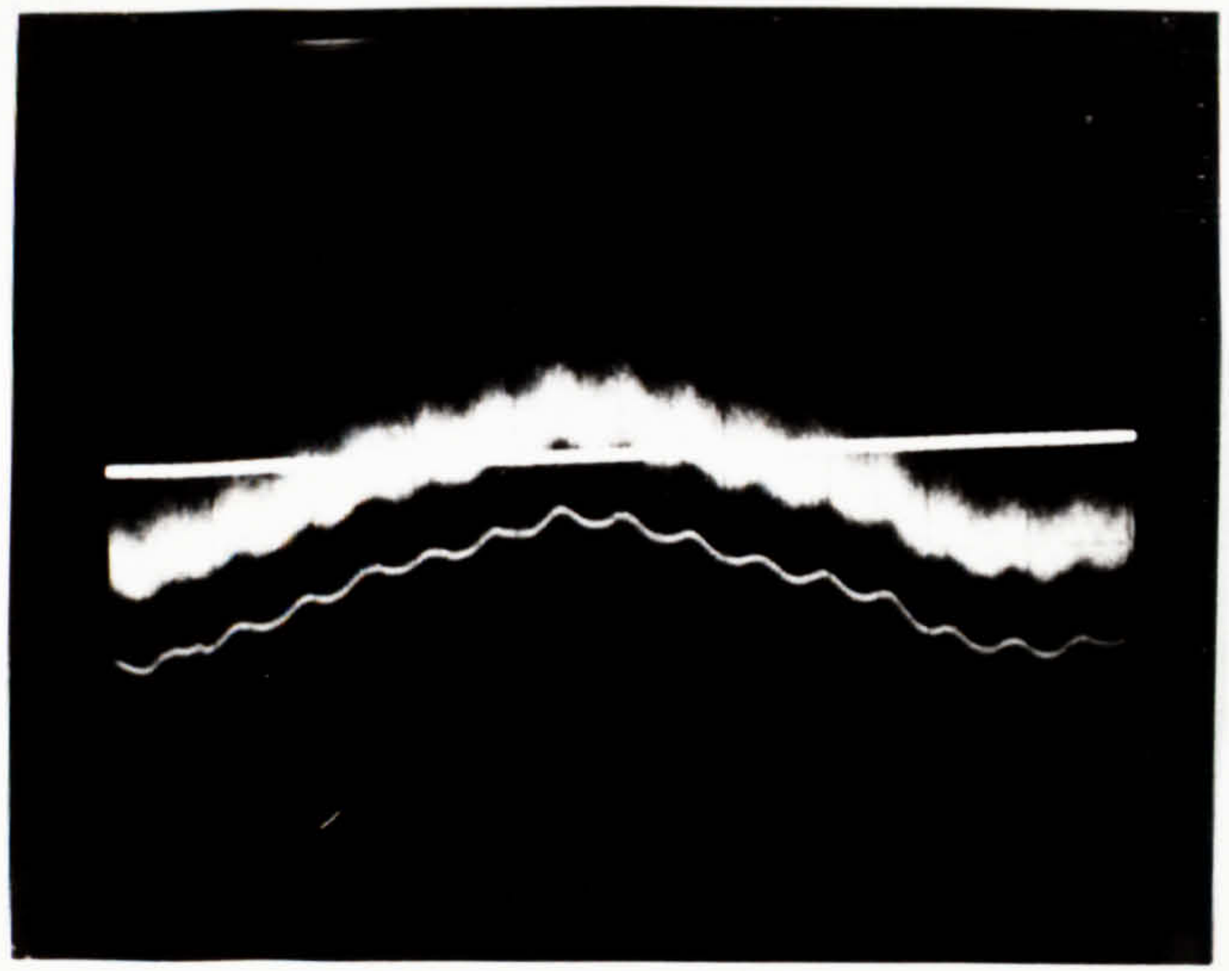

Q = 50 cc/s δm = 124 μm

ω = 300 rpm

R = 15 cm

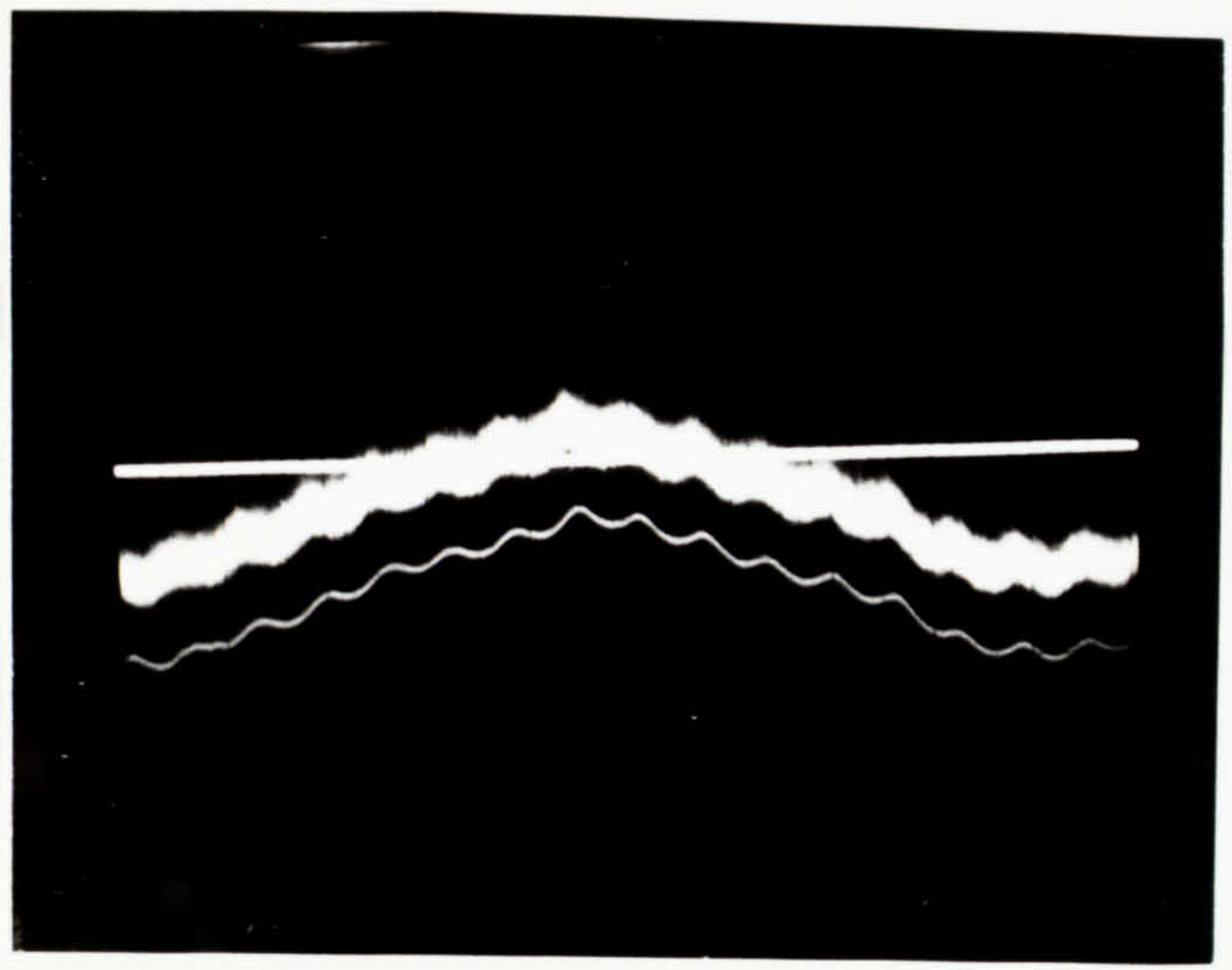

Q = 100 cc/s δm = 154 μm

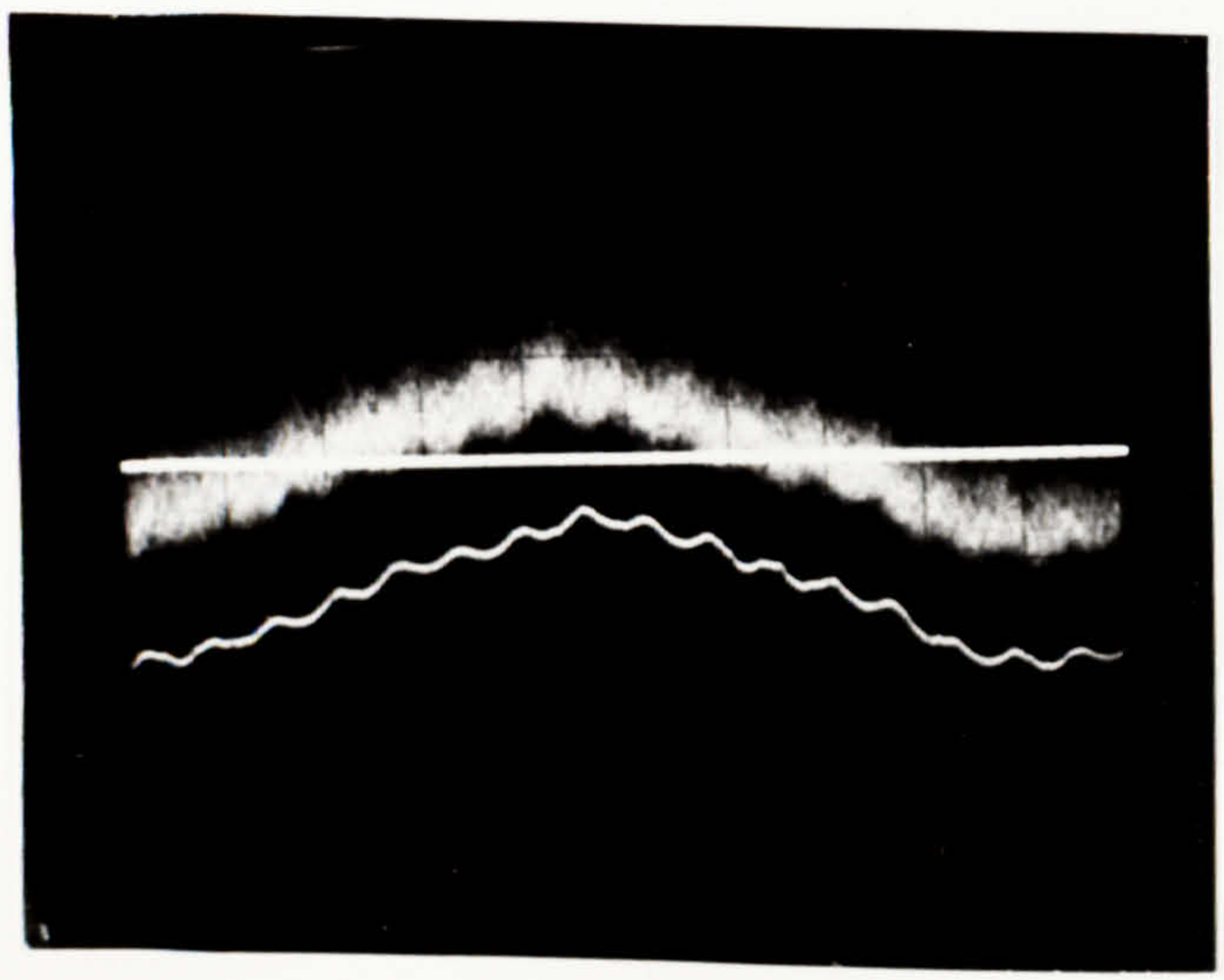

Q = 200 cc/s δm = 195 μm

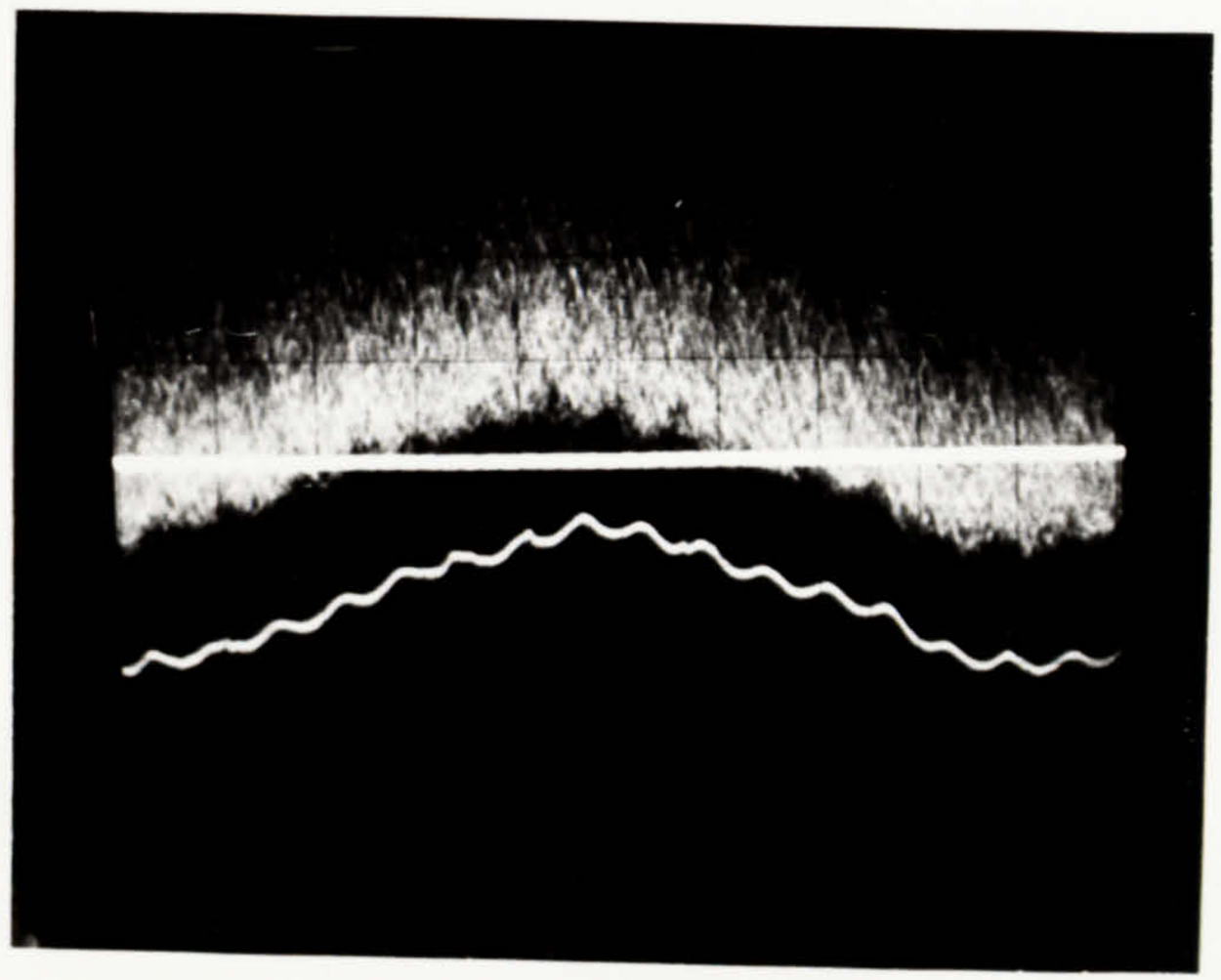

Q = 300 cc/s δm = 225 μm

It should be noted that the traces made of the film 'wavy' thicknesses are done so over a considerable area (some 1 cm diameter) due to the restrictions of the capacitive technique employed. This strictly reduces the value of the results to an indicative level although comparison to CHARWAT et al's results (see later) shows some agreement. CHARWAT et al employed a sensing technique over a 1 mm square area.

2.7. RESULTS AND DISCUSSION

A: GENERAL

Reference to FIGURE 50 shows the typical regimes observed on the disc with water at varying flowrates and disc speeds. Three boundary radii are used, 9, 14 and 19 cm and the significance of the diagram can be understood if one considers the action of increasing disc speed with a constant flowrate of some 100 cm^3/s. At low speeds ($\omega<2$ rev/s) the entire disc surface appears to be covered with a smooth flat film (in area marked SMOOTH FILM). If the speed is increased, to say 20 rad/s, then the Q/w intersection on FIGURE 50 is now to the right of the 19 cm radius line and to the left of the 14 and 9 cm lines. At this speed the entire disc is no longer covered by a smooth film. The smooth film now occupies a smaller area of the disc limited to radii less than about 14 cm. At greater radii the liquid film is characterised by regular ripples. These ripples appear to be the spiral waves noted by CHARWAT et al (143). Increasing the speed further to say 40 rad/s places the intersection to the right of the descending 19 and 14 cm lines and to the left of the 9 cm line. Thus the liquid surface is smooth up to at least a radius of 9 cm, then forms ripples and by a radius of 14 cm has developed into a 'gray' film. The 'gray' film is a marked contrast to the smooth film in that the surface appears very agitated and the reflections from the polished disc surface are not visible.

Increasing the flowrate from zero at a speed of say 15 rad/s reveals the following series of events. Initially the film is broken and flows as rivulets (in BROKEN FILM area). At a flowrate of some 25 cm^3/s mechanical brushing of the disc surface causes the rivulets to join and form a stable film. At a flow of some 50 cm^3/s the film is smooth to a radius of 9 cm and exhibits regular ripples over the remainder of the disc. A flowrate of 100 cm^3/s extends the smooth film to at least 19 cm radius. Increasing the flowrate further gives signs of jetting from the inlet, presumably due to imperfections in inlet design. Increasing the speed of the disc once the liquid shows signs of jetting causes the film to progress directly to the gray film regime (without any regular ripples). It seems likely that the gray film results from centrifugal action causing the crests of ripples or jets to break off and impact upon following fluid. With this in mind, the appearance of the gray film closely resembles a liquid film impacted by many small droplets.

FIG 50 FLOW REGIMES

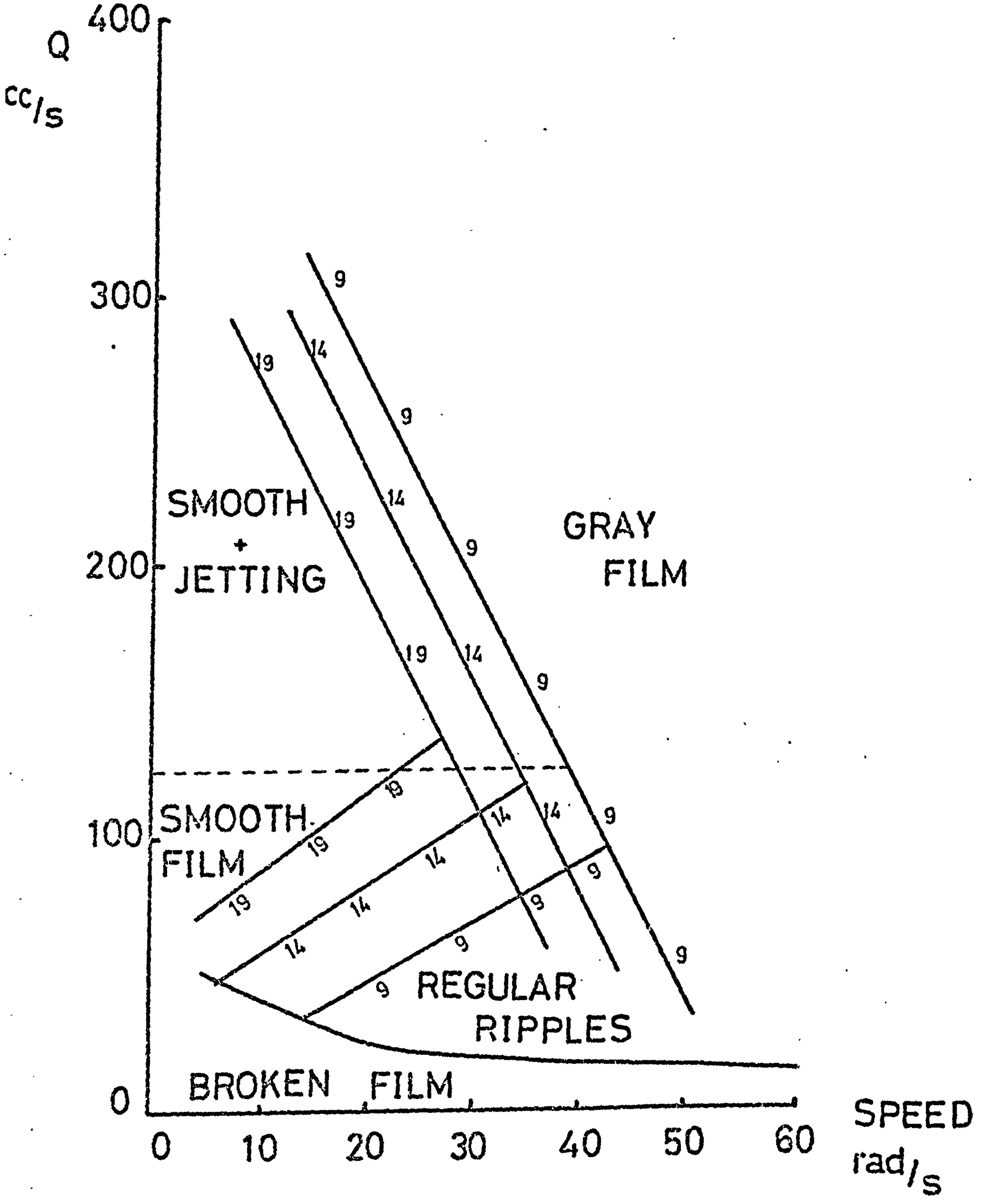

FIGURE 51 shows the same information as FIGURE 50 in schematic form with the radius plotted as a third dimension. FIGURE 50 may be regarded as a plan view of FIGURE 51. The gray film regime in FIGURE 51 is towards the reader, normal to the plane of the diagram. FIGURE 52 details the Re/Ta area previously investigated for which independent Re and Ta values are available or computable. Shown on the diagram are the practical limitations of the equipment used in this investigation and the actual area investigated. It will be seen that the present work covers and extends much of the previously collected information. Also shown on the diagram is the dividing line for (Re^2/Ta) greater than unity. The area <u>above</u> the dividing line corresponds to Re^2/Ta <u>less</u> than unity.

B: FILM THICKNESS

Some 549 measurements of film thickness were made for varying system parameters, ($8.3 < Q < 750$ cc/s, $6 < r < 20$ cm, $5 < w < 95$ rad/s). These measurements were made at radii at which film thickness was not influenced by the inlet conditions, namely distributor gap and initial liquid velocity. A further 210 measurements are presented which demonstrate the influence of inlet conditions on film characteristics.

The first 549 measurements are presented as raw data in APPENDIX A, and as computed dimensionless groups in APPENDIX C. Each entry is given a unique number for ease of identification.

The data is presented graphically in FIGURES 53, 54 and 55 correlated in terms of (Re/Ta^2, δ/r), ($\frac{Re^2}{Ta}$, $\frac{\delta}{r}$ Re) and ($\frac{Re^2}{Ta}$, $\frac{\delta}{r}(Ta)^{\frac{1}{2}}$) respectively.

It will be immediately apparent that FIGURE 54 shows the best correlation and shows that the centrifugal model relationship, viz.

$$\frac{\delta}{r} \cdot Re = \left(\frac{3}{2\pi}\right)^{1/3} \left(\frac{Re^2}{Ta}\right)^{2/3} \qquad 68.2$$

is obeyed up to values of Re^2/Ta of aboutunity. Further comparison of FIGURES 54 and 37 shows that when deviation occurs the Coriolis model fits the data to a remarkable degree. It can be concluded, therefore, that the analytical prediction of Coriolis influence for Re^2/Ta greater than about unity is correct and providing Re^2/Ta is much less than .1 the centrifugal model will apply. The significant scatter of FIGURE 53 may be explained in terms of the Coriolis influence. FIGURE 54 and SECTION 2.4A show that there is a one to one relationship between $\frac{\delta}{r}$.Re

FIG 51 FLOW REGIME SCHEMATIC

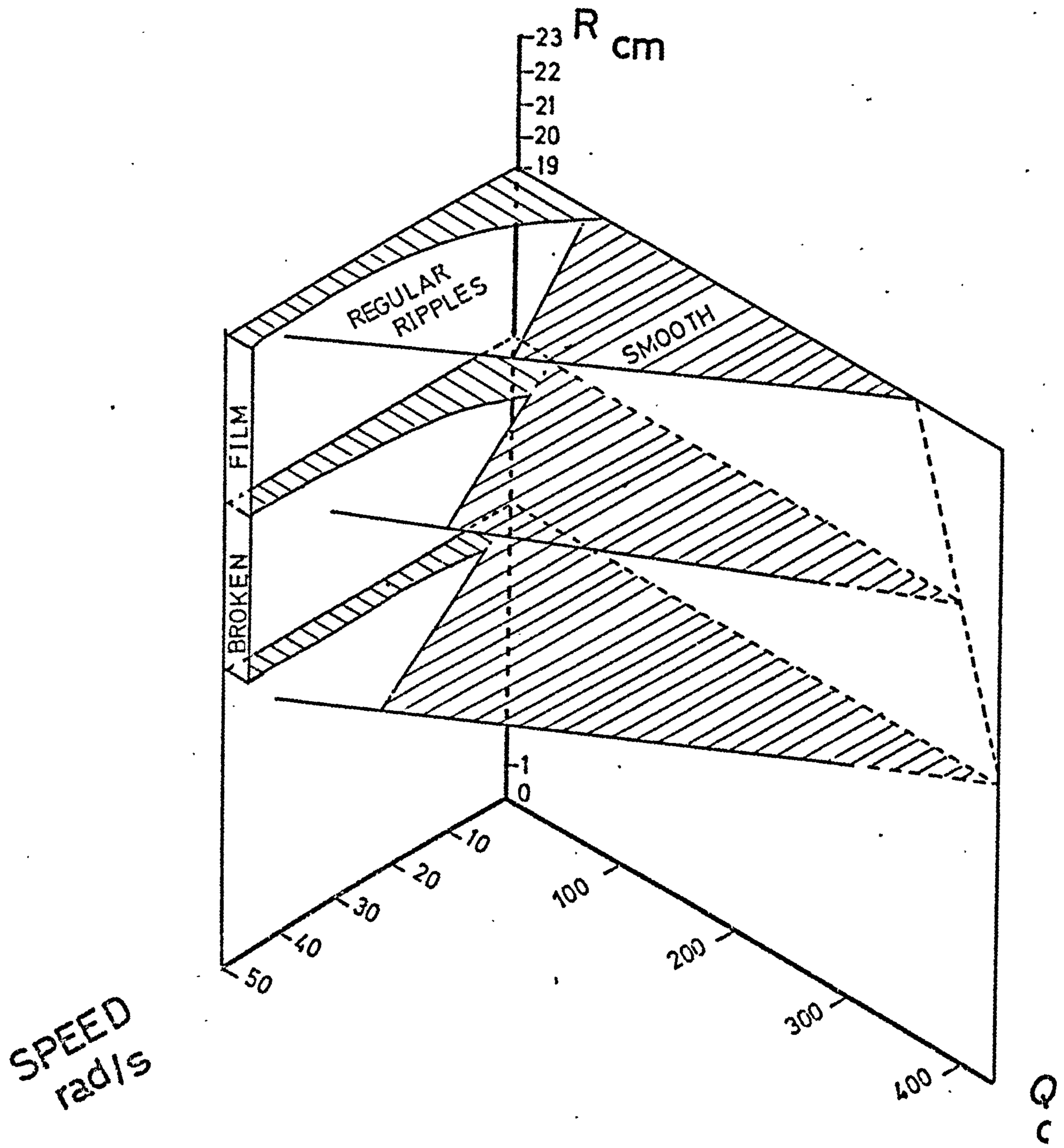

FIG 52 PARAMETER RANGES

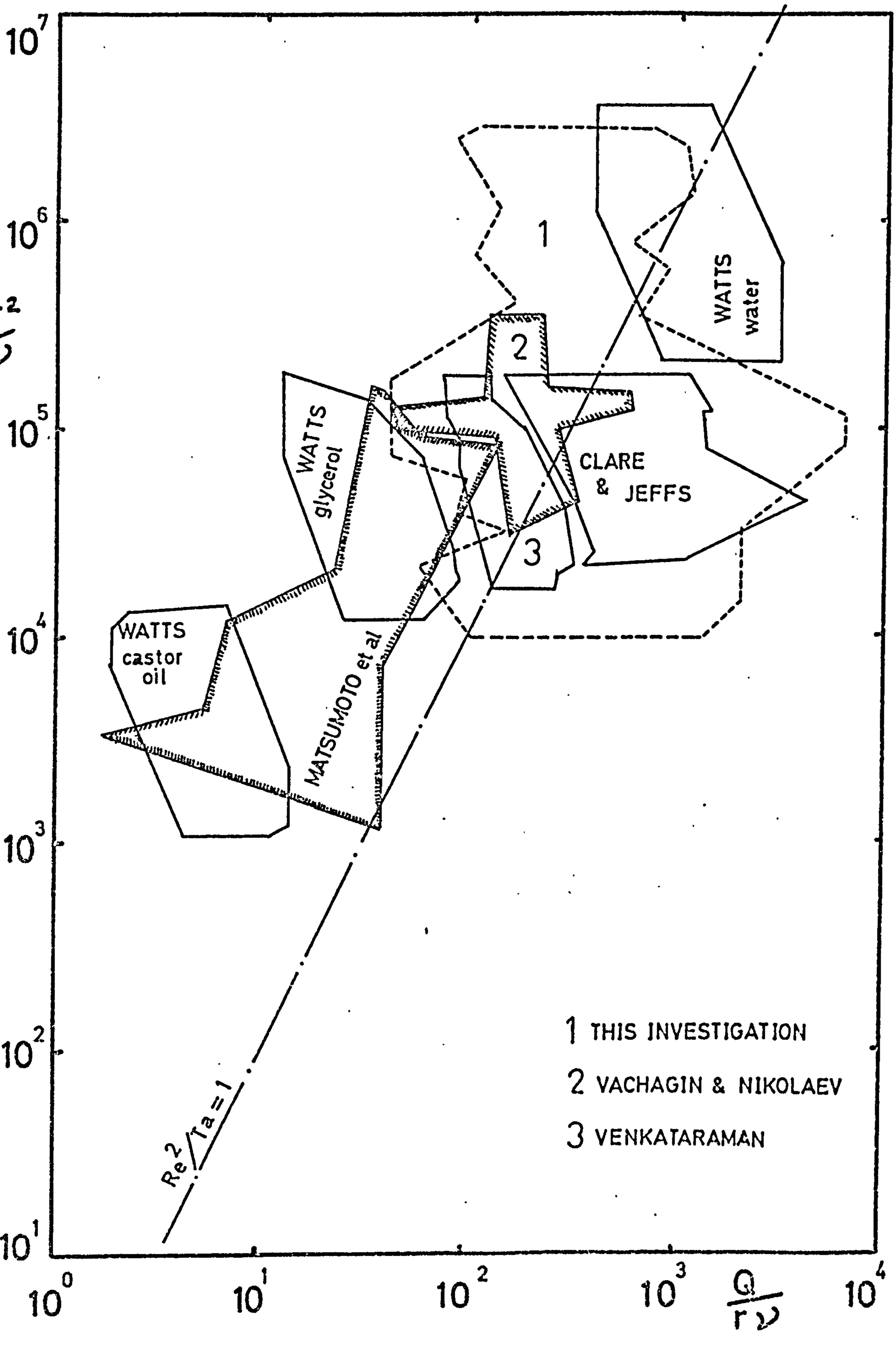

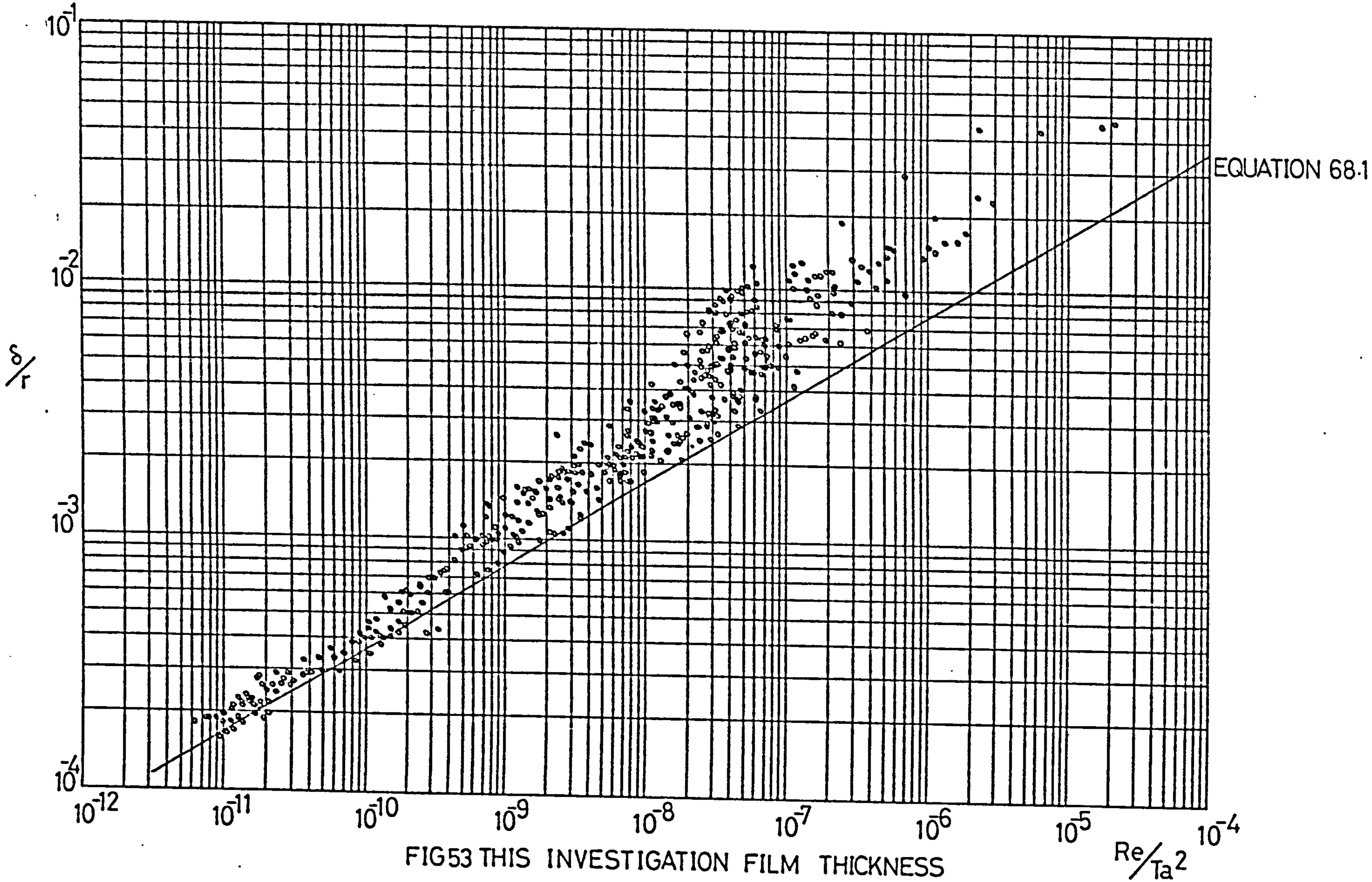

FIG 53 THIS INVESTIGATION FILM THICKNESS

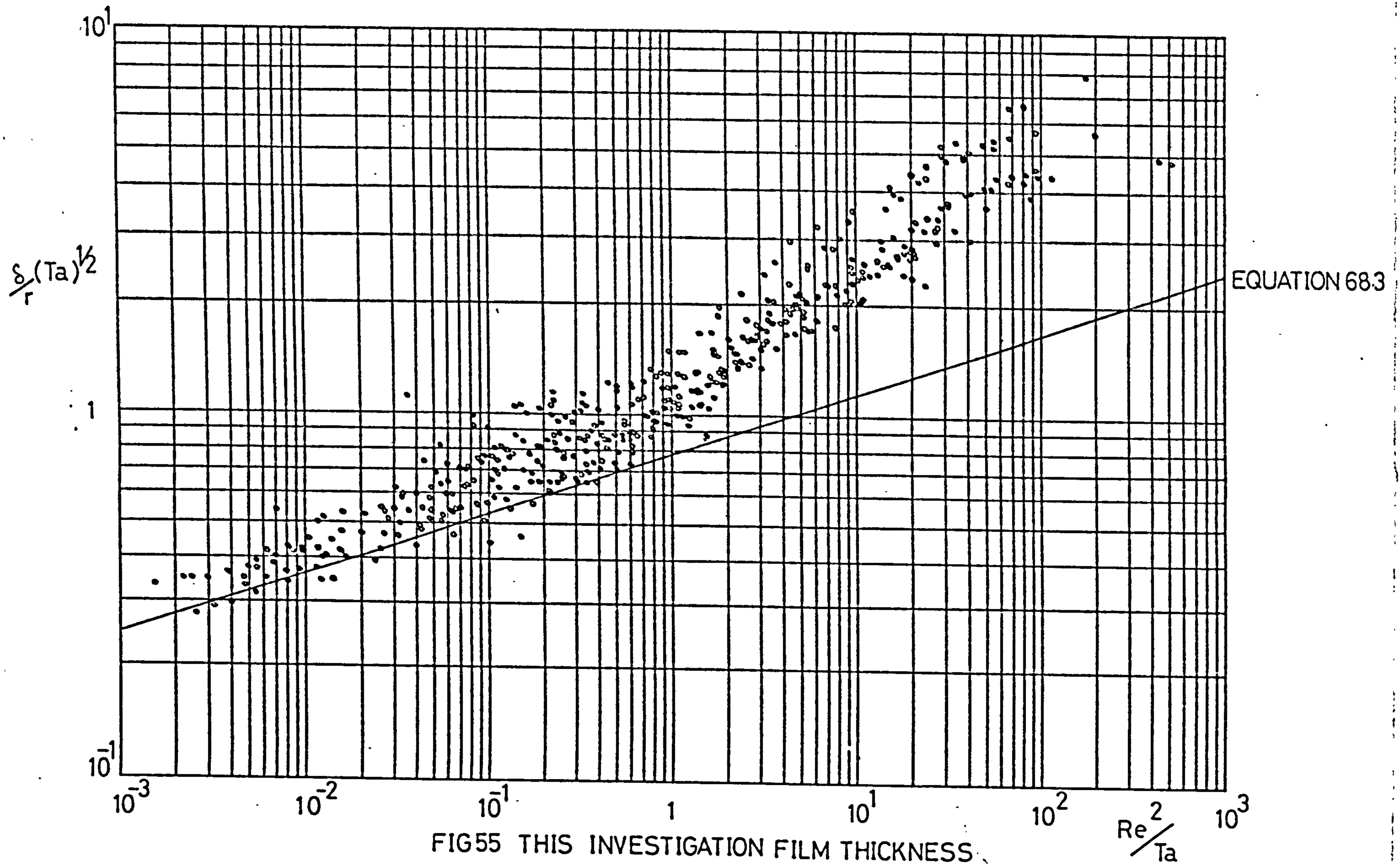

FIG55 THIS INVESTIGATION FILM THICKNESS

and Re^2/Ta. Should the desired correlating groups be δ/r and Re/Ta^2, it is simple to show that a third parameter, Re^2/Ta enters into the calculations thus

$$\frac{\delta}{r} = \frac{Y}{X^{\frac{2}{3}}} \left(\frac{Re}{Ta^2}\right)^{\frac{1}{3}}$$

where X and Y are conjugate values of Re^2/Ta and $\delta/r \cdot Re$ respectively. When Re^2/Ta is less than unity, the centrifugal model is appropriate and $Y/X^{\frac{2}{3}}$ reduces to $(3/2\pi)^{\frac{1}{3}}$. When the Coriolis force has an influence the factor has a unique value depending upon the value of Re^2/Ta specified. Thus correlating data on δ/r and Re/Ta^2 coordinates will produce sets of parallel lines, with Re^2/Ta the additional parameter. This is shown in FIGURE 56.

The scatter of FIGURE 55 is more apparent than real since the ordinate is scaled some 3 x larger than the other figures. FIGURE 55 illustrates that a slight advantage may be had in correlating the data in terms of $\frac{\delta}{r}(Ta)^{\frac{1}{2}}$ rather than $\frac{\delta}{r}Re$ in that the numerical spread of the data is so lessened by a factor of about 3.

FIGURE 54 shows that the film thicknesses measured tended to be slightly above the line and had a spread of some $\pm$ 7%. Error calculations in APPENDIX L show that the <u>maximum</u> error to be found will be some $\pm$19% in ($\frac{\delta}{r} \cdot Re$).

Values of Re^2/Ta studied in this investigation ranged from 1.6×10^{-3} to 500. All previous reports of investigation of the influence of the Coriolis force (see SECTION 2.3.2:A) have given experimental data which have maximum values of Re^2/Ta of order (3), that is, the experimental evidence collected has been mainly applicable to the non-Coriolis region. The upper limit for Re^2/Ta of 500 reported in this work represents a significant extension of available data.

C: <u>SURFACE VELOCITY</u>

Twelve measurements of surface velocity were made using the pointer technique outlined in SECTION 2.2:B.

The radial surface velocity is plotted against Re^2/Ta in FIGURE 57. Also shown on the plot is the data collected by VENKATARAMAN (120) and the theoretical line given by equation 60.1 evaluated at the free surface and non-dimensionalised by (ωr). The equivalent results of

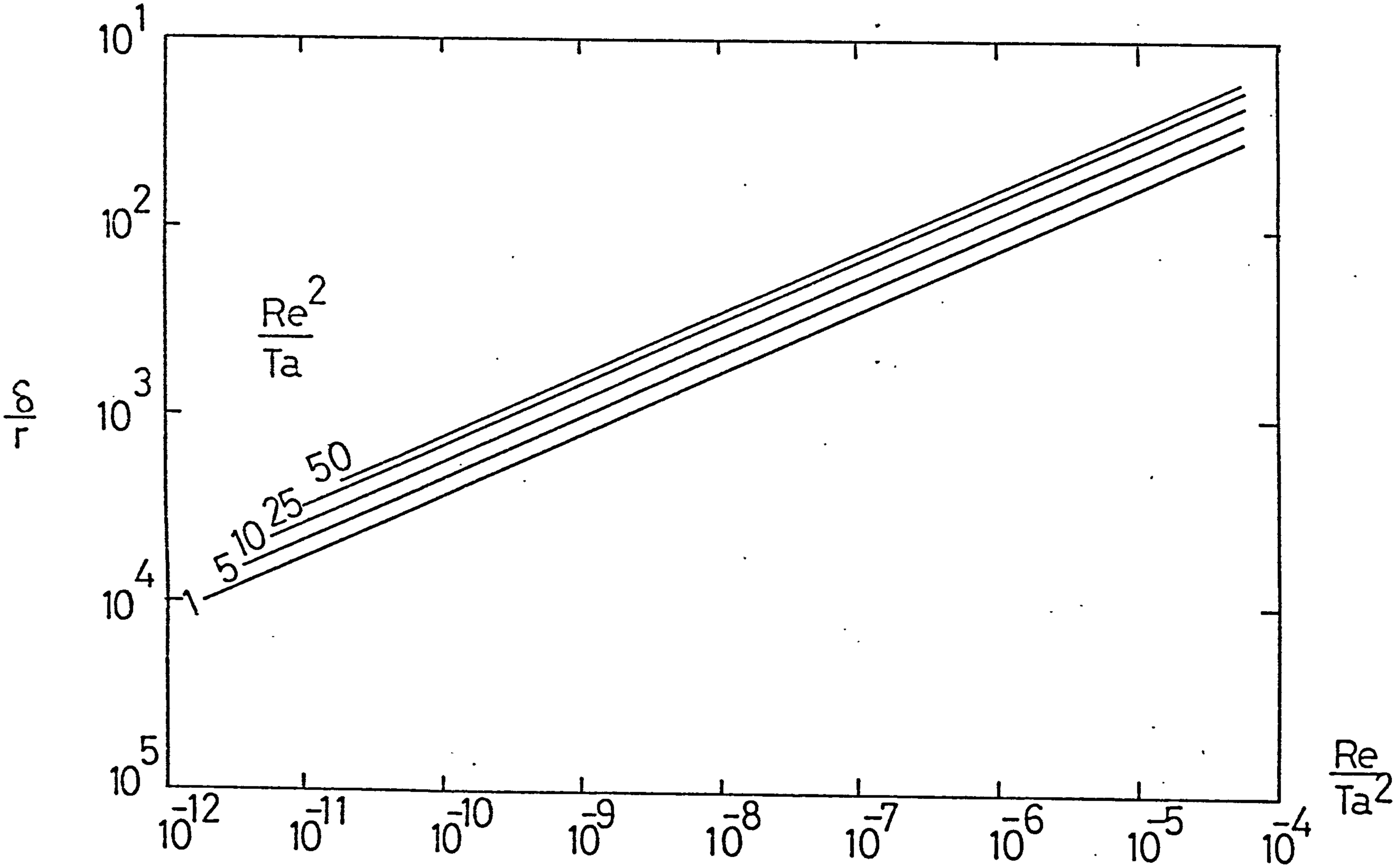

FIG 56 EFFECT OF (Re/Ta) UPON SIMPLE CORRELATION (EQUATION 68·1)

FIG 57 SURFACE VELOCITY VARIATION

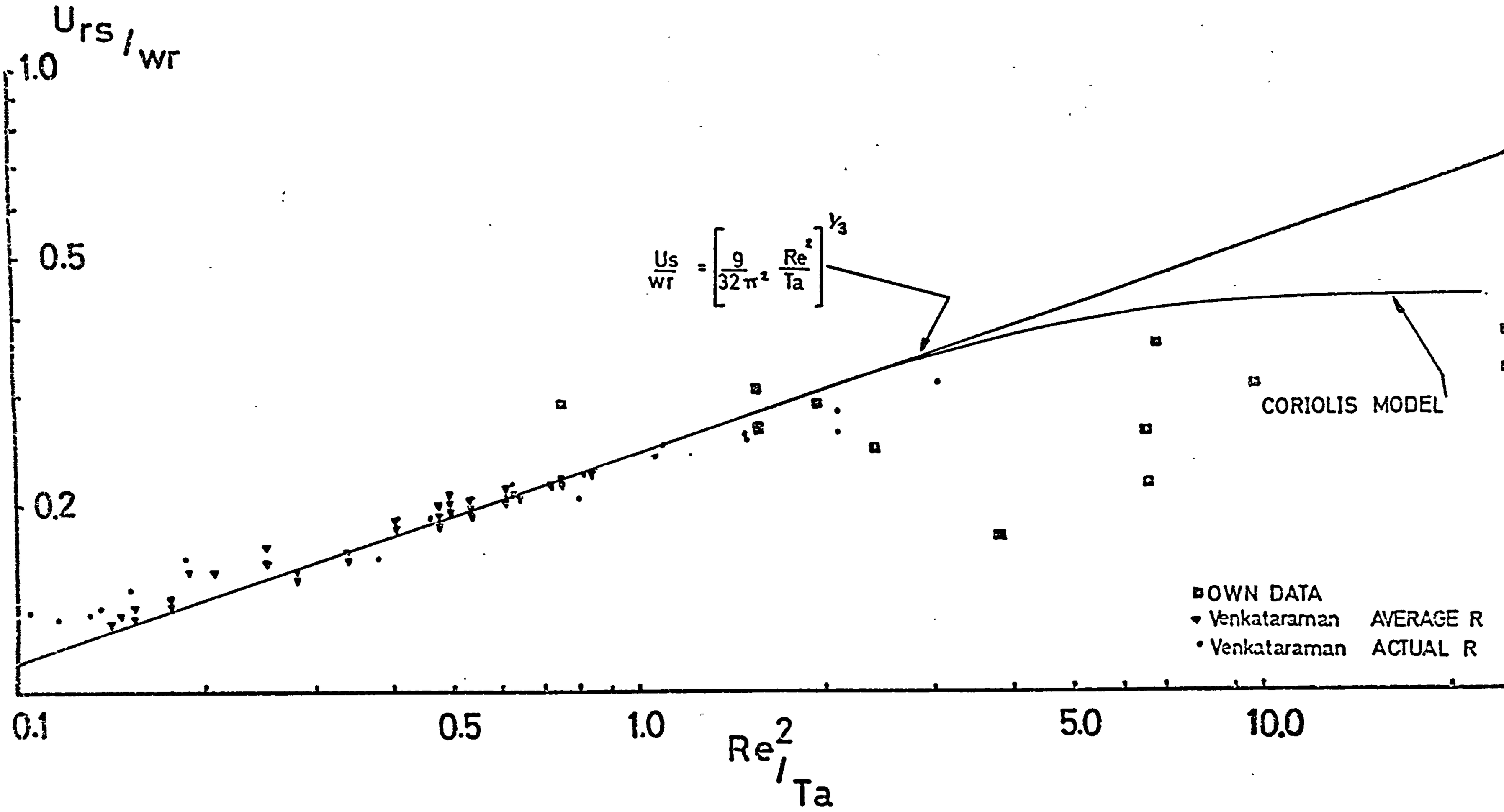

the analogue model have been included. VENKATARAMAN'S data has been included as being the most reliable low valued (Re^2/Ta) data available. The data is shown with the radius used both actual and average since VENKATARAMAN presents 20 surface velocities measured at specified radii and 37 further velocities averaged over the disc since the observed radial variation was small.

It can be seen from FIGURE 57 that the data of VENKATARAMAN and that of this study intersect at a value of Re^2/Ta of O(1) and that both sets of data tend to deviate from the simple model for higher values of Re^2/Ta. The effect of the Coriolis force is to reduce the surface radial velocity.

This point is emphasised in FIGURE 58 where the ratio of experimental to centrifugal model radial velocities (both surface and average) are plotted against Re^2/Ta. It can be seen that as (Re^2/Ta) increases from unity to about 25 both these ratios decrease from the theoretical value of 1 to about 0.4. The figure also has plotted the ratio of centrifugal to Coriolis model velocities. Again the inclusion of the Coriolis force gives a closer fit to the experimental data.

FIGURE 59 shows the observed experimental wake angle from the tangent at the pointer. Equation 99.3 is also shown and it can be seen that the wake angle increases rapidly with increasing Re^2/Ta at first. The agreement for Re^2/Ta less than about 10 is excellent (as was found by CHARWAT et al). Beyond this there is a progressive divergence between predicted and measured values. However it should be noted that the pointer shows a considerable wake at the higher values of Re^2/Ta and locating the mid-wake line is prone to error.

The results of this work confirm the conclusions of the previous section concerning the onset and existence of Coriolis influenced flow.

D: TURBULENCE

If VENKATARAMAN'S turbulent film thickness expression (equation 93.3) is expanded as an infinite series in $X(\equiv b \delta^+)$, then the following equation can be established (after grouping like terms)

$$Re = \frac{2\pi}{b^2}\left(\frac{1}{3}X^2 - \frac{1}{30}X^4 + \frac{1}{105}X^6 - \frac{1}{252}X^8 + \ldots.\right) \qquad 127.1$$

The coefficient of the term in X^{2n} is $\left(\frac{(-1)^n}{n} + (-1)^{n+1}\left(\frac{4n}{4n^2-1}\right)\right)$ 127.2

FIG 58 VELOCITY DEVELOPMENT (RADIAL)

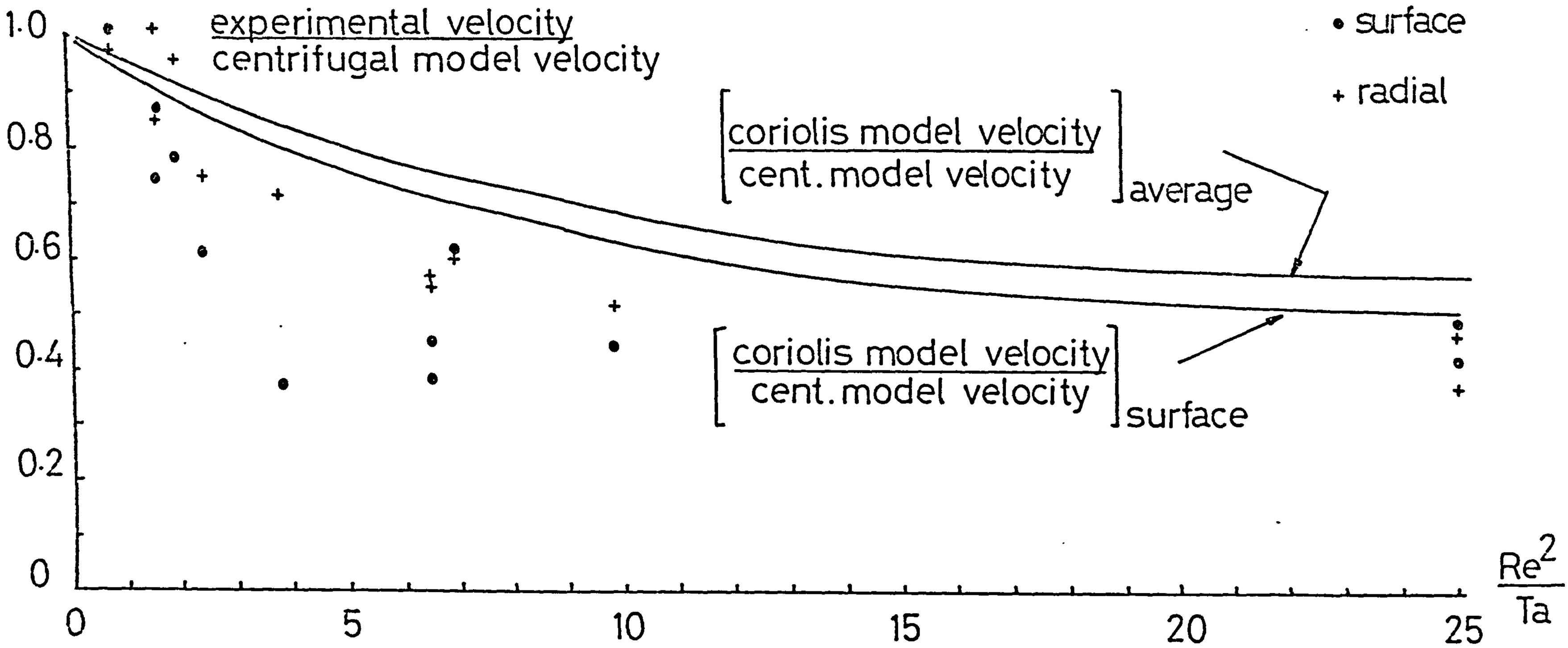

FIG 59 WAKE ANGLE VARIATION

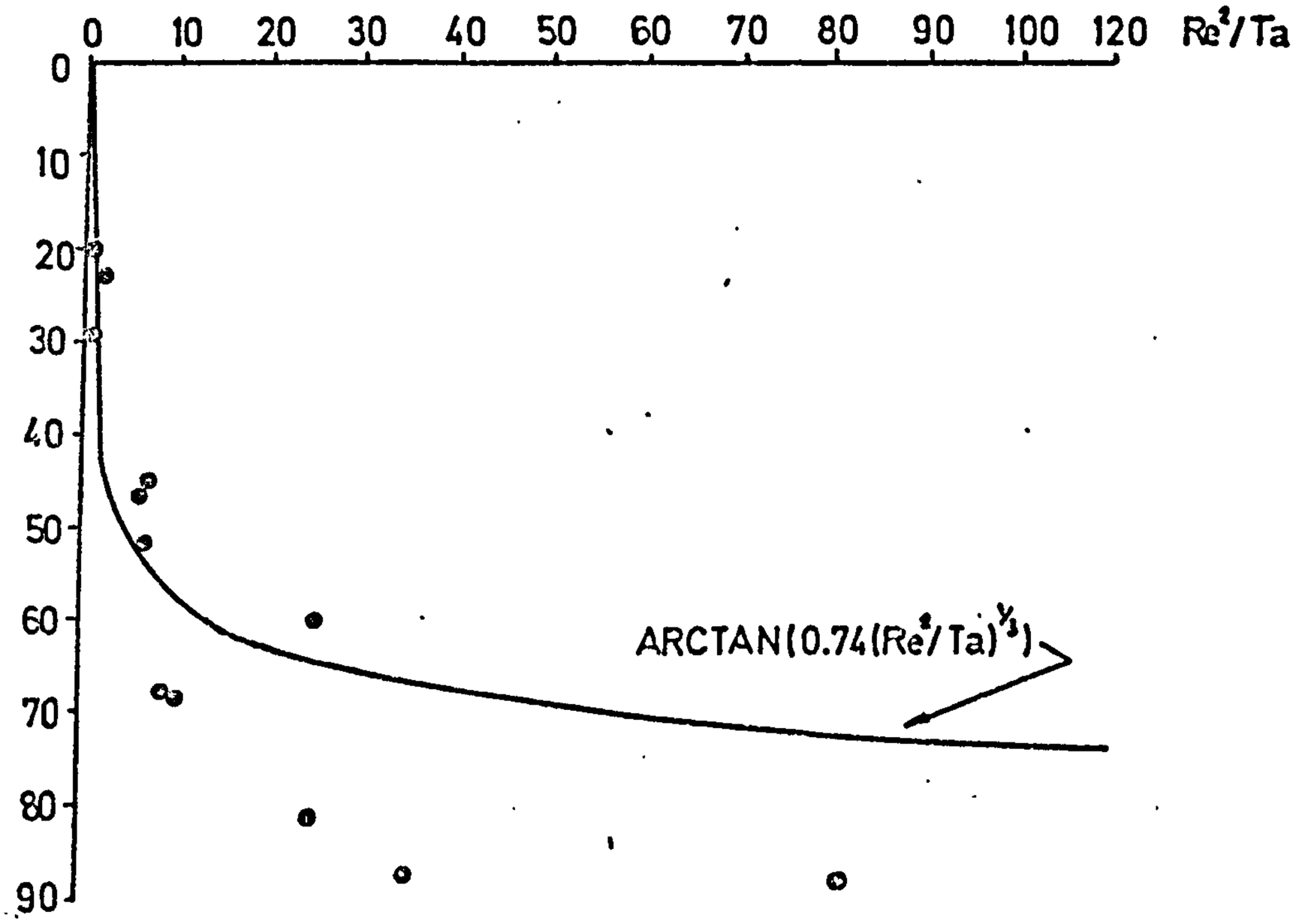

If the first term of equation 127.1 is reduced by the definitions of X and δ^+, then the simple centrifugal model film thickness results. For this solution to be valid remaining terms of the expansion must be very small. This leads to the limitation

$$Re < \frac{2\pi}{3} \frac{1}{b^2} \quad \text{or} \quad < 250 \qquad 127.3$$

for non-turbulent flow.

Equation 127.1 enables the effect of turbulence as proposed by this model to be seen. As more terms in X are included in the expansion, then Re is reduced for any specified X value. Thus, inversion of this logic suggests that increasing the order of the terms held will increase the value of X for any Re, the turbulent film will be thicker than the laminar at any Re.

The film thickness data collected in this investigation is plotted in the co-ordinates of δ^+ and Re in FIGURE 60. As may be seen the data approximately agrees to the centrifugal model, viz

$$\delta^+ = \left(\frac{\delta}{r}\right)^{\frac{3}{2}} Ta = \left(\frac{3}{2\pi}\right)^{\frac{1}{2}} Re^{\frac{1}{2}} \qquad 128$$

for values of Re $<$ 500. The data shows significant deviation at higher values of Re but this can be explained in terms of the Coriolis deviation. As with the treatment of film thickness in δf and Re/Ta^2 co-ordinates (SECTION 2.7:B earlier), the present data is strictly correlatable against

$$\left(\frac{\delta}{r}\right)^{3/2} Ta = \frac{Y^{3/2}}{X} Re^{1/2} \qquad 129$$

(when X and Y are conjugate Re^2/Ta and $\frac{\delta}{r}$. Re values) rather than simply equation 128. Thus FIGURE 60 should strictly be plotted with Re^2/Ta as a third parameter.

YURCHENKO et al (124) and RIFERT (149) hold that turbulence is controlled by the value of the parameter (Re.Ta). YURCHENKO et al state that this parameter was shown to be applicable by dimensional considerations, however, the reasoning was not presented.

The critical value defined by these workers is some 4×10^8. For laminar flow (Re.Ta) must be less than this critical value. Evaluating the implied limitations on speed and flowrate for radii of 9, 14 and 19 cm

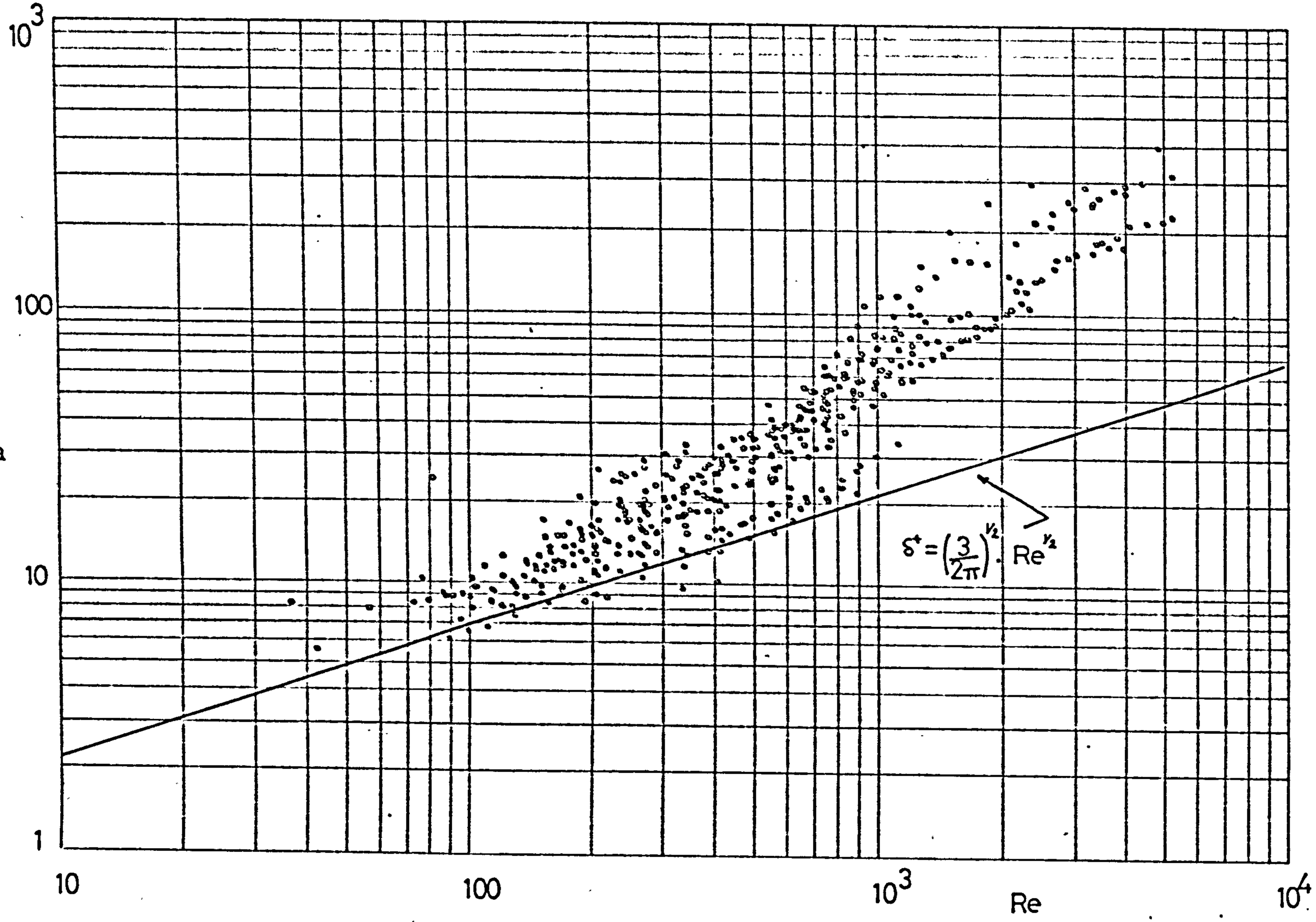

FIG 60 EFFECT OF INCREASING Re.

gives transition lines in the same area as the gray film transition noted in FIGURE 50 earlier.

The data collected in the experimental program has a range of (Re Ta) values from 2.6×10^6 to 2.4×10^9 with 154 points greater than 3.0×10^8 and 34 greater than 1×10^9. Thus any evidence of turbulence as controlled by the parameter (Re Ta) should be visible by selective plotting of these points. FIGURES 61 and 62 contain the points referred to plotted on the $\frac{\delta}{r}$ Re vs Re^2/Ta system. It will be noted that the points are distributed fairly evenly over the full range of Re^2/Ta with many agreeing to the centrifugal model line when the Coriolis influence is negligible. There is no evidence of any 'turbulent' film thickening. The conclusion to be drawn from this work is that YURCHENKO et al's criteria is strictly applicable to interfacial agitation and at least to a value of (Re Ta) of 2×10^9 does not give any indication of being a correlating group for full film turbulence.

E: INERTIA

The 210 film thickness measurements taken with the distributor gap as a major variable are presented in APPENDIX B in basic form and in APPENDIX D in computed dimensionless group form. The distributor gap was varied from 635 to 6350μm in 635μm steps for three distinctive system parameters Q = 128.6 cm^3/s, ω = 50 r.p.m.; Q = 58.6 cm^3/s, ω = 50 r.p.m. and Q = 128.6 cm^3/s, ω = 150 r.p.m. The resulting radial film depth profiles are presented in FIGURES 63, 64 and 65 respectively. As would be intuitively expected, increasing the flowrate at constant speed increases the flow path required for the film to become independent of distributor gap. Increasing speed at constant flowrate causes the reverse.

In each of FIGURES 63, 64 and 65 the data corresponding to the smallest entry gap shows that as the radius is increased the film thickness initially increases to a maxima and subsequently decreases with increasing radius. The maxima is probably related to the hydraulic jump effect found in radial flows on a stationary disc. The jump is not as well defined as for stationary situations due to the induced centrifugal force. The initial gap was selected so as to give a mean radial entry velocity greater than that predicted by the centrifugal model for that entry radius, speed and flowrate. This behaviour may be contrasted against the simple analytical models illustrated in FIGURES 10, 11 and 12 respectively. In these models the film thicknesses from the smallest

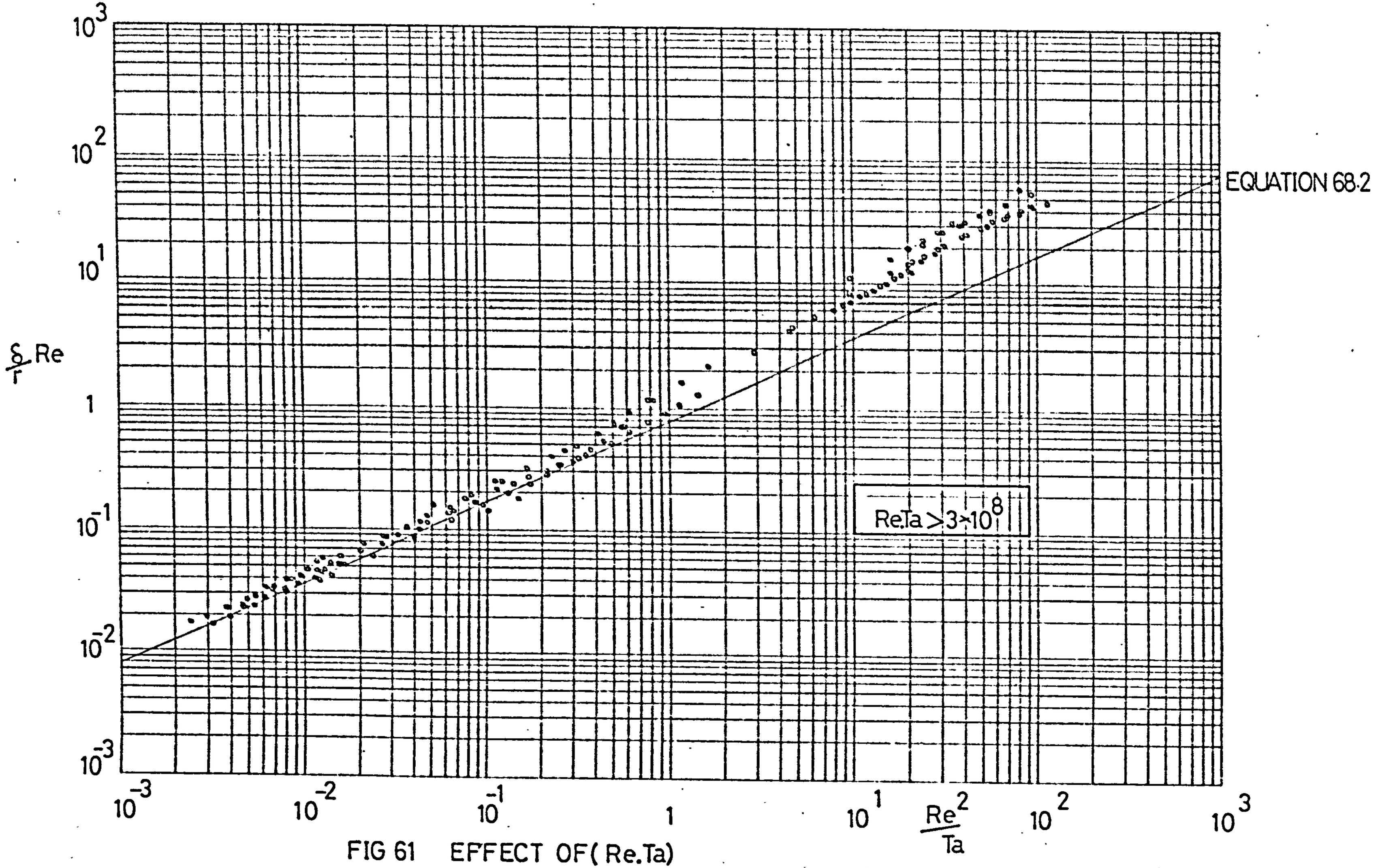

FIG 61 EFFECT OF(Re.Ta)

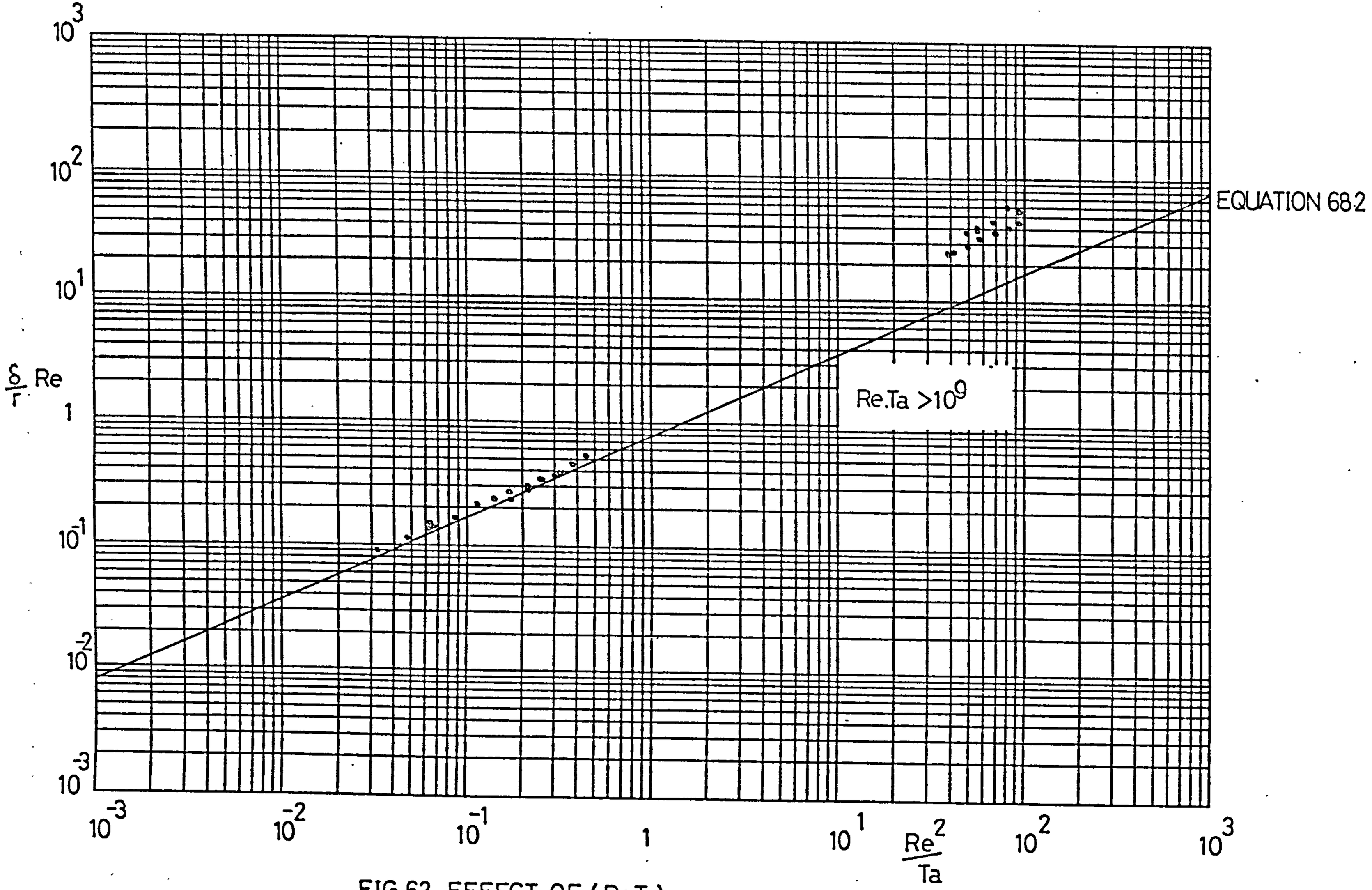

FIG 62 EFFECT OF (Re.Ta)

FIG63 ENTRY EFFECTS

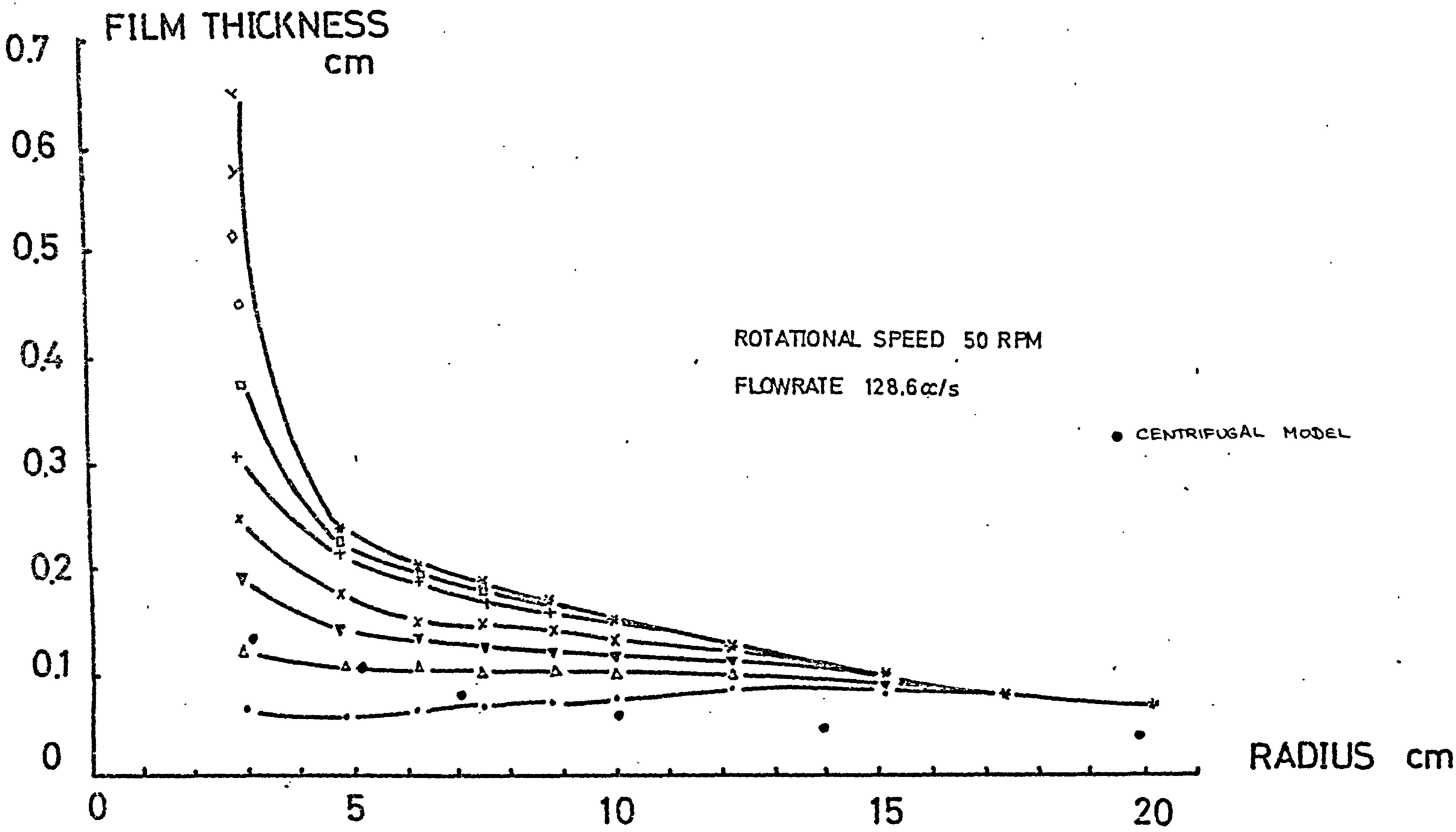

FIG 64 ENTRY EFFECTS

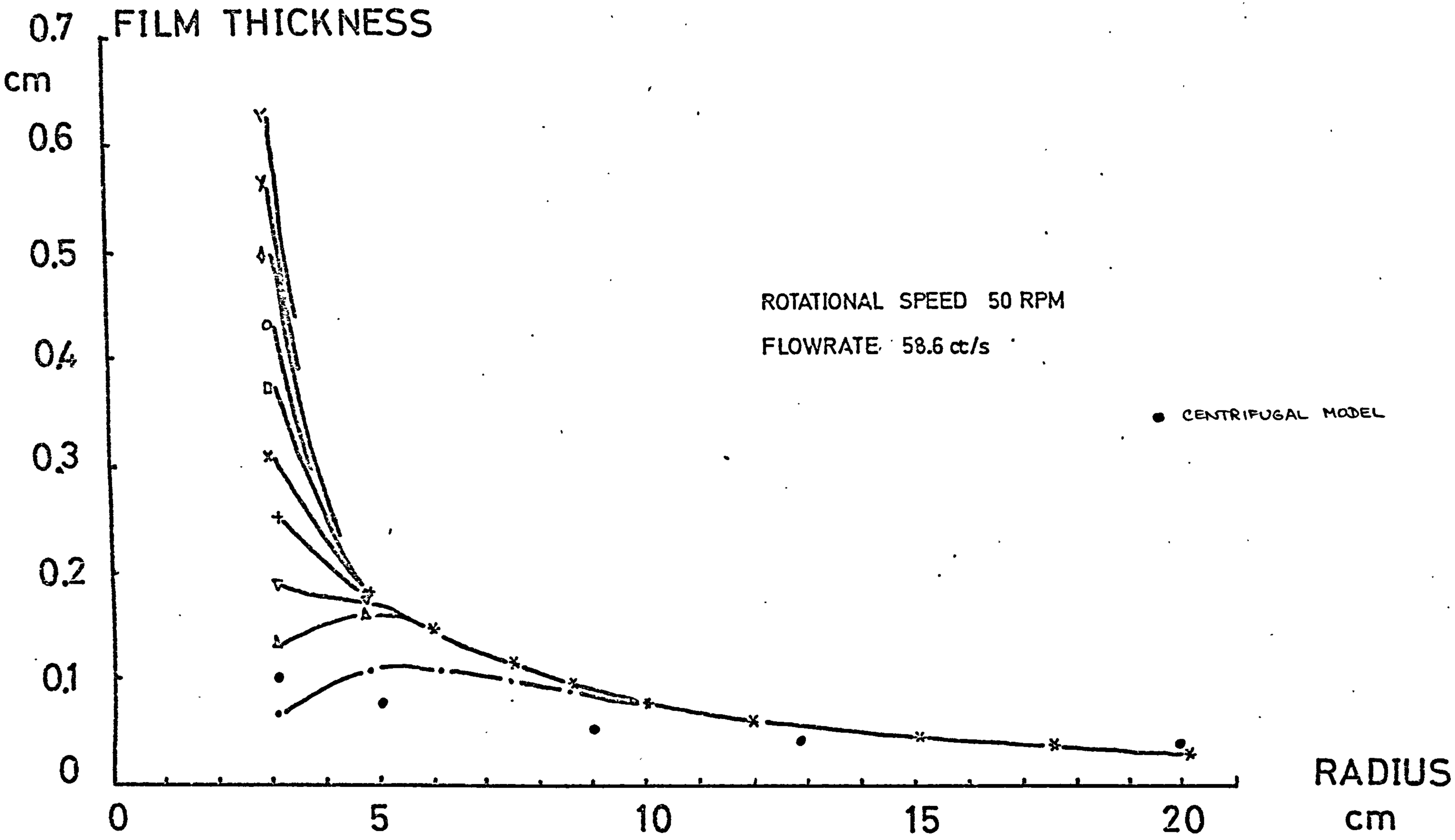

FILM THICKNESS

FIG65 ENTRY EFFECTS

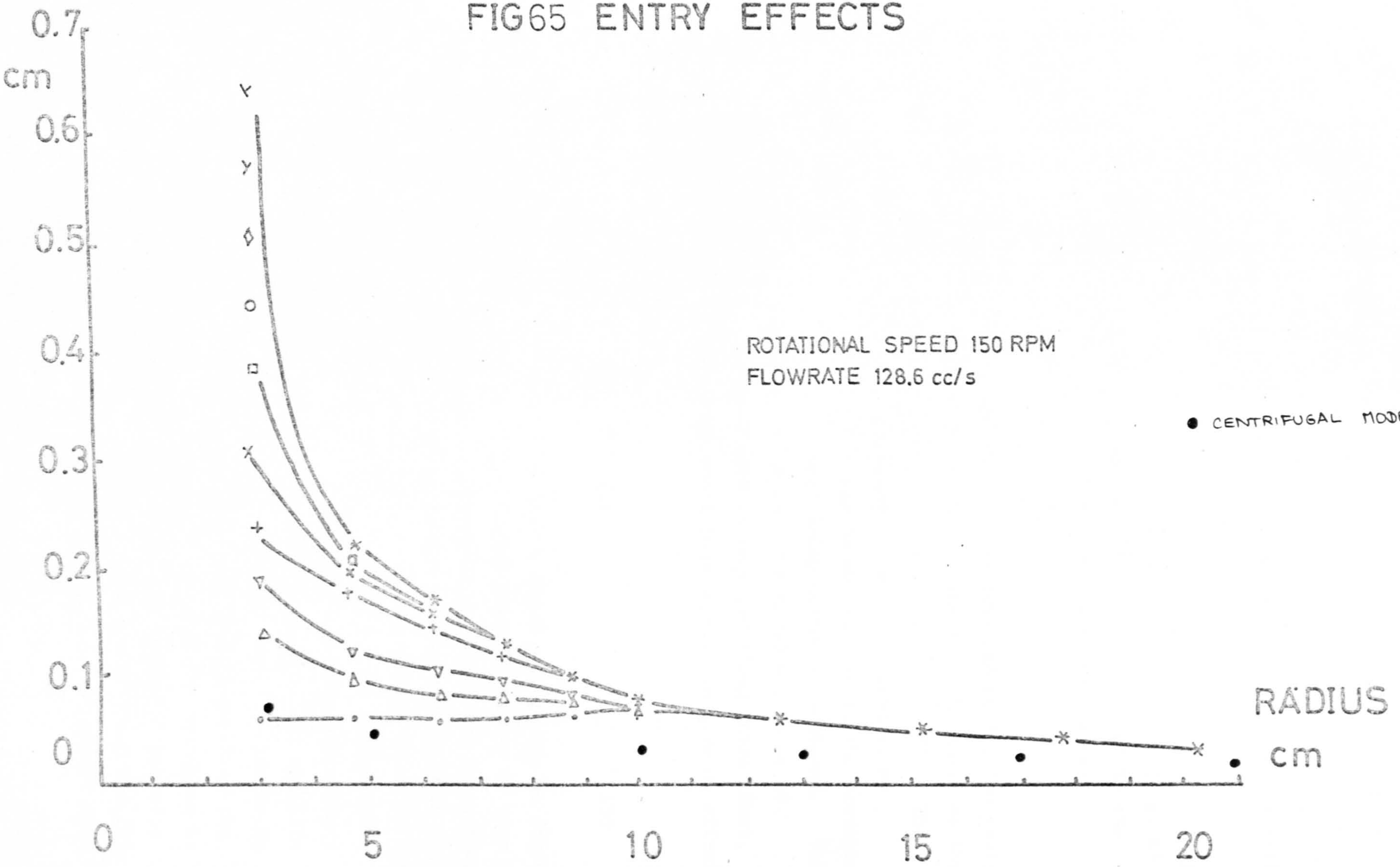

ROTATIONAL SPEED 150 RPM
FLOWRATE 128.6 cc/s

● CENTRIFUGAL MODEL

gap initially decreases before increasing to a maxima and falling away again. The analytical models attain independence of any inlet effects (viz. distributor gap and inlet velocity) at a shorter radius than found experimentally. In each case studied the analytical models reach a steady independent value at some 50% of the radius required experimentally. A more detailed model of the phenomena is obviously called for.

Dimensional analysis after the method outlined by HUNTLEY (152) in which the actual directions are not solely given a dimension (e.g. L) but have a directional significance (normal (Y) or parallel (R) to the plate), shows the parameters $\frac{Re}{Ta}$ and $\frac{r^*}{A}$ (see SECTION 2.4:C) may be best combined into a single group $\frac{Re}{Ta}\frac{r^*}{A}$ (or $\frac{Q}{\omega r^2 G}$).

Considering the three experimental systems and noting the radius at which the film from the smallest gap reaches the same thickness as that from the largest gap, the value of the above group is $1.5 \pm 30\%$. The variation of r and G to provide independence from entry conditions indicates that closing the distributor gap to one quarter of the previous setting doubles the radius at which entry independence is achieved. This behaviour can be seen experimentally in any of FIGURES 63, 64 or 65.

Obviously much further experimental work is required along these lines, but a useful point is that the entry conditions appears to have no effect upon the flow if

$$\frac{Re}{Ta}\frac{r^*}{A} = \frac{Q}{\omega r^2 G} << 1.5 \qquad 130$$

The significance of increasing flowrate with a fixed gap, as may be found in commercial equipment operating with variable throughput, may be seen from FIGURE 66. The data for this illustration was collected by setting the distributor gap to 635μm, the probe radius to 5 cm and the disc speed to 50 r.p.m. As the flowrate was increased from an initial 11 cm^3/s the film thickness (although greater than predicted due to the influence of Coriolis force since the Re^2/Ta value is O(4)) followed the centrifugal model's trends. As the flowrate is increased past 30 cm^3/s, the film thickness begins to decrease. Visual observations show the film to be "jetting" in this state - a noticeably fast, thin film issues from the distributor. When a flowrate of 145 cm^3/s is reached, the thickness is noticeably below even the centrifugal model (itself below the Coriolis model). Increasing the gap causes the jetting to diminish and the film to thicken. Each progressive incremental opening has less effect upon

FIG 66 EFFECT OF ENTRY GAP

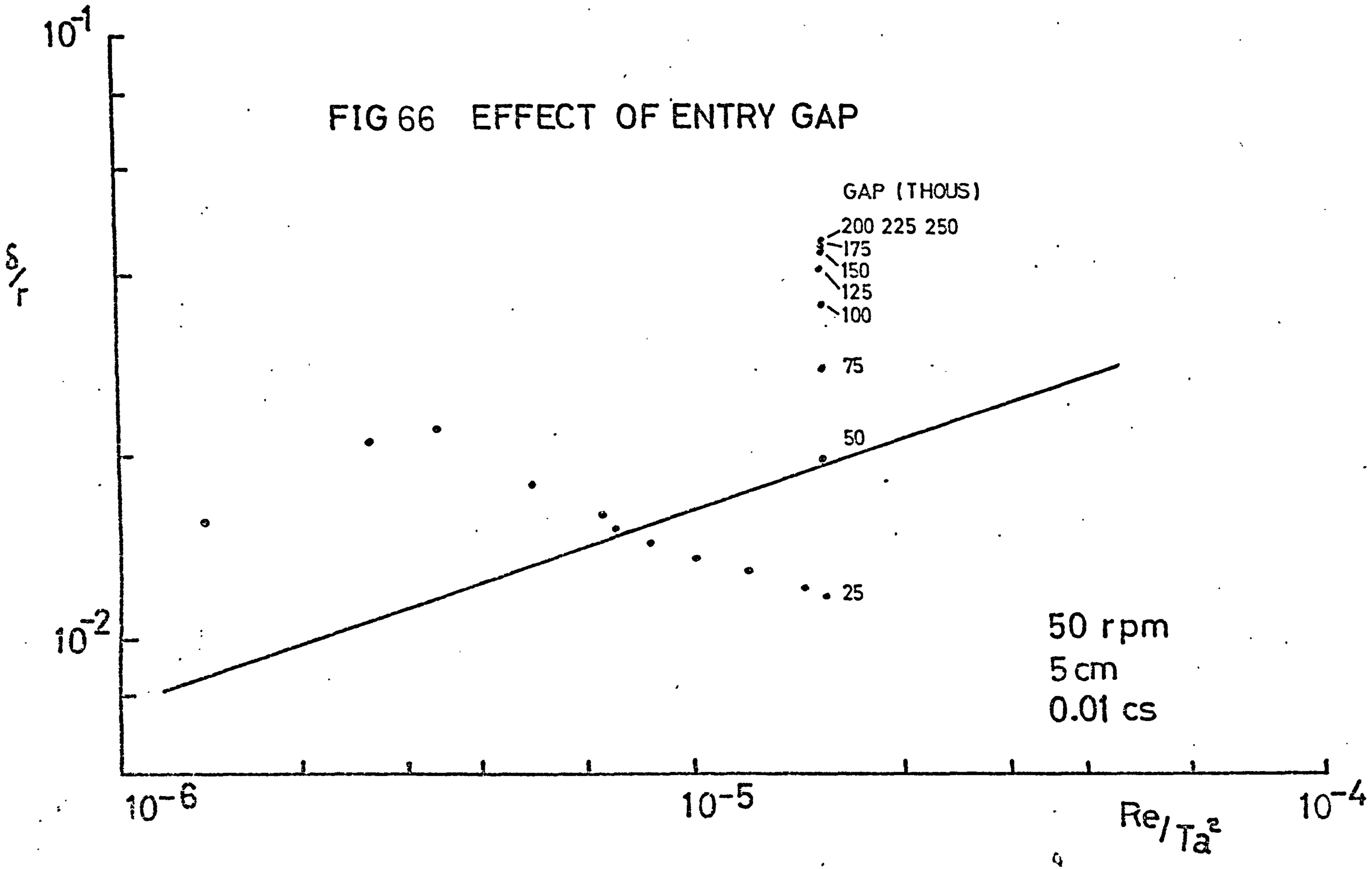

the thickness, so that the final three increments have no measurable effect at all. This demonstrates the significance of entry gaps to commercial designs of rotating disc equipment. If the results of this work are to be applied, the entry gap selected for the maximum flowrate must be such that no jetting occurs. This should be satisfied by the criteria in equation 130.

F: FILM BREAKDOWN

The results of the investigation into film breakdown are given on FIGURE 67. The radius of breakdown is taken as 20.8 $\pm$ 1 cm (since the edge of the disc is a smooth curve rather than a sharply defined edge) and both film breakdown and reformation are shown. Due to hysterisis in re-wetting, at any given speed the flowrate required for re-establishing an already broken film is greater than that at which a continuous film begins to breakdown. The difference in these two flowrates (the vertical separation of the circles and triangles in FIGURE 67) decreases with increasing disc speed.

Also shown on FIGURE 67 is the predicted influence of speed on the critical breakdown flowrate as given by equation 123. It will be seen that the experimental values are some 30% of the predicted although the influence of increasing speed seems adequately represented. One possible cause for the apparently low critical flowrates could be the effect of waves (which were always present on the disc - see SECTION 2.7:F later). The waves may produce extra momentum at the edge of an incipient dry patch and cause the film to become continuous once more. The suggestion by DORMANT (see SECTION 2.1.1:G earlier) that waves may contribute to film breakdown by temporarily thinning the film is most likely limited to a static film situation and not to the rotating disc situation. The agreement between experiment and theory is probably as good as can be expected from such a simple model.

The disc surface as used in these experiments is chromium plated, a notoriously difficult surface to wet. It would be of value to study the breakdown characteristics of other metal and/or coated surfaces. As with the distributor gap design, any design utilizing the information of this work can only be applied to those flow situations in which a continuous film exists on the disc. In this respect equation 123 should act as a satisfactory criteria for isothermal flow.

FIG 67 MINIMUM WETTING RATE vs. ROTATIONAL SPEED

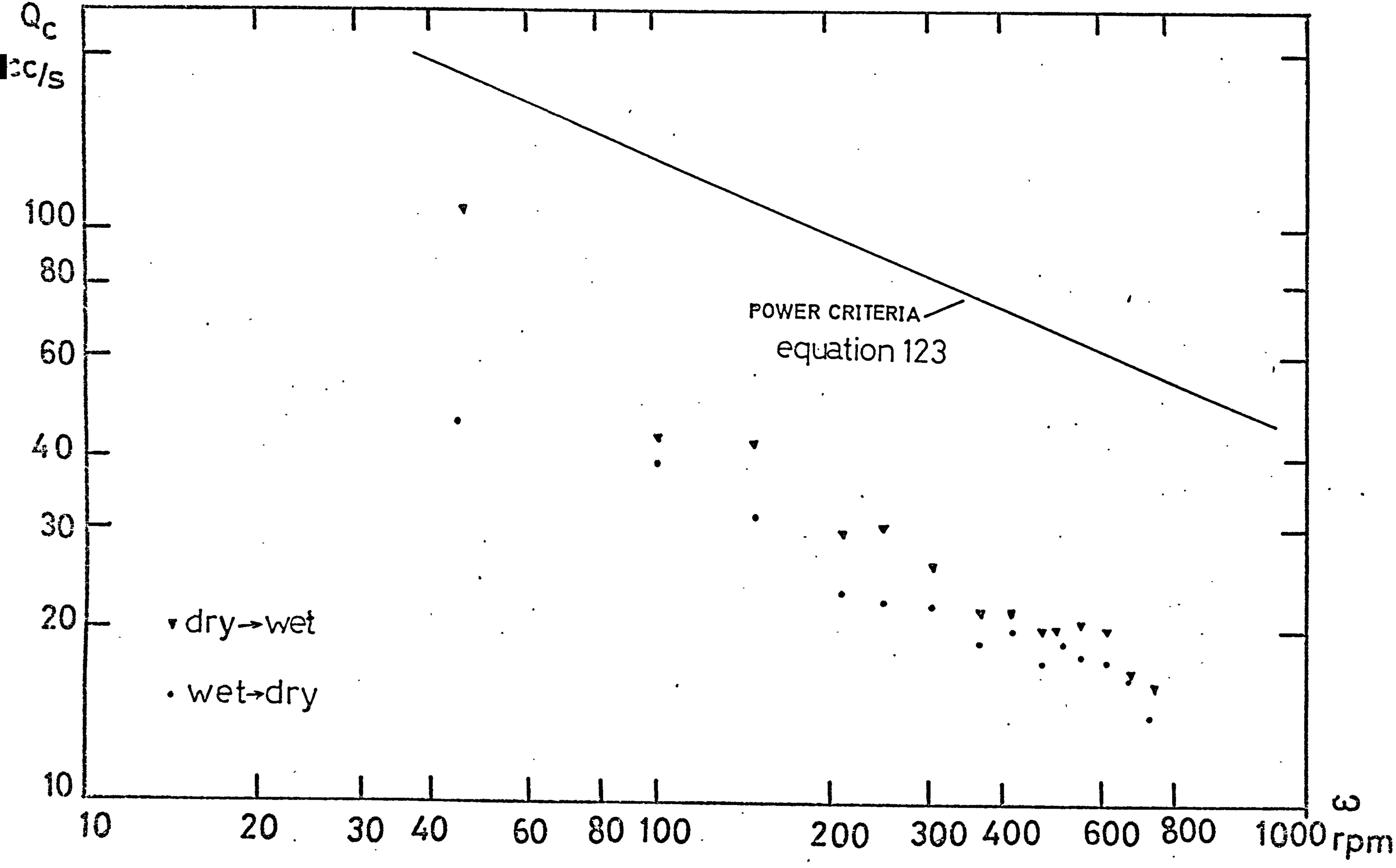

G: WAVES

A limited investigation into wavy flow was conducted as reported in SECTION 2.6.2:E. The spiral waves of CHARWAT et al were observed, but their concentric circular waves were observed only infrequently and apparently at random. This seems to justify their conclusion that such waves are induced at the liquid inlet distributor, and will be unique to each investigation.

The wave amplitudes noted from the studies are reported in FIGURES 68 and 69. The amplitude/radius variations noted by CHARWAT et al are also shown in FIGURE 68. By comparing the two figures it will be seen that increasing flowrate increases the value and radius of the maximum amplitude, at a given speed. Increasing disc speed, at constant flowrate, reverses this trend. The amplitudes of the waves studied could be quite large, of the order of 60% of the mean film depth.

Care should be taken in the interpretation of FIGURES 68 and 69. The capacitance probe employed has sizable dimensions when compared to the waves and some smoothing of the wave amplitude results must have occurred. This has already been commented upon.

FIG68 WAVE AMPLITUDE VARIATION

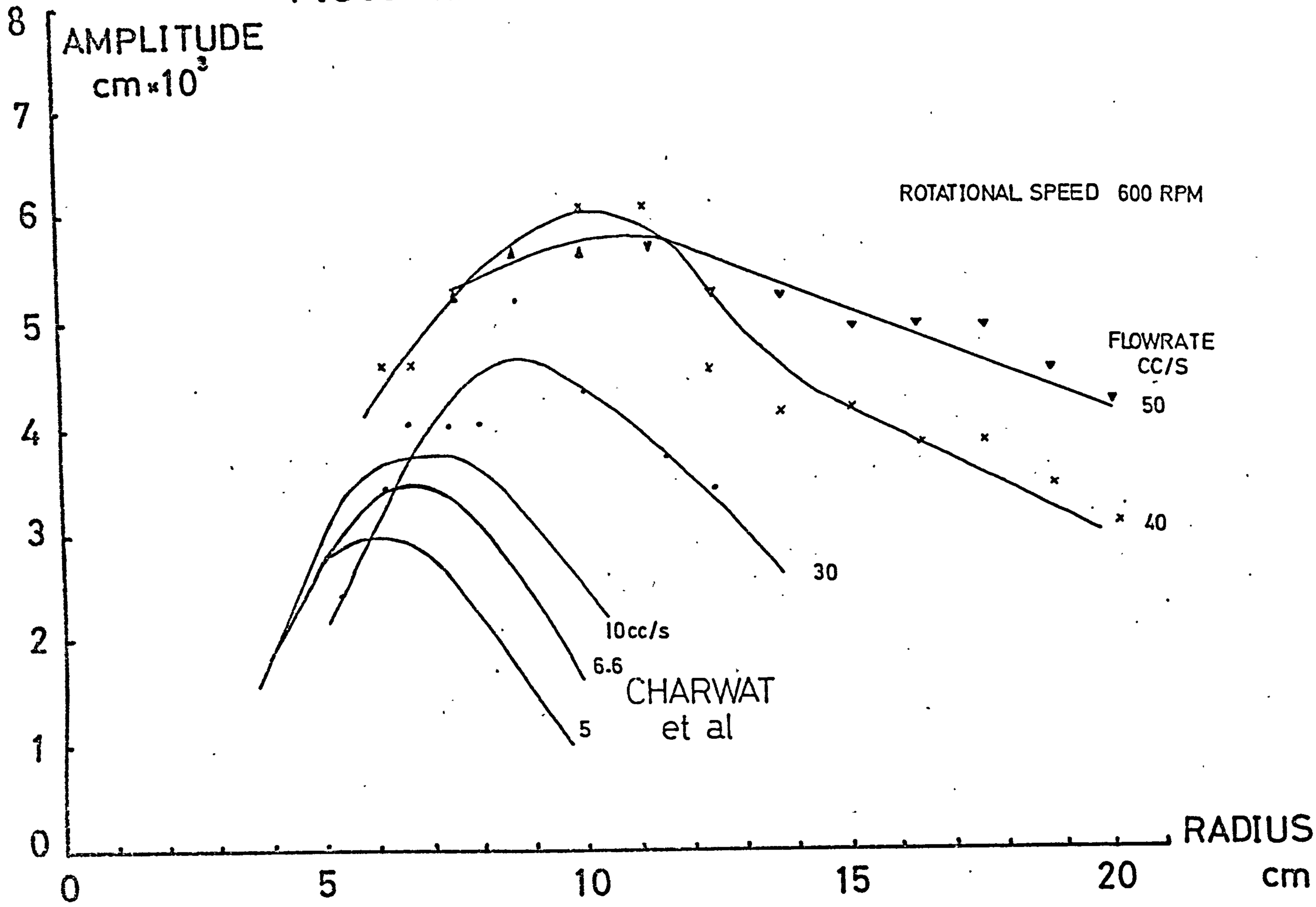

FIG 69 WAVE AMPLITUDE VARIATION

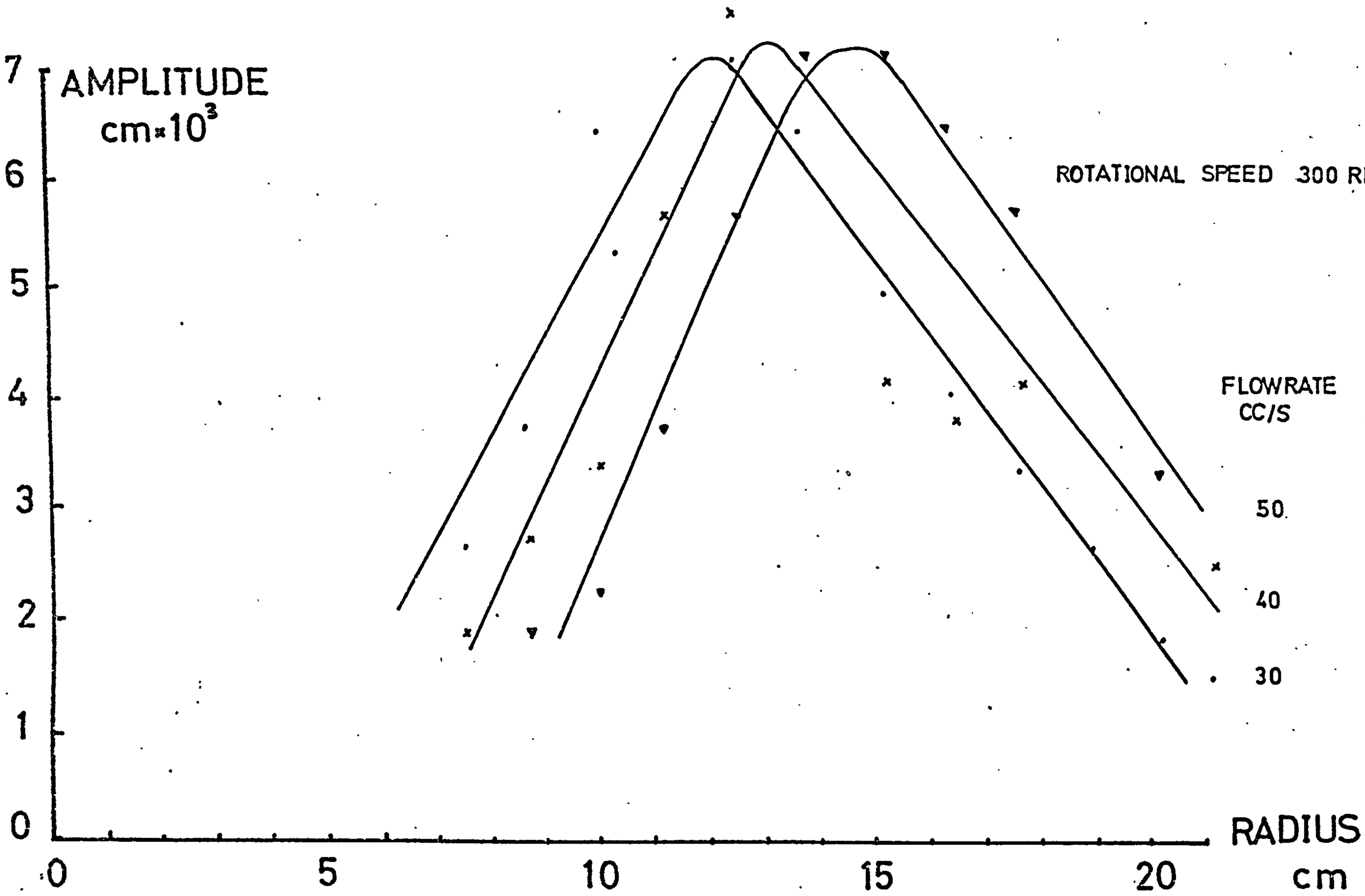

2.8. CONCLUSIONS

1. The film thickness is given by the centrifugal model result:

$$\frac{\delta}{r} = \left(\frac{3}{2\pi}\right)^{1/3} \left(\frac{Re}{Ta^2}\right)^{1/3} \qquad 68.1$$

for $\frac{Re^2}{Ta} < 1$

The corresponding radial velocity profile is

$$v_r = \frac{\omega^2 r}{\nu}\left(\delta y - \frac{y^2}{2}\right) \qquad 60.1$$

For values of (Re^2/Ta) greater than 1 the numerical result of the Coriolis model (FIGURE 37 and TABLE 4) adequately describe the hydrodynamics of the flow within the experimental conditions studied.

2. The film appears to be laminer within the experimental study,

$$30 < Re < 5000$$

$$10^4 < Ta < 5 \times 10^6$$

and no evidence of turbulence was observed. Free surface agitation is observed for values of $(Re.Ta) > 10^8$.

3. Entry gap will have no effect when the criteria

$$\left(\frac{Re}{Ta}\ \frac{r_i}{G}\right) < 1.5$$

is satisfied.

4. The film will be continuous when the criteria

$$Q_c \geq 5.5 \left(\frac{\nu r^4}{\omega^2}\right)^{1/5} \left(\frac{\sigma}{\rho}\right)^{3/5} \qquad 123$$

is satisfied.

2.9. RECOMMENDATIONS FOR FUTURE WORK

1. That the experimental work be repeated for other liquids. Purely viscous Newtonian liquids might be expected to satisfy the models proposed and compared in this study.

General models have already been developed suitable for time independent non-Newtonian fluids described by an Ostwald power law function or a Bingham plastic model. The agreement between these models and the limited experimental data available is good. Further experimental data should be collected. Models suitable for time dependent liquids (e.g. thixotropic and rheopectic fluids) have yet to be developed. Visco-elastic materials will provide the greatest analytical problems, but owing to the high shear rates upon the disc such materials will require their own model.

2. The initial experimental work on wavy flow should be extended and augmented by analysis. The effects of surfactants (which have important implications in the commercial processing of industrial liquids) should be investigated.

3. The technique applied to the measurement of surface velocity of the film should be developed to enable the useful range of Re^2/Ta used in the reported measurements to be extended.

4. More sophisticated analyses of the film breakdown should be developed and more experimental information upon the effects of edge shape, liquid properties and wetted surface nature collected.

5. Further work on establishing the validity bounds of the various models should be undertaken. This work reports several brief reviews that show that interfacial drag, for example, is usually negligible. However the presence of other surfaces in a multi-disc unit may lead to appreciable drag.

3. HEAT TRANSFER

3.1. ASSOCIATED FIELDS

3.1.1. PLANAR FILMS UNDER GRAVITATIONAL INFLUENCE

A: LAMINAR AND TURBULENT FILMS

In the following section several definitions of heat transfer coefficient will be employed, all differing only in the selection of the appropriate temperature difference for use with the definition. The definitions are outlined in the NOMENCLATURE, and where used initially.

The simplified energy equation (see APPENDIX F) which may be rewritten as

$$\rho C_p U_x \frac{\partial T}{\partial x} - k \frac{\partial^2 T}{\partial y^2} = 0 \qquad 131$$

was first solved numerically and analytically by NUSSELT (153). Utilising the simple velocity profile (equation 2) and the dimensionless groups η ($\equiv y/\delta$), x' ($\equiv \mu k x / g \rho^2 C_p \delta^4$) and T^* ($\equiv (T_o - T)/(T_o - T_i)$) then equation 131 may be written as

$$\left(\eta - \frac{\eta^2}{2}\right) \frac{\partial T^*}{\partial x'} - \frac{\partial^2 T^*}{\partial \eta^2} = 0 \qquad 132$$

The boundary conditions used to solve equation 132 are

at the inlet $x = 0$ $T = T_i$

or $x' = 0$ $T^* = 1$ 133.1

at the plate $y = 0$ $T = T_o$

or $\eta = 0$ $T^* = 0$ 133.2

at the free surface

$y = \delta$ $\frac{\partial T}{\partial y} = 0$

or $\eta = 1$ $\frac{\partial T^*}{\partial \eta} = 0$ 133.3

Boundary condition 133.3 implies that there is no convective heat loss from the free surface. The resulting solution gives the dimensionless temperature distribution as a function of η and x', the two non-dimensionalised directions. These distributions may be expressed in

the form

$$T^* = N f(\eta) \exp(-a x') \qquad 134$$

when N and a are constants and $f(\eta)$ is a single value function of η. Numerical values are available from either NUSSELT'S paper or JAKOB'S (154) book.

From the original definition of T^*, a heat transfer coefficient may be written as

$$h_N = \frac{q}{T_o - T_i} = \frac{k}{\delta} N \exp(-a x') \left[f'(\eta)_{y=o}\right] \qquad 135.1$$

or

$$Nu_N = \frac{h_N \delta}{k} = N \exp(-a x') \left[f'(\eta)_{y=o}\right] \qquad 135.2$$

The suffix N is used to indicate that the appropriate ΔT for use with this heat transfer coefficient is $T_o - T_{fi}$ when T_{fi} is the fluid temperature at the inlet to the plate and T_o the heated surface temperature.

Approximate values for N = 1.2014, a = 5.65 and $f'(\eta)_{y=0} = 1.423$, then equation 135.2 may be written as

$$Nu_N = 1.71 \exp\left(\frac{-5{:}65\, y k x}{g \rho c_p \delta^4}\right) \qquad 136$$

Notice that the local value of the Nusselt number will fall from an infinite value at entry (where the temperature profile is undeveloped) with increasing flow path length x. The fully developed asymtotic local heat transfer rate (at large values of x) will be 1.71.

NUSSELT gives the results of the numerical investigation in an alternative form thus,

$$\bar{h}_N = \frac{\rho Q' c_p}{L} \ln\left(\frac{1}{1 - \phi(x)}\right) \qquad 137$$

when $\phi(x') = 2.23\ x'(L)^{0.656}$ for $x'(L) < 0.05$

and $\phi(x') = 1 - 0.91 \exp(-5.65\ x'(L))$ for $x'(L) > 0.05$

when L is the heating length.

BAYS and McADAMS (155) investigated the flow of oils down heated vertical plates and correlated the results in the form

$$\frac{h_a \delta}{k} = \left(\frac{c_p \mu}{k}\right)^{1/3} \left(\frac{\delta}{L}\right)^{1/3} \left(\frac{Q'}{\nu}\right)^{1/3} \left(\frac{\mu}{\mu_o}\right)^{1/4} \qquad 138$$

The suffix a has been used on the heat transfer coefficient to indicate that the appropriate temperature difference to apply is $T_o - T_{fm}$ when T_{fm} is the film mean ((inlet + outlet)/2) temperature, T_o the heated surface temperature. Note that the effect of temperature variation upon the oil viscosity is accounted for by a SEIDER-TATE type correction.

The index of 0.25 on the viscosity correction has also been confirmed experimentally by AHMED and KAPARTHI (156), who obtained the correlation

$$\overline{Nu}_a = 0.005 \left(\frac{Q'}{\nu}\right)^{0.93} Pr^{0.4} \left(\frac{\mu}{\mu_o}\right)^{1/4} \qquad 139$$

The NUSSELT model is derived for an implied smooth, laminar flow and with each flow transition additional corrections to the simple model will be required. WILKE (157), for example, provides a set of experimental correlations for each flow regime noted. These are

1) developing region $\overline{Nu}_a = 0.0942 \left(\frac{Q'}{\nu}\right)\left(Pr.\frac{S}{x}\right) + 1.88$ 140.1

2) developed laminar smooth region $\overline{Nu}_a = 1.88$ 140.2

3) transition region $\overline{Nu}_a = 0.00112 \left(\frac{Q'}{\nu}\right)^{\frac{6}{5}} Pr^{0.344}$ 140.3

4) turbulent region $\overline{Nu}_a = 0.0066 \left(\frac{Q'}{\nu}\right)^{\frac{14}{15}} Pr^{0.344}$ 140.4

In regions 3 and 4 noted above, the δ value employed is given as 0.369 δ_N when δ_N is the film thickness from the simple NUSSELT model.

CHUNG and SEBAN (158) provide correlations for the laminar and turbulent regimes as

laminar smooth: NUSSELT model

turbulent $\overline{Nu}_N = 0.00952 \left(\frac{Q'}{\nu}\right)^{0.73} Pr^{0.655}$ 141

The dependency of h on Q' will be seen from the previous correlations to vary as $Q'^{-\frac{1}{3}}$ in the smooth laminar regime, tending to a variation directly with $Q'^{\frac{1}{2}}$ in the turbulent regime. This behaviour was analytically predicted by DUCKLER (31). DOMANSKII and SOKOLOV (159) have considered evaporative heating of a liquid film in which the U.V.P. analysis describes the velocity profile within the film. The analysis

results in the general equation

$$\overline{Nu}_c = 1.44\, A\, \delta^{+1/3} \left(\frac{Q'}{\nu}\right)^{1/3} Pr \qquad 142.1$$

when A is a function dependent upon the particular film thickness δ^+ $\left(\equiv \left(g\delta^3/\nu^2\right)^{1/2}\right)$ and the heat transfer coefficient is defined in terms of $(T_o - T_s)$ when T_s is the free surface temperature. Thus A is given as

$$\delta^+ < 5 : \text{laminar} \quad A = (Pr^2)^{-1}$$

$$5 < \delta^+ < 30 : \text{transitional } A = \left(5\,Pr + 5\,\ln\left(1 - Pr + \frac{Pr}{5}\delta^+\right)\right)^{-1}$$

$$\delta^+ > 30 : \text{turbulent } A = \left(5\,Pr + 5\,\ln(1 + Pr) + 2.5\,\ln\left(\frac{1 - Pr + 0.4\,Pr\,\delta^+}{1 + 11\,Pr}\right)\right)^{-1}$$

for strict laminar flow equation 142.1 becomes

$$\overline{Nu}_c = 1.73 \left(\frac{Q'}{\nu}\right)^{1/2} \frac{1}{Pr} \qquad 142.2$$

DOMANSKII and SOKOLOV report good agreement to the theory and evaporative heat transfer to water and aqueous solutions of glycerol and alcohol.

Some experimenters report experimental correlations for vertical film heat transfer which are not given in generalised form but are reported here for completeness. Thus LUKACH et al (34) investigated vertical water flow over heated polymer tubes and found

$$\bar{h} = 1.85\left(\frac{Q'}{\nu}\right)^{1.55} Pr^{2.4} \quad \left(\text{for } 100 < \frac{Q'}{\nu} < 625\right) \qquad 143$$

when h is given in $W/m^2\,{}^oC$. The definition of h is not stated. HERBERT and STERNS (160) found that, for water flowing on the inner surface of a 1" diameter tube

$$\bar{h}_a = 1.69\left(\frac{Q'}{\nu}\right)^{0.65}$$

$$\left(\text{for } 600 < \frac{Q'}{\nu} < 5000\right) \qquad 144$$

when $\bar{h}_a$ is given in $W/m^2\,{}^oC$.

McADAMS et al (161) correlated the heating of water films on the outside of vertical tubes as

$$\bar{h}_N = 120\ \Gamma^{-\frac{1}{3}} \qquad 145.1$$

$$\text{for } 250 < \frac{Q'}{\nu} < 6200$$

when Γ is in lb/hr ft and h in BTU/hr.ft^2.$^\circ$F.

McADAMS (162) suggests that the heat transfer coefficient can be written as

$$\overline{Nu}_N = 0.0228\ \left(\frac{Q'}{\nu}\right)^{\frac{2}{3}}\ Pr^{\frac{1}{3}} \qquad 145.2$$

The correlation appears to be drawn from the work reported above.

FIGURE 70 shows the variation of h (various definitions) with flow rate parameter Q'/ν .

B: <u>WAVES</u>

The effect of waves upon heat transfer has led to several experimental correlations. Thus WILKE (157) found that the correlation

$$Nu_a = 0.061\ \left(\frac{Q'}{\nu}\right)^{8/15}\ (Pr)^{0.344} \qquad 146$$

best correlated the wavy laminar regime, whilst CHUNG and SEBAN (158) provide the correlation

$$Nu_c = 0.874\ \left(\frac{Q'}{\nu}\right)^{0.11} \qquad 147$$

TROMMELAN (163) repeated WILKES' work on water and ethenol and glycol solutions with both heating and cooling. The influence of surface tension variation, as given by the Weber number ($\equiv \rho Q^2/\sigma\delta$) was given by

$$\frac{h}{h_w} = 0.42\ We^{0.34} - 0.2 \qquad 148.1$$

$$\text{for } 0.2 < We < 15$$

and

$$\frac{h}{h_w} = 0.85 \qquad 148.2$$

$$\text{for } We > 15$$

In equations 148.1 and 148.2, h_w is the heat transfer coefficient predicted

by WILKES' correlation (equation 146).

A simple semi-empirical analysis was performed by KAPITSA (109) to describe the enhancement of heat transfer by waves. The film profile is described by

$$\delta(x) = \bar{\delta}\left(1 + \frac{a}{\bar{\delta}} \sin\left(\frac{2\pi x}{\lambda}\right)\right) \qquad 149.1$$

when a is half the film amplitude about the mean film $\bar{\delta}$, and λ is the wave length. Equation 149.1 describes a simple sine wave profile. Representing the instantaneous thickness of the wavy profile by δ_i, then the normal conductive heat transfer through the wavy film may be written as

$$q_w = \frac{1}{\lambda}\int_0^{\lambda} \frac{k\,(T_s - T_o)}{\delta_i}\, dx \qquad 149.2$$

when the temperature driving force is taken as the difference between the solid and free surface temperatures separated by the instantaneous film thickness. The integration is performed over one wavelength. Using the result of the standard integral

$$\frac{1}{\lambda}\int_0^{\lambda} \frac{dx}{a + b\sin(nx)} = (a^2 - b^2)^{-1/2} \qquad 149.3$$

equation 149.2 gives, after substitution for δ_i from equation 149.1

$$q_w = \frac{k(T_s - T_o)}{\bar{\delta}}\left(1 - \left(\frac{a}{\bar{\delta}}\right)^2\right)^{-1/2} \qquad 149.4$$

Had the film been taken as smooth over the entire flow length, then the equivalent smooth film heat transfer could be written as (see equation 149.2)

$$q_s = \frac{k\,(T_s - T_o)}{\delta_o} \qquad 149.5$$

when δ_o is the smooth film thickness.

The enhancement of heat transfer in a wavy flow compared to a smooth flow is thus

$$\frac{q_w}{q_s} = \frac{\delta_o}{\bar{\delta}\,(1 - a^2/\bar{\delta}^2)^{1/2}} \qquad 149.6$$

FIG 70 FALLING LIQUID FILMS: HEAT TRANSFER

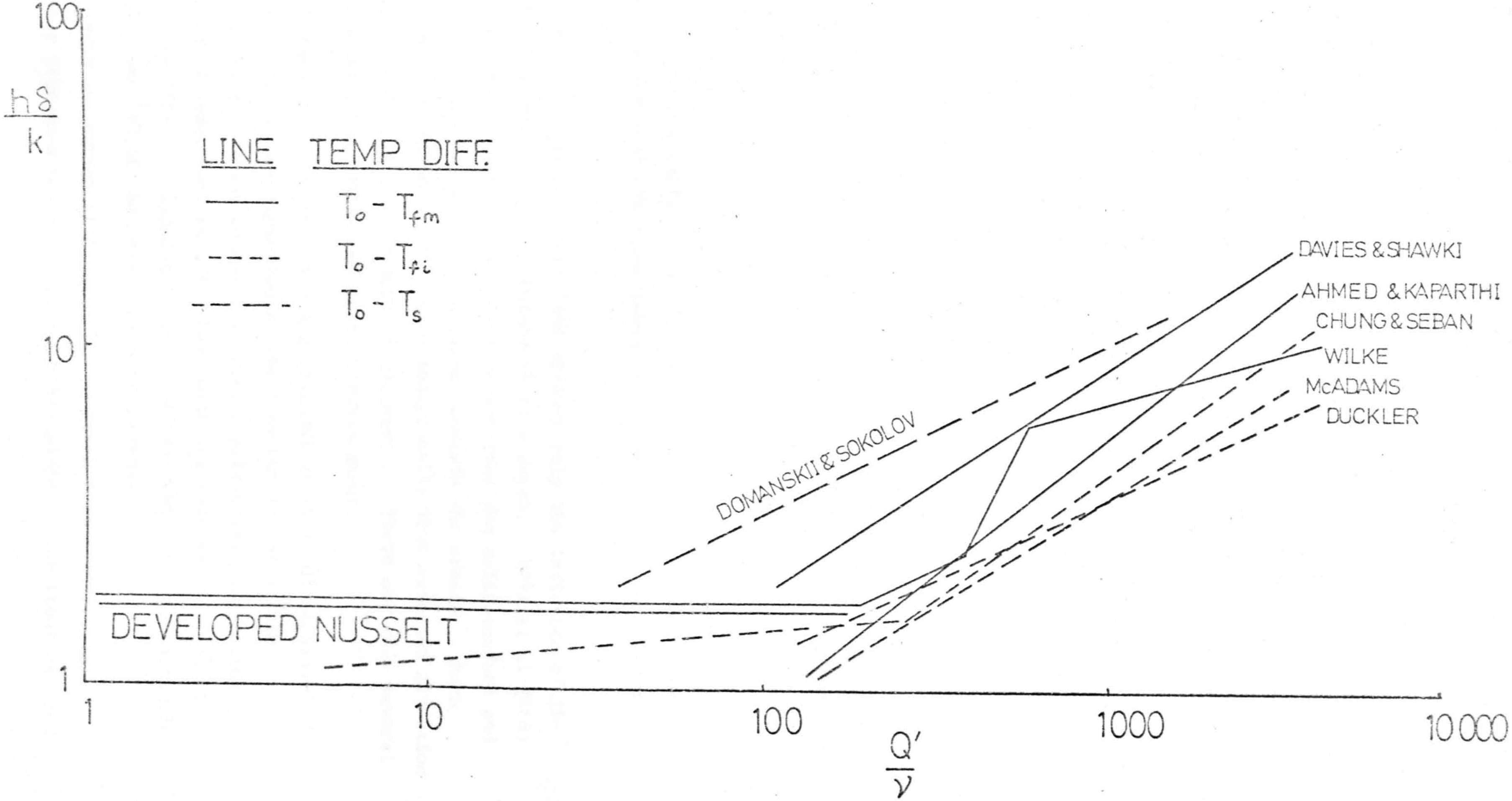

KAPITSA obtained theoretical values for $\frac{\bar{\delta}}{\delta_o}$ as 0.93 and for $\frac{a}{\delta}$ as 0.46 (see 109). Evaluating equation 149.6 with these figures shows that the wavy film gives 21% greater heat transfer than a smooth film, all other conditions being constant. This figure is of the correct order of enhancement noted by heat transfer investigators.

LEONARD and ESTIM (164) performed a numerical integration of the simplified energy equation (allowing for flow in the vertical direction) when the free surface is defined by the wave profile

$$\delta = \delta_o\left(1 + \frac{2a}{\delta_o}\left(-0.5 + \sin\left[\pi\left(1 - (X - I)^r\right)^2\right]\right)\right) \qquad 150$$

when $X = \dfrac{x - U_w t}{\lambda}$ and $I = 0$ for $0 < X < 1$

$I = 1$ for $1 < X < 2$ etc.

r is a variable parameter and for r = 4 a surface profile similar to those obtained by KAPITSA was found. This particular profile showed a further increase in heat transfer (of some 20% over that possible with the simple sine wave profile. The wave shape is characterised by large narrow crests and long shallow troughs.

O'BRIEN (165) considered the effect of a Gerstner-type wave for which the surface profile exhibits wave crests in the form of cusps and O'BRIEN showed that the enhancement of the wavy flow lies between zero and 100%.

The above analyses take into account only the influence of the wave in its influence of the instantaneous film depth. MIYA et al (166) measured the shear stress as roll waves passed over the solid surface and showed that the flow was probably turbulent beneath the crests. Both PORTALSKI (167) and BARBER (168) showed analytically that reversed direction flow is feasible beneath the troughs of the waves. There are thus several mechanisms whereby wavy films may produce enhancement.

EINARSSON and WRAGG (169) and IRIBARNE et al (170) separately observed the electrolytic reduction at the flow surface of a film containing ferricyanide and found that current pulsations (indicating varying rates of reduction) were in phase with the roll waves visually observed on the film. IRIBARNE et al noted that the maximum fluctuation observed was some $\pm$8% of the mean reduction current.

CHAND and ROSSON (171) studied the local heat transfer to a falling water film on a heated stainless steel plate. The front and rear

surface temperatures of the plate were used to control an electrical analogue of the process, previously calibrated against known heat fluxes. In this way instantaneous values of the heat transfer were obtained. They observed that in the range $55 < Q'/\nu < 121$ the entire flow surface was covered with ripples. With heat fluxes of less than 10^5 W/m^2 the local fluxes were steady, whereas at higher heating rates ($>2.5 \times 10^5$ W/m^2) oscillations of $\pm$10% about the mean were noted in the local fluxes. Further the frequency of these oscillations was approximately in phase with the visible ripple frequency. CHAND and ROSSON proposed that the influence of the ripples was upon the thermal boundary layer which was thickened at the higher fluxes, and interacted with the ripples to give localised thinning/thickening of the thermal boundary layer and hence variation in the heat flux.

Heat transfer to films containing surfactants has been carried out by several investigators. SHAH and DARBY (172) noted that the heat transfer coefficient for a falling water film increased linearly with surfactant concentration in the range $1000 < Q'/\nu < 2000$. DAVIES and SHAWKI (173) found an increase of up to 40% in the heat transfer coefficient predicted from their experimental correlation

$$\overline{Nu}_a = 0.046 \left(\frac{Q'}{\nu}\right)^{\frac{2}{3}} (Pr)^{0.4} \qquad 151$$

when surfactant was added to the flow.
PONTER et al (174) gradually increased the surfactant concentration of a vertically falling water film and noted the effect upon the heat transfer coefficient. Initially the coefficient increased with increasing concentration and then began to fall, eventually stabilising at some 20% over the coefficient for pure smooth water films. PONTER et al propose that the initial addition of surfactant reduces the film velocity (through increasing the interfacial tension and decreasing the free surface velocity - see STROEBAL and WHITAKER (175)) and so increases the film residence time and hence transfer coefficient. However, addition of the surfactant also causes a damping of the waves and thus reduces their enhancement. The usual maxima for the addition of the effects of one increasing and one decreasing process is eventually seen.

C: CONDENSATION

Condensation on a wall will be dealt with only briefly since the more important study is for condensation on a rotating surface, and the

wall situation is presented only for completeness.

NUSSELT (24) first developed a simple theory of laminar film condensation. NUSSELT considered the incremental thickening of a falling film of condensate due to the addition of further condensate as it flowed down a cooling surface. Utilising the results of the simple flow model NUSSELT obtained an expression for the local heat transfer coefficient h_c, which for a vertical surface is

$$h_c = \left(\frac{(\rho - \rho_v)\, h_{fg}\, k^3 g_c}{4\nu\, (T_s - T_o)\, x} \right)^{1/4} \qquad 151.1$$

The local coefficient decreases from infinity at the top of the plate ($x = 0$). An average coefficient over the total plate length is obtained by integrating equation 151.1 to obtain

$$\overline{h_c} = \frac{1}{x}\int_o^x h_c\, dx = 0{\cdot}943 \left(\frac{\rho g\, h_{fg}\, k^3}{\nu\, \Delta T\, x} \right)^{1/4} \qquad 151.2$$

when $\Delta T = T_s - T_o$

Equation 151.2 may be rewritten in a dimensionless Nusselt number form as

$$\overline{Nu_c'} = \frac{\overline{h_c}\, x}{k} = 0{\cdot}943 \left(\frac{\rho g\, h_{fg}\, x^3}{k \nu\, \Delta T} \right)^{1/4} \qquad 151.3$$

Experimental investigation has shown that in streamline flow conditions at low vapour velocities, equation 151.3 tends to be substantially low although when the equivalent equation is derived for condensation on horizontal tubes, the agreement is of the order of 15%. Various empirical relationships are available to account for the influence of non-condensable inerts, high vapour velocities, etc., for which reference should be made to any engineering text (e.g. PERRY (176)).

SPARROW and GREGG (177) have considered the numerical solution of the governing partial differential equations after reduction to an ordinary set by the similarity transform

$$\eta = \frac{cy}{x^{1/4}} \quad , \quad c = \left[\frac{g\, c_p (\rho - \rho_v)}{4 \nu k} \right]^{1/4} \qquad 152$$

The results indicate that the group ($\frac{c_p \Delta T}{h_{fg}}$) is an additional parameter. When the parameter ($c_p \Delta T / h_{fg}$) is much less than unity, the dependence of the heat transfer coefficient varies directly as predicted by the NUSSELT

equation, increasing $C_p \Delta T / h_{fg}$ causes discrepancies. . . . The effect of the included inertial term in the more general solution is negligible for values of Prandtl number much greater than unity. In this instance, the results may be correlated in the form

$$\frac{h_c x}{k} = 0.707 \left[\frac{g(\rho - \rho_v) h'_{fg} x^3}{\nu k \Delta T} \right]^{1/4} \qquad 153.1$$

when $$h'_{fg} = h_{fg} \left(1 + 0.68 \left(\frac{C_p \Delta T}{h_{fg}} \right) \right) \qquad 153.2$$

A recent review is presented by DHIR and LIENHARD (178).

3.1.2. RADIAL FLOW ON A STATIONARY DISC

The heat transfer to a film flowing normally onto the centre of a stationary disc has recently been studied theoretically by CHAUDHURY (179) and experimentally by HEALEY (180).

CHAUDHURY supplemented the flow equations used by WATSON (88) (equation set 37) with the boundary layer energy equation

$$u_r \frac{\partial T}{\partial r} + u_y \frac{\partial T}{\partial y} = \frac{\nu}{\rho_r} \frac{\partial^2 T}{\partial y^2} + \frac{\nu}{c_p} \left(\frac{\partial^2 u_r}{\partial y^2} \right) \qquad 154.1$$

with the boundary conditions

$$y = 0 \qquad T = T_o \qquad 154.2$$

$$y = 0 \qquad \left(\frac{\partial T}{\partial y} \right)_{y=0} = C \qquad 154.3$$

$$y = \delta \qquad \frac{\partial T}{\partial y} = 0 \qquad 154.4$$

In equation 154.3, C is a specified constant (corresponding to a known heat flux). CHAUDHURY considered the similarity flow section found by WATSON and integrated equation set 154 written in terms of the similarity variables used by WATSON. The resulting equations form a convergent infinite series and CHAUDHURY gives numerical and analytical equations for the evaluation of the terms.

HEALEY studied the heating of a water film fed to the centre of a small (5 cm diameter) brass disc surrounded by a larger (12 cm diameter) stainless steel annular ring. The brass disc was in fact the end face of a brass bar around which an electrical heater was wound. HEALEY arranged the experimental conditions such that the hydraulic jump

occurred outside the heating ring. HEALEY'S data and CHAUDHURY'S analysis for Pr = 6 and Pr = 7 (which bounds HEALEY'S data) are shown in FIGURE 71.

It will be noticed that HEALEY'S results are some 30 - 100% greater than those proposed by CHAUDHURY. It will be seen that the best agreement occurs for the maximum values of $r_o/r_i \left(\frac{r_i \nu}{Q}\right)^{1/3}$, and as this parameter reduces then the agreement worsens. A possible explanation for this behaviour is as follows. For the parameter $\left(\frac{r_o}{r_i} \cdot \left(\frac{r_i \nu}{Q}\right)^{1/3}\right)$ to reduce then the flowrate Q must increase, since in this work r_o and r_i were fixed and ν varied only slightly. From WATSON'S analysis, increasing Q increases the radius at which the similarity model is appropriate. Taking the maximum and minimum values of $\left(\frac{Q}{r_i \nu}\right)$ used by HEALEY (1.35×10^4 and 2.3×10^4) and thus utilising equation 42.1 then the variation in radii below which the similarity criteria cannot be satisfied is from 0.75 to 0.9 cm which corresponds to a variation of 10 to 14% of the total flow area. Thus HEALEY'S data contains an appreciable area in which the flow conditions will obviously be much different from those assumed by CHAUDHURY'S analysis. The experimental data does indicate that the heat transfer is increased by increasing Prandtl number as indicated by CHAUDHURY'S model.

3.1.3. ROTATING DISC IN AN INFINITE MEDIUM

A: CONVECTIVE HEAT TRANSFER

MILLSAPS and POHLHAUSEN (94) were first to perform a numerical investigation into the heat transfer of a disc rotating in a uniform environment of infinite extent. The hydrodynamic equations considered by COCHRAN were re-solved and the results employed in solving the heat transfer boundary layer equation

$$\rho\left(v_r \frac{\partial T}{\partial r} + \frac{v_\theta}{r} \frac{\partial T}{\partial \theta} + v_y \frac{\partial T}{\partial y}\right) = k\left(\frac{\partial^2 T}{\partial r^2} + \frac{1}{r}\frac{\partial T}{\partial r} + \frac{1}{r^2}\frac{\partial^2 T}{\partial \theta^2} + \frac{\partial^2 T}{\partial y^2}\right) + \frac{\Phi_v}{\rho} \qquad 155$$

when Φ_v is the viscous dissipation term (see APPENDIX F).
Physical properties were assumed independent of temperature and the temperature distribution was assumed to be of the form

$$T(r,y) = r^2 s(y) + q(y) + T \qquad 156$$

when s and q are functions of y only.
The results of the analysis are presented in graphical form to enable the

FIG 71 RADIAL FLOW ON A STATIONARY DISC: HEAT TRANSFER

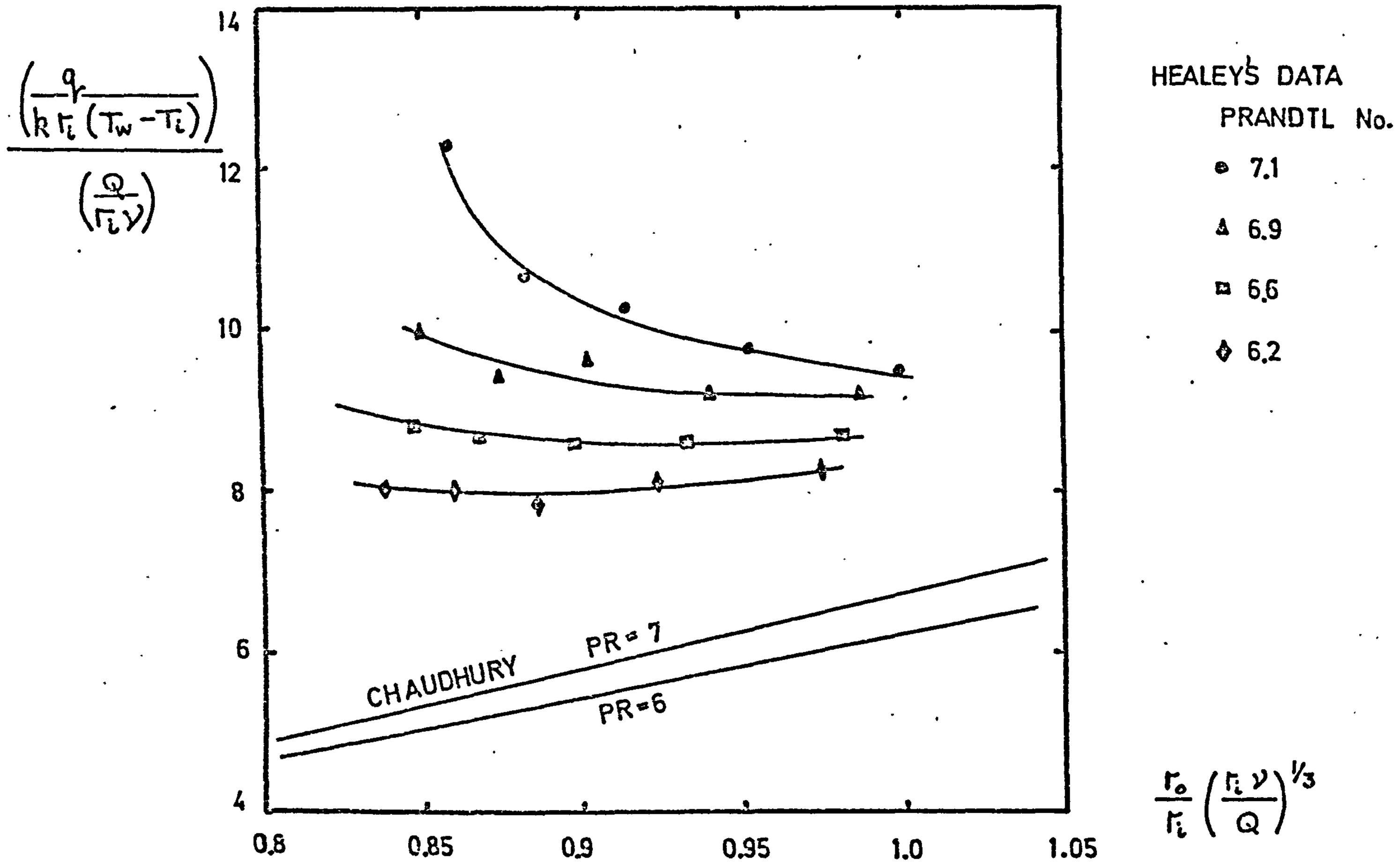

heat transfer or temperature profile away from the disc to be found. OUDART (181) obtained similar results analytically after assuming polynomial expansions for T. For air the results may be written as

$$\frac{q}{T_o - T_{ambient}} - h_\infty = 0.28\, k \left(\omega/\nu\right)^{1/2} \qquad 157.1$$

or $$Nu_\infty = \frac{h_\infty r}{R} = 0.28\, Ta^{1/2} \qquad 157.2$$

It will be noticed that the heat transfer coefficient is independent of radius.

WAGNER (182) considered equation 155 neglecting the circumferential distributions and viscous dissipation. By using the polynomial expressions for U_y and U_r as given by Von KARMAN, WAGNER obtained two analytic expressions for the heat transfer coefficient depending upon the manner of formulation. These two expressions should be identical, but in fact differed by a very small amount. This difference may be ascribed to approximations in the velocity profile descriptions. The result for air (Pr = 0.74) gave

$$h_\infty = 0.337\, k \left(\frac{\omega}{\nu}\right)^{1/2} \qquad 158.1$$

or $$Nu_\infty = 0.337\, Ta^{1/2} \qquad 158.2$$

OSTRACH and THORNTON (92) repeated MILLSAP and POHLHAUSEN'S analysis neglecting the viscous dissipation term. The resolution of COCHRAN'S hydrodynamic set was carried out to higher accuracy and Cp, the specific heat at constant pressure, rather than Cv used in the heat transfer equation. OSTRACH and THORNTON showed that Φ_v the viscous dissipation may be ignored when

$$\frac{(\gamma - 1)(P_r) M^2}{(T_o/T_\infty - 1)} \ll 1 \qquad 159.1$$

when M = Mach number of the flow and $\gamma = Cp/Cv$

The numerical result found for air was

$$Nu_\infty = 0.329\, (Ta)^{\frac{1}{2}} \qquad 159.2$$

SPARROW and GREGG (93) extended the range of Prandtl numbers of the previous investigations and give analytic results for Pr (0.01, .1,

1, 10, 100) and asymptotic bounds for Pr $<$ .01 and $>$ 100. These are

$$Nu_\infty = 0.88447\ (Ta)^{\frac{1}{2}}\ Pr \qquad \text{for Pr} \ll 0.01 \qquad 160.1$$

and $$Nu_\infty = 0.62048\ (Ta)^{\frac{1}{2}}\ (Pr)^{\frac{1}{3}} \qquad \text{for Pr} \gg 100 \qquad 160.2$$

for air, $$Nu_\infty = 0.33\ (Ta)^{\frac{1}{2}} \qquad Pr = 0.73 \qquad 160.3$$

Several investigators have provided expressions for extending the useful range of Prandtl numbers served by the numerical results. Thus, LIU and STEWART (183) give three such correlations, the most accurate being

$$Nu_\infty = (Pr)^{\frac{1}{3}} \left[1.61173 + \frac{0.4803}{(Pr)^{\frac{1}{3}} - .4870} \right]^{-1} (Ta)^{\frac{1}{2}} \qquad 161.1$$

which gives $Nu_\infty = 0.325\ Ta^{\frac{1}{2}}$ for air (Pr = 0.73)

LEVART and SCHUHMANN (184) give an analytical solution to the transfer equation

$$U_y \frac{\partial T}{\partial y} = \frac{k}{c_p} \frac{\partial^2 T}{\partial y^2} \qquad 162.1$$

with the velocity profile described by COCHRAN'S equations. The result of the investigation is

$$Nu_\infty = \frac{1}{M\ Pr} (Ta)^{\frac{1}{2}} \qquad 162.2$$

when $$M = 1.611731\ (Pr)^{-\frac{1}{3}} + 0.480306\ (Pr)^{-\frac{2}{3}} + 0.233931\ (Pr)^{-1} + ... \qquad 162.3$$

for Pr = 0.73, equation 162.3 gives a value of M = 2.816, so from equation 162.2

$$Nu_\infty = 0.486\ (Ta)^{\frac{1}{2}} \qquad 162.4$$

RILEY (185) allowed viscosity to vary linearly with temperature and employed COCHRAN'S hydrodynamic solution to solve equation 155 neglecting circumferential gradients and viscous dissipation. The resulting expression is valid for Pr $>$ 1 only,

$$Nu_\infty = (0.6315\ Pr^{\frac{1}{3}} - 0.035\ Pr^{-\frac{1}{3}} - 0.185)\ Ta^{\frac{1}{2}} \qquad 163$$

HAYDAY (186) considered the solution of the simple boundary layer energy equation for bodies of arbitrary shape. The result for the disc shape was

$$Nu_\infty = 0.3325\ Ta^{\frac{1}{2}} \qquad \text{for Pr} = 0.73 \qquad 164$$

DORFMAN (187) considered the solution of the simple energy equation when the plate radial temperature distribution is given as proportional to r^n with n as some integer. DORFMAN showed that for n = 2, the circumferential velocity and radial energy equations were similar and a Reynold's analogy could be applied. Using equations for the disc shear stress in laminar flow from COCHRAN'S work and his own for turbulent flow expressions for Nu_∞ were obtained. A more general analytical solution allowing n to vary was then conducted. For a Prandtl number of unity with a constant disc temperature, this results in the expressions

$$Nu_\infty = 0.436\ (Ta)^{\frac{1}{2}} \qquad \text{for Ta} < 10^6,\ \text{Pr} = 1 \qquad 165.1$$

and

$$Nu_\infty = 0.0198\ (Ta)^{0.8} \qquad \text{for Ta} > 10^6,\ \text{Pr} = 1 \qquad 165.2$$

for Pr = 0.73, these equations may be approximated by

$$Nu_\infty = 0.318\ Ta^{\frac{1}{2}} \qquad \text{for Ta} < 10^6 \qquad 165.3$$

and

$$Nu_\infty = 0.0144\ Ta^{0.8} \qquad \text{for Ta} > 10^6 \qquad 165.4$$

DORFMAN reports that the numerical solution of the equations considered gave the relationship

$$Nu_\infty = 0.399\ Ta^{\frac{1}{2}} \qquad 165.5$$

although the Prandtl number is not specified.

KREITH and TAYLOR (188) performed an analytical solution of the simple radial energy equation using Prandtl's $^1/_7$th power law and a logarithmic velocity profile . Two expressions resulted, the simplest of which gave

$$Nu_\infty = 0.0116\ (Ta)^{0.8} \qquad 166.1$$

Equation 166 is valid only for the situation Pr = 1 when the thermal and momentum boundary layers are of equal thickness. The other expression

gave Nu_∞ implicitly as a function of Ta. KREITH and TAYLOR extended the useful range of the Prandtl number by assuming the full pipe flow U.V.P. analysis to fit the laminar and buffer layers separately. The result was

$$Nu_\infty = 0.0265\ Ta^{0.8}\left[\frac{Pr}{1+\frac{0.1325(Pr-1+\ln(1+5/6(Pr-1)))}{Ta^{0.1}}}\right] \qquad 166.2$$

for $0.5 < Pr < 25$

which evaluates for Pr = 0.73 to give

$$Nu_\infty = 0.0210\ Ta^{0.8} \qquad 166.3$$

with less than 2% error for $Ta > 10^6$.

DAVIES (189) employed Von KARMAN'S velocity profiles and a Reynold's analogy to the flow on the disc. The analysis results in the expression

$$Nu_\infty = K\ Pr\ Ta^{4/5} \qquad 167.1$$

when K is a number depending solely upon the velocity profile chosen. Although equation 167.1 should be strictly only evaluated at Pr = 1, evaluation at Pr = 0.73 gives results close to the experimental values found (see later). The correlation is thus

$$Nu_\infty = 0.012\ Ta^{0.8} \qquad 167.2$$

(note that the coefficient given in DAVIES paper is 0.014, 0.002 too high).

HARTNETT et al (190) repeated DAVIES analysis for a variable disc temperature profile, after DORFMAN'S technique using the circumferential velocity profile rather than the radial profile, to provide the momentum equation for the analogy. The results of the analysis were

$$Nu_\infty = 0.0198\ Pr\ Re^{0.8} \qquad 168.1$$

or $$Nu_\infty = 0.0145\ Re^{0.8} \quad \text{for air Pr} = 0.73 \qquad 168.2$$

Suitable reviews of the theoretical developments of discs in infinite environments are supplied KREITH (191) and DORFMAN (192).

COBB and SAUNDERS (193) and YOUNG (194) both investigated

experimentally the heat transfer properties of disc flows. . In the laminar flow regime both investigators found the best fit to the data was obtained as

$$Nu_{\infty} = 0.36\ Ta^{\frac{1}{2}} \qquad 169.1$$

whilst in the turbulent regime, COBB and SAUNDERS found the data to agree to

$$Nu_{\infty} = 0.015\ Ta^{0.8} \qquad 169.2$$

The transition value of Ta was found to be 2.4×10^5.
COBB and SAUNDERS measured the velocity profiles existing within the flow above the disc and found close agreement to COCHRAN'S profile in laminar flow and Prandtls $^1/7$th law profile in the turbulent regime. In the low Ta value work of YOUNG a dependency was found on the disc temperature and OSTRACH and THORNTON ascribe these discrepancies as being due to the influence of natural convection from the disc.

To observe the true influence of the Prandtl number, experiments have to be performed with a heated disc surrounded by fluids of differing Prandtl number. RICHARDSON (195) measured the heat transfer rate from heated discs enclosed in a water tank. The results indicated that the heat transfer coefficient was only some 30% of the theoretical from the work of MILLSAPS and POHLHAUSEN, being correlated by the equation

$$Nu_{\infty} = 0.3\ Ta^{\frac{1}{2}} \qquad 170$$

$$Pr = 5.8$$

No dimensions of the tank used were given by RICHARDSON and a simple explanation of the low results may be that the tank was so small as to cause the presence of the walls to interact with the flow on the disc (note that the analyses previously considered all assume that the fluid is of infinite extent). In this respect the work of GREGORY and RIDDIFORD (196) and LEHMKUHL and HUDSON (197) should be noted. GREGORY and RIDDIFORD demonstrated that mass transport to a rotating disc is not affected by the diameter of the retaining vessel if

$$\frac{\text{vessel diameter}}{\text{disc diameter}} \geqslant 2 \qquad 171.1$$

and LEHMKUHL and HUDSON place the criteria as low as 1.02 providing that the

additional criteria

$$\frac{\omega H^2}{\nu} > 50 \qquad 171.2$$

(when H is the disc edge/wall clearance)is also satisfied.

Due to the difficulty experienced in transferring energy to the heated discs in experimental work, an analogy method of study has been developed. In this technique use is made of the fact that the governing transfer equations for both heat and mass transport are of the same form.

KREITH et al (198) used a cast naphthalene disc for a mass transfer study and correlated the laminar regime results by

$$\frac{k_m r}{D_v} = Sh = 0.635\ Ta^{\frac{1}{2}} \qquad 172.1$$

when Sh is the Sherwood number.
This information can only be interpreted as an analogous heat transfer result if Pr = Sc (when Sc is the Schmidt number ≡ 2.4 for air). Applying the LIU-STEWART correlation as describing the effects of varying Prandtl number, equation 172.1 can be "corrected" to give the equivalent result for Pr = 0.73

$$Nu_\infty = 0.335\ Ta^{\frac{1}{2}} \qquad 172.2$$

This result is in approximate agreement with the theoretical analyses and the experimental system has several advantages.

Recently MABUCHI et al (199) studied the transfer of naphthalene from a discontinuous surface in suction flow. The technique is obviously a useful research tool but has severe limitations in the requirement that the Schmidt and Prandtl numbers of the analogous systems be equal.

KREITH et al (200) employed the mass transfer analogy to investigate the influence of a close fitting shroud over the disc surface. It was found that the shroud caused the flow to become turbulent at lower values of the group Ta. METZGER (201) showed that the effect of the shroud is negligible if

$$\frac{Z_o}{r_o} > 0.17 \qquad 173$$

when Z_o is the disc-shroud clearance.

SPARROW and GREGG (202), LEE (203) and MABUCHI (204) have studied the theoretical effect of suction and transpiration from the disc surface. The overall effect of suction is to decrease the thermal boundary layer and hence promote heat transfer. Transpiration from the disc surface causes the reverse process to occur.

Heat transfer from unsteadily rotating plates has been theoretically studied by ANDREWS and RILEY (205), and LEVART and SCHUHMANN (184). ANDREWS and RILEY show that the response time of the system is given by

$$t_R = 0.1954 \frac{(Pr)}{\omega} \qquad 174$$

for $Pr \leq 7$

Thus for most situations a step change in the speed of the disc will only require a few revolutions of the disc for a new steady state to establish.

IYENGAR and RATH (206) considered the same problem as ANDREWS and RILEY when the fluid was power law non-Newtonian. The results are expressed in terms of the rates of change of the speed and its differentials (i.e. $\beta_1 = \omega'/\omega$, $\beta_2 = \omega''/\omega^2$ etc.) and the instantaneous value of the Nusselt number is given as a function of β_i. The general observation is made that the flow of the non-Newtonian fluid establishes faster and the heat transfer more slowly compared to that found for Newtonian fluids.

SHULMAN et al (207, 208) provide recent reviews of mass transfer work to non-Newtonian fluids from rotating discs. A comparison is made of the various coefficients proposed for the dependency of Nu_∞ on Ta in TABLE 5.

B: CONDENSATION

SPARROW and GREGG (209) obtained a similarity solution to the boundary layer hydrodynamic equations (equation set 48) augmented by the simple energy equation

$$c_p v_r \frac{\partial T}{\partial r} = k \frac{\partial^2 T}{\partial y^2} \qquad 175$$

Condensate energy liberation and the film thickening effect of the addition of the condensate mass were accounted for by an overall energy balance also solved simultaneously. The results are presented graphically for values of $0.003 < Pr < 100$ and $0.0001 < \frac{c_p \Delta T}{h_{fg}} < 1$. Here ΔT is defined as $(T_s - T_o)$. The results were found to tend to the limiting equation

INVESTIGATOR	CONST.	E T A	REF.
MILLSAP & POHLHAUSEN	0·28	T	94
WAGNER	0·337	T	182
OSTRACH & THORNTON	0·329	T	92
SPARROW & GREGG	0·33	T	93
LIU & STEWART	0·325	T	183
LEVART & SCHUHMANN	0·486	T	184
RILEY	0·347	T	185
HAYDAY	0·3325	T	186
DORFMAN	0·318	T	187
COBB & SAUNDERS	0·36	E	193
YOUNG	0·36	E	194
KREITH	0·335	A	198

LAMINAR FLOW $\frac{\omega r^2}{\nu} < 200\,000$

TABLE 5 HEAT TRANSFER FROM A ROTATING DISC IN AN INFINITE MEDIA (PR = 0·72)

INVESTIGATOR	CONST.	E T A	REF.
DORFMAN	0·0144	T	187
KREITH & TAYLOR	0·0116	T	188
" " " " " " "	0·0210	T	188
DAVIES	0·012	T	189
COBB & SAUNDERS	0·015	E	193
HARTNETT et al	0·0145	T	190

TURBULENT FLOW $\frac{\omega r^2}{\nu} > 1\,000\,000$

KEY E:EXPERIMENTAL T:THEORETICAL A:ANALOGUE

$$\frac{hr}{k} = (\text{CONST.})\left(\frac{\omega r^2}{\nu}\right)^y$$

laminar flow $y = 0.5$
turbulent flow $y = 0.8$

$$\frac{h_c r}{k} = 0.904 \left(Pr \Big/ \left(\frac{C_p \Delta T}{h_{fg}} \right) \right)^{1/4} Ta^{1/2} \qquad 176$$

for small values of $C_p \Delta T / h_{fg}$ and Prandtl numbers close to unity. The effect of increasing Prandtl number was to increase the coefficient, whilst decreasing Prandtl numbers from unity lowered the heat transfer coefficient. SPARROW and GREGG show that equation 176 may be deduced analytically by employing the centrifugal model velocity profiles in the vertical and circumferential directions (equations 82.2 and 82.3) and the assumption of a linear film temperature profile to solve the expression for the overall heat balance

$$\rho h_{fg} \int_0^\delta 2\pi r u_t dy + \int_0^\delta \rho 2\pi r v_t C_p (T_s - T_o) dy = k \left(\frac{dT}{dy} \right)_{y=o} \pi r^2 \qquad 177.1$$

The direct solution of equation 177.1 using the normal boundary conditions for velocities and temperatures is

$$\frac{C_p \Delta T}{h_{fg}} = \frac{2}{3} Pr \left[\delta \left(\frac{\omega}{\nu} \right)^{1/2} \right]^4 \qquad 177.2$$

and defining the heat transfer coefficient, h_c, as

$$h_c = \frac{q}{(T_s - T_o)} = \frac{k \Delta T}{\delta \Delta T} = \frac{k}{\delta} \qquad 177.3$$

then equation 176 results.

Note that equation 176 indicates the $h_c \propto \omega^{1/2}$.

SPARROW and GREGG combined equation 176 with ROHSENOW'S (210) equivalent local equation derived for flow down a vertical wall. For the average heat transfer coefficient ROHSENOW gives

$$\frac{\bar{h}_c}{k} = 0.943 \left(\frac{g(\rho - \rho_v) h_{fg}}{k \nu \Delta T x} \right)^{1/4} \left(1 + 0.68 \frac{C_p \Delta T}{h_{fg}} \right)^{1/4} \qquad 178$$

Note that the $\bar{h}_c$ in equation 178 is the average value over the wall height x = 0 to x = x. For small values of $C_p \Delta T / h_{fg}$ and when $\rho_v << \rho$, then equations 176 and 178 give

$$\frac{h_r}{h_x} = 0.96 \left(\frac{\omega^2 x}{g} \right)^{1/4} \qquad 179$$

where the suffices r and x indicate the coefficients in heat transfer for the rotating disc and vertical plate respectively. Thus a rotating disc device will condense a greater amount per unit surface area than a plate

condenser if

$$\omega > \left(\frac{g}{x}\right)^{1/2} \qquad 180$$

Obviously if x is made sufficiently short the speed required of the disc can be raised beyond reasonable limits, but if x = 0.1 m, then $\omega >$ 100 r.p.m. will satisfy the criteria.

SPARROW and GREGG compared the results of NANDAPURKAR (see 209) to their analysis and found the experimental results some 30% low. The discrepancy was initially explained as being caused by the lack of interfacial drag in the theoretical model giving theoretically thinner film that would be experimentally obtained. Subsequent analysis allowing for interfacial drag (211) gave little improvement. BECKETT et al (212) also found little theoretical dependency of the heat transfer coefficient upon interfacial drag. A possible explanation for the disagreement between SPARROW and GREGG'S analysis and the data of NANDAPURKAR could be the presence of non-condensible gases or wave formation etc. in the experimental runs. Unfortunately, NANDAPURKAR'S thesis is not readily available for study.

CHIRANJIVI et al (213) used various velocity profiles in the film to solve the simple energy balance and compared the results to SPARROW and GREGG'S analysis. An equation is given which reproduces the numerical results of SPARROW and GREGG thus

$$\frac{h_c r}{k} = \left(\frac{1}{4}\right)^{1/4} \left(\frac{b}{2.5 + \frac{74}{49}\left(\frac{c_p \Delta T}{h_{fg}}\right)\frac{1}{b P_r}}\right)\left(\frac{\mu}{c_p \Delta T / h_{fg}}\right)^{1/4} Ta^{1/2} \qquad 181.1$$

when $$b = 1 + \frac{82}{210}\,\frac{c_p \Delta T}{h_{fg}} \qquad 181.2$$

These equations are applicable for the ranges

$$0.001 < \frac{c_p \Delta T}{h_{fg}} < 1.0 \qquad 181.3$$

$$1 < Pr < 100 \qquad 181.4$$

The error in reproduction of equation 181.1 is < 7%.

A similar analysis is presented by APPARAO et al (214) and the results are some 5 - 10% lower than those of SPARROW and GREGG. The analysis is valid only for Pr > 1 due to the neglect of inertia terms in

the boundary layer momentum balance conducted.

ROETZEL (215) has conducted a general analysis applicable to the condensation of fluids of Pr > 1 in general force fields on bodies of various radius of curvature. For condensation on a disc, ROETZAL gives

$$\frac{h_c r}{k} = \left[\left(\frac{2}{3}\left(\frac{Pr}{\frac{c_p \Delta T}{h_{fg}}}\right) Ta^2\right)^{\frac{23}{16}} + \left(\frac{0.86}{3}\frac{1}{(Pr)\left(\frac{c_p \Delta T}{h_{fg}}\right)}\frac{g r^3}{\alpha_H^2}\right)^{\frac{23}{20}}\right]^{\frac{4}{23}} \quad 182$$

when α_H is the thermal diffusivity $= k/c_p\rho$
For high Prandtl number fluids, when the second group in equation 182 may be ignored, equation 182 reduces to equation 176.

Condensation on bodies of general surface shape has been considered theoretically by GUNERATNE (216).

ESPIG (141) studied the condensation of steam on a horizontal, water cooled, disc and found that the experimental data was best correlated by

$$\frac{h_c}{h_c^*} = \frac{113}{\omega^{0.415}\ \Delta T_c^{0.6}} \qquad 183$$

$250 < \omega < 2000$ r.p.m.

when ω is in R.P.M., ΔT in ^oF and h_c^* is given by equation 176 - the laminar case. Notice that the experimental dependency on ω is almost negligible.

NANDAPURKAR and BEATTY (217) studied the condensation of various vapours on a cooled rotating disc. The data obtained was some 25% below equation 176 which, for the various Pr and $c_p \Delta T/h_{fg}$ values of the vapours used, should, according to SPARROW and GREGG, have agreed to within 5%. NANDAPURKAR and BEATTY propose that waves may have been present on the disc causing a thickening of the film. The presence of Coriolis forces are allowed for in SPARROW and GREGG'S model and thus the film thickening effect of the Coriolis force cannot be proposed as an explanation.

ASTAF'EV and BAKLASTO (218) studied the condensation of steam to the underside of an upward facing horizontal disc. It was observed that h_c showed a varying dependency on ω. When the disc speed was less than 300 r.p.m., condensate drops tended to fall from the disc surface rather than flow radially along the disc surface. For speeds greater than some 600 r.p.m., ASTAF'EV and BAKLASTO give a correlating equation which is unfortunately dimensionally incorrect. However, the authors state

that the heat transfer coefficients were some 50% of the theoretical values and the dependency of ω in the regime in which the theory was expected to hold was to the power of 0.43 (cf. equation 176, power of $\omega = 0.5$).

In a subsequent paper, ASTAF'EV and BAKLASTO (219) consider the condensation of steam on the upward facing side of the cooled disc. Dependency of h_c on rotational speed is again noted, this time due to the non-wetting properties of the disc edge. At speeds greater than 600 r.p.m. the condensate left the disc freely and the heat transfer results were correlated by the equation

$$\overline{Nu} = 1.38 \left(\frac{\rho_r}{\frac{c_p \Delta T}{h_{fg}}} \right)^{1/4} Ta^{0.43} \qquad 184$$

Unfortunately the definition of $\overline{Nu}$ is not given. Notice that equation 184 predicts a slight dependency of h_c on radius. The data of NANDAPURKAR and BEATTY are also shown to fit the data and if Nu is defined as hd/k with d the disc diameter, coefficients some 30% below equation 176 are obtained.

BUTUZOV et al (220, 221) considered heat transfer to the underside of an upward facing disc. As with ASTAF'EV and BAKLASTO, at low speeds drop formation in the condensate layer gave erroneous coefficients, but at sufficiently high speeds (ω>500 r.p.m.) the data was some 10% below the theoretical. The authors suggest that Coriolis force may cause local thickening and therefore reduce the heat transfer coefficients.

Condensation of several organic vapours on short annular fins along a rotating tube have recently been studied by WILLIAMS et al (222). The data was well correlated by

$$h_c = 0.655 \left(\frac{k^3 \rho^2 h_{fg}}{\mu \Delta T} \right)^{1/4} \left(\frac{G'}{L'} \right)^{1/4} \qquad 185.1$$

when $G' = (g^2 + (w^2 r_o)^2)^{1/2}$

and r_o is the fin outer radius, L' is the fin to fin separation along the tube. If $L' \rightarrow 0$ and $\omega^2 r \gg g$, then equation 185 tends to become

$$\frac{h_r}{k} = 0.655 \left(\frac{\rho_r}{\frac{c_p \Delta T}{h_{fg}}} \right)^{1/4} Ta^{1/2} \qquad 185.2$$

or some 28% below the theoretical equation 176.

3.2. LITERATURE SURVEY

3.2.1. THEORETICAL DEVELOPMENTS

DORFMAN (130) supplemented the hydrodynamic equations considered earlier by the energy equation

$$v_r \frac{\partial T}{\partial r} + v_y \frac{\partial T}{\partial y} = \frac{k}{c_p \rho} \frac{\partial^2 T}{\partial y^2} \qquad 186$$

The energy equation was solved simultaneously with the hydrodynamic model (constant physical properties assumed). DORFMAN showed numerically that adjusting the entry velocity of the film onto the disc had only slight effect upon the heat transfer at small radii and almost no effect at larger radii. The effect of increasing disc speed was more pronounced, however, with the heat transfer coefficient varying almost with $\omega^{\frac{1}{2}}$. DORFMAN defined the Nusselt number of the flow as

$$Nu_c = \frac{h_c \delta}{k} = \frac{q \delta}{(T_o - T_s) k} \qquad 187$$

BRUIN (223) has considered equation 186 (less the vertical convection term) written for flow on the inner surface of a cone. The numerical results, obtained using the fully developed centrifugal model velocity profiles, indicate that the film may be considered in two distinct portions. The first portion corresponds to the developing temperature profile. As the fluid moves to increasing radii, a critical radius is reached where the temperature profile becomes fully developed. BRUIN'S results indicate that the critical radius is dependent upon the group $Pr(Re^2/Ta)_o^{2/3}$. If the value of this group is zero the critical radius is equal to the inlet radius. As the parameter $Pr(Re^2/Ta)_o^{2/3}$ increases, then the critical radius increases tending to the asymptote of some 1.12 times the inlet radius for values of $Pr(Re^2/Ta)_o^{2/3}$ greater than about 4. BRUIN gives expressions for the analytic determination of the film temperature profiles in the developing and developed regions.

WATTS (115) considered the co-current heating of a cold liquid flowing radially on one side of a rotating disc by a hot fluid flowing on the reverse side. The velocity and temperature profiles are considered to be fully developed and the energy equation is given as

$$\frac{d}{dr}\left(\rho c_p Q T_m\right) = -2\pi r k \left(\frac{dT}{dy}\right)_{y=o} \qquad 188$$

Equation 188 is in essence a simple radial balance between heat conducted from the disc surface and additional sensible film heat.

Employing the boundary conditions

$$y = \delta \qquad \frac{dT}{dy} = 0 \tag{189.1}$$

$$y = \delta \qquad T = T_s \tag{189.2}$$

$$y = 0 \qquad \frac{d^2T}{dy^2} = 0 \tag{189.3}$$

to determine the appropriate constants for a cubic temperature profile gives

$$\frac{T - T_o}{T_s - T_o} = \frac{3}{2}\left(\frac{y}{\delta}\right) - \frac{1}{2}\left(\frac{y}{\delta}\right)^3 \tag{189.4}$$

Notice that boundary condition 189.3 implies heating by conduction only. Defining a mean film temperature T_m as

$$T_m = \frac{\int_o^\delta (v_r T)\, dy}{\int_o^\delta v_r\, dy} \tag{190}$$

then equation 189.4 may be re-written as

$$\frac{T - T_o}{T_m - T_o} = \frac{40}{61}\left(3\left(\frac{y}{\delta}\right) - \left(\frac{y}{\delta}\right)^3\right) \tag{191}$$

when the centrifugal model velocity profiles are assumed in the integration of equation 190. The local heat transfer coefficient may be evaluated from equation 191 using the definition

$$h = \frac{k\left(\frac{dT}{dy}\right)_{y=o}}{T_m - T_o} \tag{192.1}$$

WATTS found that

$$Nu = \frac{h\delta}{k} = \frac{\delta}{k}\,\frac{q}{(T_m - T_o)} = \frac{120}{61} = 1.97 \tag{193.2}$$

Equation 193.2 is deduced for a film in which the centrifugal model describes the velocity profile and the temperature profile is described by a cubic equation. WATTS performed a numerical investigation of the energy equation 186 with the velocity profiles given by the centrifugal model and the temperature profile specified in terms of boundary

conditions only. The results indicate that the temperature profile requires a greater radius for full development with increasing flowrate and decreasing rotational speed.

WATTS developed an approximate turbulent model as follows. The heat flux is given by

$$q = -(k + \rho c_p \epsilon)\frac{dT}{dy} = -k\left(1 + \frac{A\epsilon}{\nu}\right)\frac{dT}{dy} \qquad 194.1$$

and the heat flux varies linearly with depth

$$\frac{q_r}{q_o} = 1 - \frac{y}{\delta} \qquad 194.2$$

A dimensionless temperature T^+ is defined as

$$T^+ = \frac{U^* k}{\nu q_o}(T - T_o) \qquad 194.3$$

when U^* is the friction velocity (see SECTION 2.1.1. earlier). Using equations 194.2 and 194.3, equation 194.1 becomes

$$\frac{dT^+}{dy^+} = \frac{1 - y^+/\delta^+}{1 + \frac{P_r \epsilon}{\nu}} \qquad 194.4$$

with y^+ and δ^+ as defined in SECTION 2.1.1.
Following the reasoning of the first model described, the heat transfer coefficient is given by

$$\frac{1}{h} = \frac{2\pi\nu}{U^* Re\, k}\int_o^{y^+} T^+ U^+ dy^+ \qquad 194.5$$

Equation 194.4 was integrated to give a temperature/depth profile which enables equation 194.5 to be integrated. REES (131) repeated WATTS' work and obtained similar results.

3.2.2. EXPERIMENTAL RESULTS

BROMLEY et al (224) investigated heat transfer to films on grooved discs. In these investigations either or both sides of the disc were machine grooved or scratched with glass-paper. The experimental study was primarily concerned with condensation and evaporation of liquid on the disc. It was found that the machined disc (on which the groove profile was shaped to give the optimum drainage due to surface tension forces) gave improved condensation heat transfer coefficients of up to 65%

greater than those of a smooth disc. Grooving the evaporation face of the disc gave only slight improvement (of the order of 13%) over those coefficients found for the smooth disc. In each case the glass papered discs gave some three quarters of the grooved discs' improvements.

BUTUZOV and RIFERT (225) have developed a simple theory to account for evaporation from the free film surface. The work of JONES (see 225) is erroneously quoted as giving the mean wavy film thickness as 0.83 of the smooth film thickness at the equivalent controlling parameters. KAPITSA gives the value of 0.93 for planar gravity films. However, the ratio 0.83 is employed here. Using the centrifugal model's result for film thickness this gives a wavy film thickness as

$$\delta_w = 0.65 \left(\frac{\nu Q}{\omega^2 r^2} \right)^{1/3} \qquad 195.1$$

Defining the heat transfer coefficient similar to equation 177.3, $\frac{k}{\delta_w}$, then

$$h_c = 1.54 \left(\frac{k^3 \omega^2 r^2}{\nu Q} \right)^{1/3} \qquad 195.2$$

Since the fluid is evaporating from the disc, Q is strictly equal to $Q_i - Q_e$ when Q_i is the feed to the disc and Q_e the evaporated portion of the film flow.

A thermal balance at radius r gives

$$\frac{dQ_e}{dr} = \frac{h\, 2\pi r \Delta T}{h_{fg} \rho} \qquad 195.3$$

Substituting for h from equation 195.2 and integrating equation 195.3 from r_i to r_o with the lower limit for Q_e set to zero gives an expression for the total evaporation from the disc. Equating this evaporation to a total heat balance, one obtains an expression for the average heat transfer coefficient as

$$\bar{h}_c = 1.54 \frac{Q_d}{\left[Q_i^{4/3} - (Q_i - Q_d)^{4/3} \right]} \frac{r_o^{8/3} - r_i^{8/3}}{r_o^2 - r_i^2} \left(\frac{k^3 \omega^2}{\nu} \right)^{1/3} \qquad 195.4$$

or

$$\frac{\bar{h}_d r_i}{k} = 1.54\, \Phi_1\, \Phi_2 \left(\frac{Ta^2}{Re} \right)_i^{1/3} \qquad 195.5$$

when the suffix i denotes conditions at the inlet and the functions Φ_1, and Φ_2 are given by

$$\Phi_1 = \left(\frac{Q_e}{Q_i}\right) \Big/ \left(1 - \left(1 - \frac{Q_e}{Q_i}\right)^{4/3}\right) \qquad 195.6$$

$$\Phi_2 = 1 - \left(\frac{r_i}{r_o}\right)^{8/3} \Big/ 1 - \left(\frac{r_i}{r_o}\right)^{2} \qquad 195.7$$

Notice that equation 195.5 is only valid for $(Re^2/Ta) < 1$, wherever this may occur.

BUTUZOV and RIFERT found (work reported in 226) good agreement to equation 195.4 in that area where the liquid evaporated without significant vapour bubbling. BUTUZOV and RIFERT (148) also found that the influence of feed flow rate was small and that the data from the evaporation of 8% NaCl solutions for $\omega >$ 20 rad/s could be correlated approximately by

$$\frac{\bar{h} r_o}{k} = 0.256 \left\{\frac{\omega r_o^2}{\nu}\right\}^{0.64} (Pr)^{0.35} \qquad 196$$

Notice that the effect of ω upon $\bar{h}$ is approximately as given by equation 195.4, which also agrees to the work of HICKMAN (227).

GUBENKO and LEONCHIK (228) have considered the effect of liquid evaporation upon the bulk exit temperature of the liquid leaving a heated disc. Unfortunately the stated correlation is not dimensionally consistent and no preferred units are stated.

CLARKE and BROMLEY (229) investigated experimentally the evaporation of sea water on the plates of a multiple effect rotary evaporator.. The average overall heat transfer coefficient was reported to be dependent on $\omega^{\frac{2}{3}} r_o^{\frac{2}{3}} Q^{-\frac{1}{3}}$. Notice that this dependency is exactly as predicted in the above equations.

RIFERT (149) appears to have attempted to extend into turbulent flow the analysis of BUTUZOV and RIFERT given above. The standard U.V.P. analysis for pipe flow appears to have been used and some limited agreement with experimental data seems to be found. However, this work is as yet untranslated and full appraisal is not possible.

3.3. THEORETICAL

3.3.1. GENERAL

The hydrodynamic investigation has shown that the film may be considered in at least three definite sections, viz. an entry region, a developed region in which Coriolis forces are important and a developed region in which the simple centrifugal model may be applied. In addition the film may become turbulent at a sufficiently large value of (Re Ta) and the film free surface may or may not exhibit waves.

To expect any heat transfer analysis to be generally applicable in all regions of flow must be considered over optimistic. Instead, this work will limit itself to the full study, and implementation, of a heat transfer model to that area where the centrifugal model may be considered to apply. In addition the hydrodynamics of the flow will be considered to be established directly at entry to the disc and that the fluid properties are all independent of temperature. These latter two assumptions are obviously major and a desirable future project would be an investigation into the significance of these assumptions. The inclusion of a developing fluid velocity distribution and temperature (and hence positional) dependence of physical properties would make the basic model developed in the next section soluble only by iterative numerical or analogue techniques. However, some indication of the effects of the assumptions may be made. The work of SECTION 2.1.1:F shows that the hydrodynamic entrance length for isothermal gravity flows is quite small, usually less than 20 film thicknesses. As regards variable physical properties, the most important will be viscosity. BIRD et al (230) show that the simple NUSSELT model for film flow of a viscous oil gives the expression for film thickness as

$$\delta = \left(\frac{A Q' \nu_0}{g} \right)^{1/3} \qquad 197.1$$

when $$A = \left[\left(\frac{1}{\alpha} - \frac{2}{\alpha^2} + \frac{2}{\alpha^3} \right) \exp(\alpha) - \frac{2}{\alpha^3} \right]^{-1} \qquad 197.2$$

and α is defined from the viscosity variation

$$\frac{\nu}{\nu_0} = \exp\left(-\alpha \frac{y}{\delta} \right) \qquad 197.3$$

For isothermal flow of a non temperature dependent material ($\alpha = 0$)

BIRD et al show that equation 197.1 reduces to the basic equation 4.2 derived earlier. Equation 197.3 is equivalent to a linear temperature profile acting upon a fluid in which viscosity varies exponentionally with temperature. For water from 20°C to 100°C α is approximately 1.26 which means that compared to an isothermal water film at 20°C, an isothermal film at 100°C is 28% of the thickness (equation 4.2), a film which has a linear temperature is 0.38 as thick (equation 197.1) and a film at the mean temperature (60°C) is some 0.55 as thick. Thus assuming an isothermal film flow of an average temperature will give a film thickness some 30% in error if the true thickness is best represented by a linear temperature distribution. It is obvious that the assumption of constant physical properties will be a very major assumption.

3.3.2. LAMINAR FLOW HEAT TRANSFER

The basic model considered is that used by SPARROW and GREGG (209) in their condensation work, viz.

$$v_r C_p \rho \frac{\partial T}{\partial r} = k \frac{\partial^2 T}{\partial y^2} \qquad 175$$

To make the solution more general equation 175 is first normalised by using the expressions

$$Y = \frac{y}{\delta} \qquad T^* = \frac{T_o - T}{T_o - T_i}$$

$$R = \frac{r}{r_i}$$

when T_o is the disc solid surface temperature and T_i is the fluid temperature at entry to the disc (radius r_i). Employing the velocity profile appropriate to the centrifugal model (equation 60.1) and using the above normalisations, equation 175 may be re-written as

$$\frac{\rho C_p}{k} \frac{\omega^2 r}{\nu} \frac{\delta^4}{r_i} \left(Y - \frac{Y^2}{2}\right) \frac{\partial T^*}{\partial R} = \frac{\partial^2 T^*}{\partial Y^2} \qquad 198$$

Substituting from equation 61 for δ and rearranging the groups equation 198 becomes

$$\frac{1}{2}\left(\frac{3}{2\pi}\right)^{4/3}\left[\Pi\left(\frac{Re^2}{Ta}\right)_i^{2/3}\right]\left(\frac{1}{R}\right)^{5/3}(2Y - Y^2)\frac{\partial T^*}{\partial R} = \frac{\partial^2 T^*}{\partial Y^2} \qquad 199$$

The boundary conditions appropriate to equation 199 are (normalised form in brackets)

$$y = 0 \ (Y = 0) \ , \ T = T_o \ (T^* = 0) \text{ for all } r \ (R) \qquad 200.1$$

$$y = \delta \ (Y = 1) \ , \frac{dT}{dy} = 0 \ (\frac{dT^*}{dY} = 0) \text{ for all } r \ (R) \qquad 200.2$$

$$r = r_i (R = 1), \quad T = T_i (T^* = 1) \text{ for all } y \ (Y) \qquad 200.3$$

Thus equation 199 defines the temperature distribution in R and Y with boundary conditions defined for Y = 0, Y = 1 and R = 1.

Define a heat transfer coefficient as

$$h = \frac{-k\left(\frac{dT}{dy}\right)_{y=o}}{T_s - T_m} \qquad 201.1$$

when

$$T_m = \frac{\int_o^\delta (Tv_r)dy}{\int_o^\delta v_r dy} = \frac{2\pi r}{Q}\int_o^\delta (Tv_r)\,dy \qquad 201.2$$

In terms of the normalising variables equation 201.1 becomes

$$h = \frac{k}{\delta}\left(\frac{T_s - T_i}{T_s - T_m}\right)\left(\frac{dT^*}{dy}\right)_{y=o} \qquad 202.1$$

or

$$\frac{h\delta}{k} = \left(\frac{T_s - T_i}{T_s - T_m}\right)\left(\frac{dT^*}{dy}\right)_{y=o} \qquad 202.2$$

Define a dimensionless velocity U^* as

$$U^* = \frac{U}{\overline{U}} = 3\left(y - \frac{y^2}{2}\right) \qquad 202.3$$

then it is possible to show that

$$\int_o^1 U^* T^* \, dy = \frac{T_o - T_m}{T_o - T_i} \qquad 202.4$$

so from equations 202.4 and 202.2

$$Nu = \frac{h\delta}{k} = \left(3\int_o^1 \left(y - \frac{y^2}{2}\right) T^* dy\right)^{-1} \left(\frac{dT^*}{dy}\right)_{y=o} \qquad 202.5$$

Thus solution of equation 199 supplies T^* as a function of Y and R. Further integration of T^* with Y (according to equation 202.5) and evaluation of the gradient at Y = 0 enables the local Nusselt number to be found.

The only variable parameter is the group $(Pr(Re^2/Ta)_i^{\frac{2}{3}})$. APPENDIX I details the solution method employed which was use of the Thomas algorithm on a Crank-Nicholson representation of equation 199. Solution was made for a range of the variable parameter from 1 to 10,000 and a Crank-Nicholson parameter (r step/(Y step)^2) of 0.25. In general the IBM 360 computer required 100 seconds of CPU time to progress 1 cm (with the film divided into 50 vertical divisions). The program used is detailed in SECTION G: PROGRAM HEAT. The resultant output from this program is a temperature profile for any radius parameter value, and the integrated mean temperature and NUSSELT number. TABLES 6, 7, 8 and 9 give the radius, R (as tabular entries) at which for any given value of $(Pr.(Re^2/Ta)_i^{\frac{2}{3}})$(head of columns) the specified value of T_m^* is reached. T_m^* is defined as

$$T_m^* = \int_o^1 U^* T^* \, dY = \frac{T_o - T_m}{T_o - T_i} \qquad 203$$

It will be seen that at entry to the disc (R = 1), $T_m^* = 1$. As the fluid heats and T_m tends to T_o, then T_m^* tends to zero. Thus regarding TABLE 6, for a parameter value of 5, $T_m^* = 0.5$ at a radius of 1.17 r_i and the film has heated to within 99% of the disc surface temperature by a radius of 1.80 r_i.

TABLES 10, 11, 12 and 13 present the local Nusselt number as entries with the parameter $(Pr(Re^2/Ta)_i^{\frac{2}{3}})$ as column headings and the radius as the independent variables. Regarding TABLE 10 and a parameter value of 5, the Nusselt number has fully developed by a radius of 1.1 r_i.

Careful study of the program output reveals that increasing the variable parameter causes the local Nusselt number at any radius to increase and the radius at which a developed temperature and Nusselt number exists increases. In addition notice that the developed Nusselt number is 1.89, quite close to that analytically given by WATTS for a cubic temperature profile (equation 193.2).

Note that the model makes the major assumptions of no free surface heat loss, Re^2/Ta less than 1 everywhere and no evaporative loss along with the assumptions made by the hydrodynamic model employed.

TABLE 6: NUMERICAL RESULTS

	$Pr\left(Re^2/Ta\right)_i^{2/3}$									
T \ P	1·0	2·0	3·0	4·0	5·0	6·0	7·0	8·0	9·0	10·0
0.9	1·01	1·01	1·01	1·02	1·02	1·02	1·02	1·03	1·03	1·03
0.8	1·01	1·02	1·03	1·04	1·04	1·06	1·06	1·07	1·08	1·09
0.7	1·02	1·03	1·05	1·06	1·08	1·10	1·11	1·13	1·14	1·16
0.6	1·02	1·05	1·08	1·10	1·12	1·14	1·16	1·17	1·21	1·22
0.5	1·03	1·06	1·10	1·14	1·17	1·20	1·22	1·25	1·28	1·30
0.4	1·05	1·10	1·14	1·18	1·22	1·26	1·30	1·33	1·36	1·39
0.3	1·07	1·13	1·18	1·24	1·28	1·34	1·38	1·42	1·46	1·49
0.2	1·09	1·17	1·24	1·31	1·37	1·42	1·48	1·52	1·57	1·62
0.1	1·12	1·23	1·32	1·40	1·48	1·56	1·62	1·68	1·74	1·80
0.01	1·24	1·42	1·56	1·68	1·80	1·90	2·02	2·10	2·16	2·26

entries are R^*

TABLE 7 NUMERICAL RESULTS

$Pr\left(Re^2/Ta\right)_i^{2/3}$

T \ P	10	20	30	40	50	60	70	80	90	100
0.9	1·03	1·06	1·09	1·12	1·14	1·17	1·19	1·22	1·24	1·26
0.8	1·09	1·16	1·24	1·30	1·35	1·41	1·46	1·50	1·55	1·60
0.7	1·16	1·28	1·39	1·48	1·57	1·64	1·72	1·78	1·84	1·91
0.6	1·22	1·40	1·54	1·66	1·78	1·87	1·96	2·05	2·12	2·20
0.5	1·30	1·52	1·70	1·85	1·98	2·10	2·20	2·30	2·40	2·48
0.4	1·39	1·66	1·86	2·04	2·20	2·32	2·45	2·56	2·67	2·77
0.3	1·49	1·80	2·04	2·24	2·42	2·58	2·72	2·84	2·96	3·08
0.2	1·62	1·98	2·26	2·50	2·69	2·87	3·03	3·18	3·30	3·44
0.1	1·80	2·24	2·56	2·84	3·06	3·28	3·46	3·62	3·78	3·94
0.01	2·26	2·88	3·32	3·66	3·96	4·24	4·50	4·74	4·92	5·12

entries are R

TABLE 8 NUMERICAL RESULTS

T \ P	$Pr\left(Re^2/Ta\right)_i^{2/3}$									
	100	200	300	400	500	600	700	800	900	1000
0.9	1·26	1·46	1·62	1·74	1·88	1·98	2·08	2·18	2·26	2·34
0.8	1·60	1·96	2·24	2·46	2·66	2·82	2·98	3·14	3·26	3·40
0.7	1·91	2·39	2·75	3·04	3·30	3·52	3·72	3·92	4·10	4·26
0.6	2·20	2·78	3·22	3·58	3·88	4·15	4·40	4·62	4·82	5·00
0.5	2·48	3·17	3·67	4·08	4·42	4·74	5·02	5·26	5·50	5·70
0.4	2·77	3·54	4·11	4·58	4·96	5·32	5·64	5·92	6·18	6·42
0.3	3·08	3·96	4·59	5·12	5·56	5·94	6·30	6·62	6·90	7·18
0.2	3·44	4·44	5·15	5·74	6·24	6·66	7·06	7·44	7·76	8·06
0.1	3·94	5·08	5·90	6·58	7·16	7·66	8·12	8·54	8·92	9·24
0.01	5·12	6·64	7·74	8·60	9·34	10·02	10·62	11·16	11·64	12·03

entries are R

TABLE 9 NUMERICAL RESULTS

	$Pr\left(Re^2/Ta\right)_i^{2/3}$									
T \ P	1000	2000	3000	4000	5000	6000	7000	8000	9000	10000
0.9	2·34	2·92	3·34	3·68	3·98	4·24	4·44	4·66	4·84	5·00
0.8	3·40	4·34	5·02	5·56	6·02	6·44	6·78	7·14	7·44	7·72
0.7	4.26	5·48	6·36	7·06	7·66	8·18	8·66	9·08	9·48	9·86
0.6	5·00	6·46	7·52	8·36	9·08	9·70	10·28	10·78	11·26	11·70
0.5	5·70	7·38	8·58	9·56	10·38	11·12	11·76	12·36	12·92	13·42
0.4	6·42	8·30	9·66	10·76	11·68	12·52	13·26	13·92	15·54	15·12
0.3	7·18	9·30	10·80	12·04	13·08	14·00	14·84	15·60	16·28	16·96
0.2	8·06	10·44	12·14	13·52	14·70	15·74	16·68	17·54	18·34	19·06
0.1	9·24	12·00	13·96	15·54	16·90	18·10	19·18	22·14	21·06	21·92
0.01	12·08	15·66	18·24	20·30	22·08	23·64	25·06	26·34	27·54	28·62

entries are R

TABLE 10 NUMERICAL RESULTS

R \ P	$Pr(Re^2/Ta)_i^{2/3}$									
	1	2	3	4	5	6	7	8	9	10
1·02	1·92	2·10	2·28	2·45	2·60	2·73	2·87	2·99	3·09	3·18
1·1	1·89	1·89	1·89	1·89	1·91	1·93	2·0	2·02	2·06	2·1
1·2	1·89	1·89	1·89	1·89	1·89	1·89	1·90	1·90	1·91	1·92
1·3	1·89	1·89	1·89	1·89	1·89	1·89	1·89	1·89	1·89	1·90
1·4	1·89	1·89	1·89	1·89	1·89	1·89	1·89	1·89	1·89	1·90
1·5	1·89	1·89	1·89	1·89	1·89	1·89	1·89	1·89	1·89	1·89
1·6	1·89	1·89	1·89	1·89	1·89	1·89	1·89	1·89	1·89	1·89
1·8	1·89	1·89	1·89	1·89	1·89	1·89	1·89	1·89	1·89	1·89
2·0	1·89	1·89	1·89	1·89	1·89	1·89	1·89	1·89	1·89	1·89
3·0	1·89	1·89	1·89	1·89	1·89	1·89	1·89	1·89	1·89	1·89

entries are Nusselt numbers

TABLE 11 NUMERICAL RESULTS

	$Pr(Re^2/Ta)_i^{2/3}$									
R \ P	10	20	30	40	50	60	70	80	90	100
1·02	3·19	3·93	4·47	4·90	5·26	5·58	5·87	6·01	6·37	6·59
1·20	1·92	2·07	2·18	2·39	2·53	2·65	2·76	2·87	2·96	3·06
1·40	1·89	1·91	1·89	2·02	2·10	2·17	2·24	2·31	2·37	2·43
1·60	1·89	1·89	1·89	1·92	1·95	1·99	2·03	2·07	2·11	2·16
1·80	1·89	1·89	1·89	1·90	1·90	1·91	1·94	1·96	1·98	2·01
2·0	1·89	1·89	1·89	1·89	1·89	1·90	1·90	1·91	1·92	1·94
3·0	1·89	1·89	1·89	1·89	1·89	1·89	1·89	1·89	1·89	1·89
4.0	1·89	1·89	1·89	1·89	1·89	1·89	1·89	1·89	1·89	1·89
5·0	1·89	1·89	1·89	1·89	1·89	1·89	1·89	1·89	1·89	1·89
6·0	1·89	1·89	1·89	1·89	1·89	1·89	1·89	1·89	1·89	1·89

entries are Nusselt numbers

TABLE 12 NUMERICAL RESULTS

R \ P	$Pr(Re^2/Ta)^{2/3}$									
	100	200	300	400	500	600	700	800	900	1000
1·02	6·59	8·28	9·45	10·38	11·16	11·82	12·41	12·94	13·40	13·84
1·24	2·96	3·52	3·99	4·37	4·69	4·97	5·22	5·46	5·67	5·87
1·50	2·27	2·70	3·02	3·29	3·52	3·72	3·90	4·06	4·22	4·37
1·76	2·03	2·32	2·57	2·77	2·96	3·11	3·26	3·39	3·52	3·63
2·0	1·94	2·13	2·31	2·48	2·63	2·76	2·88	3·00	3·10	3·20
4·0	1·89	1·89	1·89	1·90	1·90	1·92	1·93	1·95	1·98	2·00
6·0	1·89	1·89	1·89	1·89	1·89	1·89	1·89	1·89	1·89	1·89
8·0	1·89	1·89	1·89	1·89	1·89	1·89	1·89	1·89	1·89	1·89
10·0	1·89	1·89	1·89	1·89	1·89	1·89	1·89	1·89	1·89	1·89
12·0	1·89	1·89	1·89	1·89	1·89	1·89	1·89	1·89	1·89	1·89

entries are Nusselt numbers

TABLE 13 NUMERICAL RESULTS

R \ P	$Pr(Re^2/Ta)^{2/3}$									
	1000	2000	3000	4000	5000	6000	7000	8000	9000	10000
1·02	13·84	16·64	18·34	20·14	22·36	24·94	27·74	30·61	33·47	36·26
1·20	6·30	7·90	9·02	9·91	10·65	11·29	11·86	12·37	12·83	13·25
1·40	4·80	6·00	6·84	7·51	8·08	8·58	8·84	9·43	9·80	10.14
1·60	4.04	5·03	5·72	6·28	6·76	7·17	7·55	7·89	8·20	8·12
1·80	3·55	4·41	5·00	5·48	5·89	6·26	6·58	6·88	7·15	7·40
2·0	3·20	3·96	4.49	4·91	5·27	5·59	5·88	6·14	6·39	6·61
6.0	1·89	1·92	2·00	2·09	2·18	2·27	2·34	2·43	2·50	2·56
10.0	1·89	1·89	1·89	1·89	1·89	1·90	1·91	1·93	1·94	1·96
20.0	1·89	1·89	1·89	1·89	1·89	1·89	1·89	1·89	1·89	1·89
30.0	1·89	1·89	1·89	1·89	1·89	1·89	1·89	1·89	1·89	1·89

entries are Nusselt numbers

3.4. EQUIPMENT

3.4.1. GENERAL

As was mentioned in SECTION 2.5.1. the design work for the heat transfer equipment was conducted in parallel with the hydrodynamic design. One of the initial decisions to be made which affected both designs was the selection of a heating method and the method by which the heat transfer coefficients were to be measured.

The heating methods investigated were electrical heating and steam heating. Electrical heating has several obvious advantages over steam heating, viz. accurate and convenient power measurements, choice of constant flux or constant surface temperature conditions and flexible and relatively simple arrangements are possible to bring the supply to the disc. The electrical systems studied were

(a) surface plated heaters
(b) embedded wire heaters
and (c) infra-red emitters situated beneath the plate.

In the first case the possibility was considered of plating a resistance metal film onto a non-conducting substrate subsequently using the plating as a heating resistance. Major objections to this idea included

1. the deposition method of the plating
2. the thinness of the plating required and hence the mechanical weakness
3. effective sealing of the electrical paths ring to ring (the heating surface was visualised as either a collection of annular rings of constant thickness per ring or a spiral band of varying thickness) and ring/fluid/ring.

and 4. choice of a suitable resistance metal.

The major objections to an embedded wire scheme were

1. effective wire/wire insulation
2. machining of insulant plate
3. effective thermal contact of wires/top plate

and 4. method of smoothing of the heat flux from individual wires into a uniform flux.

In addition in each case the transfer of electrical power from a stationary supply to the rotating disc presents a major problem. Sizing calculations showed that a flux of the order of 20 kW would be required and cost, size and supply of slip rings to suit this load proved a serious problem. In addition if a broken liquid film occurred, serious overheating or even 'burn-out' could occur with electrical heating, as was found by RICHARDSON (195). Direct electrical surface heating was therefore discarded.

The major problem with infra-red under disc heaters lay in their inability to give an accurately defined radial distribution of heat flux and the little previous use of such heaters. Considerable development work would be required to implement such a technique.

The heating method chosen, therefore, was steam heating. Although this enables (at least in theory) only an isothermal plate surface to be studied at least the use of steam will be in keeping with its probable use as the heating medium in future commercial developments.

The use of steam as the heating medium requires use of an accurate condensate collection method and dryness measurement to ascertain the heat flux. These methods will be investigated later.

The remaining variables to be measured or computed required for the calculation of heat transfer coefficients are the film mean and disc surface temperature.

Dealing first with the film mean temperature it was realised that due to the extreme thinness of the film any probe introduced into the film would cause severe turbulence and hence automatically invalidate the natural heat transfer process. In addition, damage to the disc surface may be caused. Several ideas were considered in which the fluid was scooped clean from the surface but owing to the slight fluctuations in plate level the devices would become unreasonably complicated. The most realistic method of evaluating the mean film temperature was finally decided to be an indirect method. From the heat flux at that radius and from the heat fluxes to the preceding film the total cumulative heating of the film is known. If the fluid temperature at inlet and the flowrate of the fluid are known, a simple heat balance will give the mean film temperature at the radius under consideration.

The surface temperature could be inferred in a similar manner if desired. If the heat flux is known and assumptions made of the plate thickness, thermal conductivity and steam condensation coefficient then by

normal heat conduction calculations the disc surface temperature could be calculated. However, the assumptions to be made are more unreasonable than those used in the mean film temperature and an absolute measurement of surface temperature is more desirable. The selection and implementation of the technique chosen is discussed below.

3.4.2. HEAT TRANSFER EQUIPMENT DESIGN

A: DISC SURFACE TEMPERATURE MEASUREMENT

Probes which reach the surface from above (SASAJI (231)) were rejected due to the impracticallity of touching the fluctuating, rotating surface without disturbing the film. Deposited resistance films (WATSON (232)) were rejected due to the manufacturing difficulties. An elegant method developed by BENDERSKY (233) was considered. This method consists of threading a nickel wire covered with an oxide layer through a stainless steel tube. The assembly is then drawn to compress the tube onto the wire. By coating the end of the tube with nickel a neat thermocouple is produced. The method was rejected due to the length of unbroken oxide film required to inlay the thermocouple in the disc at appreciable radii. CHAND and ROSSON (171) have also used this technique. Thermistors half buried in the disc and then ground flat were rejected for availability reasons.

The method finally chosen was a variant of the last two techniques. Trials with a small metal plate showed the method to be practical. The disc top surface was machined with six radial grooves (to correspond to the condensate measurement radii see SECTIONS E/D later) of radial lengths 4, 6, 8, 10, 12 and 14 cm. At the end of each groove a short (some 2 cm) circumferential arc was machined. The grooves are visible in PHOTOGRAPHS 7b and 8a. Notice from PHOTOGRAPH 8a that the radial groove consists of a basic groove 3 mm broad by 0.8 mm deep with, at the centre of the groove base, a further groove 1.5 mm wide by 0.8 mm deep (PHOTOGRAPH 8 shows two circumferential arcs. By error the initial arc was wrongly positioned and had to be re-machined). The grooves originate from a 1" diameter centre boss and from the detail in FIGURE 38 it can be seen that each groove ending is radiused.

The basic thermocouple is formed from a length of copper-constantan wire double insulated with glass cloth. The wire diameters are some 170μm bore, 300μm with a single insulation and some 0.7 mm overall. The preparation of the thermocouples was as follows. The outer insulation

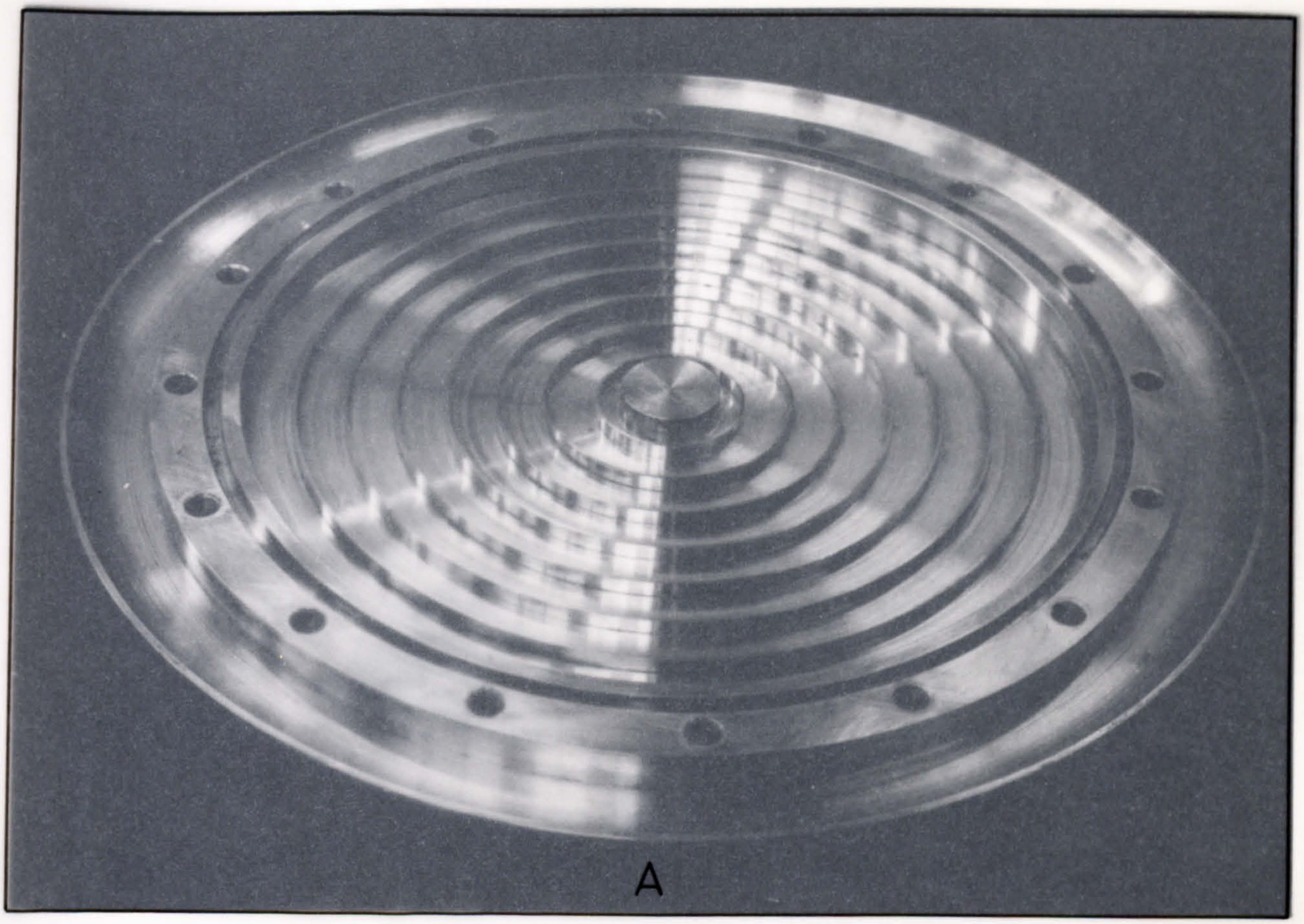

A

PHOTOGRAPH 7

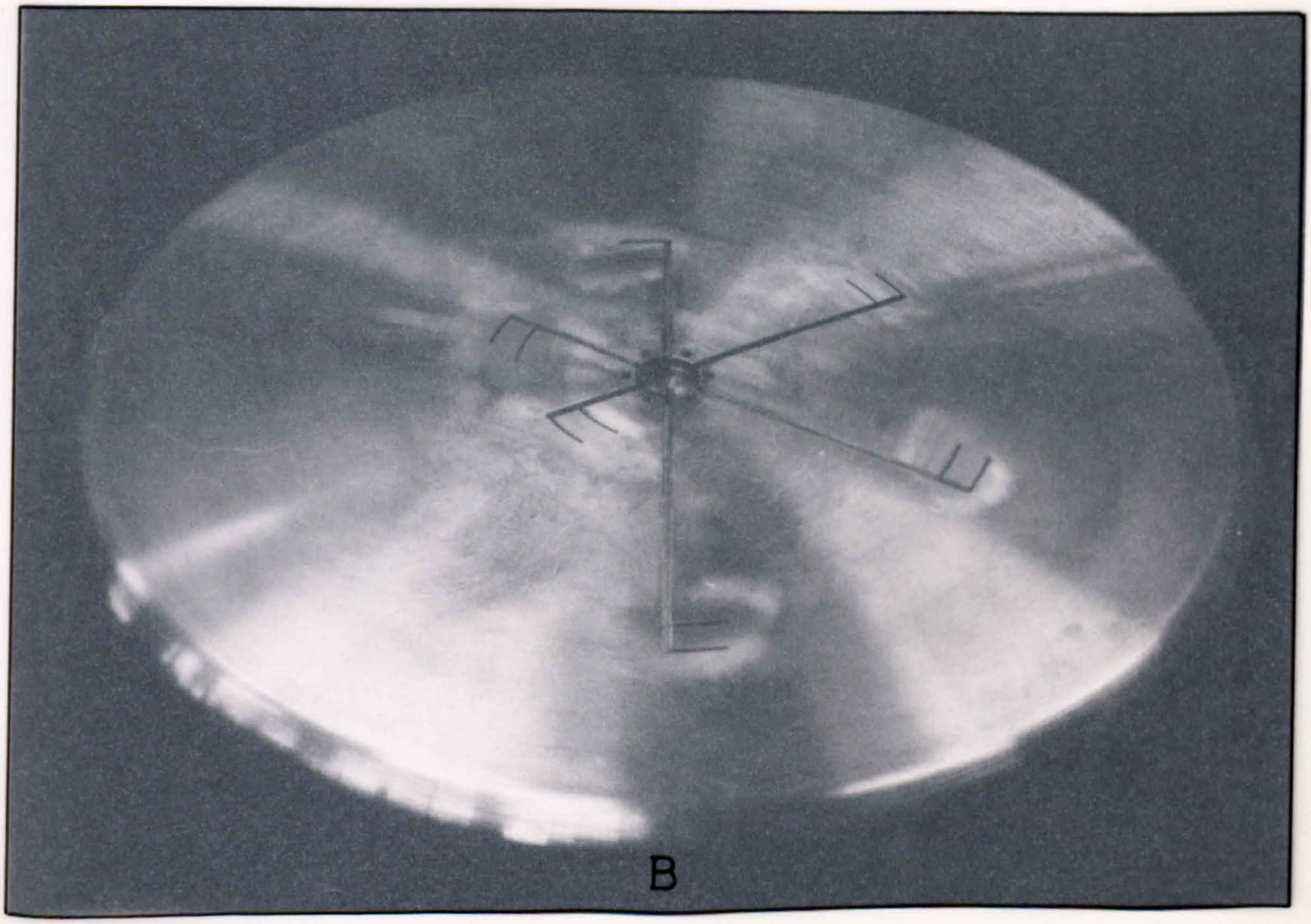

B

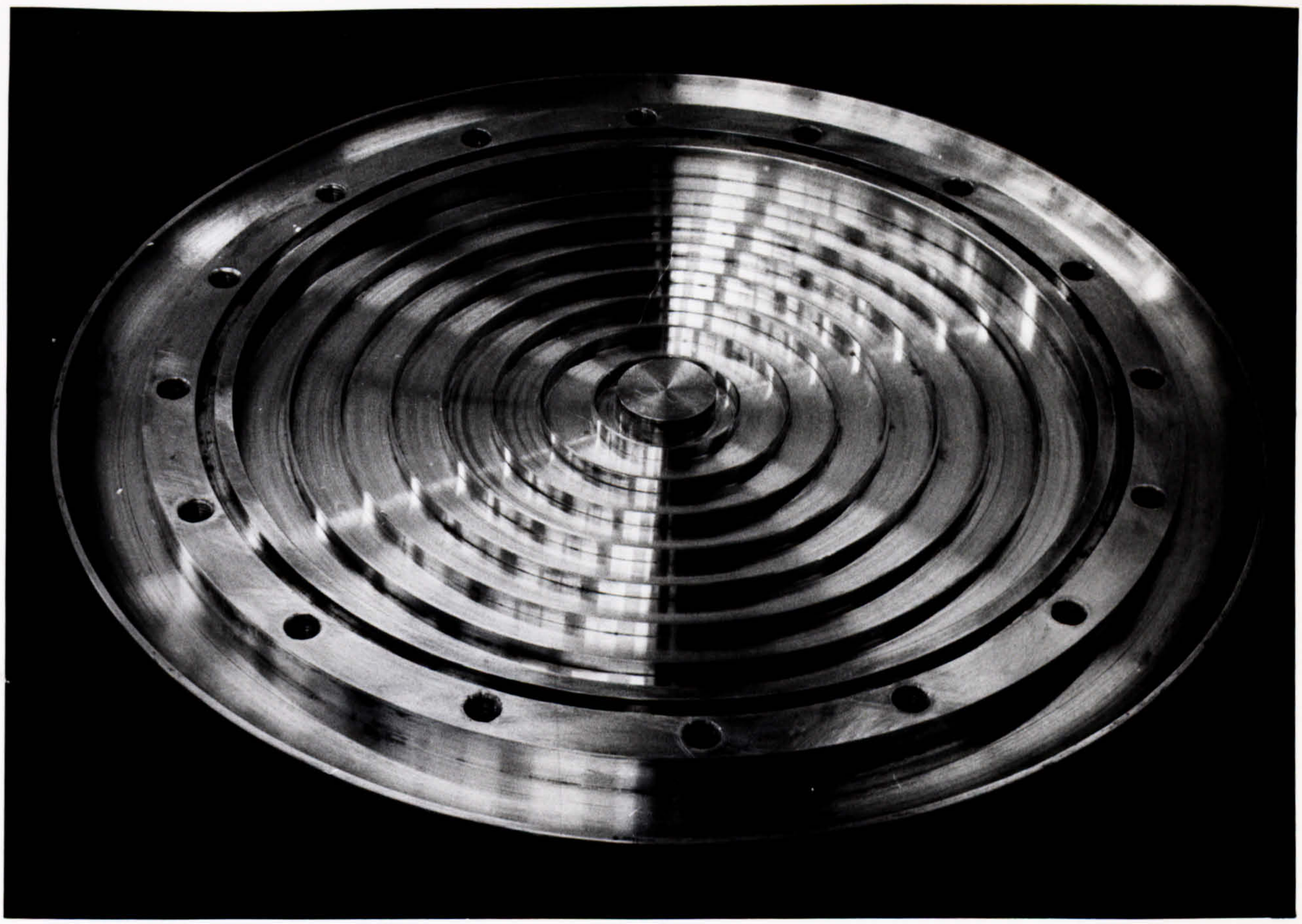

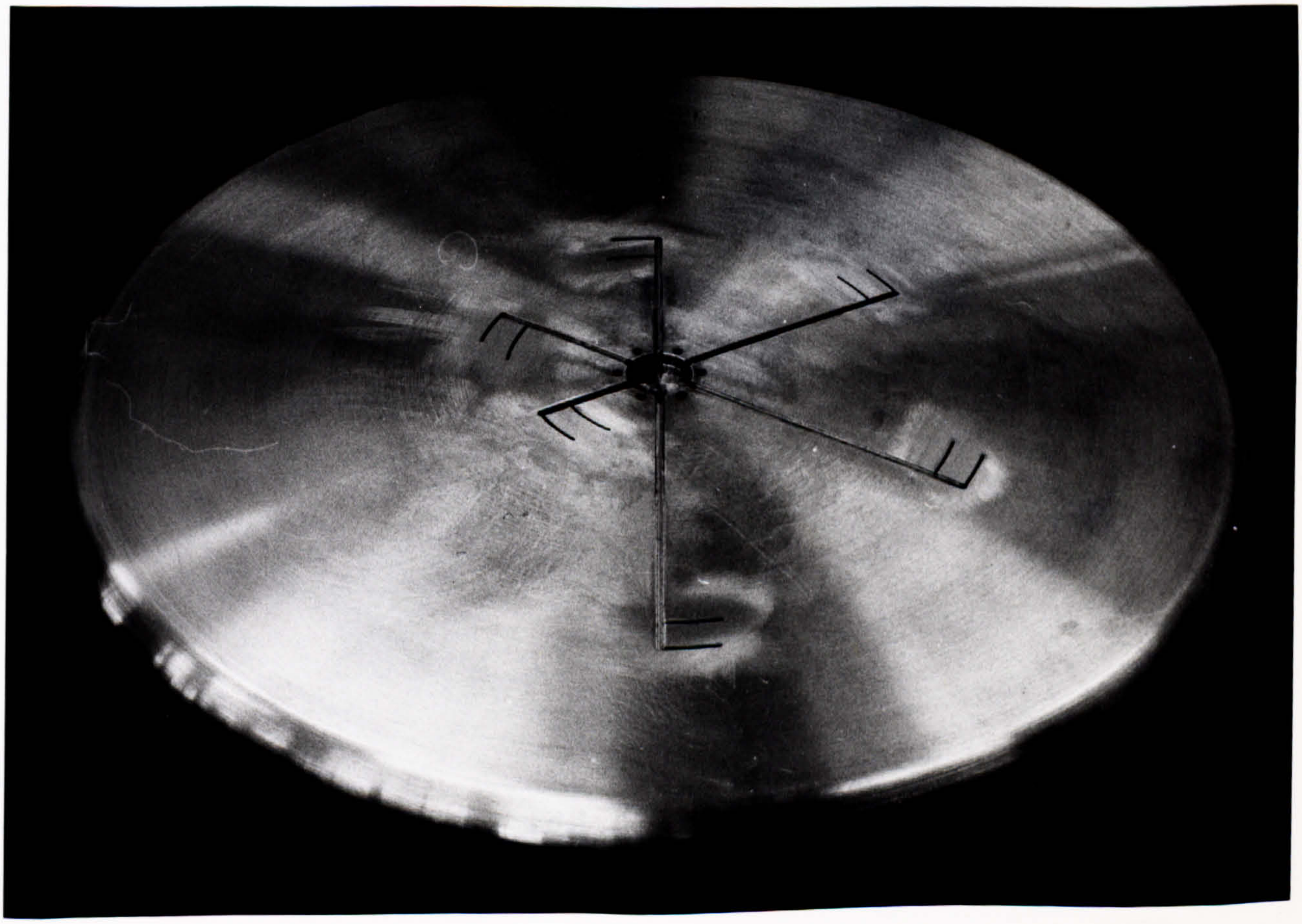

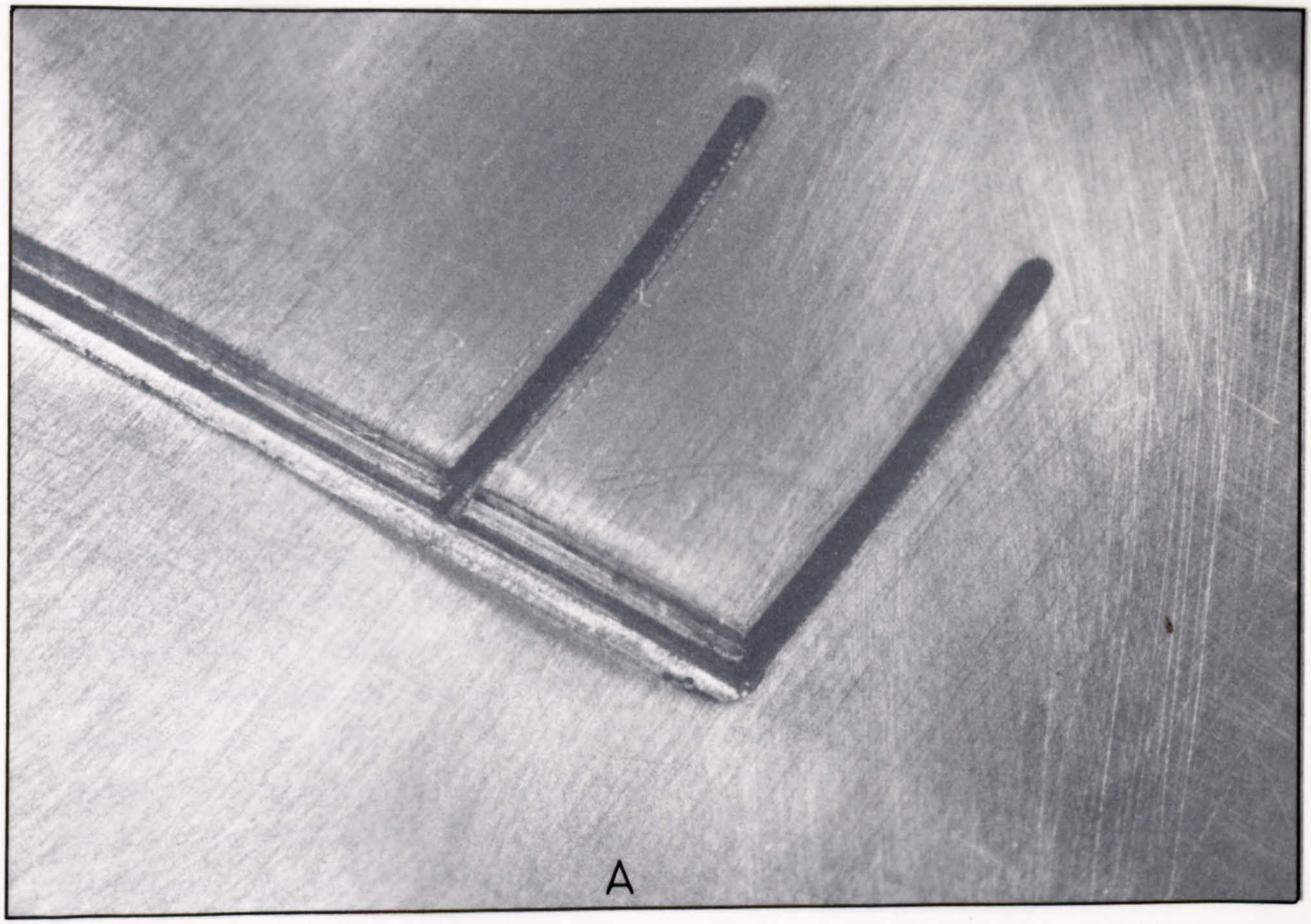

PHOTOGRAPH 8

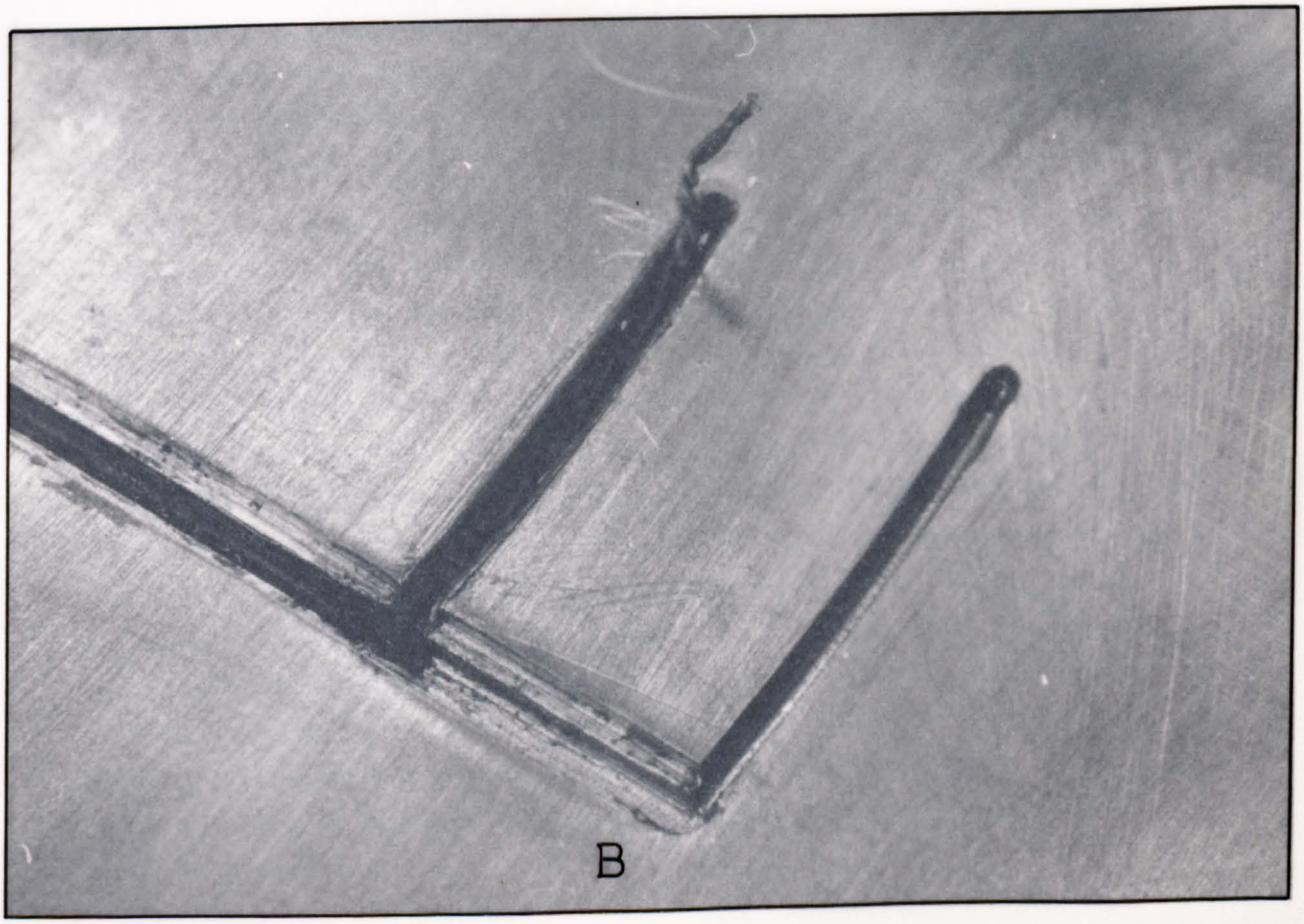

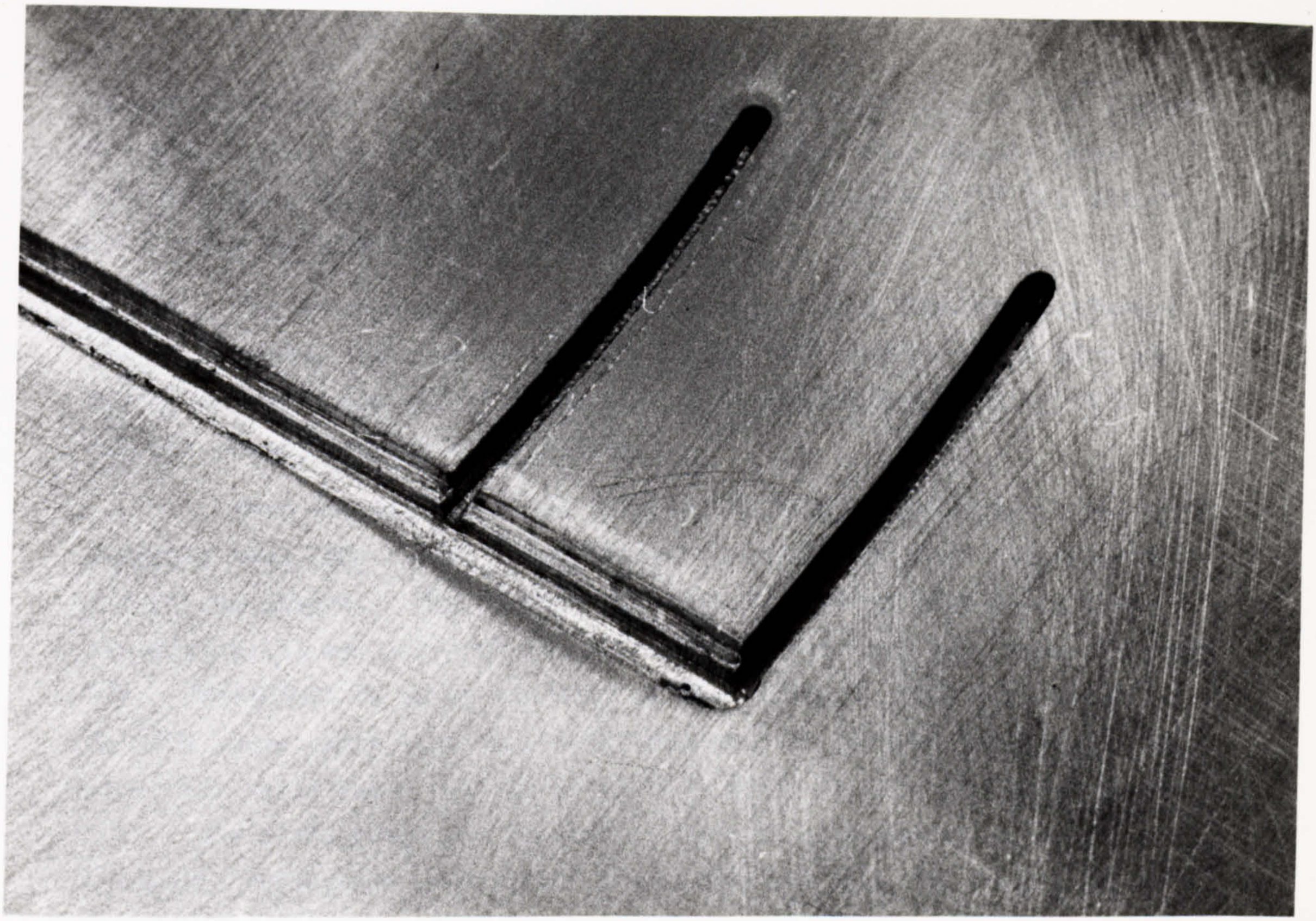

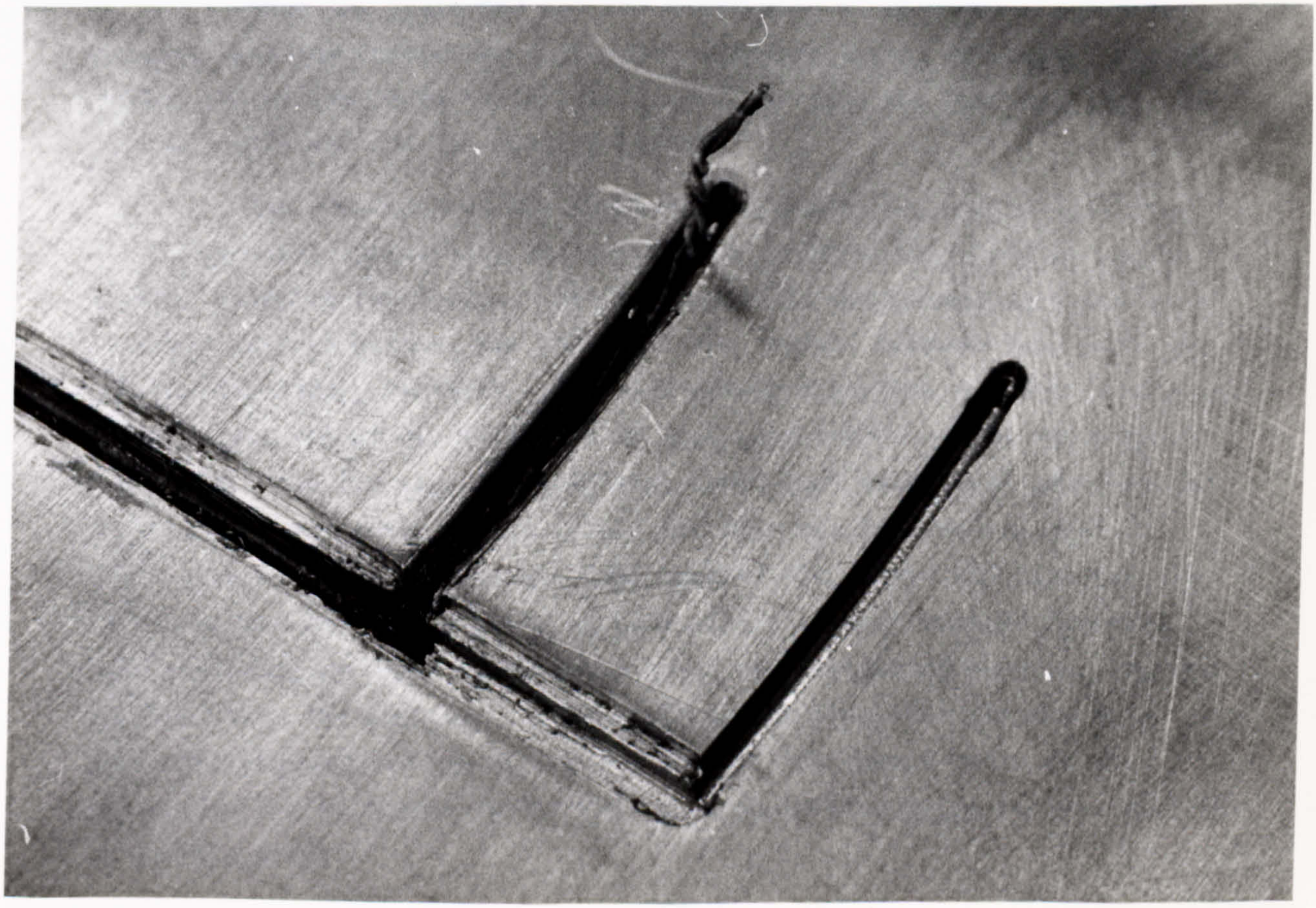

was carefully unwound for some 4 cm at one end taking care not to damage the single wire insulation. The two loose wires thus exposed were twisted into a loose spiral, degreased in acetone and tested for insulation using an AVOMETER (model 8 Mk II).

The thermocouple grooves in the plate were thoroughly cleaned by wire brushing followed by probing with a fine needle. The disc was then washed in soapy water, DECON and water and swabbed with acetone with air drying between each process.

When all six wires and grooves had been prepared the wires were carefully bent into shape, using tweezers, and forced into the deepest part of the groove. The twisted separate wires were laid along the circumferential arc and bent so as to stand clear some 3 mm from the very end. PHOTOGRAPH 8b shows the wire at this stage. Next a batch of ARALDITE epoxy resin type CY 219 and hardener HY 219 were prepared. When mixed this resin has a very low viscosity which ideally suited it to the task. The mixed resin was applied in turn to each groove so as to thoroughly impregnate each wires' insulation and fill the deeper groove to a smooth contour. Care was taken to ensure that no air was trapped and that the circumferential arc was not overfilled with resin.

When the resin had set the continuity of wire was checked for breakage and the insulation (wire-wire and wire-plate) checked. At this stage, two of the leads failed the insulation test and were removed, the grooves recleaned and new wires inserted.

The remainder of the thermocouple groove now had to be filled with a material approaching the properties of brass but could be applied without damaging the resin. Several materials were tried in trial runs on other grooved plates, viz. electricians solder, bismuth-lead eutectic, LOY plastic metal, araldite and araldite/copper powder, and dental amalgam. Electricians solder was difficult to apply and caused slight charring of the plastic and the plastic materials showed poor mechanical adhesion and resistance to expansion tests (since the disc was required to heat to 100°C several times the thermal expansion of the filler had to match that of the parent brass as closely as possible). Dental amalgam appeared very satisfactory until the heating tests were conducted when mercury was expelled from the amalgam. It was first felt that this was due to incorrect mixing/handling of the amalgam but subsequent tests at the University Dental School showed that amalgam several <u>years</u> old was unstable to boiling water.

The most successful material was the bismuth-lead (44.5 Pb, 55.5 Bi) eutectic prepared in the Department of Metallurgy. PHOTOGRAPH 9a shows a microphotograph of typical impregnated thermocouple lead after surrounding with the eutectic, cooling and rough polishing. The wires, plastic impregnated glass cloth and surrounding eutectic are clearly discernible.

To cast the eutectic into the grooves, retaining walls of a cellulose material, POLYFILLA, were built to some 3 mm height around the grooves. The disc was brought to 410 K in a thermostatically controlled oven and just molten eutectic (397 K) poured along the groove. When all six grooves had been filled the disc was removed and slowly cooled. As the eutectic began to solidify a small 15 W soldering iron was used to "puddle" problem areas (corners, ends, narrow sections) to ensure complete wetting of the brass by the eutectic.

When the disc was quite cool excess thermocouple wire protruding from the eutectic was clipped off and the eutectic smoothed to the disc surface by file, emery paper (coarse, fine, worn fine), carborundum grits and finally metal polish until a fine mirror-like finish was achieved and no scratches were visible to the naked eye. When completed the remains of the metal polish were removed with carbon tetrachloride swabs. Each thermocouple was tested and the insulation (wire-wire and plate-wire) found to be of the order of 10^{14} ohms. PHOTOGRAPH 9b shows a typical groove after this process.

To form the actual surface thermocouple all that is required at this stage is to create a metal film (preferably one of the wire metals) over the free end of the wire. Electrolysis-less metal deposition was considered but discussions with the local plater revealed that subsequent electrolytic deposition onto the metal substrate would not give a satisfactory plating. The trial junctions previously prepared were then plated (soft copper, hard copper, nickel, final chromium flush) without further attention. Upon return it was seen that the plastic insulation around each junction was covered over by plating and the junction now functioned as a thermocouple. The procedure was then repeated with the disc itself. From measurements made on the disc before and after plating and from the current-time information supplied by the plater it appears that the disc is covered by some 160μm of copper and 18μm of nickel. PHOTOGRAPHS 10a and b show the finished disc before and after plating. The central unplated area of the disc is due to the presence of a protective

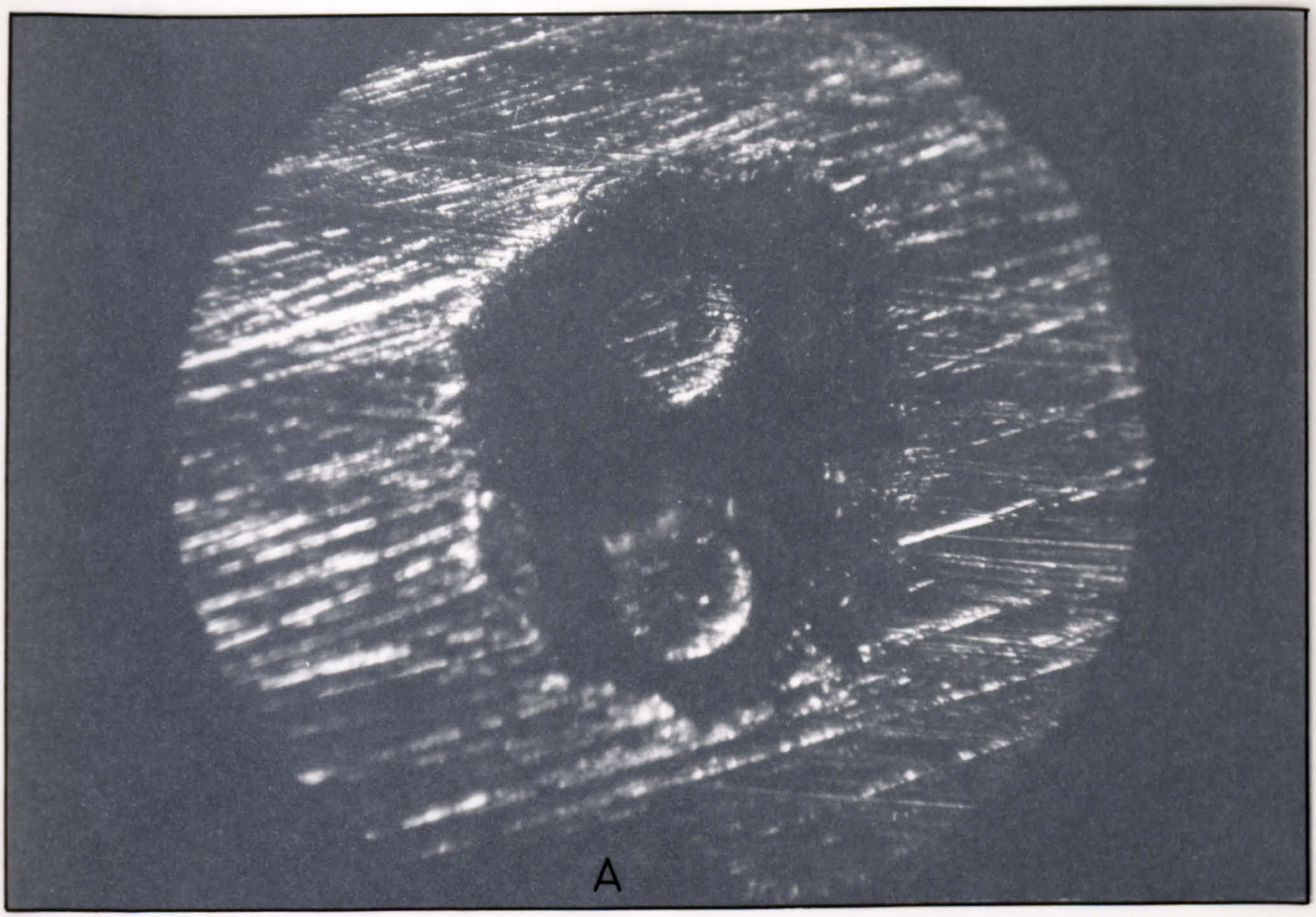

A

PHOTOGRAPH 9

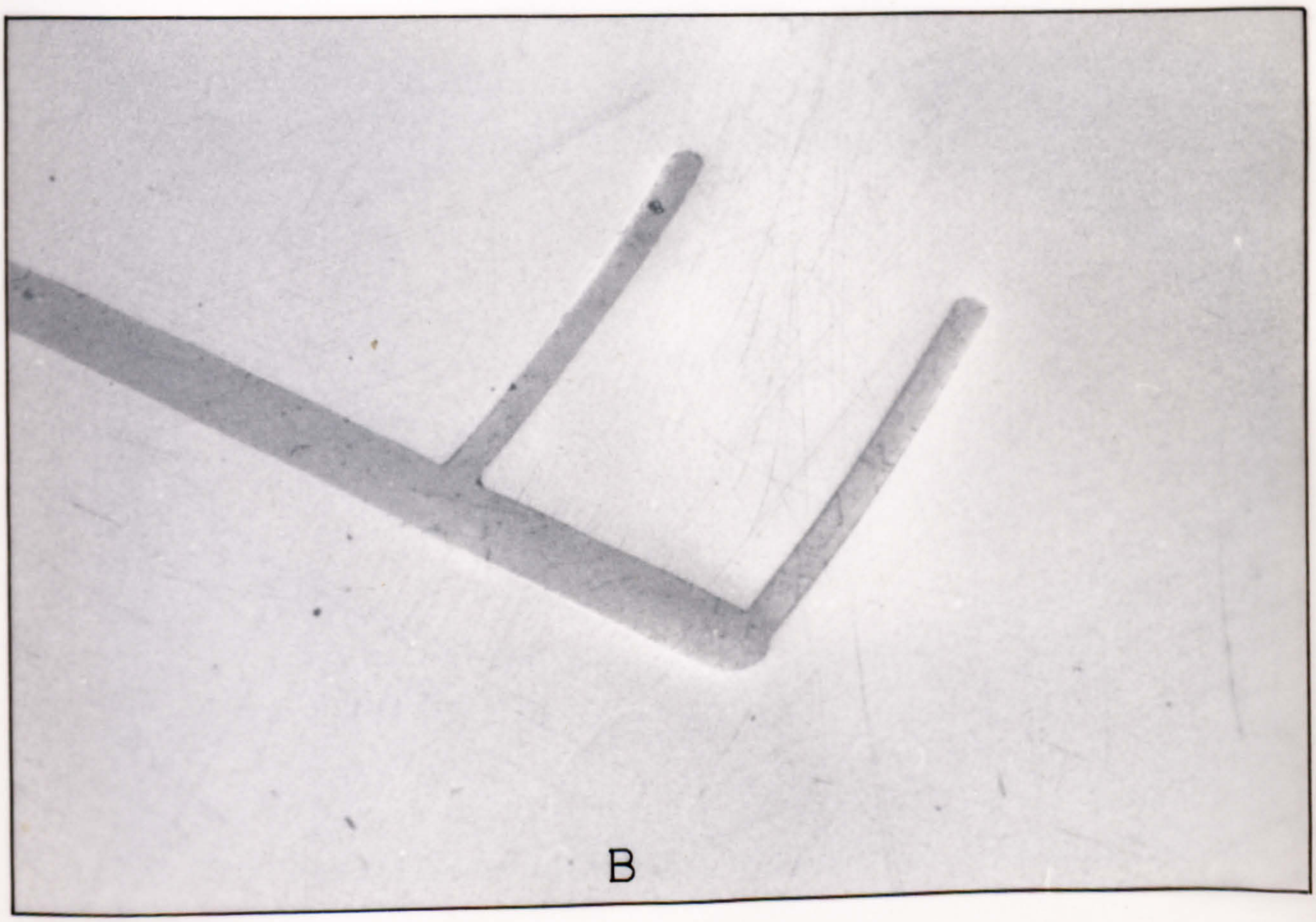

B

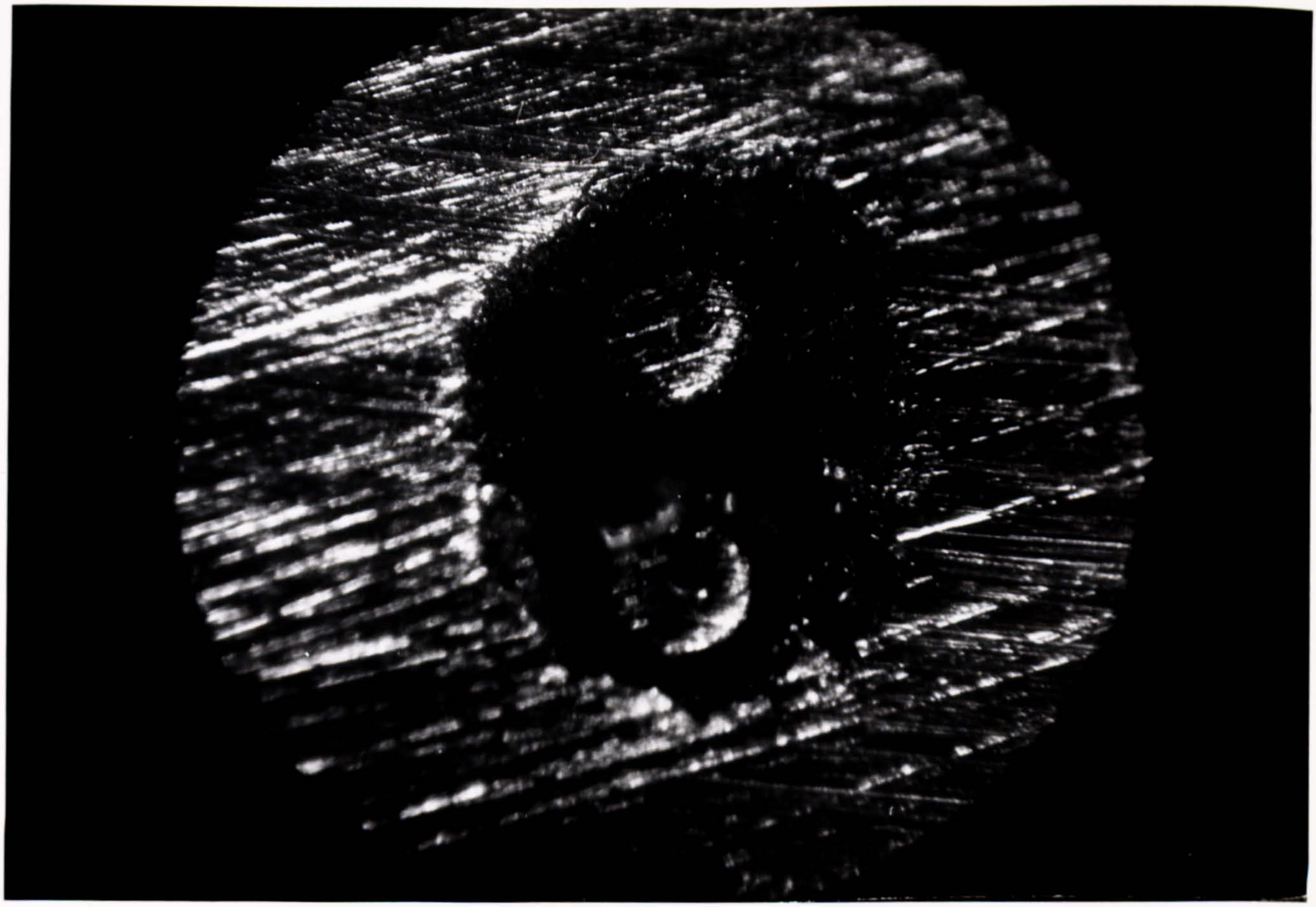

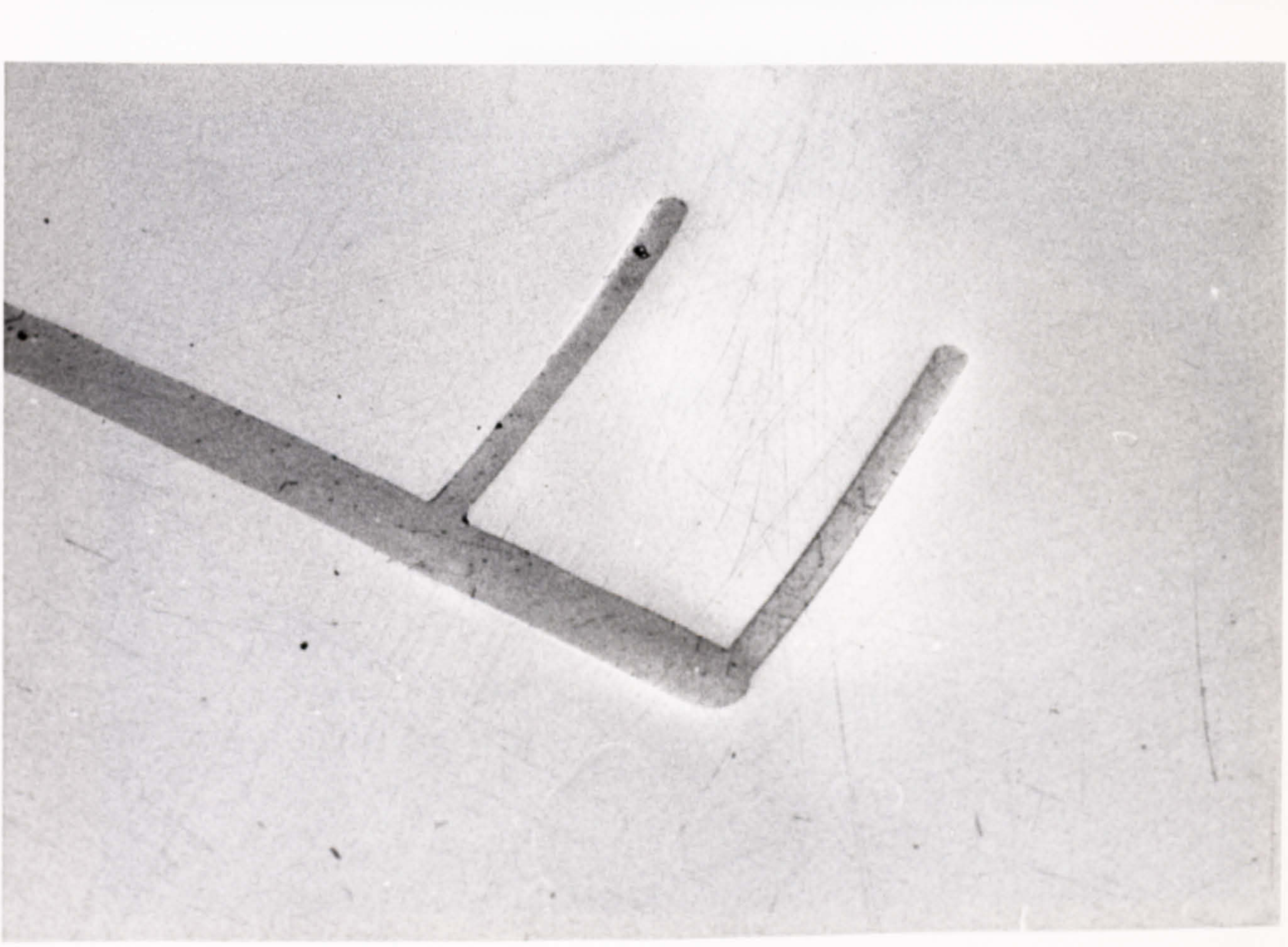

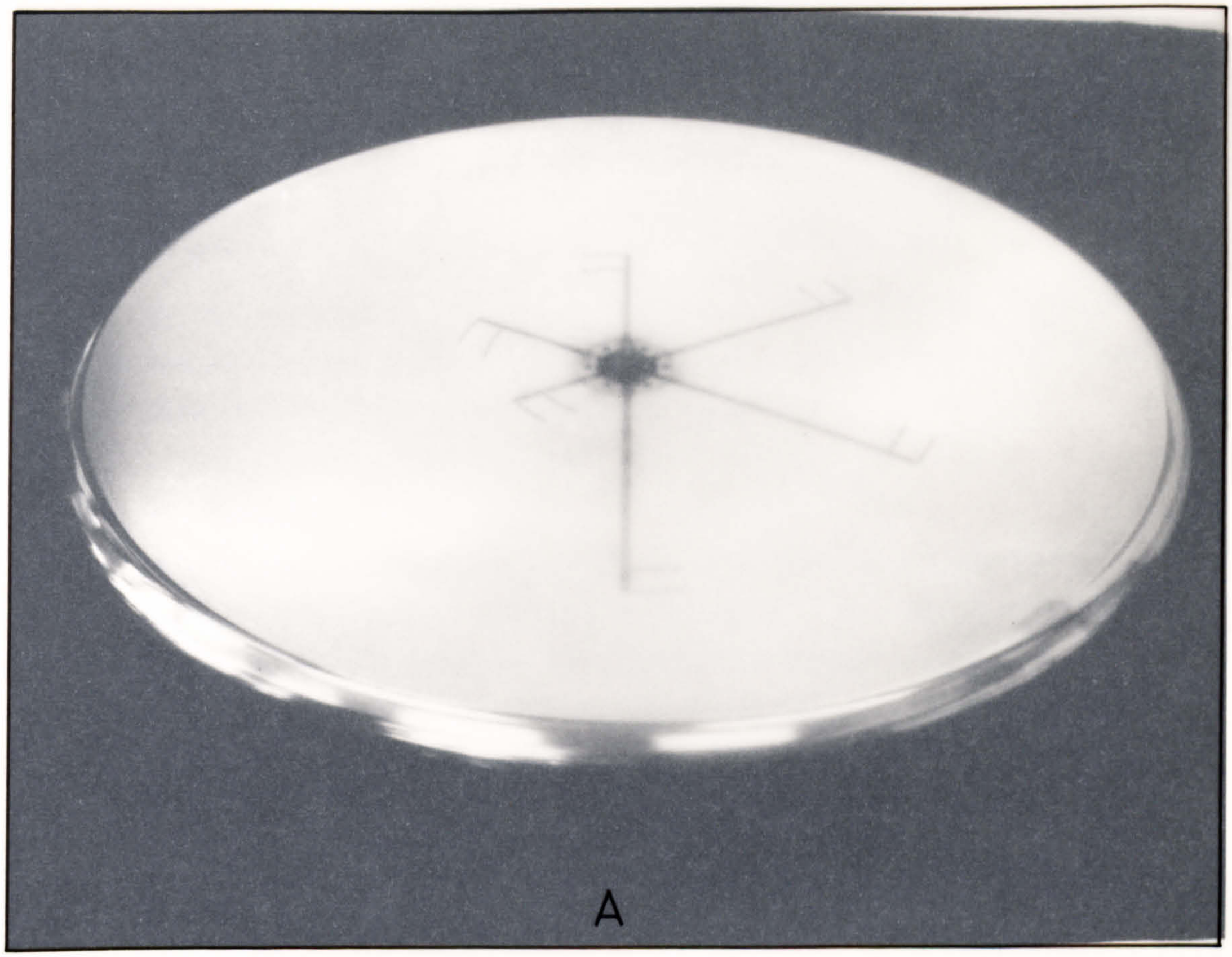

PHOTOGRAPH 10

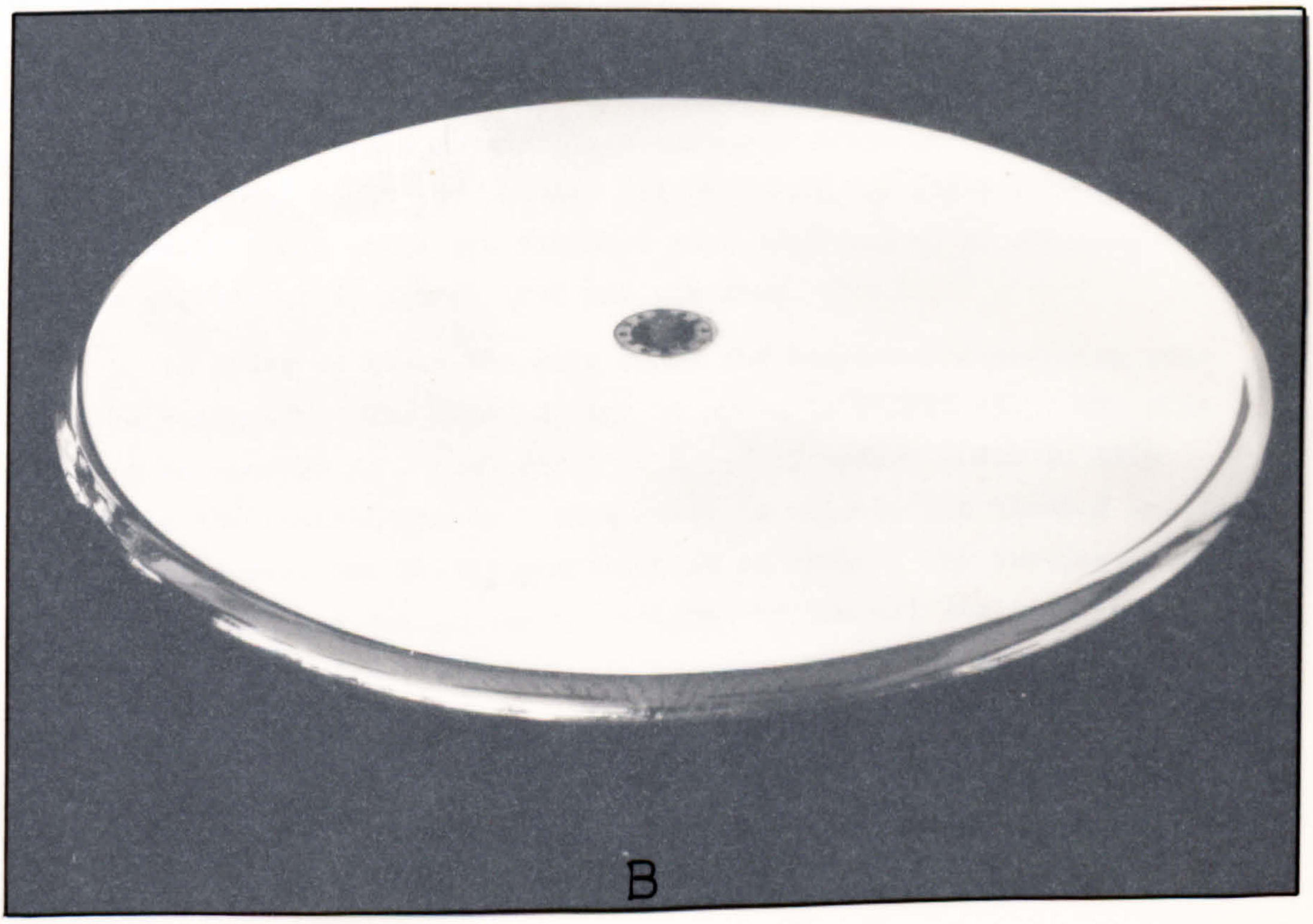

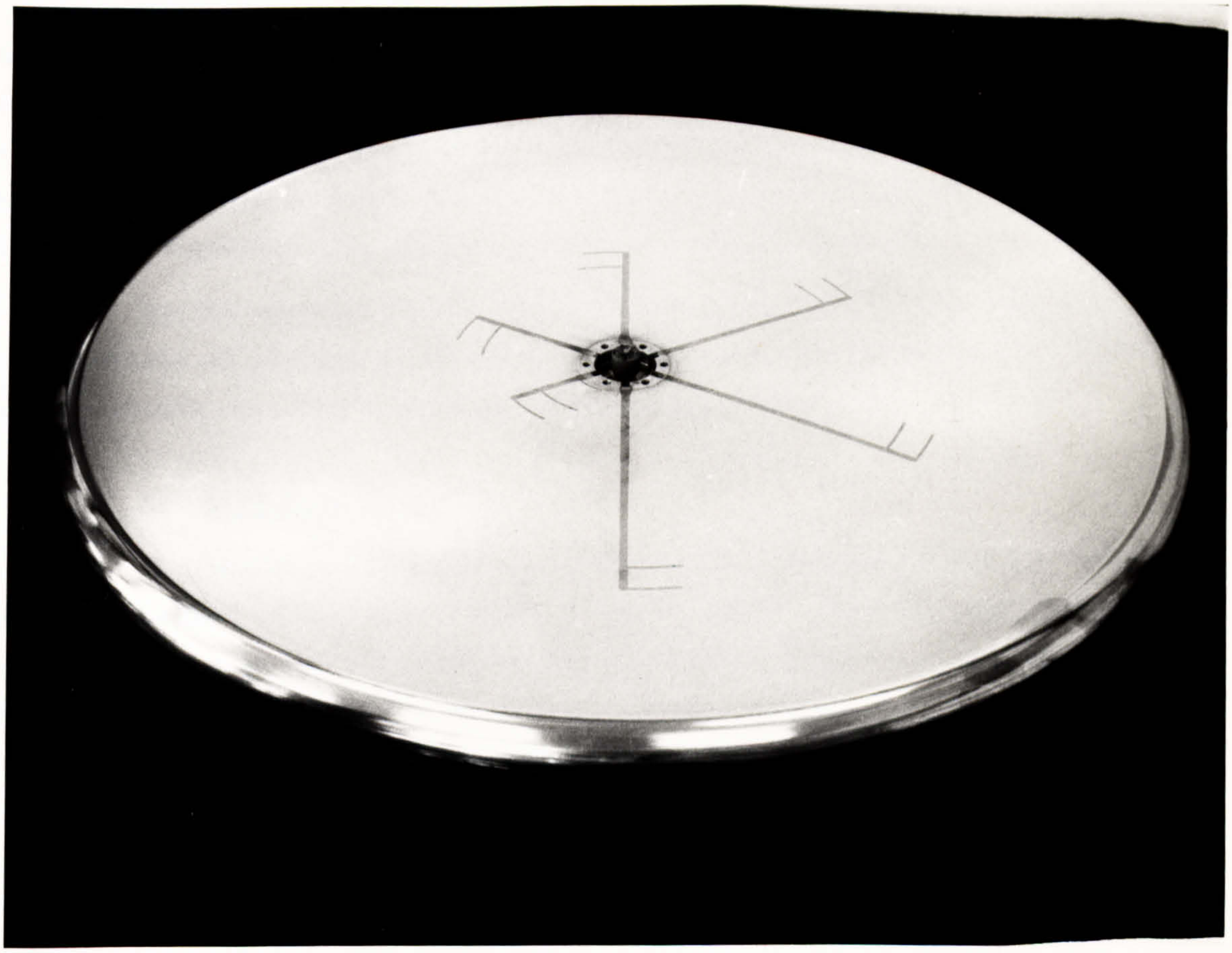

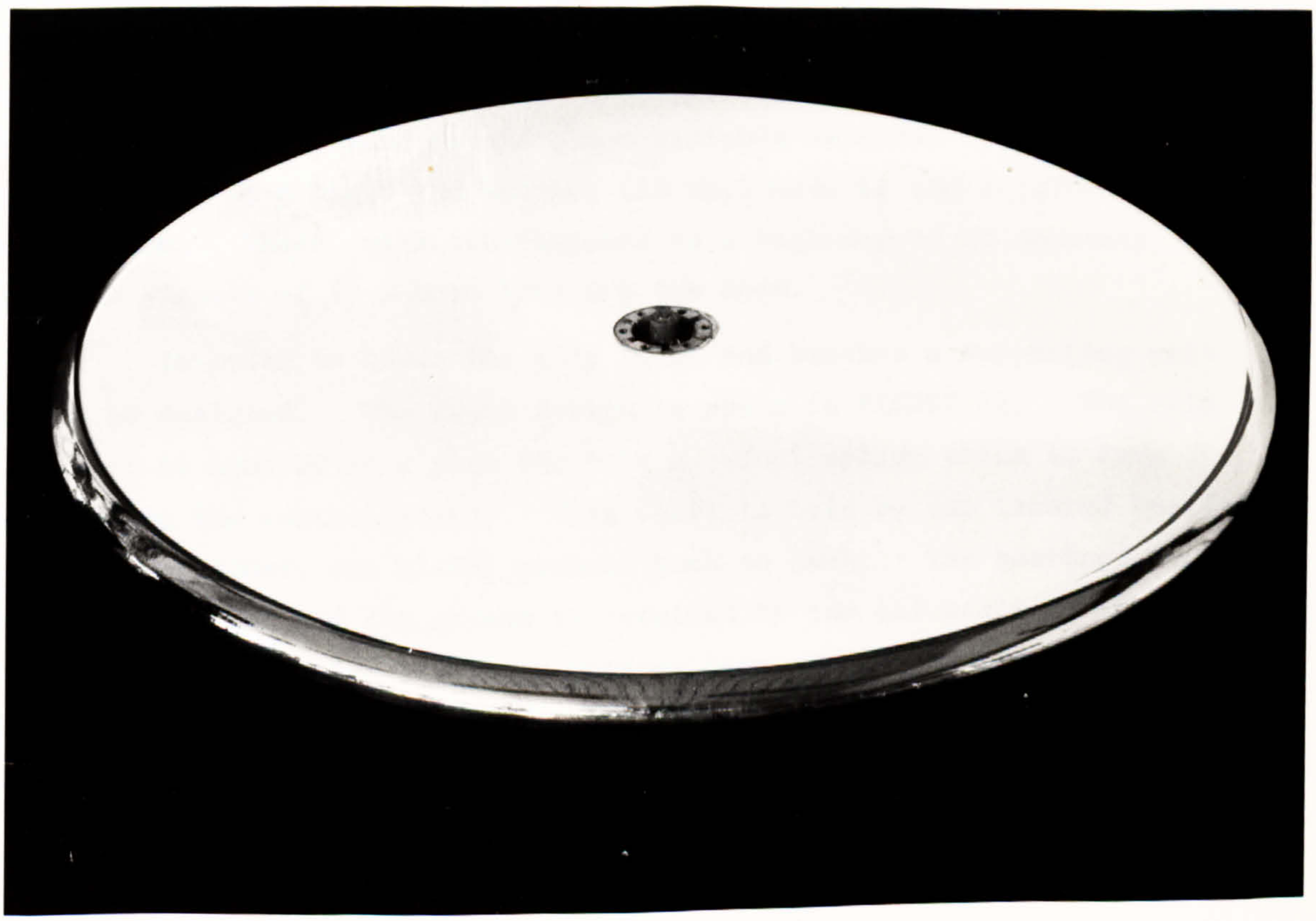

cap during plating. The cap prevented the free ends of the thermocouple leads from being attacked by the plating process. The wires themselves are attached to a small tufnol block at the very centre. The purpose of this block is to reduce the strain of any attachment to the thermocouple wires and to prevent the thermocouple leads from fracturing.

At the maximum fluxes found in the experiments (some 400 kW/m^2) the thickness of plating material above the "surface" thermocouples leads to an apparent temperature some $0.3^{o}C$ greater than the true value.

B: SLIP RING UNIT

The thermocouple leads from the surface thermocouples are not common connected in any way. This is so to ensure that the thermal E.M.F. of the junction is not affected by the rotational E.M.F. of the leads or of the disc itself. Thus from the six thermocouples, twelve leads remove the individual outputs. A slip ring/brush unit is obviously required to connect the rotating source to the stationary data logger. There are several reports in the literature of slip ring units produced by individual investigators (e.g. 141, 171, 194, 195 and 201), however, only limited success is reported. For power input these units may be adequate but for thermocouple purposes considerable 'noise' may be generated unless the unit is finished to a very high standard. In addition, discussion with commercial manufacturers (ADENCO (234)) suggests that use of common materials (copper, brass etc.) can give apparently random spurious signals and only use of the noble metals gives reliable results. For this reason 24 carat gold slip rings and brushes (12 way) made by IDM ELECTRONICS Ltd. were chosen. These units are finished to a high degree of accuracy, and spurious signals of less than $1\mu V$ are the norm.

In order to house the slip rings and brushes a supporting unit had to be designed. The final design is shown in FIGURE 72. The slip ring unit is mounted as a push fit into a tufnol spigot which in turn mounts into the central shaft. This shaft is held by two tapered bearings (TIMKEN cone A2047, cup A2126) mounted back to back. The bearings are grease lubricated and the grease is retained by two oil seals on the shaft. The upper oil seal also retains a perspex body around the slip rings. This shell is designed to provide protection to the rings and brushes and is drilled to accept a cooling air supply.

The twelve way slip ring is wired to a twelve way tufnol socket at the lower end of the central shaft. This socket utilises gold plate

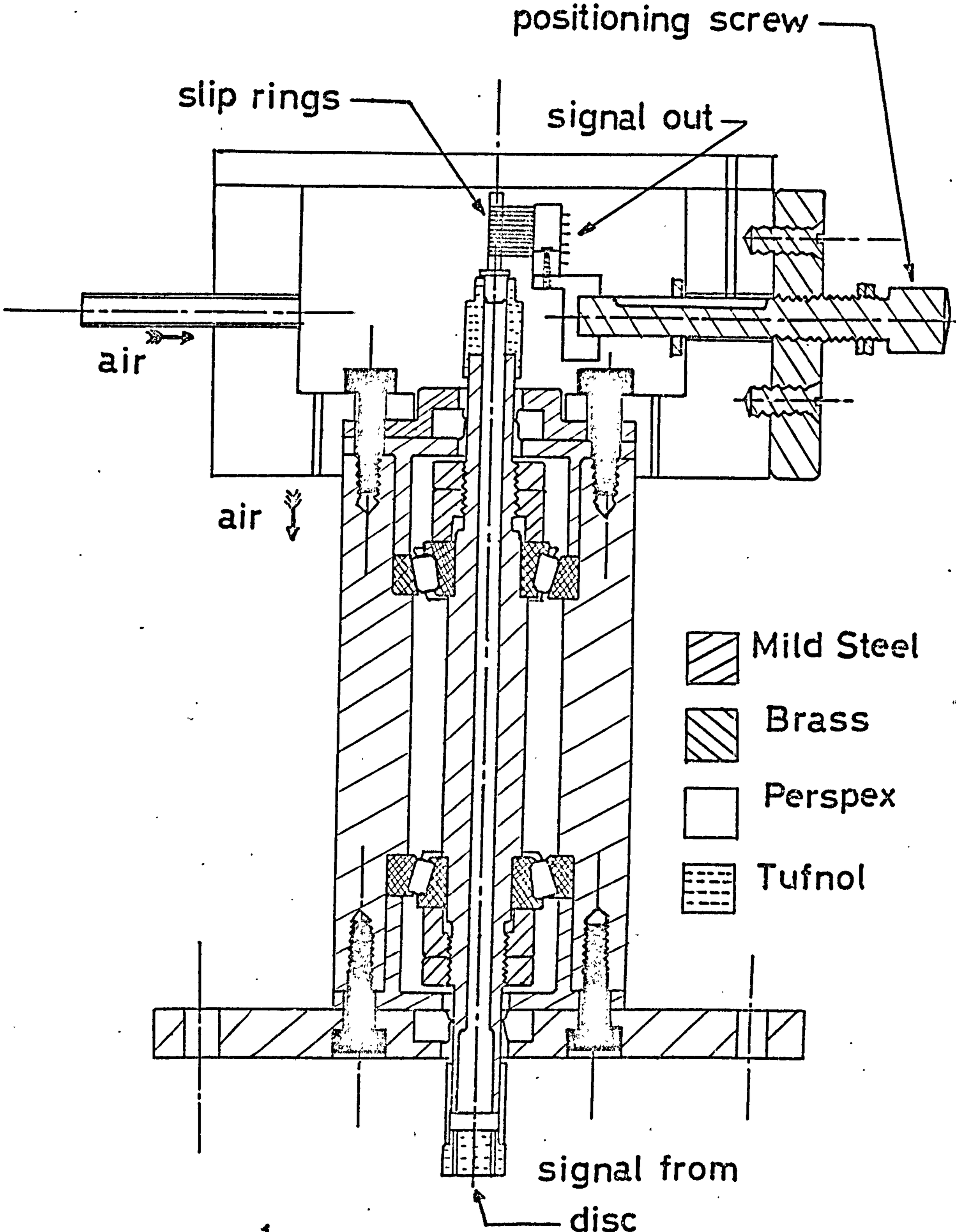

FIG 72 SLIP RING UNIT

integrated circuit socket tubes 250/µm in diameter.

The brushes are mounted on a carrier which may be adjusted so as to engage the slip rings or allow the slip rings to rest without wear in the triangle formed by the brushes (2 arms) and the brush base. Each position is preset by 'stops' fitted to the carrier spindle.

The unit bolts into position on the rig over the distributor body and leads from the rotating disc thermocouples are brought up from the centre 'stalk' of the disc (FIGURE 41a) and are connected to the socket at the lower end of the centre shaft of the slip ring unit. Drive plates attached to the disc stalk and the unit shaft turn the slip ring unit with the disc. Signals from the thermocouples pass via the slip rings onto the brushes and thence by multicore screened cable to ice point and data logger.

In practice no spurious E.M.F. in the thermocouple output was observed attributable to the slip ring unit.

The finished unit is shown in PHOTOGRAPH 11.

C: CONDENSATE COLLECTION

As may be seen from PHOTOGRAPH 7a the underside of the disc has the heat transfer area divided into annular sections. The dividing walls of each annular ring are some 1.0 cm high and 1.5 mm broad. The inner edges of the rings are located at 3, 5, 7, 9, 11, 13 and 15 cm radii and the seven rings divide the heat transfer area into six sections. Each area is 1.85 cm broad and commences at the outer root of the inner fin. The area occupied by the dividing wall varies from 5% (at the inner ring) to 4% (at the outer ring) of the total area for each ring. The disc is some 3 mm nominally thick in the heat transfer direction between fins.

FIGURE 39 shows a cross-section through the rotating equipment previously referred to in the hydrodynamic work. The tracing front has a blacked area covering those parts of the equipment especially used in the heat transfer work. The major elements of the additional equipment are seen in PHOTOGRAPH 12a, b and c. A set of 7 plain cylindrical rings of 1 mm thick stainless steel are pressed into grooves cut into a brass base plate. When vertical, the inner edges of these rings are some 2 mm greater in diameter than the equivalent disc ring. The base plate is specially machined to have a sloping gutter between each ring and one drainage hole per gutter. The plate is held by retaining cap screws to a

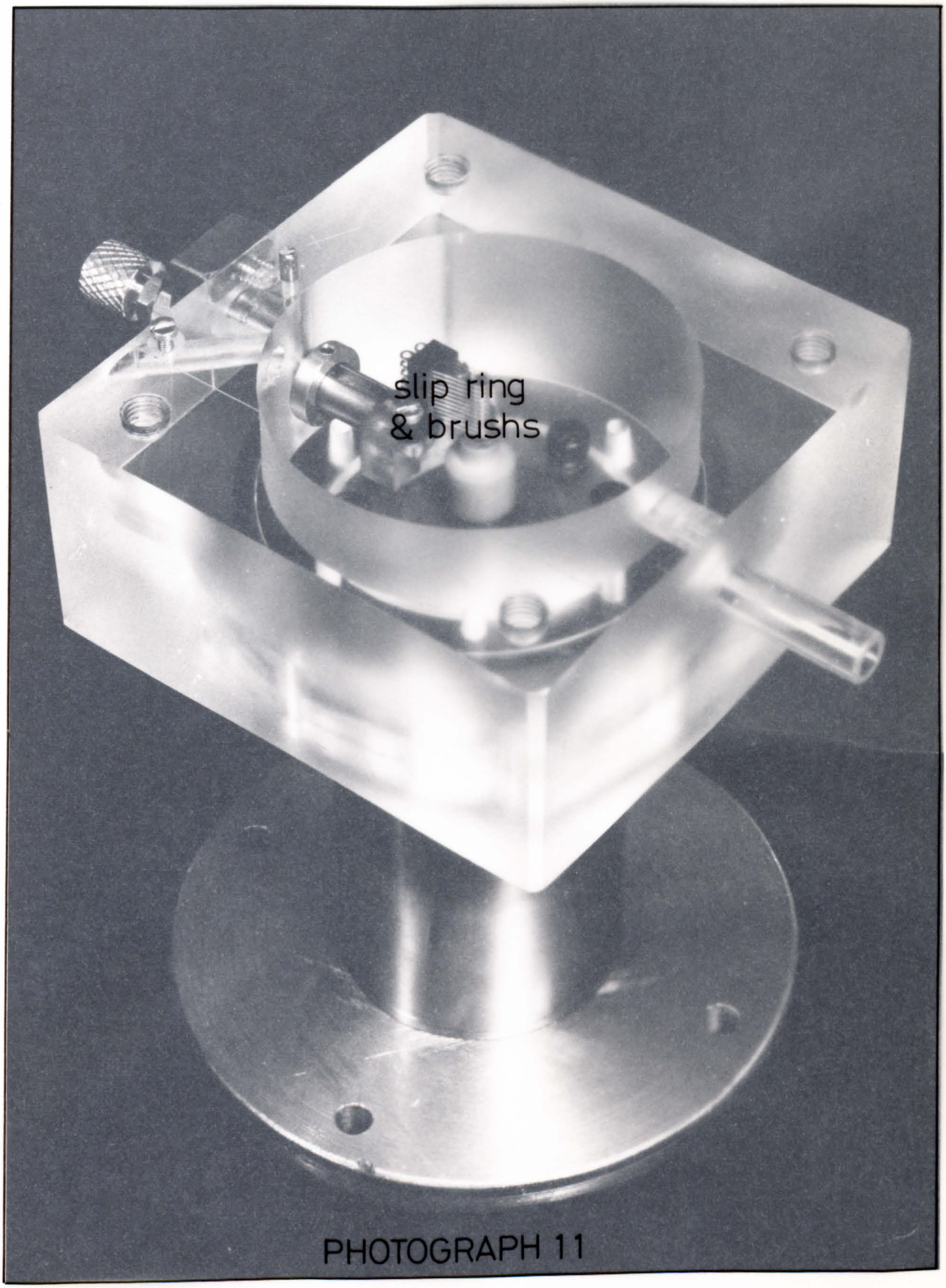

PHOTOGRAPH 11

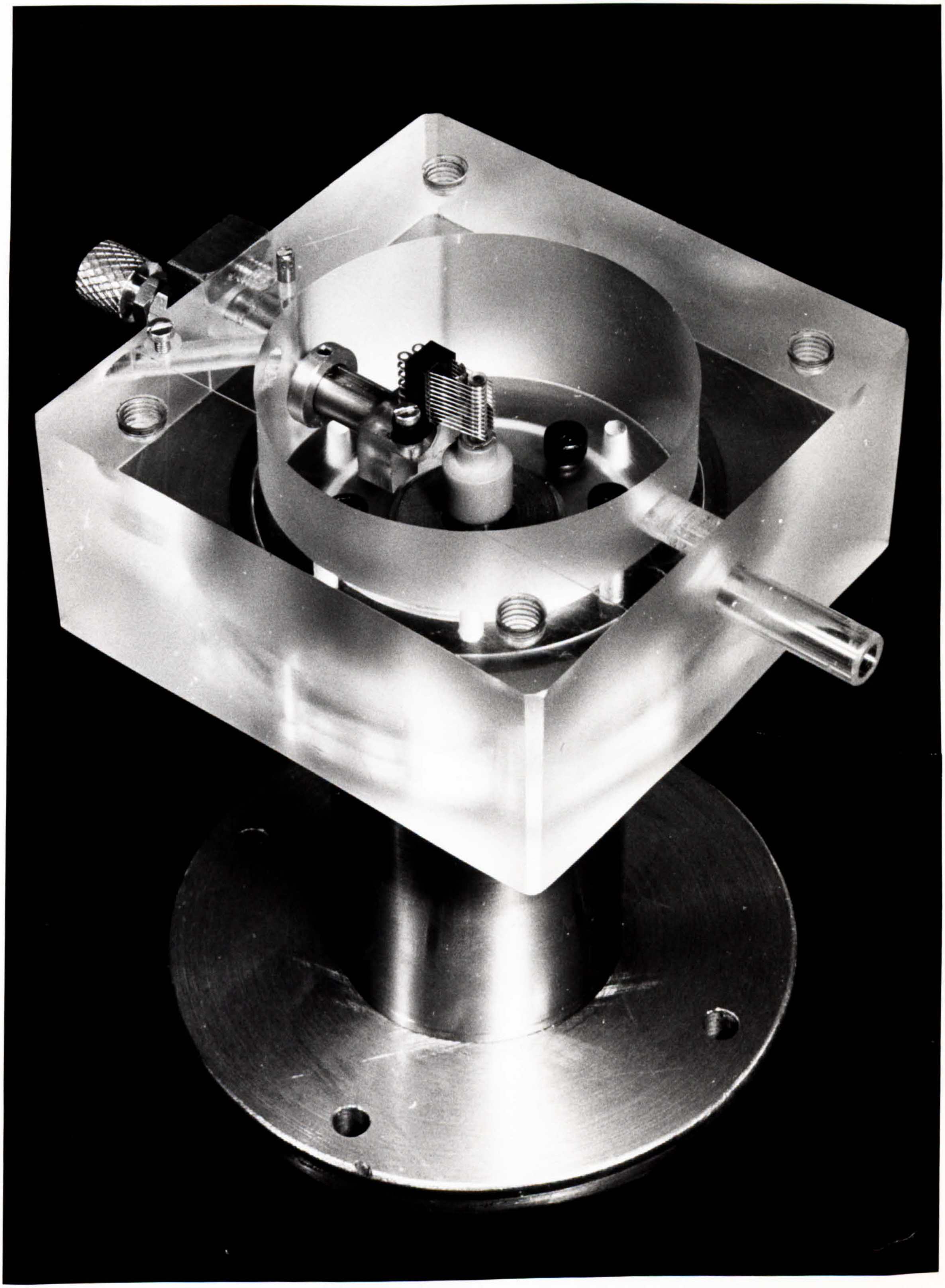

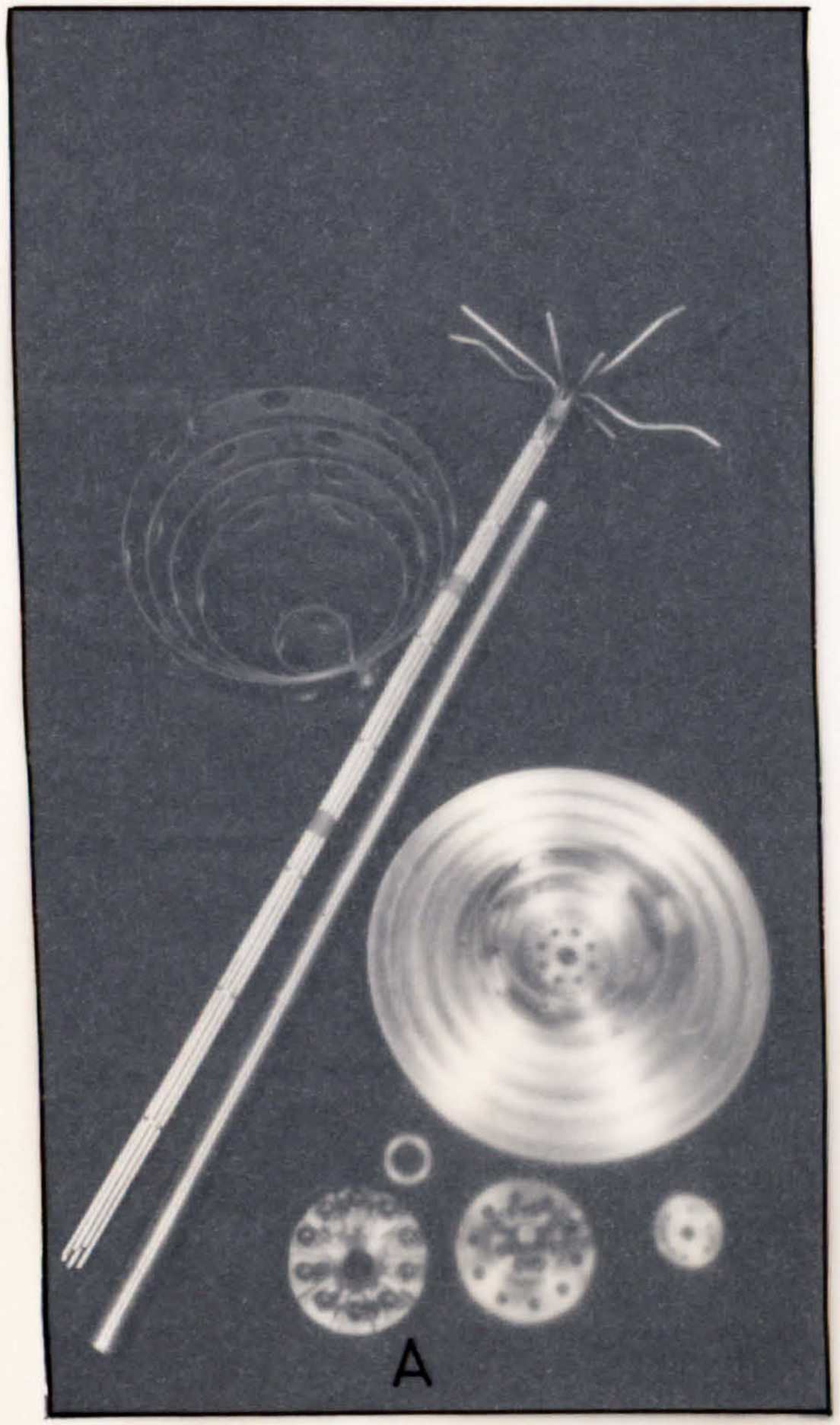

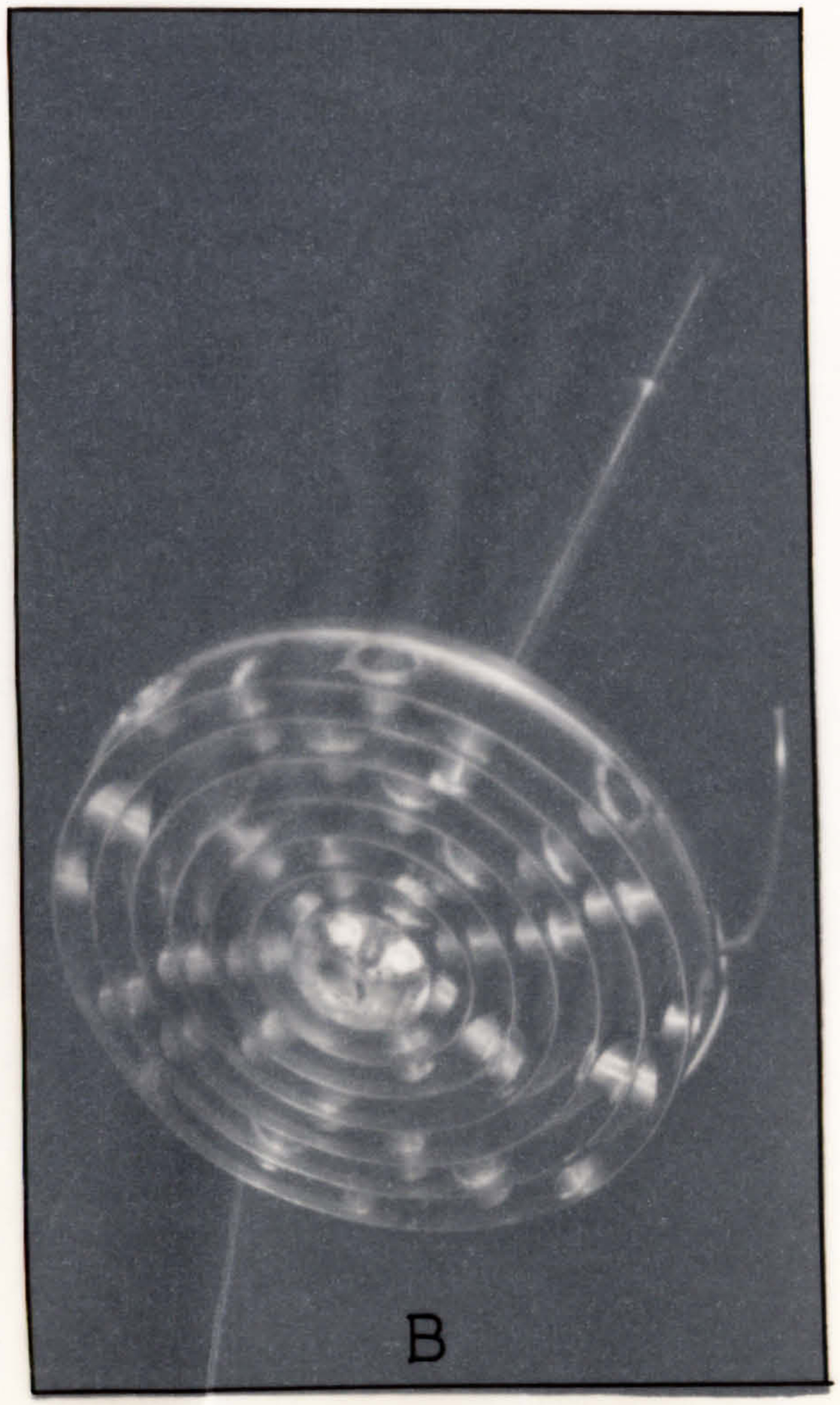

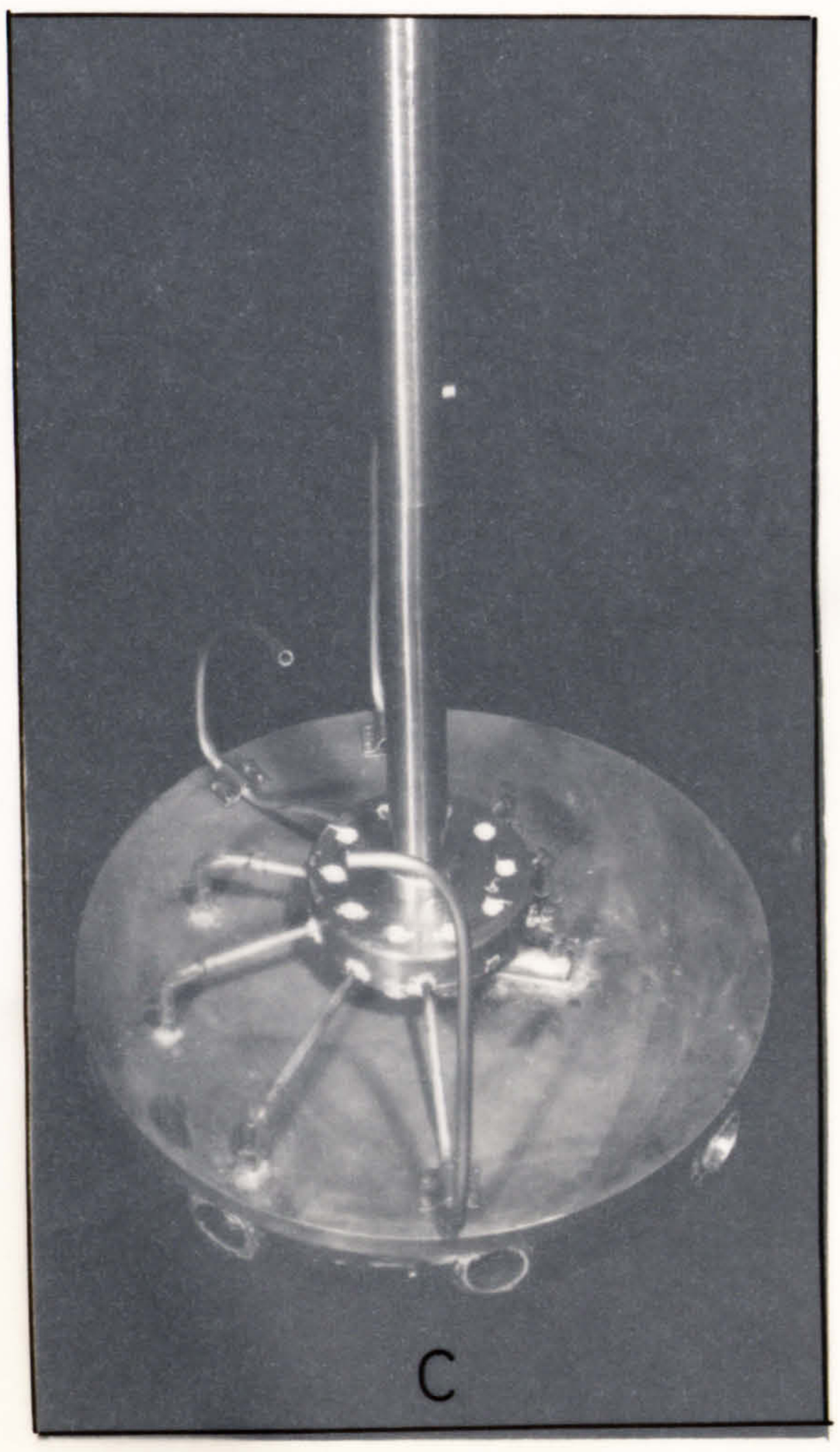

PHOTOGRAPH 12

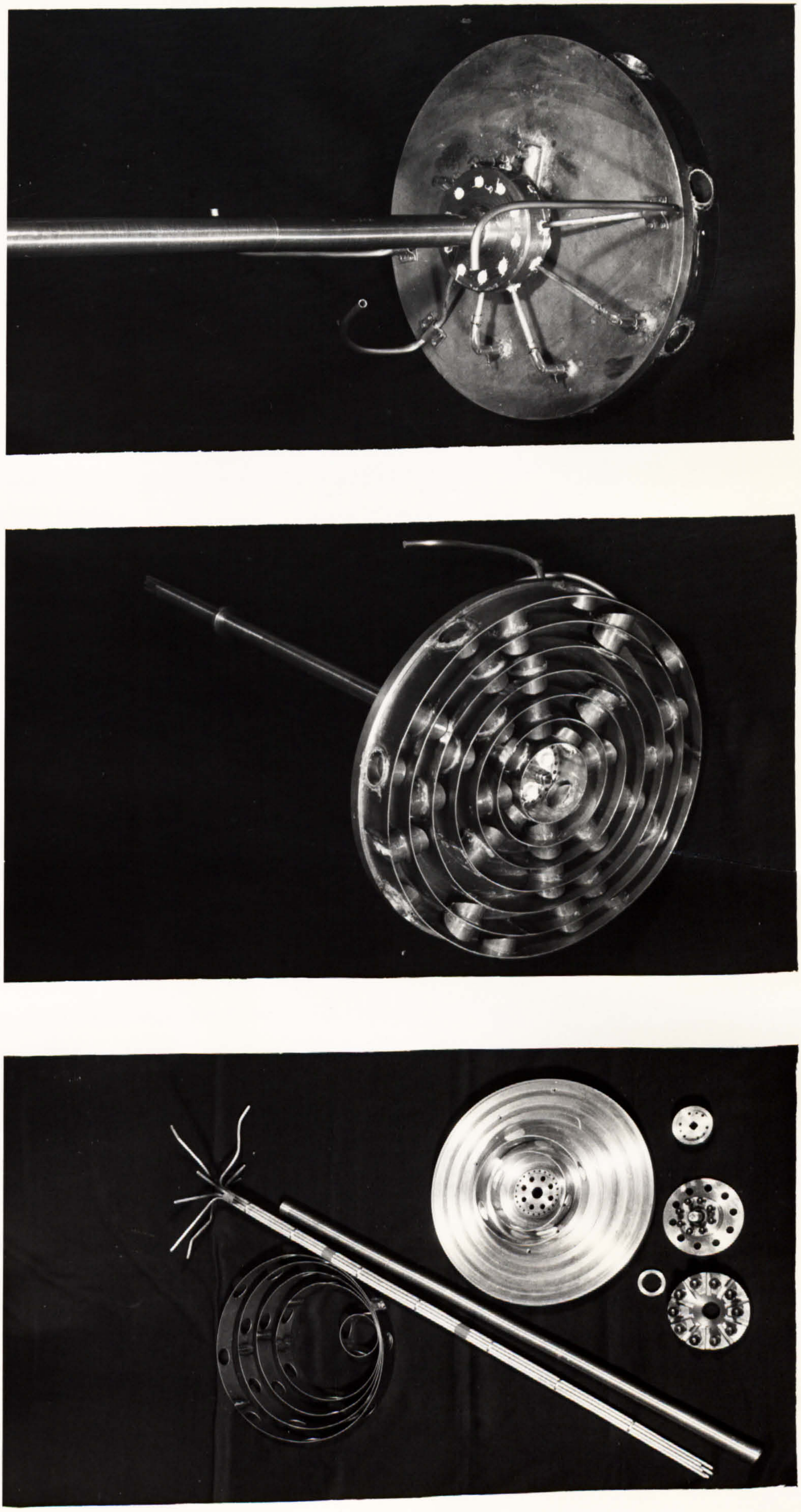

heavy mild steel block which is in turn screwed to one end of a long (60 cm) mild steel tube (2.5 cm diameter). This tube contains a tube bundle of nine $^{3}/16$" brass tubes held by spacer baffles. These tubes are led free at the lower end and at the mild steel block end are bent through a ninety degree curve. The nine tubes are laid in 9 equally spaced slots machined in the lower half of the mild steel block. Before bolting the upper portion of the block into place any gaps were filled with silicone rubber. Six of the nine tubes are connected to the six drainage holes of the brass plate (see PHOTOGRAPH 12c and FIGURE 39), two are bent into a gentle curve twisting clockwise looking down and the remaining tube is cut short to about one half of the plate radius and positioned half way between the plate and the ends of the two previously mentioned tubes.

The mild steel block carries a 1.25 cm diameter stainless steel bar mounted in a grease packed bearing (TIMKEN cone A2047, cup A2126). The bar is free to move vertically for small distances (order of 3 mm). The free end of this bar is square sectioned to suit a square hole machined in a stainless steel block cap screwed to the centre bush of the disc underside.

The assembly and operation of the equipment is as follows. The completed unit is lowered into the open steam chamber with the disc removed. The free mild steel tube is threaded through the rotary union and the two free tubes attached to the brass plate are bent in situ so as to rest freely in the lower portion of the steam chamber. The disc is then replaced and fixed and the free end of the mild steel tube raised, by means of the jacking clamp screwed into the rotary unit, until the square section of the central stainless steel rod mates to the square hole of the block on the disc underside. In practice this took some care to achieve. The jacking clamp was then locked into place. The dimensions of the various pieces of the equipment were arranged so that in this position the stainless steel rings would be set exactly 1.0 mm from the disc underside and 1.0 mm radially separated from the outermost face of the disc's undersurface fins. Any radial eccentricity of the disc when rotating is transferred to the firmly held stainless steel bar which, due to the unrestrained action of the bearing, causes the collection equipment to pivot about its support (the jacking clamp) and so follow this eccentricity. Thus the small clearances between the rotating disc fins and the stationary collecting rings are maintained at all speeds.

The stainless steel rings (PHOTOGRAPH 12a and b) have a number of large holes punched into them. When arranged in the brass plate these holes are off-set. The purpose of these holes is to transfer, with as low a pressure drop as possible, steam from the surrounding chamber to each of the heat transfer rings. To equalise any significant back pressure a set of holes was drilled through the base plate at the very centre to permit an alternative access.

When the disc rotates condensate formed on each ring undersurface is thrown outwards by the centrifugal force until it meets the downward facing fin of that ring. It is then thrown off onto the stationary stainless steel ring and drains to the gutter beneath to eventually flow out of one of the six brass tubes at the base of the mild steel tube. To prevent any possible carry over into other rings via the steam access holes, these holes are provided with mitred tubing 'hoods' (see FIGURE 39 and PHOTOGRAPH 12a, b and detail in FIGURE 73). Condensate from the steam chamber itself, the outer edge of the disc and moisture droplets in the steam gather due to centrifugal force in the lower portion of the steam chamber. The liquid is then drained by the two stationary tubes fixed to the brass base plate.

D: STEAM CIRCUIT

The steam circuit is shown in FIGURE 73. The steam is untreated wet ($x_f \approx 0.85$) low pressure mains steam supplied as a departmental service. The steam is fed via isolating valves and a pressure governor to the flexible hoses fixed to the rotary union and the end of the mild steel drive shaft for the disc equipment. A sample of the steam is taken from the steam chamber of the disc via the ninth brass tube mentioned in SECTION C above. This sample line is also used to monitor the plenum pressure which was held to between 2 and 4 psig for best operation. Condensate forming in the annular gap between the rotating support shaft and the collection support tube (SECTION C above) is drained from the supply hose by a T piece drain on the rotary union leading to a float operated steam trap. Wherever possible, hoses, tubing and fittings are lagged with asbestos rope.

E: CONDENSATE MEASUREMENT

The condensate from each of the six heat transfer areas of the disc drains from six brass tubes at the foot of the collection equipment.

FIG 73 STEAM CIRCUIT

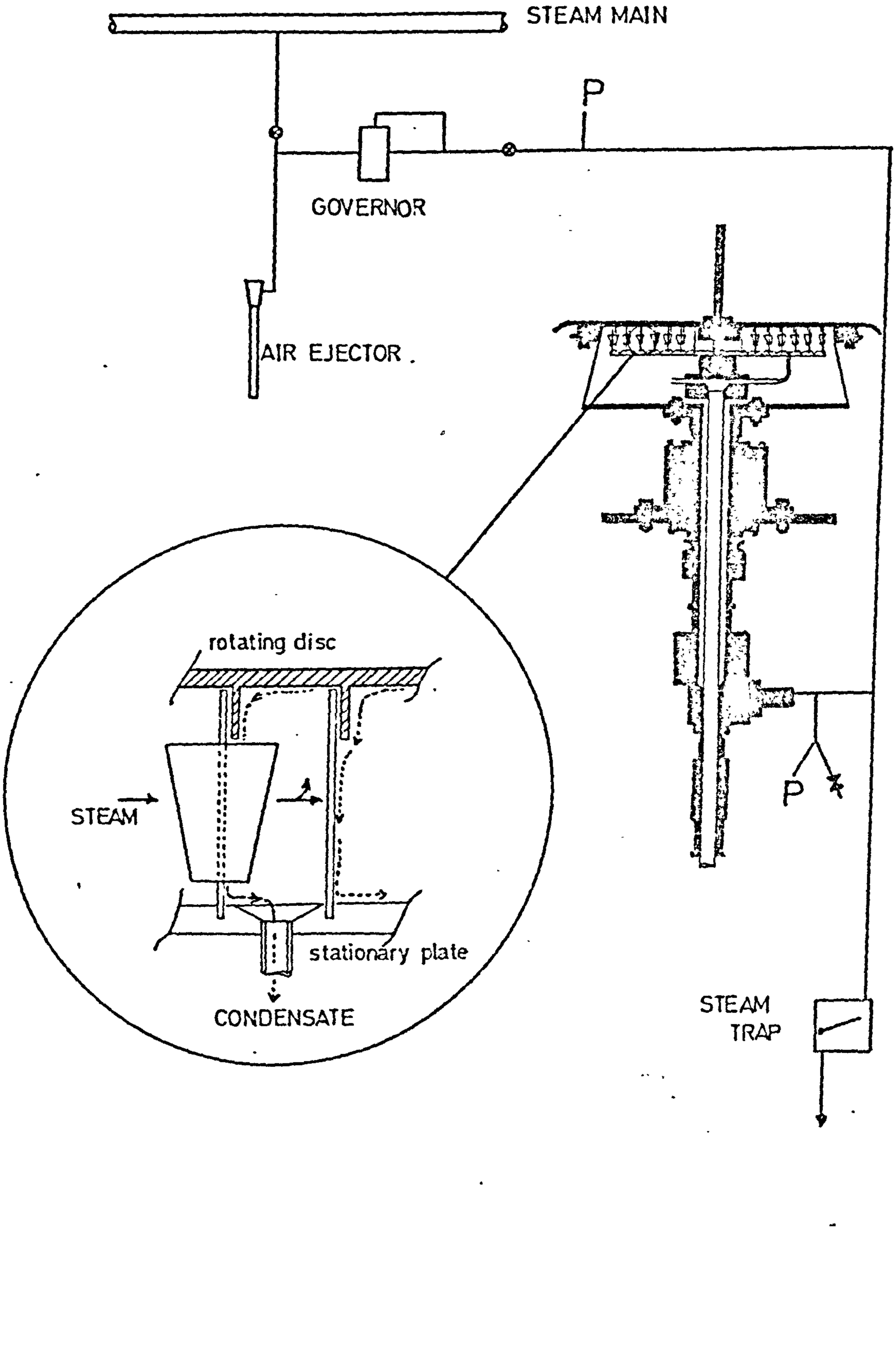

In practice, due to the plenum pressure, an intermittent mixture of condensate and steam is ejected. Since the passage of the mixture from the plenum through the mild steel support tube is essentially through a steam jacket the only heat losses that this mixture can suffer occurs in the short flow after issue from this tube. Thus a negligible amount of steam entering at the top of the collector will appear as condensate at the base.

In practice the rate of condensate production was measured very simply. The six tubes were led by flexible hoses to six preheated and weighed glass flasks. The time that each hose was allowed to discharge to the flask was noted on a stop watch accurate to 0.25s and the contents reweighed. The method appeared reproducible to within 2% when steady state conditions prevailed. All six hoses were discharged simultaneously.

It was hoped that an electronic method of timing the time required to fill a collector of known volume automatically and continuously could be used. However due to difficulties in drainage of the collectors, which would require major redesign to overcome, the technique was shelved. The method is presented here in abridged form. For fuller details consult reference 235.

The electronic circuit is given in FIGURE 74. Essentially two probes are placed at differential heights in a collector tank of known (or calibrated)volume (FIGURE 41b). The probes are connected to the circuitry as noted by trigger 1 and 2. When condensate reaches trigger 1 a relay is closed by means of the fired thyristor (which could be used to start a timer) and a light signal given. When the water level reaches trigger 2 the second relay is closed (which could stop the timer) and a drainage valve opened to reset the system. The values of the components given have been tested and perform satisfactorily in cold and boiling water and do not operate in steam. Although voltage levels of $\pm$ 30 V exist within the circuit the probes sense a ground signal only, contributing to inherent safety. The circuits were built on small printed circuit boards and provide a compact unit (the unit can be seen in the top left corner of PHOTOGRAPH 3). The probes were constructed of brass rod covered with heat shrinking insulant tubing and no electrolytic effects were found. The collector tank was jacketed by exhaust steam, and the jacket itself protected by vermiculite packing to minimise heat losses.

PHOTOGRAPH 13a, b, c, d show respectively a set of the brass condensate collector tanks, the setting up procedure showing the probes used,

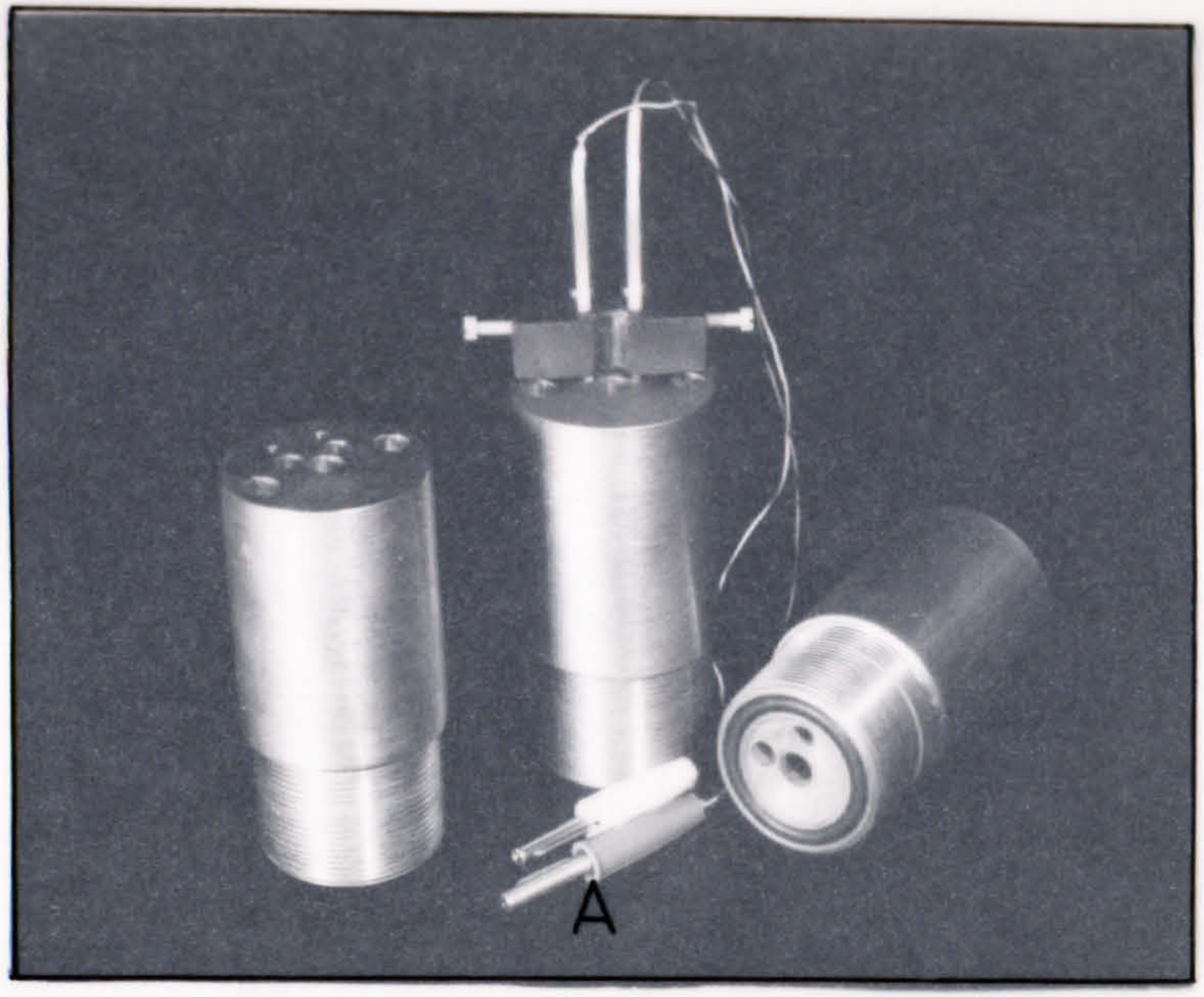

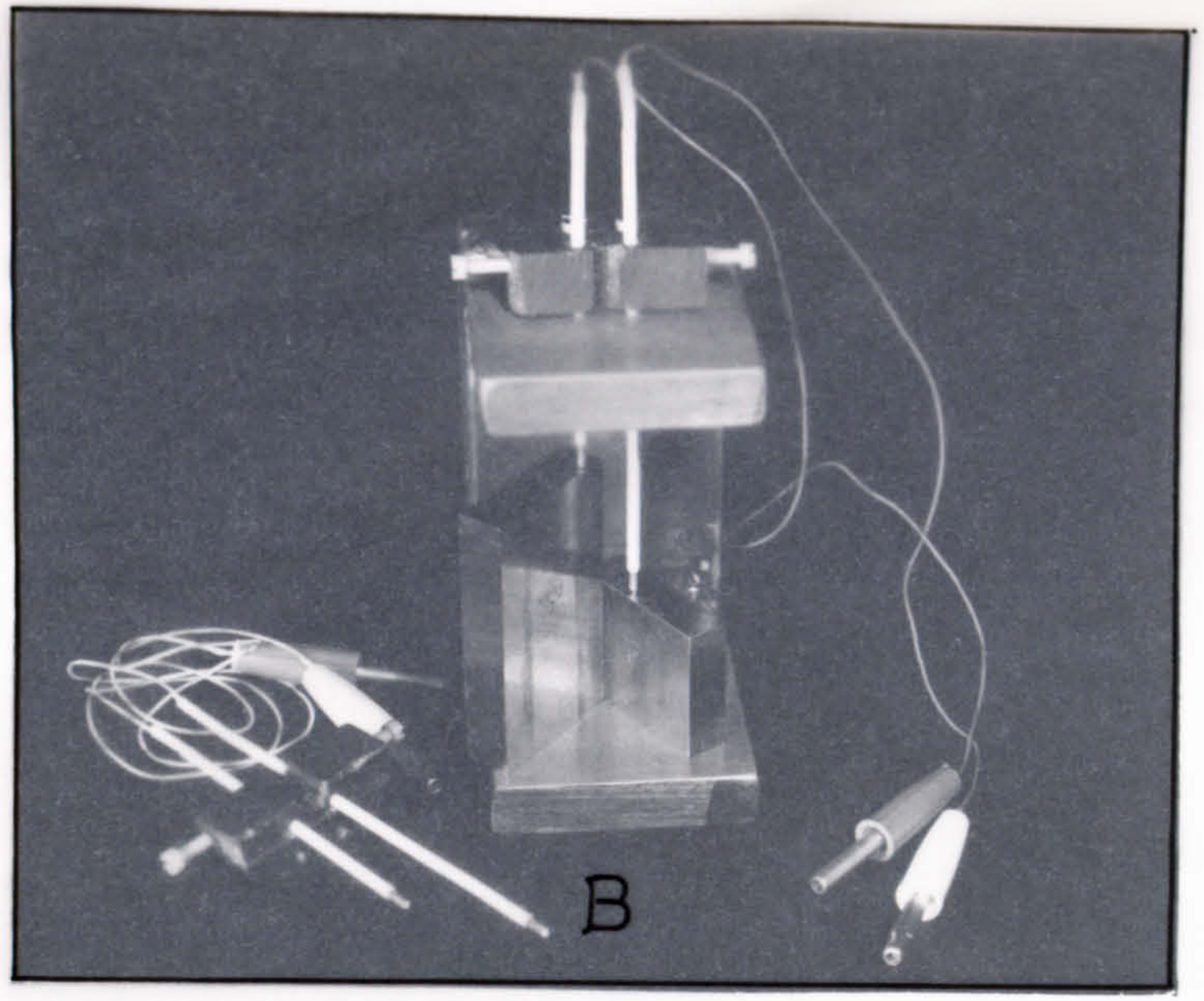

PHOTOGRAPH 13

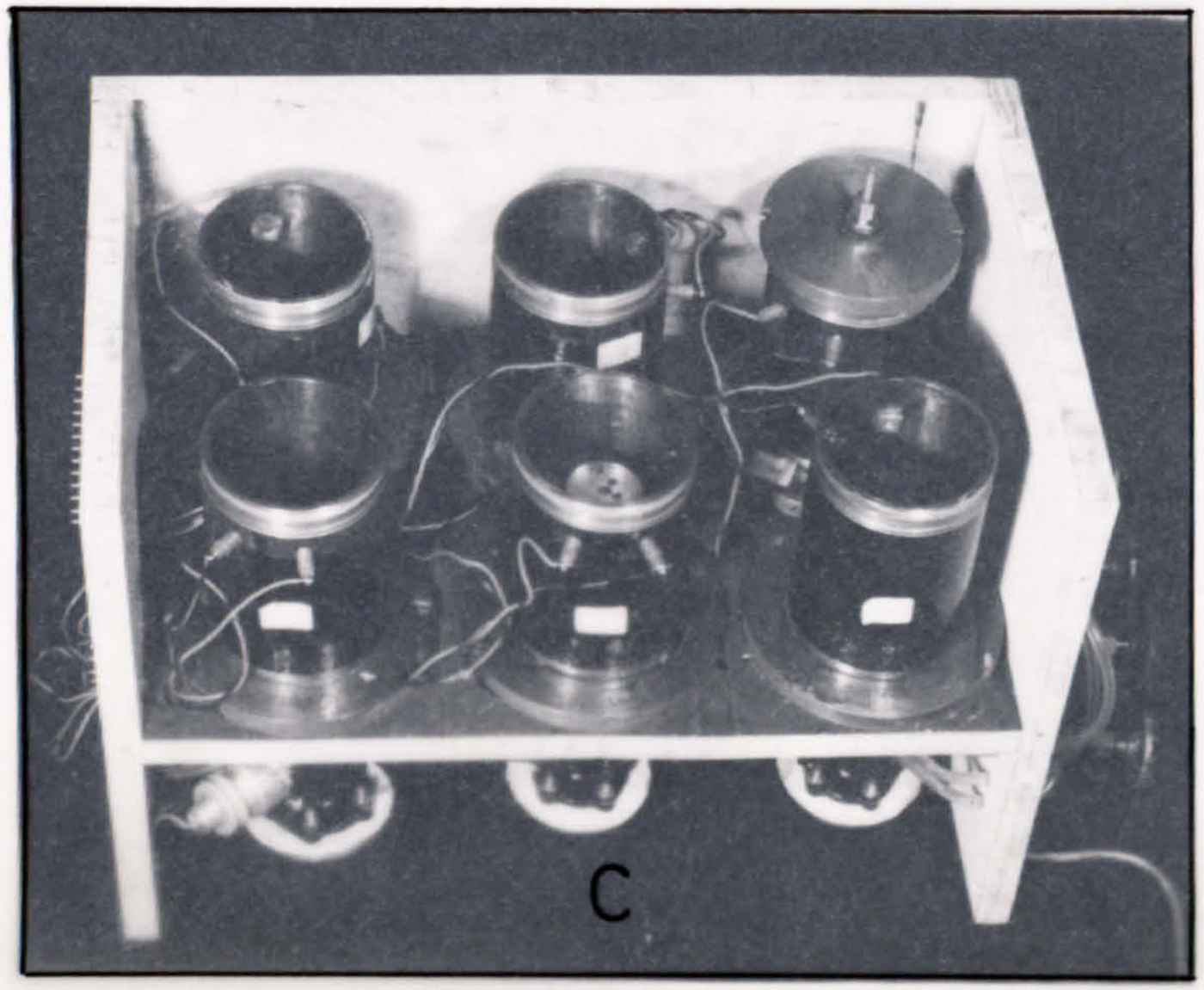

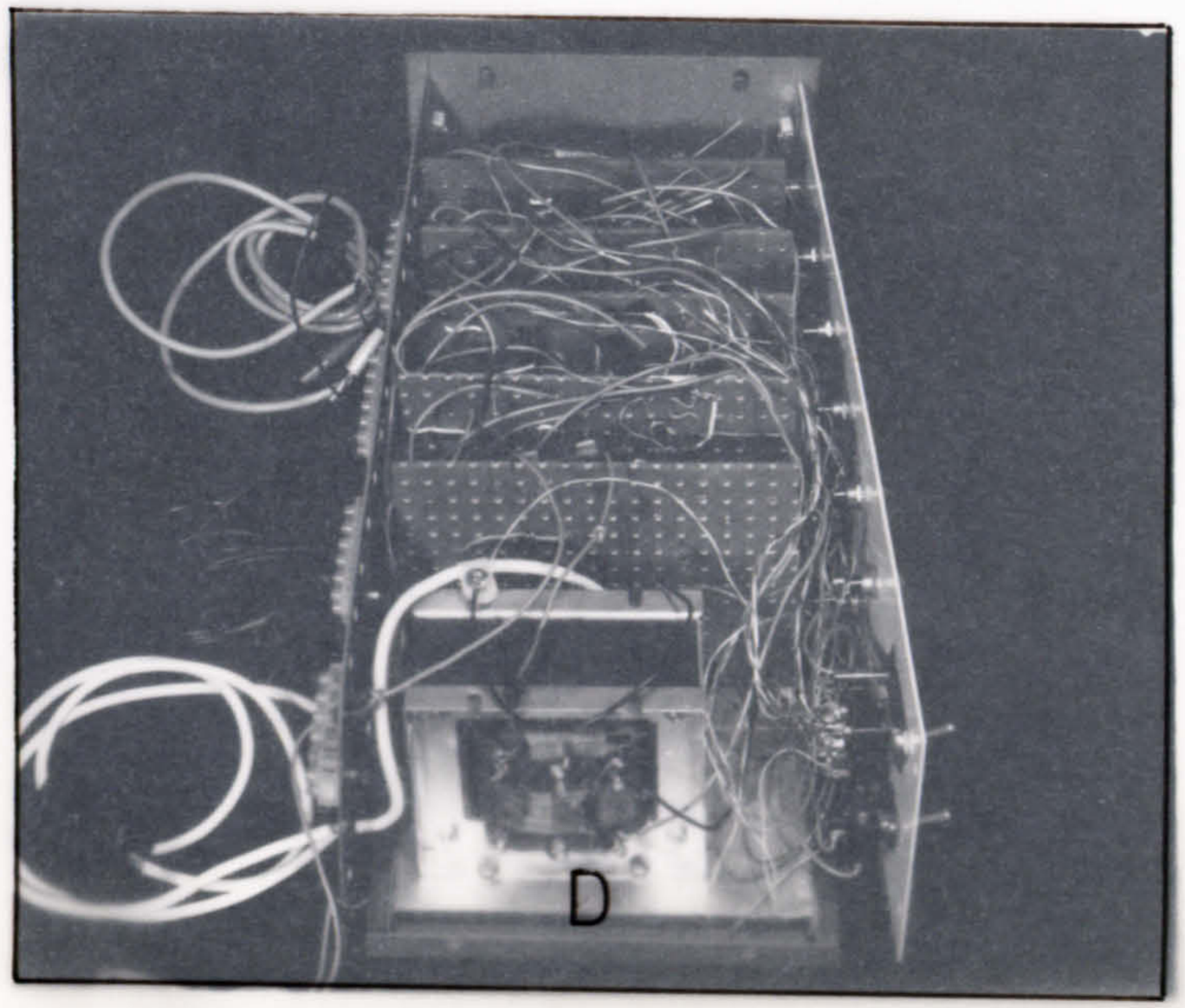

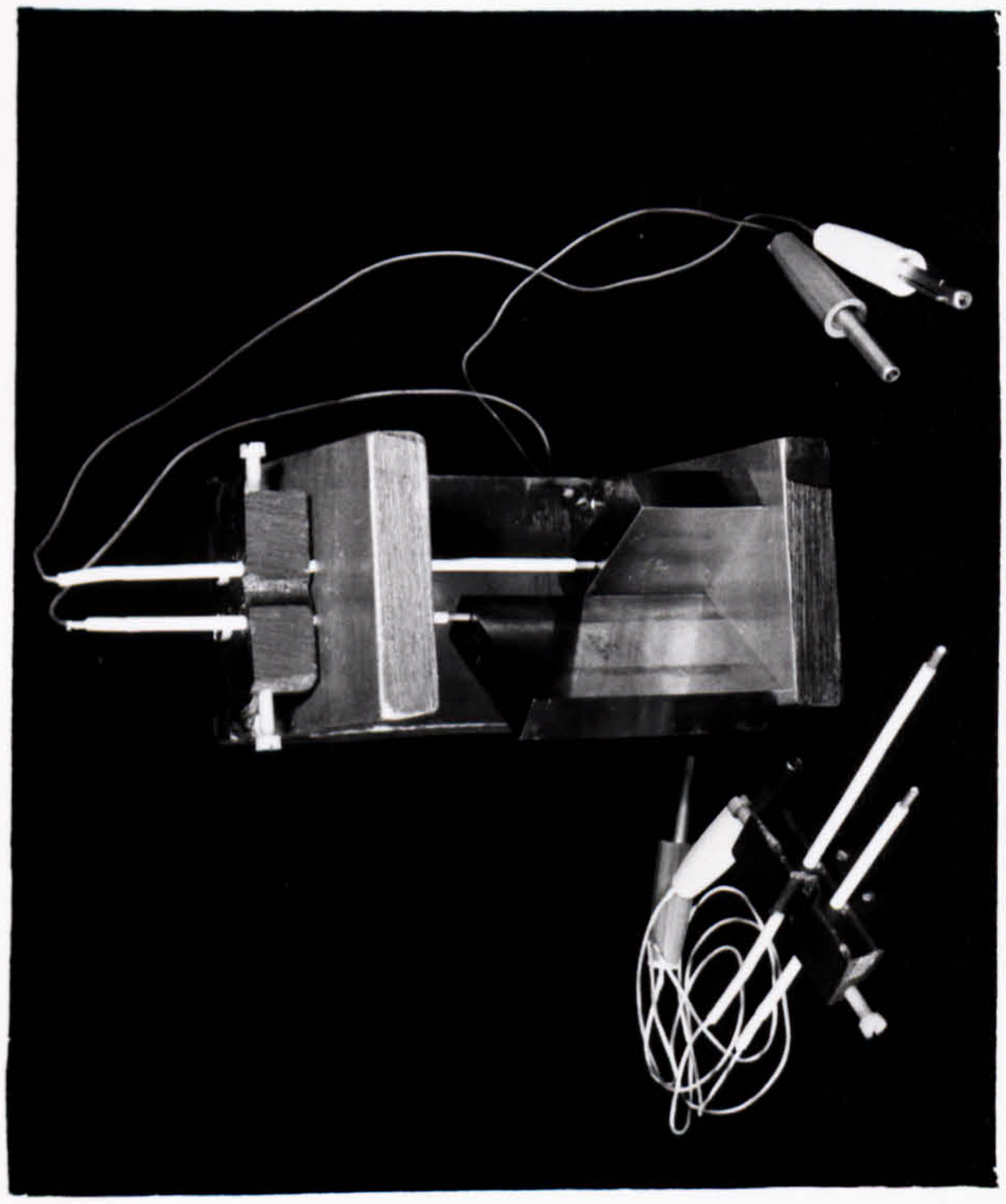

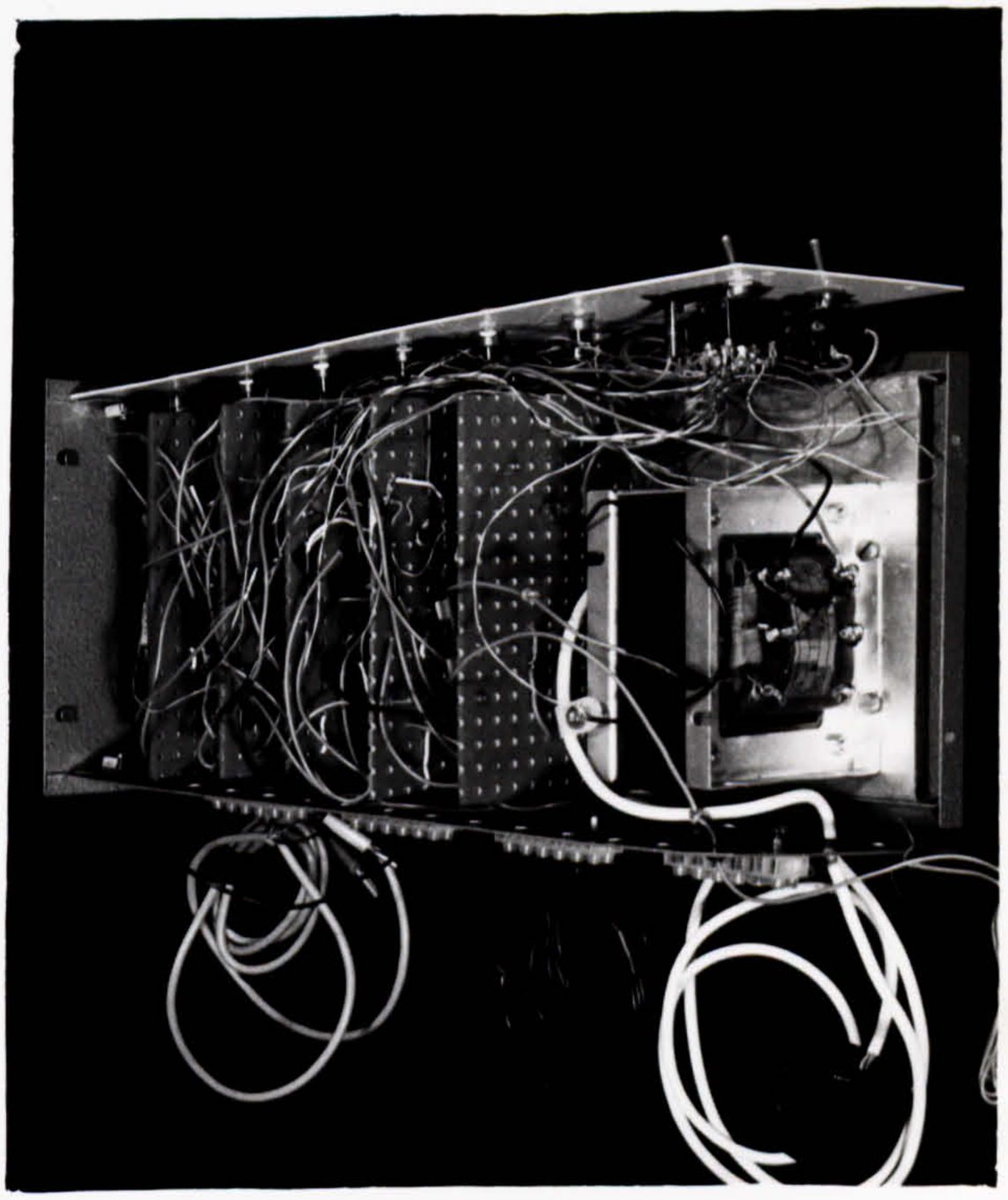

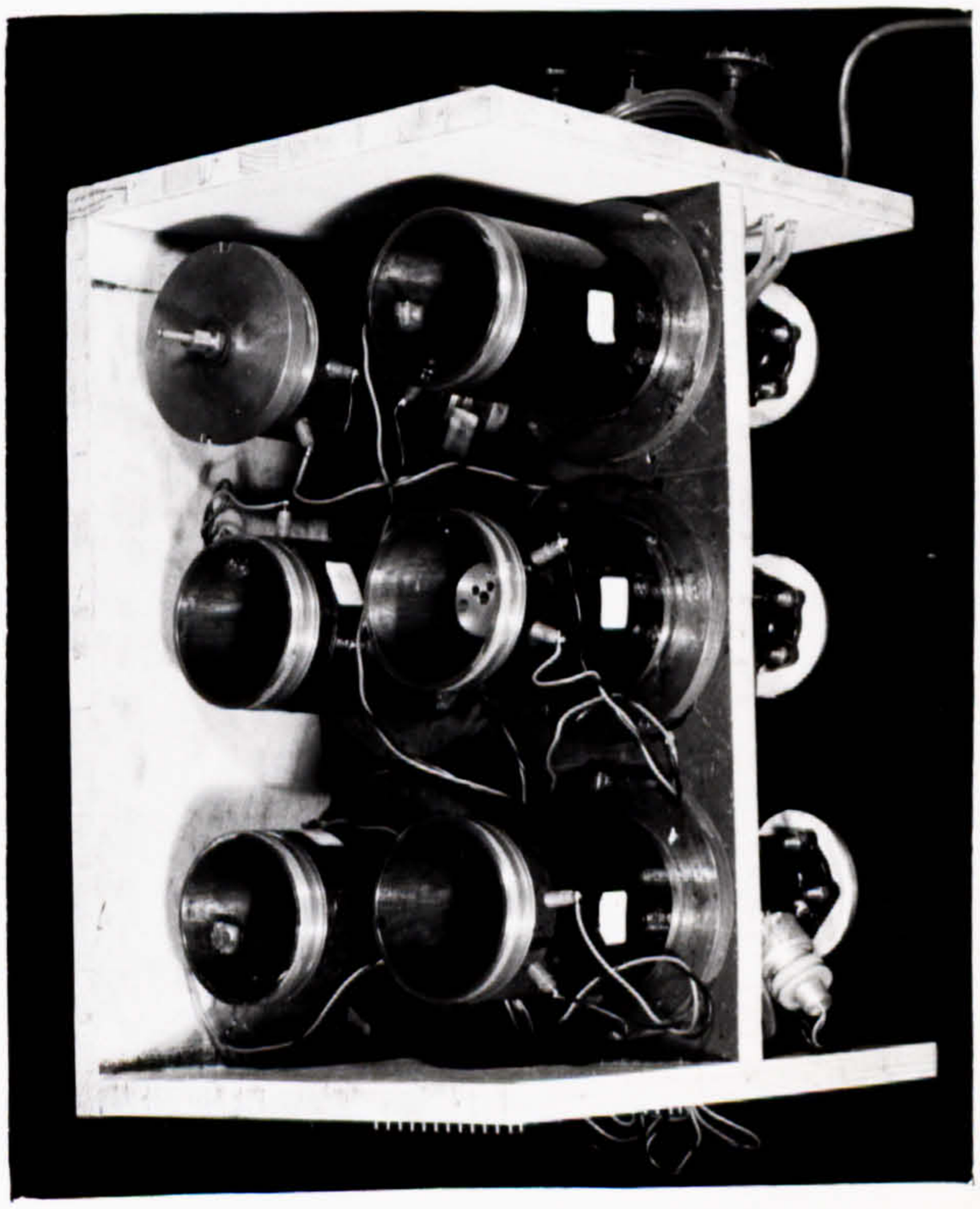

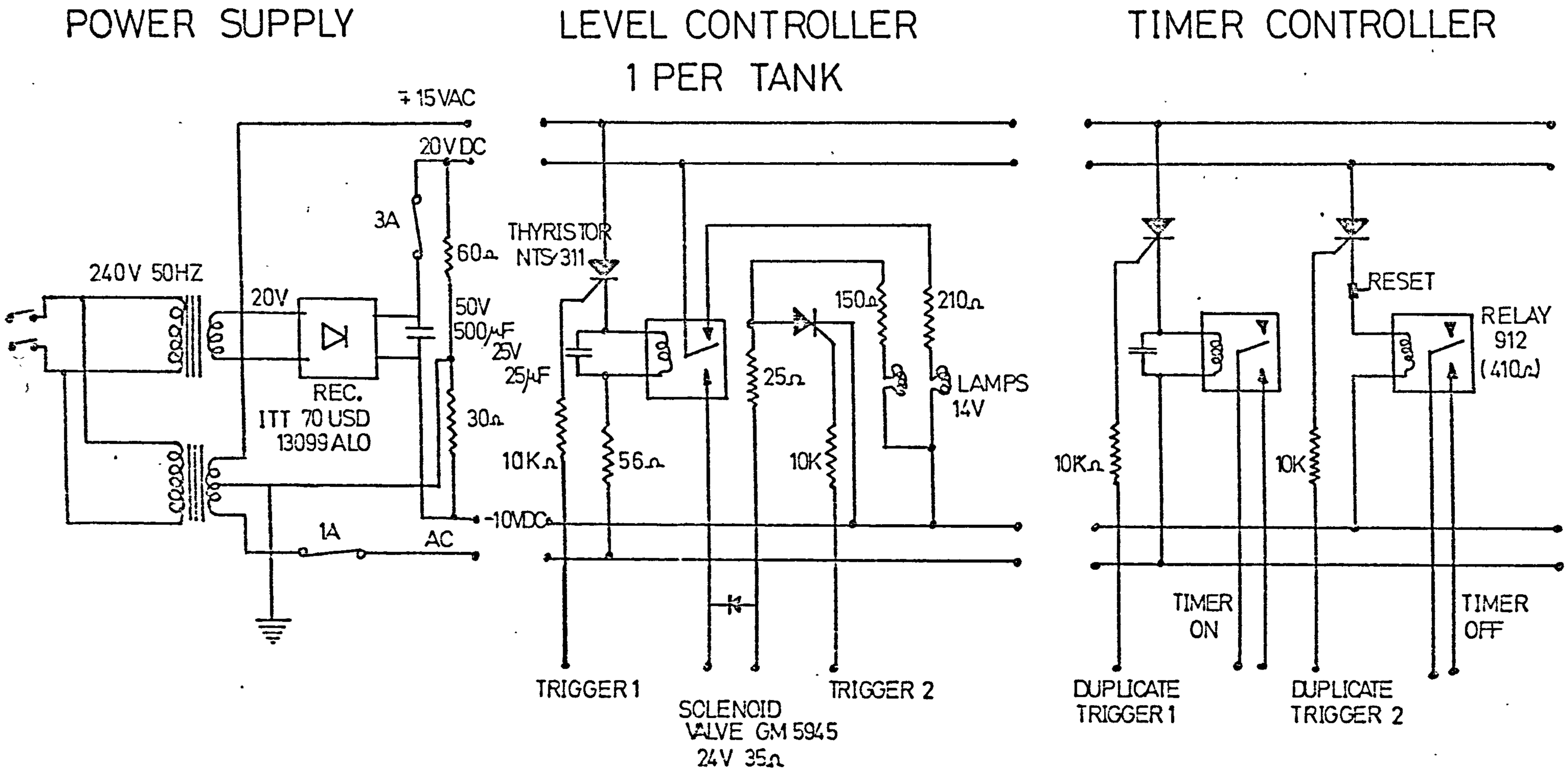

FIG 74 ELECTRONIC CONDENSATE MEASUREMENT

the steam jacket and the electronic controller circuit layout.

F: DRYNESS MEASUREMENT

A steam sample was removed from the steam plenum at a point approximately central to the chamber. The sample line was well lagged to minimise heat losses and terminates in a needle valve. Dryness measurements were made by a calorimetric method. A wide necked thermos flask was fitted with a stirrer, thermometer (^{o}F) and a glass sparger pipe. The water equivalent of the unit was found by experiment (see SECTION 3.5.1. later) and the exact experimental method used to measure dryness is detailed later.

Typical dryness fractions from 0.8 to 0.98 were found.

3.5. EXPERIMENTAL

3.5.1. CALIBRATION

A: SURFACE TEMPERATURE

The six surface thermocouples of the disc were calibrated against the four inlet and three outlet thermocouples whose calibration procedure is described earlier in SECTION 2.6.1:C.

The disc was bolted into position and a steady flowrate of some 500 cm^3/s set up on the disc. The heaters and cooler on the supply side were adjusted to give a steady temperature of fluid delivered to the disc. A maximum temperature of 50°C was used. The equipment was allowed about 1 hr to come to equilibrium. The output from the inlet and outlet thermocouples was logged and an average value of the surface thermocouples output noted. Some cooling of the fluid was noted from inlet to outlet, for example at 50°C the temperature fell by some 1°C according to the difference in the thermocouple readings. At any temperature the surface thermocouples agreed to each other to within $\pm$ 0.7°C and to within $\pm$ 1°C of the mean fluid temperature. The calibration curve applicable to the inlet/outlet thermocouples was therefore applied to the surface thermocouples.

B: WATER EQUIVALENT OF CALORIMETER

A known quantity (m) of cold water was placed within the thermos flask and allowed to equilibrate to the flask's temperature. The water temperature was measured (T_c), and the flask and contents weighed (M). A quantity of water was heated to a steady temperature (T_H) and quickly added to the flask. The mixture was quickly stirred and the resultant temperature (T_m) and weight (G) noted. The water equivalent of the thermos flask is given by

$$W.E = \frac{m(T_m - T_c) + (G - M)(T_m - T_H)}{T_c - T_m} \qquad 204$$

The process was repeated several times and the water equivalent of the flask found to be 51 g $\pm$ 3 g.

C: PROCEDURE

The steam supply to the disc was gradually opened (over 10 minutes)

until the plenum pressure was some 1 - 2 psig and the drainage steam traps appeared to function satisfactorily. The electronic equipment was switched on, supply tank water checked and the ice point thermos flask recharged. About one hour was allowed for the main disc bearings to come to operating temperature (60°C) as indicated by the thermocouple fixed to the housing.

The steam was then turned down and the main supply and drainage pumps started. The disc was brought up to a steady low speed (some 100 r.p.m.) and the liquid supply to the disc carefully opened. Initial liquid caused the remaining plenum steam to condense and when the plenum pressure gauge indicated zero the hydrodynamic procedure for creating a steady thin film was followed as quickly as possible (SECTION 2.6.2:A).

When the film was established the steam supply to the disc was gradually opened in 5 psig steps (according to the governor pressure reading) until the plenum pressure indicated some 3 - 5 psig. The flow-rate and speed required for this experimental run were then set, cooling applied to the supply fluid if necessary, and the equipment allowed some 30 minutes to stabilise.

The calorimeter thermos flask was weighed empty, half filled with cold water and re-weighed. The flask was placed ready by the steam sample line. The sample valve was partly opened to heat the sample line thoroughly, and the six glass flasks to be used in the condensate collection runs warmed (by steam sparging), dried and weighed.

The data logger was started to note the inlet, surface and outlet temperature EMF's. In turn the condensate drain lines were placed into the receiver flasks and the appropriate stop-watch started. The water temperature in the calorimeter thermos flask was noted and the steam sparger connected to the steam sample line, and a stop watch started.

When sufficient condensate had been collected in a receiving flask, the condensate hose was put to drain and the appropriate stop watch stopped. When all six receivers were so filled the logger was stopped and note made of the disc speed and liquid flowrate (visual checks during the run confirmed that these values held steady). When the calorimeter flask had reached some 140°F or higher the sampling was stopped and the elapsed time noted. The flask was re-weighed and the temperature noted. The steam sample process was again repeated, but this time at a slightly different sample rate. APPENDIX K details the way in which, assuming

that the steam quality was steady over the subsequent samples, knowledge of the differing 'apparent' dryness fractions can be used to indicate the true dryness.

The data logger tape was removed, labelled and later analysed to give the inlet, outlet and surface temperatures. The condensate flasks were reweighed and dried and the disc speed and liquid flowrate reset for the next run.

After some time surface thermocouple number 2 (at 6 cm radius) ceased to function (presumably due to breakage of the brittle leads) and the surface temperature at this point was estimated by interpolation from the remaining five values.

3.6. RESULTS AND DISCUSSION

Some sixty heat transfer runs were performed and the results are tabulated in APPENDIX E. Heating rates ranged from 9.6 to 29 kW (equivalent to fluxes from 140 to 430 kW/m^2), speeds from 187 to 728 r.p.m., flowrates from 35 to 420 cm^3/s, steam dryness fractions from 0.8 to 0.98 and film temperature gains of some 50°C on average.

In general increasing the liquid flowrate, increasing the rotational speed and decreasing the feed temperature all caused the heat flux to increase.

An approximate heat balance may be conducted by knowledge of the film inlet and outlet temperatures and flowrate compared to the heat liberated by the condensate collected. Since the collected condensate is applicable only for the heat transfer area up to 15 cm radius the additional likely condensate heat for the remaining uncollected area (up to 20 cm radius) is estimated from the average of the condensate collected by the outer collecting rings. This can be used to provide a second heat balance. Under normal circumstances the first balance should indicate a greater heat content of the film and the second should indicate a nearer balance (or reverse situation). In practice this was found for nineteen of the sixty runs. In twenty six of the runs the second heat balance still indicates that the film contains greater heat than the actual + estimated condensate rates can account for. Of these twenty six runs, eight indicated an imbalance from 10 - 20% and eight more an imbalance from 20 - 29%. One presumes that for (19 + 10) runs the heat balance is satisfactory, for a further sixteen runs the heat balance may indicate unusually increased heat transfer at the very outer edge of the disc. Loss of collected condensate is ruled out due to the satisfactory heat balances obtained at some higher fluxes, i.e. the collectors functioned satisfactorily at heavier loading.

In fifteen of the sixty runs both heat balances indicated greater heat transferred from the steam than was accounted for in the film side heat balance. It was noted experimentally that these runs were accompanied by significant steaming and evaporation from the film surface. A special amendment was made to the processing program (APPENDIX G: PROGRAM EXPAN) which used the final heat balance mismatch to proportion out the evaporation loss over the disc and adjusted the film temperature and condensate heat accordingly.

FIGURE 75 shows all the data collected correlated against the general groups $(Re^2/Ta)^{\frac{1}{2}}(R)^{\frac{3}{2}}(Pr)$. The correlation found is

$$Nu = 10^{-2} \cdot \left(\frac{Re^2}{Ta}\right)^{\frac{1}{2}} R^{\frac{3}{2}} Pr^2 \qquad 205$$

suitable for the ranges

$$0.05 < \frac{Re^2}{Ta} < 30000$$

$$1.33 < R < 4.66$$

$$8.2 > Pr > 2.2$$

Equation 205 is representative of the data to $\pm$ 50%.

FIGURES 76 - 81 show some heat transfer data plotted against the inlet parameter $((Re^2/Ta)_i^{\frac{2}{3}} Pr)$. Only data for which $Re^2/Ta < 4$ and the mismatch between the second heat balance was less than 10% has been plotted. In addition if any evaporation correction was involved the plotting symbols are marked more heavily.

It will be seen that no data at the first radius (R = 1.33) satisfies these criteria. In each of the remaining figures the data lies about the theoretical line with little difference between those points with and those without any evaporation correction. Thus to some extent the evaporation correction has been validated (see for example the overlapping of data in FIGURE 79). In general, data for very low Re^2/Ta (circles) lies below the theoretical solution, contrary to expectations since one of the theoretical assumptions is that the hydrodynamics are represented by the non-Coriolis model ($Re^2/Ta < 1$). However one possible explanation may be offered. The low values of Re^2/Ta were obtained mainly at very low flowrates for which significant evaporation occurred. It is suggested that for this data the film was broken into rivulets towards the edge of the disc. Visual evidence in support of this suggestion could not be collected since the high evaporation rates and speeds rendered <u>any</u> visual examination difficult. Attempts to employ the capacitometer film thickness measurement circuit were rejected due to the invalidating condensation of steam on the probe that would surely occur.

Deviation above the theoretical line occurs at the higher values of Re^2/Ta and there is the possibility of the Coriolis force that will

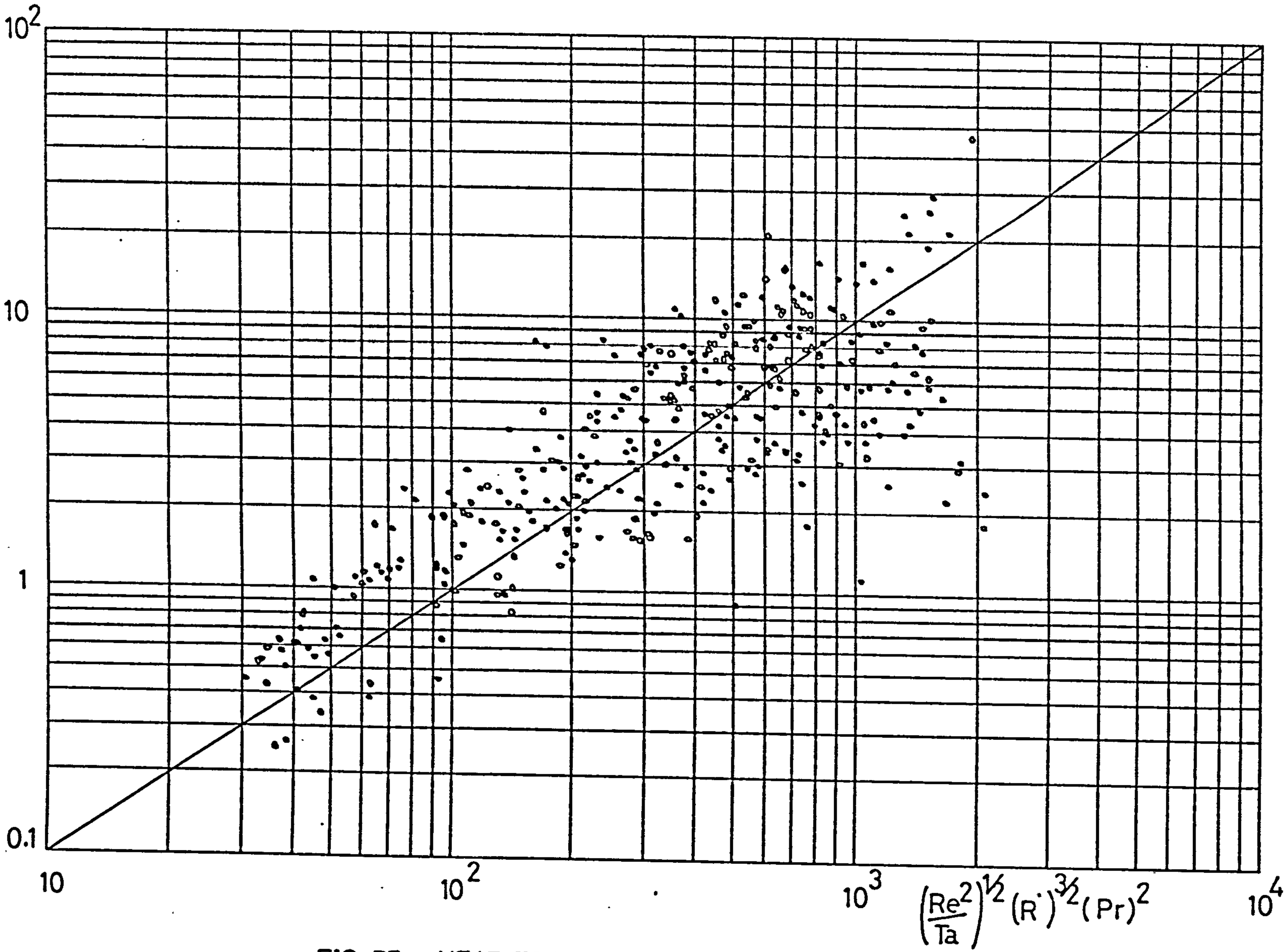

FIG 75 HEAT TRANSFER CORRELATION

FIG 76 HEAT TRANSFER

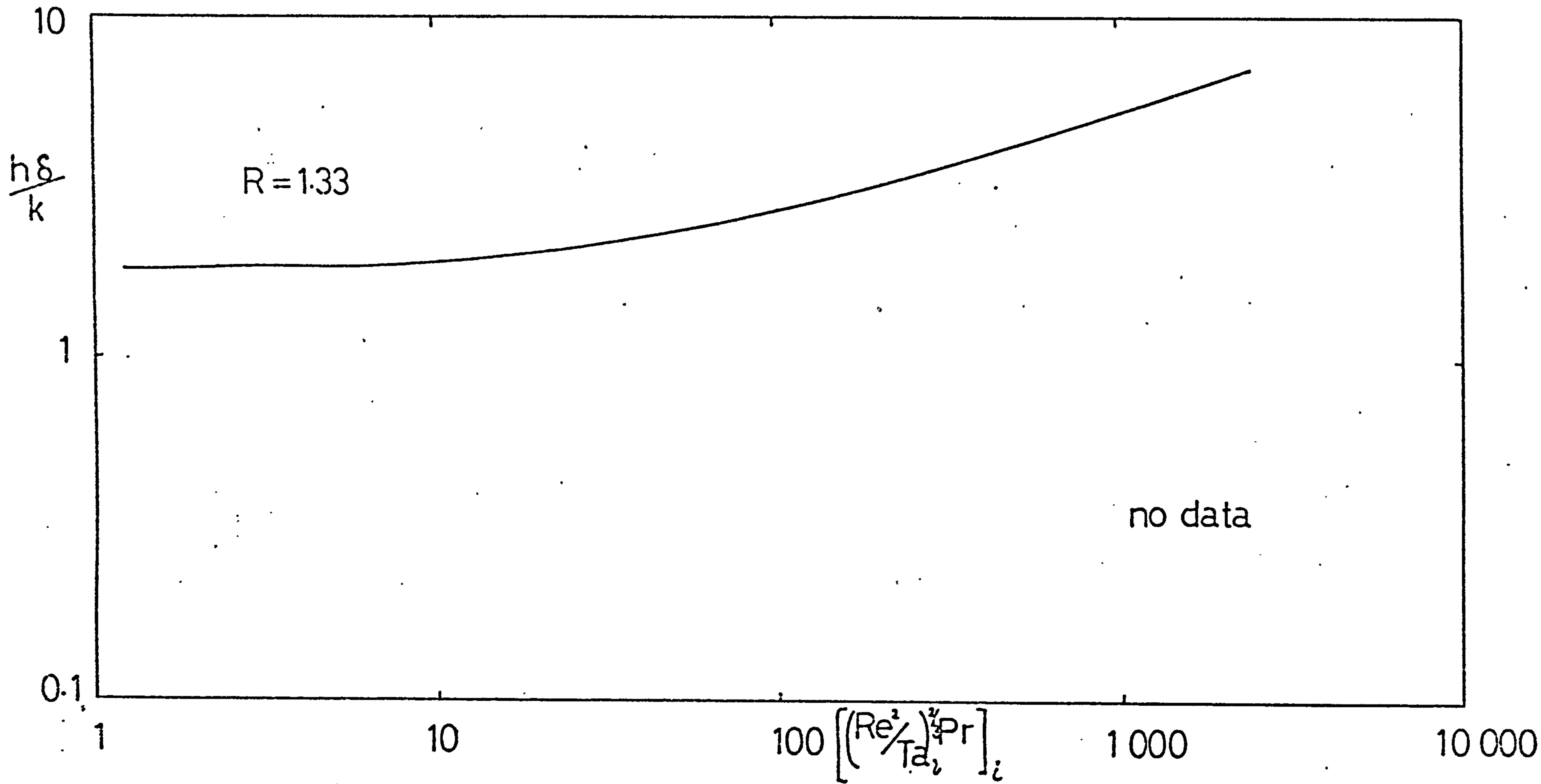

FIG77 HEAT TRANSFER

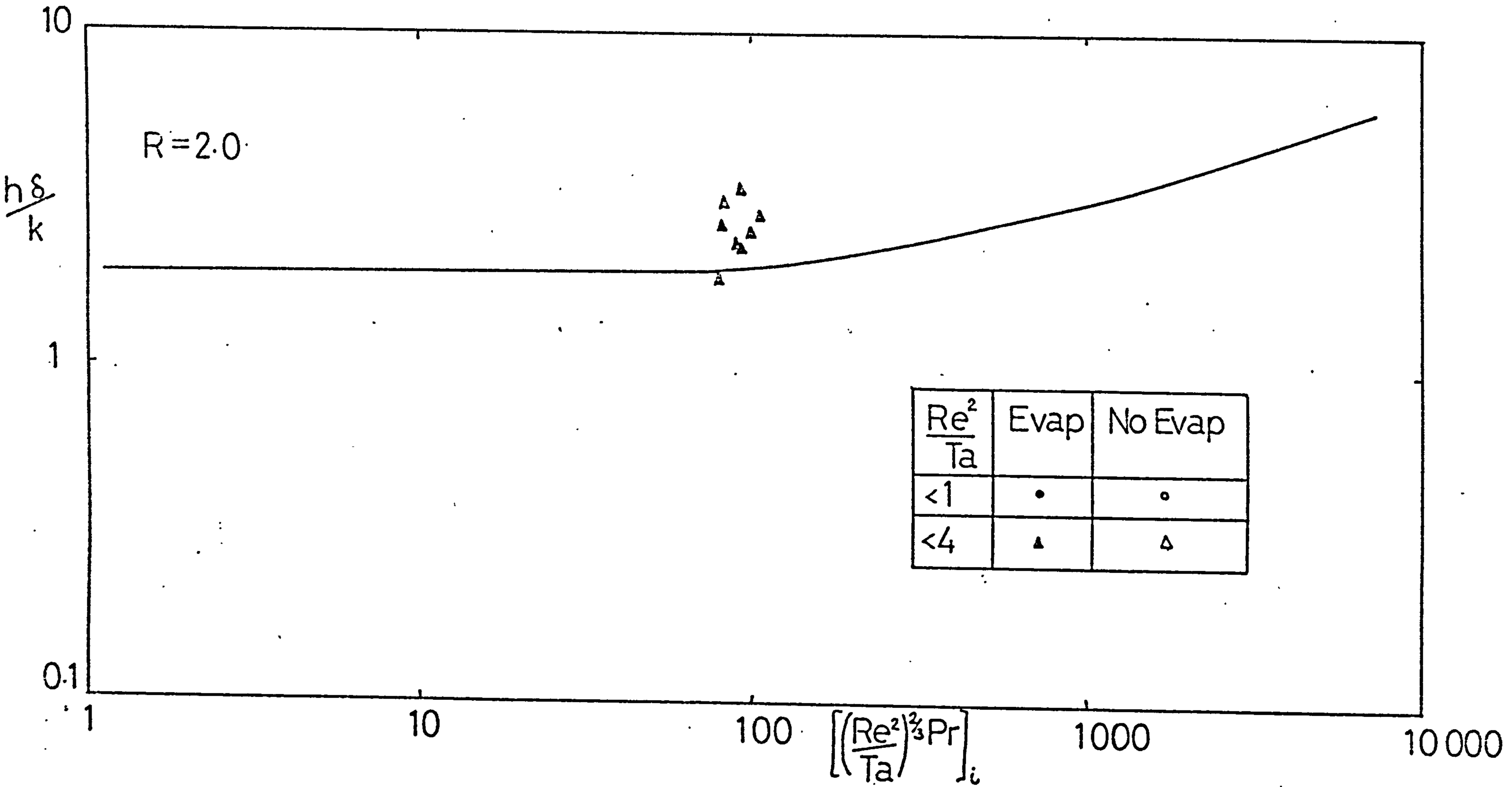

FIG 78 HEAT TRANSFER

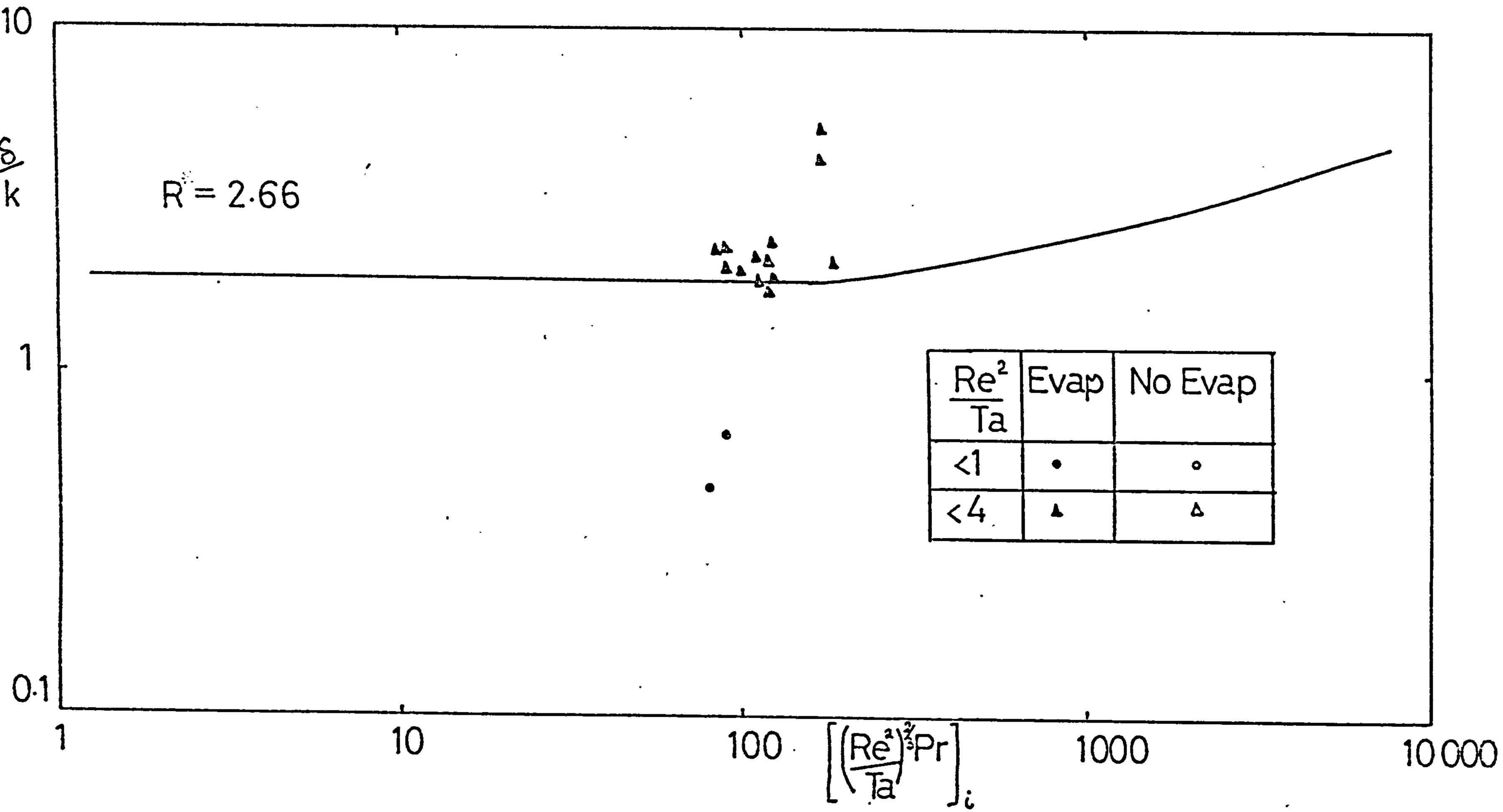

FIG 79 HEAT TRANSFER

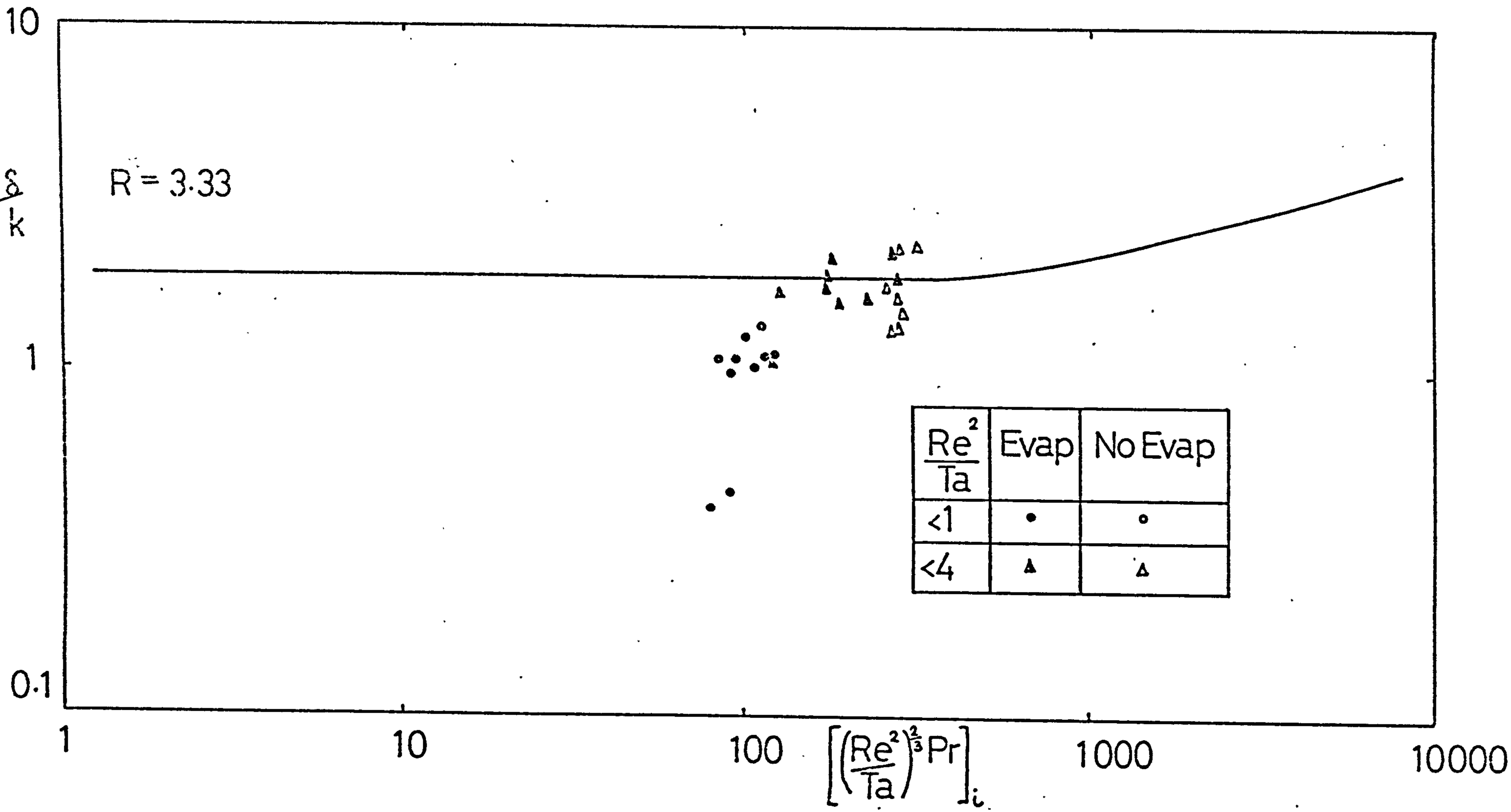

FIG80 HEAT TRANSFER

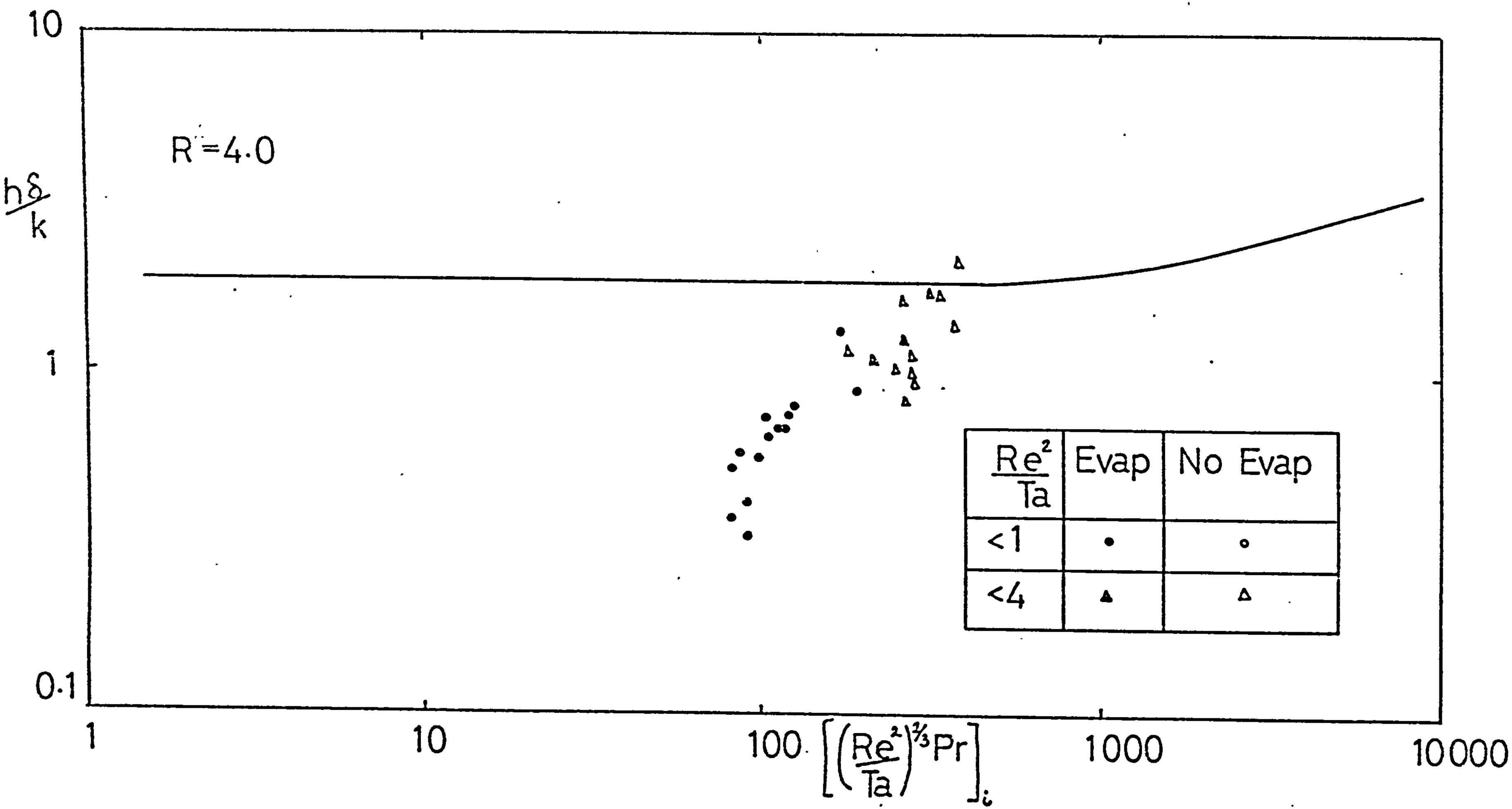

FIG81 HEAT TRANSFER

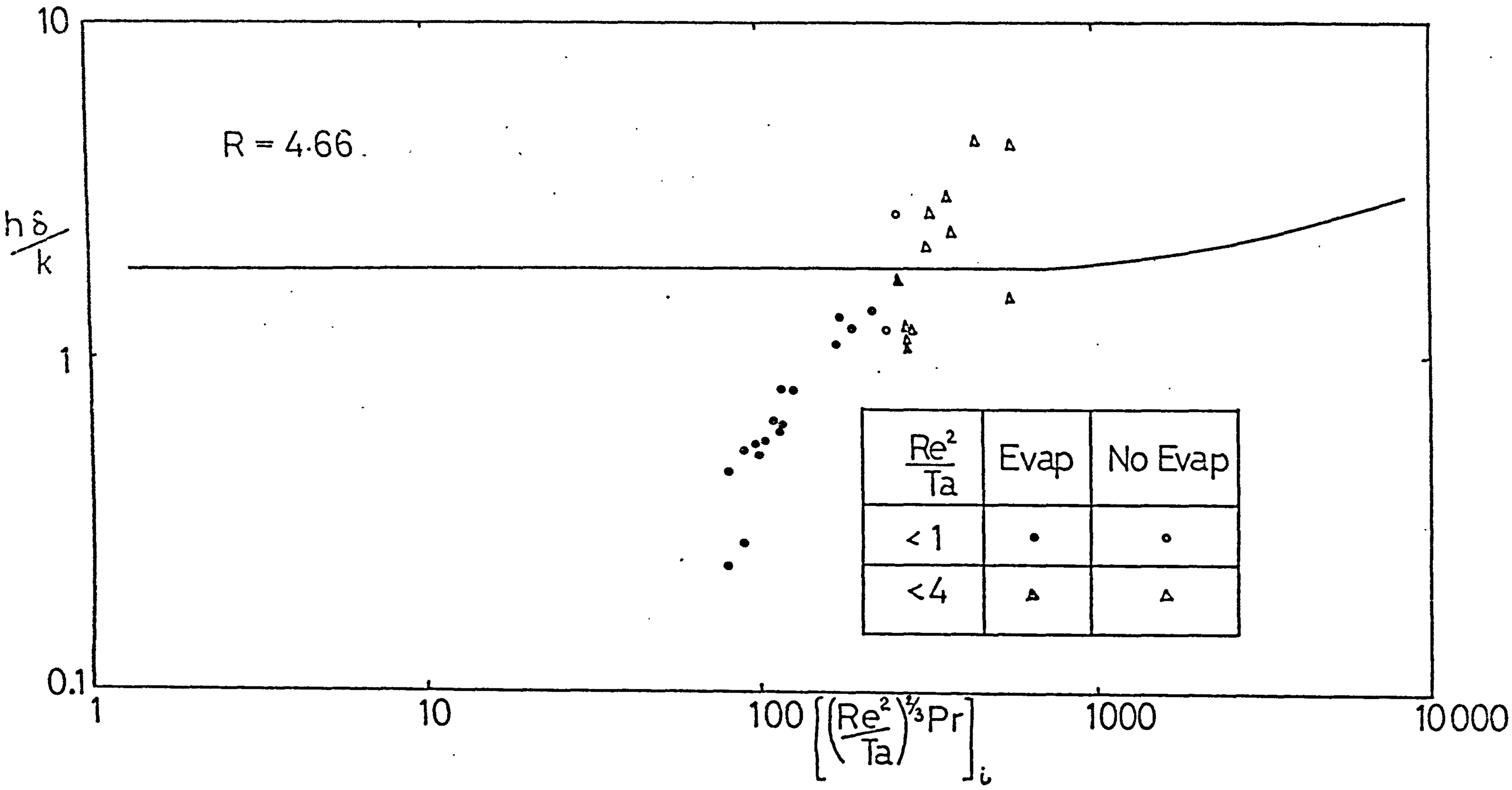

exist in these circumstances invalidating the theoretical model assumptions sufficiently to make comparison unreasonable. At each radius a line through the experimental results shows either a point of inflection or an asymptotic levelling about the theoretical line. In view of the unsatisfied assumptions of the theory (viz. that the fluid physical properties are independent of temperature, disc surface temperature is radially constant, fluid velocity and temperature profiles are fully developed at inlet and no heat or evaporation mass loss from the free surface) and the experimental inaccuracies in the measurements the agreement is surprisingly good. Obviously, however, the theoretical model requires much more experimental validation.

The steam-side heat transfer coefficients of the disc are compared against the condensation theories in FIGURE 82. It can be seen that a fairly good correlation is found independent of the radius of the measurement. This radial independence is in agreement with the models of SECTION 3.1.3:B. The group $\frac{h}{k}\left(\frac{\omega}{\nu}\right)^{1/2}$ theoretically varies with the group $\left(\frac{h_{fg}\mu}{k\Delta T}\right)$ and to a lesser extent with the steam Prandtl number. That a definite and unique relationship exists between these two groups is evident from FIGURE 82. Calculating the equivalent theoretical variation from SPARROW and GREGG (72) however shows that the experimental results are some 10 times greater than the theoretical values (see FIGURE 82). As an explanation of this phenomena it should be remembered that the disc fins which separate each heat transfer annuli will invalidate the assumptions of the theoretical model in at least two ways. Firstly the rings will produce a degree of agitation in the vapour phase which the theoretical models take to be quiescent. Secondly, each ring throws off the condensate of the preceding section. Hence each annulus consists of a short flow path condensing region over the initial portion of which high transfer rates will be produced due to the thin condensate film (the models assume that condensate at any radius corresponds to the cumulative total up to and including that radius). A further possibility for the high heat transfer rates could be the presence of drop condensation well known to give enhanced rates. An obvious possibility that the rings act as fins and enhance the heat transfer that would have occurred at the fin root were the fin removed, may be discounted on two counts. Firstly the enhancement of the fin was usually less than unity (i.e. the fin shielded the root area) and secondly the total area thus influenced is small compared to that otherwise available.

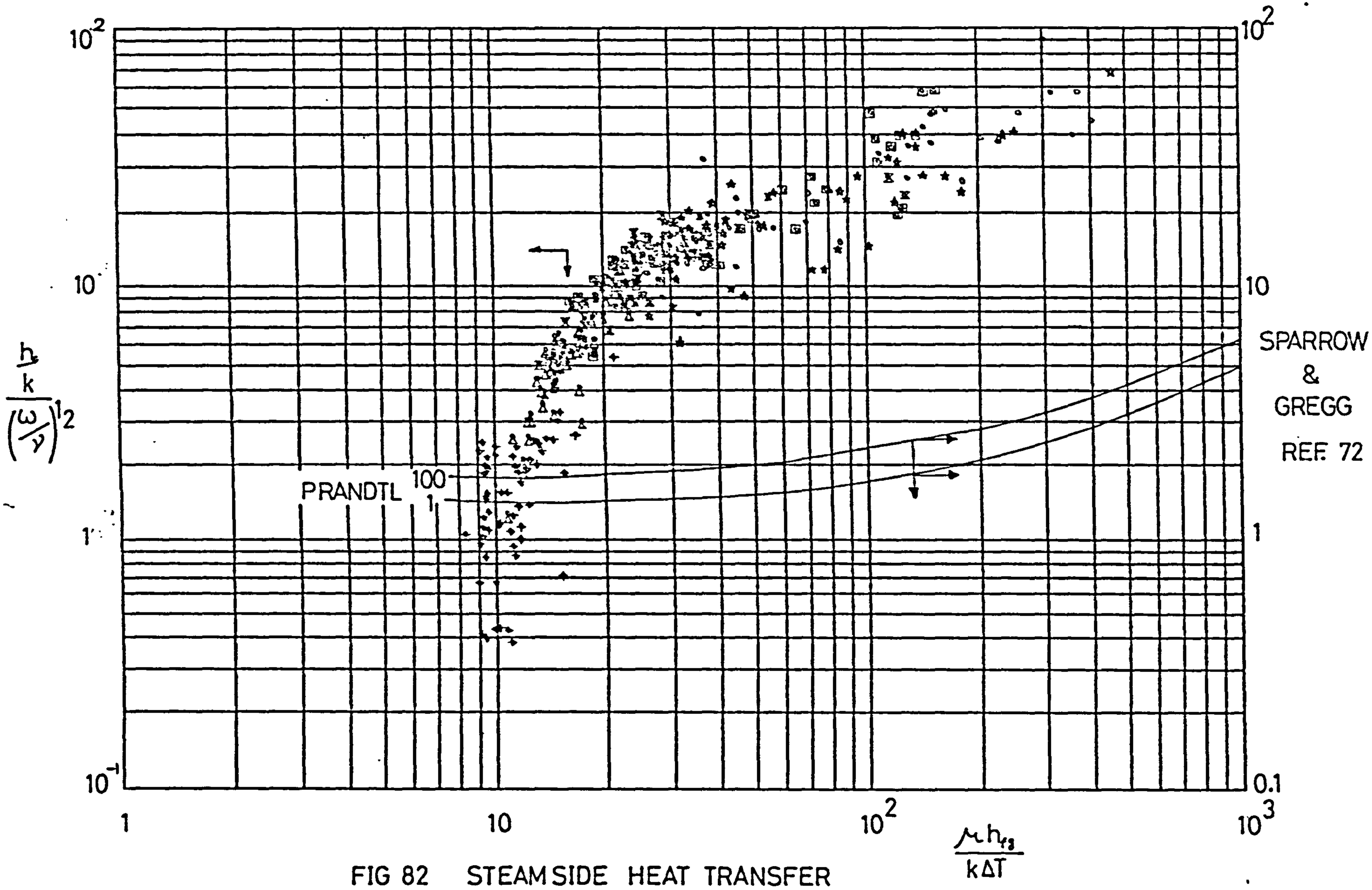

FIG 82 STEAM SIDE HEAT TRANSFER

3.7. CONCLUSIONS

1. Theoretical results are given for a simple heat transfer model for the heating film.

2. Subject to the experimental errors and bearing in mind the assumptions of the theoretical model, experimental heat transfer results are in reasonable agreement with the model.

3.8. FUTURE WORK

1. The theoretical model should be developed to include the effects of the Coriolis force found in the hydrodynamic section. This could be achieved by linking the hydrodynamic program CORIOL to a general heat transfer program. The resulting digital program is likely to be large and an analogue solution may be more suitable.

2. To augment the more general solution proposed above incorporation of the following points should be considered.

   2.1. inclusion of temperature dependent fluid properties
   2.2. provision for non-Newtonian fluids
   2.3. inclusion of interfacial drag and interfacial heat and evaporation losses
   2.4. inclusion of the vertical convective term ($v_y \partial T/\partial y$)

3. The experimental program should be extended to include

   3.1. non-evaporative (low vapour pressure) and temperature sensitive fluids (the latter subject to the proviso of 2.1 above)
   3.2. non-Newtonian fluids of commercial and industrial significance as mentioned in the hydrodynamic sections
   3.3. tests with fluids with variable physical properties which are essentially constant at one operating temperature. For example, Diala Oil B (a transformer oil) has widely variable properties ideally suited for these tests.

4. In order that the experimental accuracy of the measurements be improved a continuous method of steam quality monitoring should be developed and installed. The condensate measurement technique proposed but not utilised for this work should be developed to completion and utilised.

5. Simultaneous heat transfer measurement with film thickness measurements for non-evaporating liquids. The entire experimental Nusselt number (utilising an experimental δ rather than a theoretical value) may then be found and compared to theory.

4. REFERENCES

1. BIGELOW, W.D.
   The Logarithmic nature of thermal death time curves
   J. Infectious Diseases 29 (1921), 528 - 536

2. VITER, A.V., ZAICHENKO, M., MARCHENKO, M., PLAUNIK, V.P.
   Concentration of solutions containing thermolabile and foaming substances
   Khim. Farmat. Zhur 12 (1968), 45 - 47

3. HICKMAN, K.C.D.
   High Vacuum Short path distillation - A review
   Chem. Reviews 34 (1944), 51 - 106

4. KODAK Ltd.
   Method for the preparation of Vitamin D in high yields
   United Kingdom Patent 482,880 (6 April 1938)

5. KODAK Ltd.
   Improved method of distilling large quantitites of liquid
   United Kingdom Patent 482,883 (6 April 1938)

6. WATT, P.R.
   Improvements in or relating to Molecular Distillation Apparatus
   United Kingdom Patent 765,743 (9 January 1937)

7. LEYLAND, J., WHITELEY, K.B.
   Improvements in Heat Exchangers
   United Kingdom Patent 835,055 (18 May 1960)

8. LEIDENFROST, W., EISELLE, E.H.
   Rotating heat exchangers and optimisation of a heat pump
   Inst. Elec. Elect. Engrs. (I.E.E.E.) Trans. on Ind. Appl.
   IG A8 (1972) 345 - 354

9. LEIDENFROST, W.
   Private Communication

10. BLAKEBROUGH, N.
    Biochemical and Biological Engineering Science Vol. II
    Academic Press (London) 1968

11. KAMIYA, T., KAYANO, A.
    Film type disintegration by rotating disc
    J. Chemical Eng. Japan 5 (1972) 174 - 182

12. KAMIYA, T.
An analysis of the ligament type disintegration of thin liquid film at the edge of a rotating disc
J. Chemical Eng. Japan 5 (1972) 391 - 396

13. MARSHALL, W.R. Jnr.
Atomisation and Spray Drying
Chemical Eng. Progress Monograph Series No. 2 Vol. 50 (1954)

14. OYAMA, Y., EGUTI, M., ENDOU, K.
Studies on the atomisation of water droplets
Kaguku Kosaker 17 (1953) 269 - 275

15. TANASAWA, Y., MIYASAKA, Y., UMEHARA, M.
On the filamentation of liquid by means of rotating discs
Trans. Japan Soc. Mech. Engrs. 25 (1958) 897 - 905

16. BOOMER, D.R., McCune, C.C., FOGLER, H.S.
Rotating disc apparatus for reaction studies in corrosive liquids
Review of Scientific Instruments 43 (1972) 225 - 229

17. DESLOUIS, C., KEDDAM, M.
Use of rotating electrode rings to study mass transfer in a laminar or turbulent regime
Int. J. Heat & Mass Transfer 16 (1973) 1763 - 1775

18. KADIJA, I.V., NAKIC, V.M.
Ring electrodes on rotating disc as a tool for investigation of gas evolving electrochemical reactions
J. Electroanalytical Chemistry 34 (1972) 15 - 19

19. LITT, M., SERAD, G.
Chemical Reactions on a rotating disc
Chem. Eng. Science 19 (1964) 867 - 884

20. DUNNING, I.W., MOSES, A.K., TOTH, M.J.
High Velocity Film Heat Exchanger
U.S.A. Patent 2,779,724 (29 January 1957)

21. ANON.
Heat sensitive materials yield to unique falling film evaporator
Chem. Eng. 70 (1963) 64 - 66

22. PONIKAROV, I.I., KAFAROV, V.V., DULATOV, Yu.A.
Limiting flow rates in a centrifugal extractor with corrugated discs
J. Applied Chem. USSR 45 (1972) 2090 - 2093

23. BEARDALL, L.R.
Liquid film flow and solid liquid separation on a rotating inclined surface
Ph.D. Thesis Loughborough University 1968

24. NUSSELT, W.
Die Oberflachenkondensation des Wasserdampfes
Z. Vereines Deut. Ing. 60 (1916) 541 - 546

25. DUCKLER, A.E., BERGELIN, O.P.
Characteristics of flow in falling liquid films
Chem. Eng. Prog. 48 (1952) 557 - 563

26. PRANDTL, L.
Neure Ergebrisse der Turbulenzforschung
Z. Vereines Deut. Ing. 77 (1933) 105 - 114

27. NIKURADSE, J.
Gesetzmassigkeiten der turbulenten stromung in glatten rohren
Vereines Deut. Ing. Forschungsheft 356 October 1932

28. CHURCHILL, S.W., CHOI, B.
A simple expression for the velocity distribution in turbulent flow in smooth pipes
Amer. Inst. Chem. Engrs. J. 19 (1973) 196 - 197

29. PORTALSKI, S.
Velocities in film flow of liquids on vertical plates
Chem. Eng. Science 19 (1964) 575 - 582

30. PORTALSKI, S.
Studies of falling liquid film flow film thickness on a smooth vertical plate
Chem. Eng. Science 18 (1963) 787 - 804

31. DUCKLER, A.E.
Fluid mechanics and heat transfer in vertical falling film systems
Amer. Inst. Chem. Engrs. 56 (1960) 1 - 10

32. DEISSLER, R.G.
Analysis of turbulent heat transfer, mass transfer and friction in smooth tubes at high Prandtl and Schmidt numbers
N.A.C.A. Tech. Note 3145 (1959)

33. FULFORD, G.D.
Gas-liquid flow in an inclined channel
Ph.D. Thesis, Birmingham University 1962

34. LUKACH, Yu. Ye., KADCHENKO, L.B., TANANAYIKO, YU. M.
Determining the average thickness of a water film during gravitational flow over the outer surface of vertical pipes made of polymers
Int. Chem. Eng. 12 (1972) 517 - 519

35. KAPITSA, P.L.
Wave flow of thin layers of a viscous fluid
Collected works of P.L. Kapitsa Vol. II
Pergammon Press (London) 1965 pp 662 - 709

36. PORTALSKI, S.
The mechanism of flow in wetted wall columns
Ph.D. Thesis London University 1960

37. FULFORD, G.D.
The flow of liquids in thin films
Advances in Chem. Eng. 5 (1969) 151 - 236

38. KASIMOV, B.S., ZIGMUND, F.F.
The relationships in film flow on a vertical cylindrical tube
Inz. Fiz. Zhur. Akad. Nauk. Belorussk 5 (1962) 71 - 74

39. JACKSON, M.L., JOHNSON, R.T., CEAGLSKE, N.H.
Surface velocities of liquid films in the streamline flow region
Proc. First Midwestern conf. on Fluid dynamics, Urbana, Illinois (1950) J.W. Edwards, Ann Arbor, Michigan (1951) pp 226 - 236

40. JACKSON, M.L.
Liquid films in viscous flow
Amer. Inst. Chem. Engrs. J. 1 (1955) 231 - 240

41. FRIEDMAN, S.J., MILLER, C.O.
Liquid films in the viscous flow region
Ind. Eng. Chem. 33 (1941) 885 - 890

42. TINNEY, E.R., BASSETT, D.L.
Terminal shape of a shallow liquid front
Proc. Amer. Soc. Civil Engrs. (J. Hyd. Div) 87 (1961) 117 - 133

43. WEST, D., COLE, R.
Surface velocities of thin liquid films
Chem. Eng. Science 22 (1967) 1388 - 1389

44. GOODRIDGE, F., GARTSIDE, G.
Mass transfer into near horizontal liquid films.

Part 1: Hydrodynamic Results
Trans. Inst. Chem. Engrs. 43 (1965) 62 - 67

45. CLAYTON, C.G.A.
The behaviour of liquid films in counter-current two phase flow
Ph.D. Thesis Cambridge University 1958

46. WILKES, J.O., NEDDERMAN, R.M.
The measurement of velocities in thin films of liquid
Chem. Eng. Science 17 (1962) 177 - 187

47. COOK, R.A., CLARK, R.H.
The experimental determination of velocity profiles in smooth falling liquid films
Canadian J. Chem. Eng. 49 (1971) 412 - 416

48. ABSJØRNSEN, O.A.
The distribution of residence times in a falling water film
Chem. Eng. Science 4 (1961) 211 - 227

49. GRIMLEY, S.S.
Effects of liquid flow conditions on the performance of packed towers
Ph.D. Thesis London University 1946

50. ATKINSON, B., CARUTHERS, P.A.
Velocity profile measurements in liquid films
Trans. Inst. Chem. Engrs. 43 (1965), 33 - 39

51. BRAUER, H.
Stromung und warmeiibergang bei rieselfilmen
Vereines Deut. Ingr. Forschungsheft 457 (1956)

52. DAVIES, J.T.
University research in Chemical Engineering
Birmingham University Chem. Eng. 12 (1961) 5 - 9

53. KIRKBRIDE, C.G.
Heat transfer by condensing vapour on vertical tubes
Trans. Amer. Inst. Chem. Engrs. 30 (1934) 170 - 186

54. STAINTHORP, F.P., WILD, G.J.
Film flow: the simultaneous measurement of wave amplitude and local mean concentration of a transfer component
Chem. Eng. Science 22 (1967) 701 - 704

55. KOSKY, P.G.
Thin liquid films under simultaneous shear and gravity forces
Int. J. Heat & Mass Transfer 14 (1971) 1220 - 1224

56. BAUER, W.J.
Turbulent boundary layer on steep slopes
Trans. Amer. Soc. Civil Engrs. 119 (1954) 1212 - 1233

57. KRANTZ, W.B., GOREN, S.L.
Stability of thin liquid films flowing down a plane
Ind. & Eng. Chemistry Fundamentals 10 (1971) 91 - 101

58. BENJAMIN, T.B.
Wave formation in laminar flow down an inclined plane
J. Fluid Mechanics 2 (1957) 554 - 574

59. PORTALSKI, S., CLEGG, A.J.
An experimental study of wave inception on falling liquid films
Chem. Eng. Science 27 (1972) 1257 - 1265

60. PLINI, C., SECUNDUS
Naturalis Historia Book II pp CVI

61. KEULEGAN, G.H.
Wind tides in small closed channels
J. Res. National Bureau Standards 46 (1951) 358 - 381

62. MOORE, W.J.
Physical Chemistry
Longmanns (London) 4th Edition 1968

63. KITCHENER, J.A.
Foams and free liquid films
Recent Prog. in Surface Science 1 (1964) 51 - 91

64. LIN, S.P.
Stabilising effects of surface active agents in a film flow
Amer. Inst. Chem. Engrs. J. 16 (1970) 375 - 379

65. SMITH, F.I.P., CRAIK, A.D.
Wind generated waves in thin liquid films with soluble contaminant
J. Fluid Mechanics 45 (1971) 527 - 544

66. ANSHUS, B.E., ACRIVOS, A.
The effect of surface active agents on the stability of characteristics of falling liquid flims
Chem. Eng. Science 22 (1967) 389 - 393

67. TAILBY, S.R., PORTALSKI, S.
Wave inception on a liquid film falling down a hydrodynamically smooth plate
Chem. Eng. Science 17 (1962) 283 - 290

68. WHITAKER, S., CERRO, R.L.
Some comments on the hydrodynamics of thin liquid films
Chem. Eng. Science 29 (1974) 963 - 965

69. CERRO, R.L., WHITAKER, S.
Entrance region flows with a free surface: the falling liquid film
Chem. Eng. Science 26 (1971) 785 - 798

70. LYNN, S.
The acceleration of the surface of a falling film
Amer. Inst. Chem. Engrs. J. 6 (1960) 703 - 705

71. AULT, J.W., ORVILLE, C.S.
Entrance effects in liquid film flow
Canadian J. Chem. Eng. 50 (1972) 318 - 322

72. NORMAN, W.S., McINTYRE, V.
Heat transfer to a liquid film on a vertical surface
Trans. Inst. Chem. Engrs. 38 (1960) 301 - 307

73. McPHERSON, G.D.
Axial stability of the dry patch formed in dry-out of a two phase annular flow
Int. J. Heat & Mass Transfer 13 (1970) 1133 - 1151

74. HARTLEY, D.E., MURGATROYD, N.
Criteria for the break-up of thin liquid layers flowing isothermally over solid surfaces
Int. J. Heat & Mass Transfer 7 (1964) 1003 - 1015

75. PONTER, A.B., DAVIES, G.A., ROSS, T.K., THORNLEY, P.G.
The influence of mass transfer on liquid film breakdown
Int. J. Heat & Mass Transfer 10 (1967) 349 - 359

76. RUCKENSTEIN, E.
On the break-up of thin liquid layers flowing along a surface
Int. J. Heat & Mass Transfer 14 (1971) 165 - 169

77. WILSON, S.D.R.
The stability of a dry patch on a wetted wall
Int. J. Heat & Mass Transfer 17 (1974) 1607 - 1615

78. NORMAN, W.S., ALGAWI, M.O., GARNER, F.H.
The cooling and dehumidification of air with refrigerated brine in a grid-packed tower.
Symposium on Gas Absorption, Inst. Chem. Engrs., 1954, S14-S37

79. PONTER, A.B., BOYES, A.P.
The rupture of isothermal vertical liquid films
J. Chem. Eng. Japan 5 (1972) 80 - 83

80. ROBERTS, A.D., TABOR, D.
Mechanical properties of very thin surface films
Thin films and boundary layers
Academic Press (London) 1971 pp 243 - 250

81. PADDY, J.F.
Discussion
Thin films and boundary layers
Academic Press (London) 1971 page 84

82. PADDY, J.F.
Cohesive properties of thin films of liquids adhering to a solid surface
Thin films and boundary layers
Academic Press (London)1971 pp 64 - 74

83. LUDVIKSSON, V., LIGHTFOOT, E.N.
The dynamics of thin liquid films in the presence of surface tension gradients
Amer. Inst. Chem. Engrs. J. 17 (1971) 1166 - 1173

84. ASTARITA, G., MARRUCCI, G., PALUMBO, G.
Non-Newtonian gravity flow along inclined plane surfaces
Ind. & Eng. Chemistry Fundamentals 3 (1964) 333 - 339

85. CHENG, D.C-H.
The determination of wall slip velocity in the laminar gravity flow of non-Newtonian fluids along plane surfaces
Ind. & Eng. Chemistry Fundamentals 13 (1974) 394 - 395

86. SYLVESTER, N.D., TYLER, J.S., SKELLAND, A.H.P.
Non-Newtonian thin films: theory and experiment
Canadian J. Chem. Eng. 51 (1973) 418 - 429

87. SYLVESTER, N.D., TYLER, J.S., SKELLAND, A.H.P.
Non-Newtonian thin films
Proc. of 1972 Heat transfer and Fluid mechanics Institute
Stanford University U.S.A.
Stanford University Press (1972) pp 39 - 53

88. WATSON, E.J.
The radial spread of a liquid jet over a horizontal plate
J. Fluid Mechanics 20 (1964) 481 - 499

89. GLINKIN, A.D., TYABIN, N.V.
Movement of a stream of viscous liquid over the surface of a stationary plane disc
Trudy Kaz. Khim. Teckn. Inst. 31 (1963) 46 - 51
also available as B.L.L. RTS 9301

90. KARMAN, von T.
Uber Laminaire und turbulente reibung
Zeit. fur Angewante Mathematik und Mechanik 1 (1921) 233 - 252

91. COCHRAN, W.G.
The flow due to a rotating disc
Proc. Camb. Phil. Soc. 30 (1934) 365 - 375

92. OSTRACH, S., THORNTON, P.R.
Compressible laminar flow and heat transfer about a rotating isothermal disc
N.A.C.A. Technical Note 4320 (1958)

93. SPARROW, E.M., GREGG, J.L.
Heat transfer from a rotating disc to fluids of any Prandtl number
J. Heat Transfer (A.S.M.E. Series C) 81 (1959) 249 - 251

94. MILLSAPS, K., POHLHAUSEN, K.
Heat transfer by laminar flow from a rotating plate
J. Aeronautical Science 19 (1952) 120 - 126

95. LEVICH, V.G.
Physiochemical Hydrodynamics
Prentice-Hall (New York) 1962

96. BODEWADT, U.T.
Die drehstromung uber festem grunde
Zeit. fur Angewante Mathematik und Mechanik 20 (1940) 241 - 253

97. POSTLETHWAITE, J., ONG, K.L., PICKETT, D.J.
Determination of diffusion coefficients for M-nitrobenzene sulphonic acid with a rotating disc elcctrode
Canadian J. Chem. Eng. 50 (1972) 245 - 247

98. GERGORY, N., STUART, J.T., WALKER, W.S.
On the stability of three-dimensional boundary layers with application to the flow due to a rotating disc
Phil. Trans. Royal Soc. (London) A248 (1956) 155 - 199

99. HANNAH, D.M.
Forced flow against a rotating disc
Aero. Research Council (London) Report Memoranda 2772
April 1947 (Published 1952)

100. GREGORY, N., WALKER, W.S.
Experiments on the effect of suction on the flow due to a rotating disc
J. Fluid Mechanics 9 (1960) 225 - 234

101. KUIKEN, H.K.
The effect of normal blowing on the flow near a rotating disc of infinite extent
J. Fluid Mechanics 47 (1971) 789 - 798

102. ROGERS, M.H., LANCE, G.N.
The rotationally symmetric flow of a viscous fluid in the presence of an infinite rotating disc
J. Fluid Mechanics 7 (1960) 617 - 631

103. KREITH, F., VIVIAND, H.
Laminar source flow between two parallel co-axial discs rotating at different speeds
J. Heat Transfer (A.S.M.E. Series C) 89 (1967) 541 - 547

104. MAROTI, L.A., DEAK, G., KREITH, F.
Flow phenomena of partially enclosed rotating discs
J. Basic Engineering (A.S.M.E. Series D) 82 (1960) 539 - 552

105. MITSCHKA, P.
Non-Newtonian liquids II: The rotary flow of Ostwald de Waele non-Newtonian liquids
Coll. Czech. Chemical Comm. 29 (1964) 2892 - 2905
also B.L.L. RTS 9735

106. ELLIOTT, L.
Elastico-Viscous flow near a rotating disc
Physics of Fluids 14 (1971) 1086 - 1090

107. HOPF, L.
Turbulenz bei einen flusse
Ann. Physik 32 (1910) 777 - 808

108. ESPIG, H., HOYLE, R.
Waves in a thin liquid layer on a rotating disc
J. Fluid Mechanics 22 (1965) 671 - 677

109. KAPITSA, P.L.
Heat conductivity and diffusion in a liquid medium under periodic flow conditions
Collected work of P.L. Kapitsa, Vol. II
Pergammon Press 1965 pp 743 - 757

110. KAMEI, Se., OISHI, J.
Hold-up in a wetted wall tower
Mem. Fac. Eng. Kyoto University 18 (1956) 1 - 12

111. HEWITT, G.F., KING, R.D., LOVEGROVE, P.C.
Techniques for liquid film and pressure drop studies in annular two phase flow
A.E.R.E. - R 3921 (1962)

112. BLACK, R.H.
Capacitance method of measuring water film thicknesses
Trans. Amer. Soc. Civil Engrs. 126 (1961) Pt 1 88 - 94

113. CLEGG, A.J.
Studies of film flow on wetted wall columns
Ph.D. Thesis Surrey University 1969

114. HEWITT, G.F.
The role of experiments in two phase flow systems with particular reference to measurement techniques
Prog. Heat & Mass Transfer 6 (1972) 295 - 343

115. WATTS, B.
The flow, heat and mass transfer characteristics of a rotating disc
Ph.D. Thesis Swansea University 1971

116. GARTSIDE, G.
Hydrodynamics and mass transfer in near horizontal channels
Ph.D. Thesis University Durham (Kings College) 1962
Now held at Newcastle upon Tyne University

117. LAMB, H.
Hydrodynamics
Cambridge University Press 6th edition 1932

118. ADLER, C.R., MARSHALL, W.R.
Performance of spinning disc atomisers Pt 1
Chem. Eng. Prog. 47 (1951) 515 - 522

119. BAR, P.
Uber die physikalishum grundlagen der zerstanbringstruckrung
Ph.D. Thesis Karlstruhe Tech. Coll. 1935

120. VENKATARAMAN, R.S.
Mass trnsfer to an expanding interface
Ph.D. Thesis Leeds University 1966

121. ZINNATULLIN, N. Kh.
The flow of a non-Newtonian liquid on a rotating disc
Trudy Kaz. Khim. Tekh. Inst. 35 (1965) 146 - 153
also available B.L.L. R.T.S. 8933

122. TYABIN, N.V., SHKLYAR, L.A., MOSIKHIN, Ye.P., VINOGRADOV, G.V.
Rheologic investigation of a grease lubricant by the centrifual method
Trudy Kaz. Khim. Tekh. Inst. 16 (1951) 133 - 150
also available: translation 14960, U.S. Dept. Commerce, Office of Technical Services, Washington

123. TYABIN, N.V., SHKLYAR, L.A., MOSIKHIN, Ye.P., VINOGRADOV, G.V.
The flow of semi-solid lubricants on a rotating disc under the action of centrifugal forces
Trudy Kaz. Khim. Tekh. Inst. 18 (1953) 123 - 141
also available B.L.L. RTS 8988

124. YURCHENKO, V.A., KOPTEV, A.A., ZAITSEN, A.I., ZHEBROVSKII, A.K., YANEV, Ya.S.
Investigation of the hydrodynamics of two phase flow on the surface of a rotating disc
Theo. foundations of Chem. Eng. 3 (1969) 341 - 345

125. EMSLIE, A.G., BONNER, F.T., PECK, L.G.
Flow of a viscous liquid on a rotating disc
J. Applied Physics 29 (1958) 858 - 862

126. VACHAGIN, K.D., NIKOLAEV, V.S.
Flow of a viscous liquid over the surface of a rapidly rotating flat disc
Izv. Khim. i Khim. Tekh. 3 (1960) 1097 - 1102
also available B.L.L. RTS 8906

127. ZINNATULLIN, N.Kh., VACHAGIN, K.D., TYABIN, N.V.
The two dimensional flow of a non-Newtonian fluid over the open surface of a rapidly rotating flat disc
J. Eng. Physics 15 (1968) 701-704

128. RAUSCHER, J.W., KELLEY, R.E., COLE, J.D.
An asymptotic solution for the laminar flow of a thin film on a rotating disc
J. Applied Mechanics (A.S.M.E. Series E) 40 (1973) 43 - 47

129. MATSUMOTO, S., SAITO, K., TAKASHIMA, Y.
The thickness of a viscous liquid film on a rotating disc
J. Chem. Eng. Japan 6 (1973) 503 - 506

130. DORFMAN, L.A.
Flow and heat transfer in a film of viscous liquid on a rotating disc
J. Eng. Physics 12 (1967) 309 - 316

131. REES, E.L. Ll.
An investigation into fluid flow and heat transfer across a rotating disc
M.Sc. Thesis Swansea University 1962

132. MATSUMOTO, S., SAITO, K., TAKASHIMA, Y.
Flow of a viscous liquid on a rotating disc
Bull. Tokoyo Inst. Techn. 109 (1972)

133. MATSUMOTO, S. SAITO, K. TAKASHIMA, Y.
Thickness of liquid film on a rotating disc
Bull. Tokoyo Inst. Techn. 116 (1973)

134. ADLER, C.R., MARSHALL, W.R.
Performance of spinning disc atomisers Pt.II
Chem. Eng. Prog. 47 (1951) 601 - 608

135. CLARE, H., JEFFS, R.A.
Some measurements of the thickness of a fluid film on a spinning disc
National Gas Turbine Establishment Draft Report 12.12.60

136. JONES, G.C.A.
Some mathematics relevant to the flow of a fluid film on a spinning disc
National Gas Turbine Establishment Eng. Res. Note No. 40, June 1962

137. SLEICHER, C.A.
Experimental velocity and temperature profiles for air in turbulent pipe flow
Trans. Amer. Soc. Mech. Engrs. 80 (1958) 693 - 704

138. ELROD, H.G.,
Note on the turbulent shear stress near a wall
J. Aeronautical Science 24 (1957) 468 - 469

139. DAVIS, E.J.
An analysis of liquid film flow
Chem. Eng. Science 20 (1965) 265 - 272

140. REICHARDT, H.A.
Vollstandige darstellung der turbulenten geschwindigkeitsverteilung in glatten leitungen
Ziet. fur Angew. Math. und Mech. 31 (1951) 208 - 219

141. ESPIG, H.R.
Heat transfer by condensation of steam on a rotating disc
Ph.D. Thesis Imperial College London 1963

142. GAZLEY, C., CHARWAT, A.F.
The characteristics of a thin liquid film on a spinning disc
Third All-Union Conf. on Heat and Mass Transfer, Minsk,
May 14 - 18, 1968

143. CHARWAT, A.F., KELLEY, R.E., GAZLEY, C.
Flow and stability of thin liquid films on a rotating disc
J. Fluid Mechanics 53 (1972) 227 - 255

144. CLARE, H., ASHWOOD, P.F.
Measurement of the thickness of a liquid film on the surface of a rapidly rotating disc
Inst. Practice 16 (1962) 70 - 71

145. VACHAGIN, K.D., NIKOLAEV, V.S.
Dvizhenie zhidkosti po poverkhnocti vvistro vrashchayuegosya konicheskogo diska
Trudy Khim i Khim Tekh. Inst. 27 (1961) 44 - 53

146. LILLEHAT, L.U., HANRATTY, T.J.
Relation of the interfacial shear stress to the wave height for concurrent air-water flow
Amer. Inst. Chem. Engrs. J. 7 (1961) 548 - 550

147. DE GRAAF, J.G.A.
The mechanism of spray drying liquids from a high speed rotating disc
High Speed Photography Editor R.B. Collings Butterworths Scientific Publications 1957 (London) pp 385 - 388

148. BUTUZOV, A.I., RIFERT, V.G.
Experimental investigation of heat transfer to evaporating liquid film on a rotating disc
Izv. Vuz. Mashin. 2 (1972) 81 - 85
Also available B.L.L. RTS 9462

149. RIFERT, V.G.
Heat transfer analysis with liquid film evaporation on a rotating disc
Inz. Fizi. Khim. 28 (1973) 232 - 236

150. SCHLICHTING, H.
Boundary Layer Theory
McGraw-Hill (New York) 4th Edition 1960 pp 87 - 89

151. GAY, B.
Studies on interfacial shear
Ph.D. Thesis Birmingham University 1958

152. HUNTLEY, H.E.
Dimensional analysis
McDonald & Co Ltd. (London) 1st Edition 1953

153. NUSSELT, W.
Der warmeaustausch am berieselelungskiihler
Zeit. Vereines Deut. Ing. 67 (1928) 206 - 210

154. JAKOB, M.
Heat Transfer Vol. II
John Wiley (New York) 1957

155. BAYS, G.S., McADAMS, W.H.
Heat transfer coefficients in falling film heaters
Ind. Eng. Chemistry 29 (1937) 1240 - 1246

156. AHMED, S.Y., KAPARTHI, R.
Heat transfer studies of falling film heat exchangers
Indian J. Techn. 1 (1963) 377 - 381

157. WILKE, W.
Warmeubergang an rieselfilme
Kaltetechnik 13 (1961) 339 - 346

158. CHUN, V.R., SEBAN, R.A.
Performance Prediction of falling film evaporators
J. Heat Transfer (A.S.M.E. Series C) 94 (1972) 432 - 436

159. DOMANSKII, I.V., SOKOLOV, V.N.
Heat transfer to a falling liquid film previously heated to boiling point
Zh. Nriklandnoi Khim. 40 (1967) 56 - 60

160. HERBERT, L.S., STERNS, U.J.
An experimental investigation of heat transfer to water in film flow Pt.I: Non boiling runs with and without swirl
Canadian J. Chem. Eng. 46 (1968) 401 - 408

161. McADAMS, W.H., DREW, T.S., BAYS, G.S.
Heat transfer to falling water films
Trans. Amer. Inst. Mech. Engrs. 62 (1940) 627 - 631

162. McADAMS, W.H.
Surface temperature measurement
Heat Transmission McGraw-Hill (New York) 2nd Ed 1942 pp 149 - 152

163. TROMMELAN, A.M.
Heat transfer to falling liquid films
Chem. Eng. Science 22 (1967) 1152 - 1154

164. LEONARD, W.K., ESTIM, J.
Heat transfer through a wavy film on a vertical surface
Amer. Inst. Chem. Eng. J. 18 (1972) 439 - 442

165. O'BRIEN, E.E.
On the flux of heat through laminar wavy liquid layers
J. Fluid Mechanics 28 (1967) 295 - 303

166. MIYA, M., WOODMANSEE, D.E., HANRATTY, T.J.

A model for wall waves in gas-liquid flow
Chem. Eng. Science 26 (1971) 1915 - 1931

167. PORTALSKI, S.
Eddy formation in the film flow down a vertical plate
Ind. & Eng. Chemistry Fundamentals 3 (1964) 49 - 53

168. BARBER, N.F.
Water Waves
Wykeham Publishers (London) Ltd. 1969

169. EINARSSON, A., WRAGG, A.A.
Instantaneous local rates of liquid - solid mass transfer in a rippling film: the effect of a co- and counter-current gas flow
Chem. Eng. Science 26 (1971) 1289 - 1292

170. IRIBARNE, A., GOSMAN, A.D., SPALDING, D.B.
A theoretical and experimental investigation of diffusion controlled electrolytic mass transfer between a falling liquid film and a wall
Int. J. Heat & Mass Transfer 10 (1967) 1661 - 1676

171. CHAND, R., ROSSON, H.F.
Local heat flux to a water film flowing down a vertical surface
Ind. & Eng. Chemistry Fundamentals 4 (1965) 356 - 359

172. SHAH, D.B., DARBY, R.
The effect of surfactant on evaporative heat transfer in vertical film flow
Int. J. Heat & Mass Transfer 16 (1973) 1889 - 1903

173. DAVIES, J.T., SHANKI, A.M.
Heat transfer from turbulent falling films of water and non-Newtonian solutions on smooth and ridged plates
Chem. Eng. Science 29 (1974) 1801 - 1808

174. PONTER, A. B., DUREPOS, S., HAIGH, C.P.
Heat transfer to falling water films containing surface active agents
Amer. Inst. Chem. Engrs. J. 17 (1971) 1241 - 1242

175. STROEBAL, W.J., WHITAKER, S.
The effect of surfactants on the flow characteristics of falling liquid films
Amer. Inst. Chem. Engrs. J. 15 (1969) 527 - 532

176. KUTATELADZE, S.S.
Fundamentals of heat transfer
Editor R.D.Cess. Edward Arnold (London) 1963 page 310

177. SPARROW, E.M., GREGG, L.
A boundary layer treatment of laminar film condensation
J. Heat Transfer (A.S.M.E. Series C) 81 (1959) 13 - 18

178. DHIR, V., LEINHARD, J.
Laminar film condensation on plane and axisymetric bodies in non-uniform gravity
J. Heat Transfer (A.S.M.E. Series C) 93 (1971) 97 - 99

179. CHAUDHURY, Z.H.
Heat transfer in a radial liquid jet
J. Fluid Mechanics 20 (1964) 501 - 511

180. HEALEY, D.
Heat transfer to a radial liquid jet from a horizontal plane
M. Sc. Thesis Newcastle University 1965

181. OUDART, A.
Exchanges thermiques pour le disque isotherm en rotation uniform
Comptes Rendue Acad. Science (Paris) 239 (1954) 27 - 29

182. WAGNER, C.
Heat transfer from a rotating disc to ambient air
J. Applied Physics 19 (1948) 837 - 839

183. LIU, K.T., STEWART, W.E.
Asymptotic solutions for forced convection from a rotating disc
Int. J. Heat & Mass Transfer 15 (1972) 187 - 189

184. LEVART, E., SCHUHMANN, D.
Analyse du transport transitoire sur un disque tournant en regime hydrodynamique laminaire et permanent
Int. J. Heat & Mass Transfer 17 (1974) 555 - 566

185. RILEY, N.
The heat transfer from a rotating disc
Quart. J. Mech. & Applied Maths 17 (1964) 331 - 349

186. HAYDAY, A.A.
On the transfer from isothermal and non-isothermal spinning bodies of revolution
J. Heat Transfer (A.S.M.E. series C) 87 (1965) 445 - 452

187. DORFMAN, L.A.
Thermal boundary layer on a rotating disc
Soviet Physics Doklady 3 (1958) 248 - 251

188. KREITH, F., TAYLOR, J.H.
Heat transfer from a rotating disc in turbulent flow
Amer. Soc. Mech. Engrs. Paper 56 - A146 (1956)

189. DAVIES, D.R.
On the calculation of eddy viscosity and heat transfer in a turbulent boundary layer near a rapidly rotating disc
Quart. J. Mech and Applied Maths. 12 (1959) 211 - 221

190. HARTNETT, J.P., TSAI, S.H., JANTSCHER, H.N.
Heat transfer to a non-isothermal rotating disc with a turbulent boundary layer
J. Heat Transfer (A.S.M.E. series C) 87 (1965) 362 - 368

191. KREITH, F.
Convection heat transfer in rotating systems
Advances in Heat Transfer 5 (1968) 129 - 251

192. DORFMAN, L.A.
Hydrodynamic resistance and the heat loss of rotating solids
Oliver and Boyd (Edinburgh) 1963

193. COBB, E.C., SAUNDERS, O.A.
Heat transfer from a rotating disc
Proc. Royal Society A236 (1956) 343 - 351

194. YOUNG, R.L.
Heat transfer from a rotating plate
Trans. Amer. Soc. Mech. Engrs. 78 (1956) 1163 - 1168

195. RICHARDSON, P.D.
Some studies of the flow and heat transfer associated with a rotating disc
Ph.D. Thesis London University 1958

196. GREGORY, D.P., RIDDIFORD, A.C.
Transport to a surface of a rotating disc
J. Chem. Society (1956) 3756 - 3764

197. LEHMKUHL, G.D., HUDSON, J.L.
Flow and mass transfer near an enclosed rotating disc: experiment
Chem. Eng. Science 26 (1971) 1601 - 1603

198. KREITH, F., TAYLOR, J.H., CHONG, J.P.
Heat and mass transfer from a rotating disc
J. Heat Transfer (A.S.M.E. series C) 81 (1959) 95 - 105

199. MABUCHI, I., KOTAKE, Y., TANAKA, T.
Studies on the convective heat transfer from rotating disc
Trans. Japan Society Mech. Engrs. 37 (1971) 1996 - 2003

200. KREITH, F., DOUGHMAN, E., KOZLOWSKI, H.
Mass and heat transfer from an enclosed rotating disc with and without source flow
J. Heat Transfer (A.S.M.E. series C) 85 (1963) 153 - 163

201. METZGER, D.E.
Heat transfer and pumping on a rotating disc with freely induced and forced cooling
J. Eng. Power (A.S.M.E. series A) 92 (1970) 343 - 348

202. SPARROW, E.M., GREGG, J.L.
Mass transfer, flow and heat transfer about a rotating disc
J. Heat Transfer (A.S.M.E. series C) 82 (1960) 294 - 302

203. LEE, M.H.
Effect of boundary layer control on heat transfer from a rotating disc
Ph.D. Thesis Imperial College 1966

204. MABUCHI, I., TANAKA, T., SAKAKIBARA, Y.
Studies on the convective heat transfer from rotating disc
Bull. Japan Society Mech. Engrs. 10 (1967) 104 - 112

205. ANDREWS, R.D., RILEY, N.
Unsteady heat transfer from a rotating disc
Quart. J. Mech. and Applied Maths. 22 (1969) 19 - 38

206. IYENGAR, S.R.K., RATH, R.S.
Flow and heat transfer of a non-Newtonian fluid about an unsteadily rotating disc
Archiwum Mechaniki Stosowanej r (1968) 513 - 527

207. SHILMAN, Z.P., POKRYVAILO, N.A., KORDONSKII, V.I. KABERDINA, E.B.
Rheodynamics and mass transfer in rotating flows of anomolous viscous fluids
Prog. Heat & Mass Transfer 5 (1970) 177 - 185

208. SHULMAN, Z.P., POKRYVAILO, N.A., KORDONSKII, V.I. NESTEROV, A.K.
Mass transfer peculiarities of a disc rotating in a non-Newtonian fluid
Int. J. Heat & Mass Transfer 16 (1973) 1339 - 1346

209. SPARROW, E.M., GREGG, J.L.
A theory of rotating condensation
J. Heat Transfer (A.S.M.E. series C) 81 (1959) 113 - 120

210. ROHSENOW, W.M.
Heat transfer and temperature distribution in laminar film condensation
Trans. Amer. Society Mech. Engrs. 78 (1956) 1645 - 1648

211. SPARROW, E.M., GREGG, J.L.
The effect of vapour drag on rotating condensation
J. Heat Transfer (A.S.M.E. series C) 82 (1960) 71 - 72

212. BECKETT, P.M., HUDSON, P.C., POOTS, G.
Laminar film condensation due to a rotating disc
J. Eng. Maths. 7 (1973) 63 - 73

213. CHIRANJIVI, C., APPARAO, K.V., CHARY, S.P.
Effect of vapour drag on condensation on a rotating disc
Indian J. Technology 8 (1970) 205 - 209

214. APPARAO, K.V. CHIRANJIVI, C., CHARY, S.P.
An approximate analysis of condensation on a rotating disc
Indian J. Technology 6 (1968) 286 - 288

215. ROETZEL, W.
Improving heat transfer in steam heated rotating paper drying drums
Int. J. Heat & Mass Transfer 18 (1975) 79 - 86

216. GUNERATNE, D.C.
Condensation on a rotating axi-symmetric surface
M.Sc. Thesis Swansea University 1967

217. NANDAPURKAR, S.S., BEATTY, K.O.
Condensation on a horizontal rotating disc
Chem. Eng. Symposium Series 56 (1960) 129 - 137 No. 30

218. ASTAF'EV, V.B., BAKLASTO, A.
Condensation of steam on a horizontal rotating disc
Thermal Eng. USSR 17 (1970) 82 - 85

219. ASTAF'EV, V.B., BAKLASTO, A.
Flow of film and heat transfer with steam condensation on a rotating disc
Thermal Eng. USSR 17 (1970) 111 - 113

220. BUTUZOV, A.I. RIFERT, V.G., PUKHOVOI, I.I.
Experimental data on heat transfer in a centrifugal condenser
Khim. Prom. Ukrainy 6 (1969) 23 - 24
also available B.L.L. RTS 9499

221. BUTUZOV, A.I., RIFERT, V.G.
An experimental study of heat transfer during condensation of steam at a rotating disc
Heat Transfer Soviet Research 4 (1972) 150 - 153

222. WILLIAMS, A.G., NANDAPURKAR, S.S., HOLLAND, F.A.
Condensation on a vertical rotating finned tube
Canadian J. Chem. Eng. 49 (1971) 51 - 55

223. BRUIN, S.
Analysis of heat transfer in a centrifugal film evaporator
Chem. Eng. Science 25 (1970) 1475 - 1485

224. BROMLEY, L.A., HUMPHREYS, R.F., MURRAY, W.
Condensation and evaporation from radially grooved rotating discs
J. Heat Transfer (A.S.M.E. series C) 80 (1966) 79 - 86

225. BUTUZOV, A.I., RIFERT, V.G.
Heat transfer in evaporation of liquid from a film on a rotating disc
Heat Transfer Soviet Research 5 (1973) 57 - 61

226. BUTUZOV, A.I., PUKHOVOI, I.I., RIFERT, V.G.
Heat transfer during distillation of sea water on a rotating disc
Heat Transfer Soviet Research 2 (1970) 187 - 190

227. HICKMAN, K.C.D.
Centrifugal boiler compression still
Ind. & Eng. Chemistry 49 (1957) 786 - 800

228. GUBENKO, N. Yu., LEONCHIK, B.I.
Experimental research on evaporation and atomisation of liquid by means of a rotating heated disc
Inz. Fizi. Zhur. 20 (1971) 151 - 153

229. CLARKE, L.R., BROMLEY, L.A.
Saline water conversion by multiple effect rotary evaporation
Chem. Eng. Progress 57 (1961) 64 - 70

230. BIRD, R.B., STEWART, W.E., LIGHTFOOT, E.L.
Transport Phenomena
John Wiley (New York) 1960 pp 41 - 42

231. SASAJI, N.
A new method for surface temperature measurement
Review Scientific Inst. 21 (1950) 1 - 3

232. WATSON, G.G.
Techniques for measuring surface temperature
Inst. Practice 20 (1966) 447 - 451

233. BENDERSKY, D.A.
A special thermocouple for measuring transient temperatures
Mech. Engr. 75 (1953) 117 - 121

234. ADENCO Ltd. Private Communication

235. BELL, C.
Hydrodynamics and heat transfer to water on a rotating disc
1972/73 report Dept. Chem. Eng. Newcastle University

236. PAI, S-I.
Viscous flow theory Vol. I Laminar flow
Van Nostrand Inc. (New Jersey) 1956 Chapter 3

237. NAVIER, C.L.M.H.
Memoire sur les lois due movement des fluides
Mem. de l'Acad. des Sciences (1823) 1823 389 - 440

238. STOKES, G.G.
On the theories of the internal friction of fluids in motion and of the equilibrium and motion of elastic solids
Trans. Cambridge Phil. Soc. 8 (1845) 287 - 319

239. VACHAGIN, K.D., ZINNATULLIN, N.Kh., TYABIN, N.V.
Differential equations representing the movement of a non-Newtonian liquid
Trudy Kazan Khim. Tekh. Inst. 32 (1964) 157 - 163
also available B.L.L. RTS 9318

240. KELLER, H.B.
Numerical methods for two-point boundary-value problems
Blaisdell Pub.Co. (Waltham, Mass. USA) 1968 pp 74 - 75

PURDUE UNIVERSITY
SCHOOL OF MECHANICAL ENGINEERING
WEST LAFAYETTE, INDIANA 47907

June 21, 1973

Mr. C. Bell
Dept. Chemical Engineering
Merz Court, Claremont Road
Newcastle upon Tyne, NE1 7RU,
England

Dear Mr. Bell:

Thank you very much for your interest in my work. Unfortunately, I cannot be of any help in respect to Reference 1 of my article in IEEE (1972) because the research conducted in Aachen was supported by an industrial firm and by the government of Nordrhein-Westfalen, Germany. The research reports were confidential and not released for publication.

The work continued here at Purdue repeated part of the studies of Aachen and is described in References 6, 7, 8, 12, and 13. All this material can be obtained from Purdue University via library loan.

Sincerely yours,

Wolfgang Leidenfrost

WL/pf

Adenco Engineering Company Limited

Please note our change of address:-

163 Godstone Road,
Whyteleafe, Surrey,
CR3 0EH.
01-668 8195

'DON · CR9 2UT · ENGLAND

Telephone :- 01-688 1010

Cables :- PRECOMPTS CROYDON

REG. OFFICE
17 JOHN STREET
LONDON W.C.1

Department of Chemical Engineering,
The University,
Newcastle upon Tyne NE1 7RU.

21st November, 1972.

For the attention of Mr. Colin Bell

Dear Mr. Bell,

Many thanks for your telephone call regarding our slip ring assemblies. As mentioned on the telephone, the precious metal units do tend to be rather expensive. However, it has been found that it is imperative to use such devices where one must differentiate between low signal levels and noise.

We would also like to take the opportunity of enclosing a leaflet on commercial slip rings which may be of interest to you. Once you have had an opportunity of studying the information, please let us know if we can be of any further assistance.

Yours sincerely,

M.S. Goodall